Year : 2021

ApoE4 effects on the structural covariance brain networks topology in Mild Cognitive Impairment

Sanabria Diaz Gretel

Sanabria Diaz Gretel, 2021, ApoE4 effects on the structural covariance brain networks topology in Mild Cognitive Impairment

Originally published at : Thesis, University of Lausanne

Posted at the University of Lausanne Open Archive http://serval.unil.ch
Document URN : urn:nbn:ch:serval-BIB_7B7E08CA70FA5

UNIL | Université de Lausanne
Faculté de biologie et de médecine

Département de Neurosciences Cliniques

ApoE4 effects on the structural covariance brain networks topology in Mild Cognitive Impairment

Thèse de doctorat en Neurosciences

présentée à la

Faculté de Biologie et de Médecine
de l'Université de Lausanne

par

Gretel SANABRIA DIAZ

Psychologue diplômée de l'Université centrale "Marta Abreu" de Las Villas, Cuba

Jury

Prof. MD. Lorenz Hirt, Président
Dr. Ferath Kherif, Directeur
Prof. Dr. MD. Jean-Francois Demonet, Co-Directeur
Dr. MD. Emmanuel Carrera, Expert
Prof. Dr. Yasser Iturria Medina, Expert

Thèse n° 298

Lausanne 2021

Programme doctoral interuniversitaire en Neurosciences des Universités de Lausanne et Genève

LEMANIC NEURO SCIENCE DOCTORAL SCHOOL

UNIL | Université de Lausanne

UNIVERSITÉ DE GENÈVE

UNIL | Université de Lausanne

UNIVERSITÉ DE GENÈVE

Programme doctoral interuniversitaire en Neurosciences des Universités de Lausanne et Genève

Imprimatur

Vu le rapport présenté par le jury d'examen, composé de

Président·e	Monsieur	Prof.	Lorenz	**Hirt**
Directeur·trice de thèse	Monsieur	Dr	Ferath	**Kherif**
Co-Directeur·trice de thèse	Monsieur	Prof.	Jean-François	**Démonet**
Expert·e·s	Monsieur	Prof.	Yasser Iturria	**Medina**
	Monsieur	Dr	Emmanuel	**Carrera**

le Conseil de Faculté autorise l'impression de la thèse de

Madame Gretel Sanabria Diaz

Master in Medical Psychology,
Universidad Central "Marta Abreu" de Las Villas, Cuba

intitulée

ApoE4 effects on the structural covariance brain networks topology in Mild Cognitive Impairment

Date de l'examen: 1 mars 2021
Date d'émission de l'Imprimatur: Lausanne, le 19 mars 2021

pour Le Doyen
de la Faculté de Biologie et de Médecine

Prof. Niko GELDNER
Directeur de l'Ecole Doctorale

ACKNOWLEDGEMENTS

Undertaking this Ph.D has been a truly life-changing experience for me, and it would not have been possible to do without the support and guidance that I received from many people.

First of all, I would like to thank my thesis director, Dr. Ferah Kherif, for his scientific advice and for allowing me to pursue my research projects without objection. To my co-supervisor, Professor Jean-Francois Demonet, for sharing his knowledge and insightful suggestions. Thanks to both of them for fruitful discussions.

I would also like to thank the PIs of LREN, Prof. Bogdan Draganski, Dr. Marcia de Lucia, and Prof. Antoine Lutti, for their advice and scientific input.

From the bottom of my heart, I would like to say a big thank you to Dr. Ulrike Toepel, the Lemanic Doctoral School coordinator, for her indefectible support during my Ph.D.

To my colleagues at the LERN, who have supported me and put up with my stresses and moans for the past years of study. Special thanks to Sandra, Jing, Elham, Lucien, Claudia, Maya, Elsa, Sandrine, Renaud, Borja, Estelle, Dave, Thomas, Mirco, Leyla, and other colleagues I cannot mention here, for the friendship, collaboration, discussions, and jokes.

To my former colleagues at the Cuban Neuroscience Center in Havana, without whom my "Ph.D trajectory" would not exist. These interactions taught me a lot about ethics and hard work; thank you.

A special thanks to my family. Words cannot express how grateful I am to my mom, sister, dad, and huge family troop for all of the sacrifices you've made on my behalf. I love them so much, and I would not have made it this far without them. You did all the difficult groundwork that made me the kind of person that'd tackle a project like this.

I want to express appreciation to my best friend, soul-mate, and husband, Lester. He's one of the smartest people I know. He provided me training, scientific advice, knowledge, and many insightful discussions and suggestions. Lester is my primary resource for getting my science questions answered and helped me crank out this thesis. He is the reason without which I would have stopped these studies a long time ago. His enthusiasm and love for science are contagious. These past several years have not been an easy ride, both academically and personally. I feel that we both learned a lot about life and strengthened our commitment and determination to each other and live life to the fullest.

Finally, to my son Gabriel, the light of my soul and the motivation to finish this project, sorry for being even grumpier than usual while I wrote this thesis! Gabriel helped me re-shuffle my priorities in life and realize that his happiness means the world to me.

"Reductionism was the driving force behind much of the twentieth century's research. To comprehend nature, it tells us, we first must decipher its components. [: : :] Divide and conquer; the devil is in the details. [: : :] Now we are close to knowing just about everything there is to know about the pieces. But we are as far as we have ever been from understanding nature as a whole. [: : :] The reason is simple: Rising reductionism, we run into the hard wall of complexity. We have learned that nature is not a well-designed puzzle with only one way to put it back together. [: : :] It [Nature] does so by exploiting the all-encompassing laws of self-organization, whose roots are still largely a mystery to us. Today we increasingly recognize that nothing happens in isolation. [: : :] We have come to see that we live in a small world, where everything is linked to everything else. We are witnessing a revolution in the making as scientists from all different disciplines discover that complexity has a strict architecture. We have come to grasp the importance of networks."

(Barabasi, 2002)

ABSTRACT

The Apolipoprotein E isoform E4 (ApoE4) is consistently associated with an elevated risk of developing late-onset Alzheimer's Disease (AD). However, little is known about his potential genetic modulation on the structural covariance brain networks during prodromal stages like Mild Cognitive Impairment (MCI). The covariance phenomenon is based on the observation that regions correlating in morphometric descriptors are often part of the same brain system.

In a first study, I assessed the ApoE4-related changes on the brain network topology in 256 MCI patients, using the regional cortical thickness to define the covariance network. The cross-sectional sample selected from the ADNI database was subdivided into ApoE4-positive (Carriers) and negative (non-Carriers). At the group-level, the results showed a significant decrease in characteristic path length, clustering index, local efficiency, global connectivity, modularity, and increased global efficiency for Carriers compared to non-Carriers. Overall, I found that ApoE4 in MCI shaped the topological organization of cortical thickness covariance networks.

In the second project, I investigated the impact of ApoE4 on the single-subject gray matter networks in a sample of 200 MCI from the ADNI database. The patients were classified based on clinical outcome (stable MCI versus converters to AD) and ApoE4 status (Carriers versus non-Carriers). The effects of ApoE4 and disease progression on the network measures at baseline and rate of change were explored. The topological network attributes were correlated with AD biomarkers. The main findings showed that gray matter network topology is affected independently by ApoE4 and the disease progression (to AD) in late-MCI. The network measures alterations showed a more random organization in Carriers compared to non-Carriers.

Finally, as additional research, I investigated whether a network-based approach combined with the graph theory is able to detect cerebrovascular reactivity (CVR) changes in MCI. Our findings suggest that this experimental approach is more sensitive to identifying subtle cerebrovascular alterations than the classical experimental designs. This study paves the way for a future investigation on the ApoE4-cerebrovascular interaction effects on the brain networks during AD progression.

In summary, my thesis results provide evidence of the value of the structural covariance brain network measures to capture subtle neurodegenerative changes associated with ApoE4 in MCI. Together with other biomarkers, these variables may help predict disease progression, providing additional reliable intermediate phenotypes.

RÉSUMÉ

L'isophorme E4 de l'Apolipoprotéine E (ApoE4) est systématiquement associé avec un risqué élevé de développer la maladie d'Alzheimer (MA) à début tardif. Cependant, on connait peu sa modulation génétique potentielle sur les réseaux cérébraux de covariance structurelle durant la phase prodromique, telle que les troubles cognitifs légers (MCI). Le phénomène de covariance est basé sur l'observation que les régions corrélant des descripteurs morphométriques font souvent parti des mêmes systèmes cérébraux.

Dans une première étude, j'ai évalué les changements liés à ApoE4 sur la topologie des réseaux cérébraux chez 256 patients MCI, en utilisant l'épaisseur corticale régionale pour définir les réseaux de covariance. L'échantillon transversal sélectionné à partir de la base de données ADNI a été divisé en ApoE4-positif (Porteurs) et négatif (non-Porteurs). Au niveau des analyses de groupe, les résultats ont montré une diminution significative des caractéristiques «longueur de chemin», «index de cluster», «efficience locale», «connectivité globale», «modularité»; et une augmentation de l'«efficience globale» chez les Porteurs comparés aux non-Porteurs.

Dans l'ensemble, j'ai trouvé que ApoE4 dans les MCI modèle l'organisation topologique des réseaux de covariance de l'épaisseur corticale. Dans un second projet, j'ai étudié l'impact d'ApoE4 sur les réseaux de matière grise au niveau de chaque sujet, dans un échantillon de 200 MCI issu de la base de données ADNI. Les patients étaient classés sur la base de critère clinique (MCI stable versus en conversion vers la MA) et du statut ApoE4 (Porteurs versus non-Porteurs). Les effets d'ApoE4 et de l'évolution de la maladie sur les réseaux cérébraux ont été examinés au point de référence ainsi que leur taux de changement. Les attributs des réseaux topologiques étaient corrélés avec des biomarqueurs établis de la MA. Les principales conclusions ont montré que la topologie des réseaux de matière grise est affectée indépendamment par ApoE4 et par l'évolution de la maladie (vers la MA) dans les MCI à début tardif. Les altérations des mesures de réseaux ont montré une organisation plus aléatoire chez les Porteurs comparés aux non-Porteurs.

Finalement, comme recherche additionnelle, j'ai étudié si une approche basée sur les réseaux associée à la théorie des graphes peut permettre de détecter les changements de réactivité cérébro-vasculaire (RCV) dans les MCI. Nos conclusions suggèrent que cette approche expérimentale est beaucoup plus sensible pour identifier les altérations cérébro-vasculaires subtiles que les designs expérimentaux classiques. Cette étude ouvre la voie à une investigation future des effets d'interaction entre ApoE4 et la réactivité cérébro-vasculaire sur les réseaux cérébraux durant la progression de la MA.

En résumé, les résultats de ma thèse prouvent la valeur des mesures de réseaux cérébraux de covariance structurelle pour saisir les changements neurodégénératifs subtils associés à ApoE4 dans les MCI. Associées à d'autres biomarqueurs, ces variables devraient aider à prédire la progression de la maladie, en fournissant des phénotypes intermédiaires additionnels fiables.

LIST OF ABBREVIATIONS

AD	Alzheimer's Disease
MCI	Mild Cognitive Impairment
ApoE	Apolipoprotein E
ApoE4	Apolipoprotein E ε4 allele
E4	Allele 4
E3	Allele 3
E2	Allele 2
CSF	Cerebrospinal fluid
Aβ	Amyloid-beta
ADNI	Alzheimer Disease Neuroimaging Initiative
P-Tau	Hyperphosphorylated tau
T-Tau	Total tau proteins
APP	Amyloid Precursor Protein
Aβ40	Amyloid-β 40
Aβ42	Amyloid-β 42
NFT	Neurofibrillary tangles
sMRI	Structural Magnetic Resonance Imaging
MRI	Magnetic Resonance Imaging
NIA-AA	Alzheimer's Association published revised guidelines
TPD-43	Transactive response DNA binding protein
CBF	Cerebral Blood Flow
PIB	Pittsburgh compound B
fMRI	Functional Magnetic Resonance Imaging
rsfMRI	Resting-state Functional Magnetic Resonance Imaging
DMN	Default Mode Network
PET	Positron Emission Tomography
SPECT	Single-photon Emission Computed Tomography
FDG-PET	^{18}F-fluorodeoxyglucose-Positron Emission Tomography
rsFDG-PET	Resting-state ^{18}F-fluorodeoxyglucose-positron emission tomography
DTI	Diffusion tensor imaging
MEG	Magnetoencephalography
EEG	Electroencephalogram
GM	Gray Matter
T1	T1-weighted image
SPM12	Statistical Parametric Mapping 12
TIV	Total Intracranial Volume
HC	Healthy Controls
aMCI	amnesic Mild Cognitive Impairment
MMSE	Mini Mental-State Examination
HIP	Hippocampus
PHG	Parahippocampal gyrus

FSC	Functional Connectivity Strength
PHF-Tau	Hyperphosphorylated tau protein
NC	Normal Controls
CVR	Cerebrovascular reactivity
PCC	Posterior cingulate cortex
NBC	Normalized Betweenness Centrality
ADNI-MEM	Alzheimer Disease Neuroimaging Initiative Composite measures of executive function and memory
ACZ	Acetazolamide
DWI	Diffusion-weighted imaging

TABLE OF CONTENTS

1 INTRODUCTION

1.1 Context and Motivation

Dementia constitutes a prevailing public health crisis nowadays, and it is considered a pandemic by the International Federation of Alzheimer's Associations. The World Alzheimer Report 2019 estimates that over 50 million people are living with dementia globally. As the demographic shifts toward older ages and increases in health and longevity globally, this number is predicted to reach 75 million in 2030 (Prince et al., 2015), causing an ever-increasing percentage of the population with dementia, an enormous burden on caregivers and health systems. Late-onset Alzheimer's Disease (AD) is the most common cause of dementia, accounting for 60% to 80% of cases (Hardy, 1997). It is a progressive condition causing behavioral changes, memory loss, and a decline in learning capacity (McKhann et al., 2011). There are no disease-modifying treatments currently available for Alzheimer's. In the past decade, clinical drug trials have had a 99.6% failure rate (Cummings et al., 2014). The general postulate is that one contributor to this negative result is that brain pathology begins years before the onset of objective cognitive symptoms and maybe irreversible by the diagnosis time. It is now recognized that; AD is best conceptualized as a biological and clinical continuum covering both the preclinical (clinically asymptomatic individuals with evidence of AD pathology) and clinical (symptomatic phases: Mild cognitive impairment (MCI) and AD dementia)) (Aisen et al., 2017). In this spectrum, MCI represents this transitional zone between the cognitive changes of aging and early AD (Ronald C. Petersen et al., 1999; Petersen, 2004) and a "window" in which it may be possible to intervene and delay dementia progression. Numerous international population-based studies have been conducted to document the frequency of MCI, estimating its prevalence to be between 15% and 20% in persons 60 years and older, with an annual rate of progression to dementia between 8% and 15% per year, implying that it is an essential condition to identify and treat (Petersen, 2016; Petersen and O'Brien, 2006).

Although multiple risk factors are involved in AD pathogenesis, the E4 allele of the Apolipoprotein E (ApoE4) gene is recognized as the most potent genetic risk factor for late-onset AD (Bu, 2009; Corder et al., 1993; Liu et al., 2013). The presence of the ApoE4 has been associated with an increased risk of progression from MCI to AD-type dementia (Elias-Sonnenschein et al., 2011; Fleisher et al., 2007; Petersen et al., 1995). Still, it is an open

question of why some MCI ApoE4 Carriers develop the disease while others seem not to be affected.

There is an emerging consensus in neuroscience that most major psychiatric disorders, including AD, arise from the dysfunction of spatially distributed, interconnected neural systems (Deco and Kringelbach, 2014; Fornito et al., 2015). Advances in the application of network science and graph theory have permitted detailed descriptions of diverse disease processes based on the highly complex brain network organization (Fornito et al., 2016; Newman, 2010). The resulting network properties can be examined as "intermediate phenotypes" that are situated in this thesis, between the genetic domain (ApoE4) and the behavior (diagnosis, disease progression, cognitive measurements), offering an opportunity for a clinical research strategy. The complex etiology and multiple pathogenesis associated with the MCI progression into AD call for a development of a system-level biomarker. In this context a network-based approach will provide key insights to fully understand the network degeneration hypothesis and its association with the disease risk factors. From the brain imaging biomarker research there is clear evidence that the risk of disease progression in MCI evolve at the system level. As such a network based-biomarker can be used as an indicator of normal biological change (including aging adaptative mechanisms), pathogenesis processes, or pharmacological responses. In particular a network approach provides quantitative characterization of the brain and integrate heterogenic data in a general mathematical body paving the way for a predictive, preventive, and personalized medicine.

Like many other approaches before, there is a challenging open question regarding the MCI population: how can we identify those patients at high risk for AD progression? Which ApoE4 Carriers are going to be more affected by the disease? Ongoing clinical trials use either the increased genetic risk or positive amyloid biomarkers as useful strategies to predict progression. However, cerebral amyloid-beta deposition is a necessary yet insufficient condition for late-onset AD (Karran et al., 2011), while the genetic is neither necessary nor sufficient (Bertram and Tanzi, 2012; Goldman et al., 2011).

In this thesis, I considered a different methodological approach that focuses on studying the network-level brain integrity in MCI, considering the ApoE4 as a risk factor. From this perspective, I may identify network attributes that predict risk for AD progression, providing an opportunity for intervention efforts. A better understanding of how the pathological changes in AD affect brain networks and how they respond to accumulating pathology might offer further insights into functional resilience.

However, AD's overt clinical phenotype is complex and comprises neurocognitive, neurobehavioral, and psychiatric symptoms (McKhann et al., 2011). Given this complexity, it is challenging to link AD's end clinical phenotype to specific genetic underpinnings like ApoE4 in the MCI phase. Using endophenotypes, or intermediate phenotypes, like brain network properties, I hope to fill in the gaps between genetic risk variability and higher-level behavioral MCI phenotypes (Gottesman and Gould, 2003).

1.2 Mild Cognitive Impairment as an intermediate phase in Alzheimer's Disease.

During AD progression, there are three broad phases: preclinical AD, MCI, and possible or probable AD (Albert et al., 2011; Jack et al., 2011; McKhann et al., 2011). AD spectrum is defined as a progressive and irreversible neurodegenerative disorder characterized by memory loss and cognitive decline that impair a person's ability to function in daily life (Masters et al., 2006) along with evidence of AD-related brain changes of accumulation of extracellular amyloid β in the form of plaques (Aβ) and the intracellular accumulation of hyperphosphorylated tau proteins as neurofibrillary tangles (NFTs) (Hyman et al., 2012; Montine et al., 2012). The length of each phase on the AD continuum is influenced by age, genetics, gender, and other factors (Vermunt et al., 2019). A definitive diagnosis of AD can only be made postmortem through an autopsy, which shows the occurrence of Aβ and NFTs pathology in the brain (McKhann et al., 1984).

Following the 2011 Alzheimer's Association published revised guidelines (NIA-AA), the concept of "MCI due to AD" is used to identify those symptomatic but non-demented individuals whose primary underlying pathophysiology is AD (Albert et al., 2011). Like AD dementia, MCI due to AD cannot be currently diagnosed by a laboratory test but requires a clinician's judgment. Also, similar to AD dementia, other pathophysiological processes may coexist in an individual who meets the criteria for MCI due to AD. MCI patients report a subjective memory concern either autonomously or via an informant or clinician. However, daily living activities are essentially preserved, there are no significant impairment levels in other cognitive domains, and no signs of dementia exist. Levels of MCI (early or late) are determined using a memory test like the Wechsler Memory Scale Logical Memory II. Diagnostic and research criteria for MCI have been suggested by Petersen (2004), who proposed two clinical subtypes of MCI amnestic and non-amnestic. In most of the studies, the criteria have focused on the amnestic form of MCI (Ronald C. Petersen et al., 1999; Petersen, 2004). The two major subtypes, amnestic and non-amnestic, can be further subdivided into single and multiple domain types (Petersen et al., 2001; Winblad et al., 2004). Both subtypes

of amnestic MCI lead to AD at a high rate (Lopez et al., 2003; Petersen, 2004). Though MCI does not always lead to AD, some patients remain stable or revert to a normal state (up to 44%) while others progress to different brain pathologies (15-41%) (Grundman et al., 2004; Hänninen et al., 2002). Identifying which MCI are more likely to develop AD or other dementias is a major goal of biomarker's current research.

In terms of clinical diagnosis is essential to clarify that this thesis follows the NIA-AA's guidelines (Sperling et al., 2011). The patient's samples were selected from ADNI, an open public database, that applies this criterium (http://adni.loni.usc.edu/). Here, AD will refer to the late-onset (non-familiar) disease form. MCI term (amnesic subtype) is considered due to AD under ADNI clinical protocol (For ADNI clinical protocols, see http://adni.loni.usc.edu/wp-content/themes/freshnews-dev-v2/documents/clinical/ADNI-1_Protocol.pdf).

In particular, ADNI I project criteria for these patients are as follows: MMSE scores between 24-30 (inclusive), a memory complaint, have objective memory loss measured by education adjusted scores on Wechsler Memory Scale Logical Memory II, a CDR of 0.5, absence of significant levels of impairment in other cognitive domains, essentially preserved activities of daily living, and an absence of dementia (R C Petersen et al., 1999; Petersen, 2003). The clinical performance characteristics of these subjects are intermediate between normal control subjects and subjects with very mild AD.

1.2.1 Pathogenesis of MCI

Despite the scientific community's effort, we still do not fully understand the cause and pathology of MCI. Previous studies showed that persons with MCI often meet the minimal pathologic criteria for AD (Bennett et al., 2005; Galvin et al., 2005; Markesbery et al., 2006; Saito and Murayama, 2007). Their AD brain pathology is typically intermediate between persons with and without clinical AD (Bennett et al., 2005; Markesbery et al., 2006; Petersen and O'Brien, 2006; Sabbagh et al., 2006). Nevertheless, MCI is a heterogeneous disorder; autopsy studies confirmed this heterogeneity with individual cases demonstrating non-AD pathology, such as hippocampal sclerosis, infarcts, or subcortical ischemic vascular disease, despite similar cognitive characterization (Jicha et al., 2006; Petersen and Morris, 2005). As an intermediate state, MCI shares, to a certain degree, the histopathological hallmarks of AD: the extracellular aggregates of Aβ plaques and intracellular aggregations of neurofibrillary tangles (NFTs) (Crews et al., 2010; Iqbal and Grundke-Iqbal, 2002; Mandelkow and Mandelkow, 1998; Trojanowski and Lee, 2000).

The leading Amyloid hypothesis (Hardy and Higgins, 1992) proposed a model where an imbalance between production and clearance of Aβ is an initiating factor of AD. Amyloid pathogenesis starts with altered cleavage of APP to produce insoluble Aβ fibrils. Aβ then oligomerizes, interfering with synaptic signaling. The $A\beta_{40}$ and $A\beta_{42}$ are two main types of Aβ polymers that directly affect plaque formation and induced neurotoxicity. In this hypothesis, increased levels of Aβ causes aggregation of hyperphosphorylated tau (P-tau) protein and NFTs (Hardy and Higgins, 1992), the second neuropathological hallmark in AD (Braak and Braak, 1991; Braak and Del Trecidi, 2015; Hyman and Gomez-Isla, 1994). When the tau protein gets hyperphosphorylated, this leads to its being oligomerized. The tubule gets unstable and aggregate into NFTs. These NFTs lead to abnormal loss of communication between neurons and, finally, apoptosis. These pathological processes' downstream consequences include neurodegeneration with synaptic and neuronal loss leading to macroscopic atrophy (Serrano-Pozo et al., 2011).

1.3 ApoE4 as a genetic risk factor for MCI and AD progression

The Apolipoprotein E ε4 allele (ApoE4) is the most prominent risk factor in late-onset AD (Bekris et al., 2010; Bookheimer and Burggren, 2009; Liu et al., 2013). As we can see in Figure 1, the lipoprotein is a carrier of cholesterol produced in ApoE alleles (ε2, ε3, ε4), which combine to generate five possible genotypes listed in order of increasing risk for AD: ε 2/2, ε 2/3, ε 3/3, ε 2/4, ε 3/4 and ε 4/4 (Kauwe et al., 2009) by a factor 3 (heterozygous) to 12 (Homozygous) (Corder et al., 1993; Farrer et al., 1997). ApoE is essential for normal lipid homeostasis in the brain (Bu, 2009; Holtzman and Herz, 2012). There is growing evidence that ApoE4 genotype influences multiple physiological pathways in AD (Mahley et al., 2006). Mechanistically, ApoE4 has been linked to virtually every AD-relevant pathogenic process both directly through Aβ binding and indirectly through Aβ-independent pathways (lipid transfer, cell metabolism, repair of neuronal injury, ischemia, inflammation, amyloid-β peptide accumulation) (Liu et al., 2013; Shi et al., 2017; Teter et al., 2002; Tiraboschi et al., 2004).
Relative to the common ε3 allele, possession of at least one ε4 allele increases the risk of AD progression of three to 15 times and earlier age on onset by 10 to 20 years as compared to non-Carriers (Farrer et al., 1997; Raber et al., 2004; Roses, 1996; Thal et al., 2006). In general, epidemiological studies have shown that members of the general population are at an approximately 10% to 12% risk of developing AD in their lifetime, while those with a first-

degree relative who has AD have a 2- to 4-fold increase in risk (Plassman et al., 2007; Slooter et al., 1998).

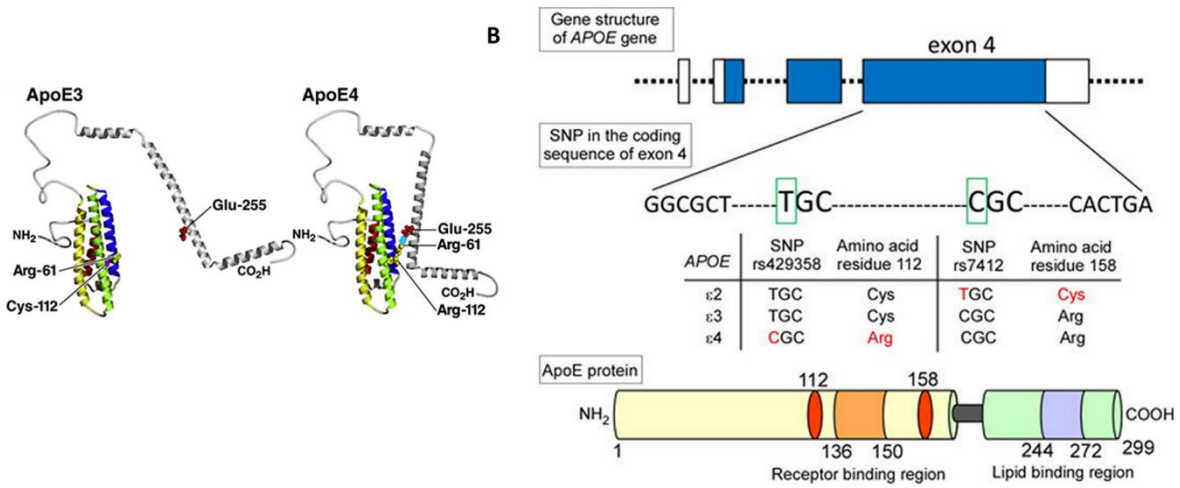

Fig 1 | ApoE isoforms and structural differences A) Structural conformation differences between Apolipoprotein E (ApoE) 3 and 4 B) ApoE gene structure, polymorphism of ApoE isoforms, and the different changes of the nucleotides and aminoacids of each isoform. Modified from (Yamazaki et al., 2016) and (Mahley and Huang, 2012).

Likewise, ApoE4 prevalence is substantially higher in MCI than in control individuals (Elias-Sonnenschein et al., 2011; Fleisher et al., 2007; Grundman et al., 2004). A meta-analysis revealed that the ApoE4 allele was associated with more than double the risk of progressing from MCI to AD across studies (Elias-Sonnenschein et al., 2011; Fei and Jianhua, 2013). During this time, ApoE4 interacts with other pathological factors to drive and shape this process. The well-documented ability of ApoE4 to accelerate and possibly induce amyloid accumulation is the most likely mechanism (Braak and Braak, 1997). Subtle pre-symptomatic changes in brain myelination, brain morphology, and cognitive functions may render ApoE4 Carriers more vulnerable (Bartzokis, 2011). A "second hit" by another age-associated pathological factor must be present in addition to amyloid accumulation (Mahley and Huang, 2009). This factor may be unrelated to the ApoE genotype or only weakly associated (e.g. tauopathy), such as any process placing increasing demand on neuronal repair during the MCI phase.

Additionally, the E4 genotype combines synergistically with other risk factors such as atherosclerosis, peripheral vascular disease, and type 2 diabetes contributing to an increased risk of AD progression (Haan et al., 1999; Peila et al., 2002). The allele is a risk factor for cardiovascular disease, suggesting that it might have compounding effects on cognitive decline in AD (Kalmijn et al., 1996)(Kalmijn et al., 1996). The overall evidence indicates that ApoE4

interacts with peripheral cardiovascular risk factors to impact cognition, and these factors share common downstream pathogenic properties: atherosclerosis, stroke, and Blood-Brain Barrier dysfunction (Tai et al., 2016). ApoE modulates Cerebral Blood Flow (CBF) when assessed using PET or SPECT. The higher CBF in MCI patients who are ApoE4 positive may indicate compensatory mechanisms in response to stress or of an ongoing pathogenic response affecting the vasculature. However, CBF is elevated in posterior brain regions with one risk factor such as ApoE4 or MCI, the presence of both results in decreased CBF and a greater likelihood of conversion to dementia.

In this direction, there is evidence that ApoE4 has effects on brain structure and function that are not in themselves pathological but appear to make the brain more susceptible to age-associated pathological mechanisms and environmental factors like diet. Diabetes, another well-known risk factor for AD, is strongly associated with disease progression among ApoE4 Carriers (Matsuzaki et al., 2010; Peila et al., 2002). Patients with diabetes who are carriers of ApoE4 have more neuritic plaques and neurofibrillary tangles than noncarriers (Peila et al., 2002)(Peila et al., 2002). Additionally, researchers have identified a close link between this allele and the cerebral iron-burden (Ayton et al., 2017, 2015). The authors' findings raise the possibility that ApoE4 confers susceptibility to AD via brain iron accumulation. Starting decades before a positive AD diagnosis, the iron influences beta-amyloid aggregation, tau and promotes neurotoxicity in the brain (Bartzokis et al., 2007; Ward et al., 2014).

Finally, it is important to clarify that AD's genetics is more complex and not limited to ApoE4. Current thinking holds that the disease's susceptibility is conferred by numerous genetic risk factors of relatively high frequency but low penetrance and, therefore, small effect size (Karch and Goate, 2015). The genome-wide association studies identified more than 20 genetic loci associated with AD's risk (e.g., BIN1, CLU, CR1, and PICALM). These genes are implicated in the immune system and inflammatory responses, cholesterol, lipid metabolism, and endosomal-vesicle recycling (Guerreiro and Hardy, 2014). However, modern-day genetic studies showed that the link between an increased risk for AD and ApoE4 continues to be the lead association finding (Bertram et al., 2010; Scheltens et al., 2016). Still, environmental and epigenetic factors likely make an important contribution in determining an individual’s risk.

1.3.1 Impact of ApoE4 on brain and cognition in MCI. Biomarkers

Even though the presence of ApoE4 does not guarantee disease progression, several cognitive dysfunctions, as well as structural and functional brain alterations, have been described among

MCI and AD patients (Fig. 2). Across studies, the more salient associations with the ApoE4 are: (1) Carriers exhibit worse cognitive performance and accelerated cognitive decline in MCI and AD subjects (Bookheimer and Burggren, 2009; Cosentino et al., 2008; Farlow et al., 2004; Ramakers et al., 2008) (2) increased hippocampal, amygdala and cerebral atrophy (particularly in the temporal lobe) (Farlow et al., 2004; Jack et al., 1999; Rusinek et al., 2003) (3) decreased cerebral blood flow and glucose metabolism (frontal, temporal, parietal and occipital lobes) (Brandon et al., 2018; Haxby et al., 1990; Small et al., 2000) (4) asymmetric atrophy effects (right hippocampus and right temporal lobe) and decreased blood flow and glucose metabolism mostly in the left hemisphere (Drzezga et al., 2005; Mosconi et al., 2004) (5) more significant Aβ deposition in the brains (Fleisher et al., 2013; Mishra et al., 2018; Murphy et al., 2013).

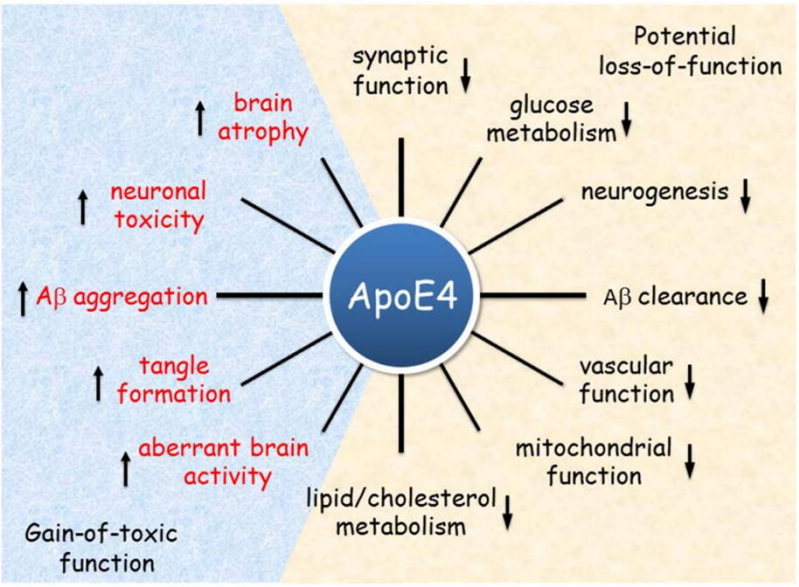

Fig 2 | The role of ApoE4 during Alzheimer disease progression. Key functional differences between ApoE4 and ApoE3 are illustrated. Abbreviations: Aβ, amyloid-β; ApoE, apolipoprotein E. Figure from (Liu et al., 2013).

Evaluating the extent of AD brain pathology using biomarkers in MCI patients may provide clues regarding the biological mechanisms underlying progression. Specifically, impairments in delayed free-recall measures from episodic memory tasks (Gomar et al., 2011; Landau et al., 2010), reduced hippocampal volumes (Devanand et al., 2007; Prestia et al., 2013; Vos et al., 2013), decreased CSF levels of $A\beta_{42}$ and elevations in T-tau and P-tau protein (Buchhave et al., 2012; Dickerson and Wolk, 2013; Hansson et al., 2006; Mattsson et al., 2009; Toledo et al., 2014; Vos et al., 2013) are the best established predictive biomarkers of AD progression in MCI (Forlenza et al., 2010).

Jack C.R et al. (2013, 2010) proposed a temporal ordering for the biomarkers mentioned above. Figure 3 shows an initial point of the development and accumulation of Aβ identified by CSF $A\beta_{42}$ or PET amyloid imaging (Jack et al., 2013, 2010).

Neuronal injury and dysfunction are identified by CSF tau or FDG-PET and neurodegenerative atrophy by sMRI. In MCI, genetic variation in the ApoE gene may shift the amyloid-beta (Aβ) and neurodegeneration curves, with individuals positive for ApoE4 showing a pathology occurring at an earlier age (Risacher and Saykin, 2013).

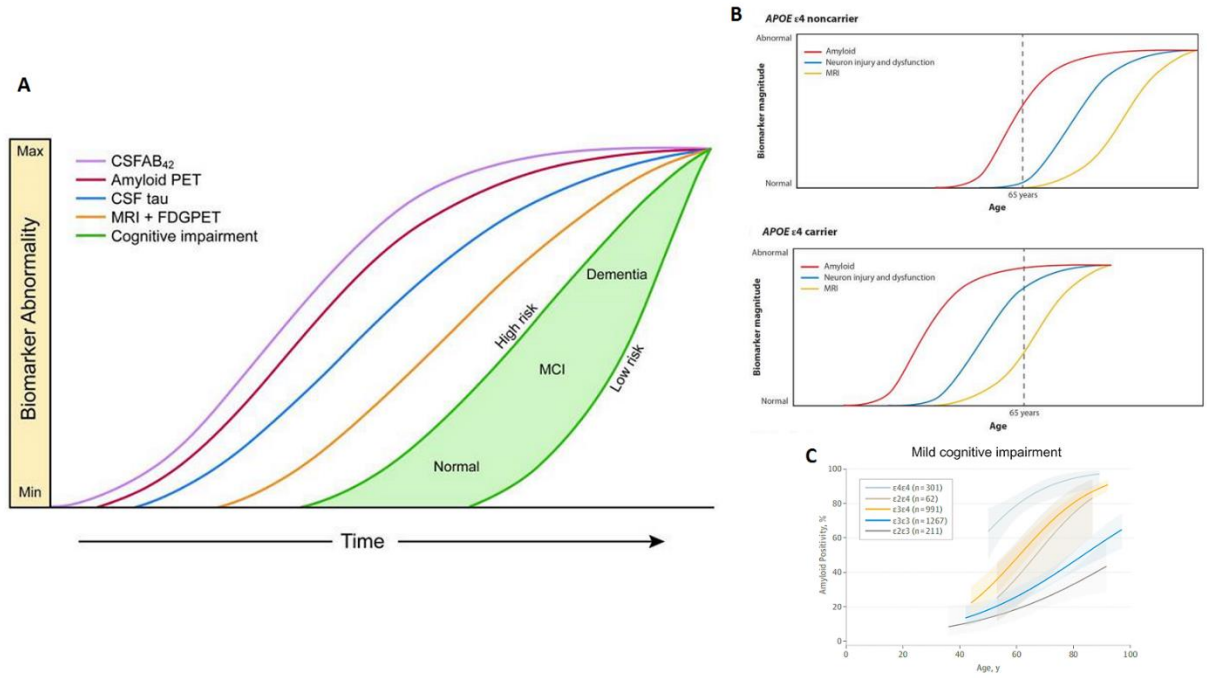

Fig 3 | A) Revised dynamic biomarkers of the AD pathological cascade model – 2012. Aβ amyloid is identified by CSF $A\beta_{42}$ (purple) or PET amyloid imaging (red). Elevated CSF tau (blue). FDG PET and structural MRI measure neurodegeneration, respectively, drawn concordantly (orange). The horizontal axis of disease progression is expressed as time. The cognitive response is illustrated as a zone (green filled area) with low and high-risk boarders. B) Panels show the modulation of biomarker curves by ApoE genotype. C) ApoE genotype and amyloid positivity. Estimated probabilities of amyloid positivity according to ApoE genotype, plotted against age in mild cognitive impairment (MCI). Shaded areas represent 95% CIs. ApoE4 individuals are more likely to be positive for amyloid pathology than individuals with any other genotype. Also, note that ApoE4 is a strong driver of Aβ positivity irrespective of ApoE2 or ApoE3. Modified from (Jack et al., 2013), (Risacher and Saykin, 2013) and (Yamazaki et al., 2019).

Recently, Jack et al. (2016) proposed a fully biomarker-based diagnostic system for research: the AT(N) system. It is a binary system in which a patient, that is, e.g., A+T−N− has amyloid pathology (amyloid positive), normal tau levels (tau negative), and no abnormal neurodegeneration (Jack et al., 2018). However, the authors point out that this biomarker-based system should not be considered a template for all research; instead, it should be applied to fit the study's specific research goals.

Nevertheless, recent multifactorial data-driven analysis in AD have shown a different tentative temporal ordering of disease progression. The authors suggest that intra-brain vascular dysregulation is an early pathological event during disease progression (Iturria-Medina et al., 2017, 2016).

During the disease course, an incremental spread of pathophysiological hallmarks between brain regions is observed, suggesting the presence of a disconnection syndrome that disrupts brain networks (Brier et al., 2014; Delbeuck et al., 2007, 2003; Pievani et al., 2011; Selkoe, 2002). However, it remains unclear which factors induce such dysfunction from a local site by interplaying adaptive and maladaptive mechanisms (Carrera and Tononi, 2014; Fornito et al., 2015; Klupp et al., 2014).

This hypothesis implies the necessary application of a brain network-based approach in MCI research because local disruptions in such complex networks may have unpredictable and widespread effects (Gratton et al., 2012).

1.4 Network neurosciences and Graph Theory to study brain networks in MCI and AD

1.4.1 Networks of structural covariance

In the *Network neuroscience* context, a network is conformed by two essential ingredients: (a) a structure (or graph, topology) that can be associated with "hardware" and (b) a function (or process, related to "software"). This approach addresses a fundamental limitation to univariate and many standard multivariate techniques that do not always represent the complex relationships between neural systems, genes, and behaviors (Bassett and Sporns, 2017; Mišić et al., 2016). The *human connectome* is a comprehensible map of the brain's circuitry, consisting of brain areas, structural connections, and functional interactions (Hagmann, 2005; Sporns et al., 2005). The connectome can be explored with various neuroimaging techniques, but sMRI has a prevalent use due to its near-ubiquity, non-invasiveness, high resolution, and broad applicability in clinical settings (Craddock et al., 2013). Depending on the neuroimaging technique, at least three different brain network classes can be studied (Friston, 1994; Sporns, 2011): functional, structural (axonal), and networks of structural covariance.

The structural covariance networks represent the statistical interdependencies of morphological features between different brain regions, as is shown in figure 3 (Bassett et al., 2008; He et al., 2007; Lerch et al., 2006; Sanabria-Diaz et al., 2010). The coordinated variations of brain morphology descriptors between functionally- or anatomically-connected areas have been

found in many sMRI studies (Andrews et al., 1997; Bullmore et al., 1998; Lerch et al., 2006; Mechelli et al., 2005; Wright et al., 1999; Zielinski et al., 2010).

It has been demonstrated that brain regions that are highly correlated in size are often part of systems subserving particular behavioral or cognitive functions. The spatial proximity between brain regions is suggestive of the presence of white matter tracts (Honey et al., 2009; Kaiser and Hilgetag, 2006), a coupling of their intrinsic functional activity (A. F. Alexander-Bloch et al., 2013; Honey et al., 2009; Salvador et al., 2005) and implies higher-than-average structural covariance. These relationships are, in turn, influenced by direct white matter connections and functional coactivation and probably also by other genetic and environmental factors (for a review, see (A. Alexander-Bloch et al., 2013).

The studies that address the structural covariance brain networks use one out of three experimental approaches: seed analysis, principal component analysis, or graph theory framework. This thesis focuses on the last method.

1.4.2 Graph theory formalism to study the topological organization of brain networks.

Graph theory– a branch of mathematics concerned with modeling systems of interacting elements – provides a unifying and robust framework for characterizing the human connectome. In general, a complex network can be represented as a graph G=[N,K], the components of this system are called nodes (N), and the relations or connections between them are called edges (K) (Boccaletti et al., 2006). The nodes anatomical location in a given network is referred to as topography, and the architecture of their connections, referred to as a topology. In addition to the type of connectivity being examined, networks can also be differentiated into binary versus weighted. A specific threshold is applied to the connections in binary networks, resulting in either present or absent edges. In weighted networks, on the other hand, edges also contain information about connection strength. Directed versus undirected is another classification of networks. Connections (edges) of an undirected network do not include any direction contrary to directed graphs that contain some direction information. Once the nodes and edges have been defined, all information can be summarized in the connectivity or adjacent matrix. In such matrices, rows and columns represent nodes, while matrix entries denote links. A network's topological properties can be examined by a rich array of graph metrics based on the connectivity matrix. In this thesis, the structural covariance analysis corresponds to a binary and undirected network.

Graph metrics can be classified mainly into measures covering segregation, integration, and centrality properties in the network (for a review, see (Rubinov and Sporns, 2010)).

'Segregation' refers to the ability for specialized processing to occur within densely interconnected groups of brain regions. For example, the 'clustering coefficient' of a node is an essential measure of segregation, quantifying the number of connections that exist between the direct neighbors of a node as a proportion of the maximum number of possible connections (Watts and Strogatz, 1998). The average clustering coefficient across all network nodes is the clustering index of the network. Modularity is another measure of segregation, which describes densely interconnected nodes (Girvan and Newman, 2002; Guimerà and Amaral, 2005).

'Integration,' on the other hand, relates to the network's capacity to rapidly combine specialized information from distributed brain regions. Measures of integration are commonly based on the path lengths representing the number of steps between two nodes. Hence, shorter paths implying a stronger potential for integration. At the network level, it is translated to the 'characteristic path length' of the network, calculated as the average shortest path length between all pairs of nodes. A related measure is 'global efficiency' (Latora and Marchiori, 2001), defined as the average inverse shortest path length.

'Centrality' measures describe the importance of network nodes and edges to network functioning. The most straightforward index of centrality is the node 'degree,' the number of links connected to a given node. Another measure of importance is 'betweenness centrality,' defined as the fraction of all shortest paths in the network that pass through a given node (edge). Both measurements are critical in global information integration between different network parts, so-called 'hubs' (Sporns et al., 2007). *Network robustness* is then typically assessed by measuring the graph's ability not to fragment into subgraphs when elements of the graph are removed (Kaiser et al., 2007; Sporns et al., 2004). To calculate the networks' resilience, two types of attacks are commonly investigated (Bullmore and Sporns, 2009): random deletion of nodes/edges and targeted attack of nodes/edges based on their centrality.

Finally, to examine Small-world (σ), the values of characteristic path length and clustering index are compared with the same metrics estimated in random networks with the same number of nodes, average degree (average of the degree over all node, where the degree of a node corresponds to the number of connections to that node), and degree distribution (the probability that a randomly selected node has k connection) as the network of interest (Achard et al., 2006; Watts and Strogatz, 1998). A small-world network is characterized by a clustering coefficient greater than that of an equivalent random network, yet it has approximately the same characteristic path length as an equivalent random network (Humphries et al., 2006). Such

network topology is commonly thought to reflect an optimal balance between segregation and integration (Watts and Strogatz, 1998). There is mounting evidence that healthy structural and functional brain networks also show this kind of organization across various modalities (Stam, 2010).

1.4.3 Networks of structural covariance: Group and single-subject-based workflows

Group level approach: It has been used in most previous studies of structural covariance brain networks in MCI and AD (Melie-Garcia et al., 2013; Sanabria-Diaz et al., 2013, 2010; Sánchez-Catasús et al., 2017). Here the morphometric properties in multiple subjects have the same statistical role for structural covariance analysis as brain activations measured at multiple time points for functional connectivity analysis. This group-based approach does not allow correlation analyses to be performed with individual clinical despite providing useful information measures (Fig.4).

The workflow comprises two main steps:

Step 1. Computation of morphometric descriptor matrices: Briefly, the cortical reconstruction and volumetric segmentation are performed using dedicated software (i.e., Freesurfer). The parcellation of the cerebral cortex based on a reference atlas (i.e., Destrieux sulci-gyral-based atlas) allows the calculation of the regional mean value descriptor (i.e., cortical thickness) for each cortical structure. The outputs are used to construct a data matrix for each group. The number of rows corresponds to the number of subjects, while the number of columns corresponds to the number of structures (For details, see Study 1, Fig 1).

Step 2. Networks of structural covariance construction: Here, the connectivity matrices are computed. First, a connection is defined as the statistical associations between each pair of brain regions for an anatomical brain parcellation scheme defined in Step 1. The synchronized changes in the morphometric descriptor between two regions are computed using an association measure (i.e., Pearson's or Partial correlation) across subjects. Thus, the interregional correlation matrix (N×N, N is the number of brain regions) of such connections is obtained using all pairs of anatomical structures. Self-connections are excluded implying zeros in the diagonal of the symmetric matrix. Before the correlation analysis, linear regression is performed in every region to remove confounding effects such as age, gender, age-gender interaction, and cerebral mean morphometric values (For details, see Study 1, Fig 2). In order to calculate the AUC network measure values a range of thresholds are explored instead of using a single value. The threshold values (different to

each connectivity matrices) are calculated to obtain different matrix sparsity denote as 'sparsity degree'. A sparsity degree of 0.9 means that 90% of the connectivity matrix is off, and only the highest 10% of the connectivity values were taking into account. The sparsity degrees are computed for sparsity degrees ranging from 0.5 to 0.9, in step of 0.02. This procedure normalizes the networks to have the same number of nodes and edges, allowing the examination of the relative network properties and morphometric descriptor obtained for each group. The range of sparsity degree was chosen to allow for all network properties to be properly estimated and the number of spurious edges in each network minimized as indicated in previous studies (Achard and Bullmore, 2007; He et al., 2007; Sanabria-Diaz et al., 2013).

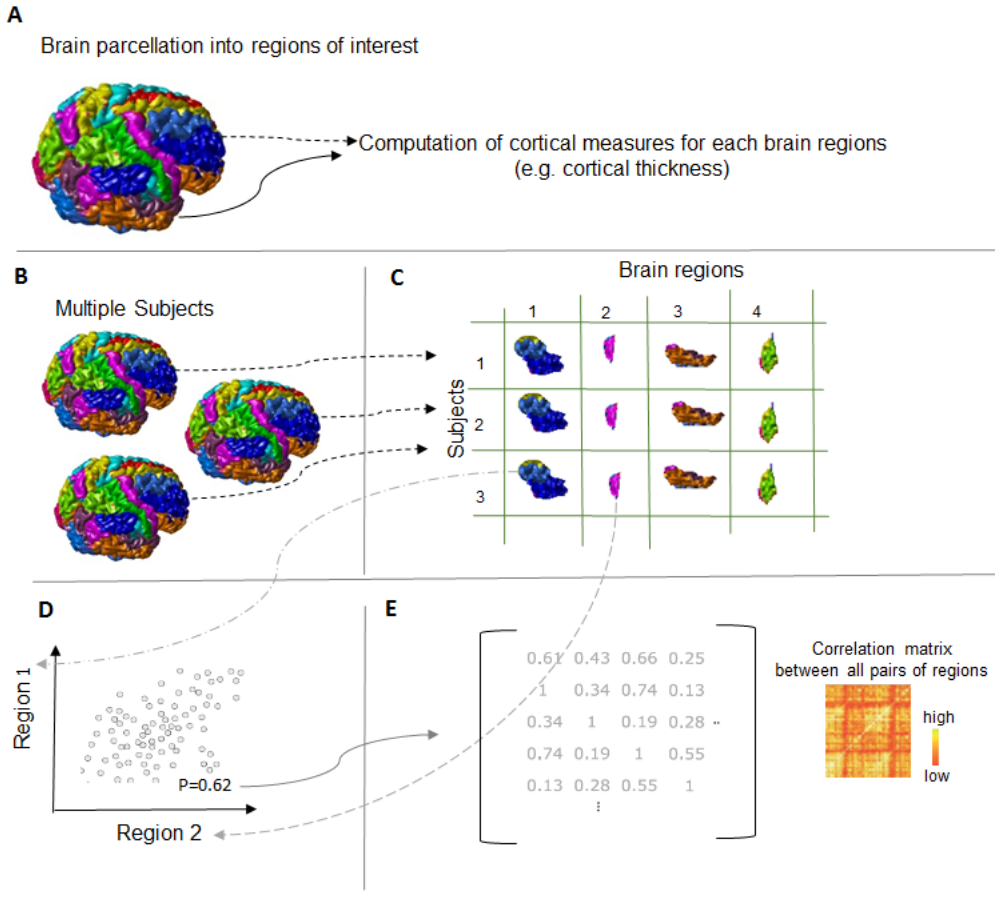

Fig 4 | Flowchart of structural covariance analysis. (A) Choice of brain atlas and computation of cortical measures. (B) Multiple subjects in one data set. (C) Data matrix construction with brain region of all subjects. Typically at this point, a confounding effects correction is performed. (D) Computation of the correlation between all pairs of brain regions. (E) Gathering all correlations in a matrix termed 'structural covariance connectivity matrix'.

Study 1 applies this approach using cortical thickness as a morphometric descriptor. Cortical thickness has been proposed as a more stable parameter for AD diagnosis than volume/density measures (Regeur, 2000; Singh et al., 2006). Cortical thickness analysis has been successfully

used in various studies as markers to separate AD patients from healthy controls and MCI subjects (Chételat et al., 2005; Desikan et al., 2009; Hutton et al., 2008; Singh et al., 2006). Besides, attempts to distinguish progressive-MCI from stable-MCI by analyzing the baseline cortical thickness have also been reported (Querbes et al., 2009).

Single-subject-based approach: Figure 5 illustrates the flowchart of the automated method used to construct the single-subject gray matter networks, which has been described previously (Batalle et al., 2013; Dicks et al., 2018, 2020; Rimkus et al., 2019; Tijms et al., 2013a, 2014, 2018). It is overcome the group level approach's main limitation by providing a method that can create individual structural covariance networks.

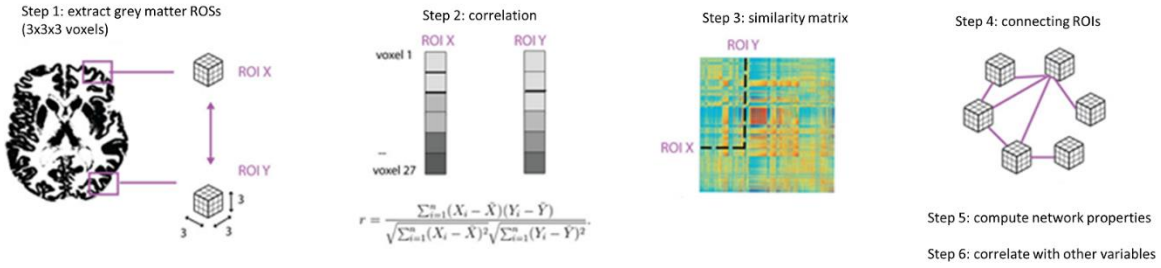

Fig 5 | Schematic overview of the pipeline to extract single-subject gray matter networks. The resulting gray matter segmentation is divided into voxel cubes (1). The similarity between all cubes is computed with the correlation coefficient (2), and the maximum similarity value over multiple rotations is stored in a similarity matrix (3). This matrix is then thresholded to include similarity values that crossed the significance threshold of 0.05, corrected for multiple comparisons. For each binarized graph, random graphs are generated that kept intact the size and degree distribution (4). For all graphs, the network attributes are computed (5). Finally, are determined across subjects the correlation between the network properties and other measures (6). Figure modified from (Tijms et al., 2014).

The workflow is composed of two main steps:

Step 1. Image acquisition and preprocessing: Anatomical images are segmented into gray matter, white matter, and cerebrospinal fluid. In the native space gray matter segmentation of each subject, anatomical areas are identified based on an automated anatomical labeling atlas (i.e., AAL; (Tzourio-Mazoyer et al., 2002)).

Step 2. Single-subject gray matter network computation: the network's nodes are defined as small regions of interest of N x N x N voxel cubes (e.g., 3 x 3 x 3) in the native space gray matter segmentations. The correlation coefficient expresses the similarity between nodes in the network. Given that the cortex is a curved object, two similar cubes could be located at an angle from each other, decreasing their similarity value. Therefore, the maximum correlation value is computed over different rotations of the seed cube. Regions with zero variance in gray matter values are excluded since the correlation coefficient is

undefined. Next, the similarity matrices are binarised to construct unweighted and undirected graphs after determining each graph's threshold correcting for multiple comparisons. Finally, network attributes are assessed (Rubinov and Sporns, 2010).

Study 2 applies this approach using gray matter volume similarity extracted from sMRI (Tijms et al., 2012). Intracortical similarity has been associated with coordinated growth patterns, functional coactivation, and axonal connectivity (A. Alexander-Bloch et al., 2013; Gong et al., 2012). Previous studies have shown that gray matter networks are disrupted in AD (Pereira et al., 2016; Tijms et al., 2013a; Yao et al., 2010), associated with cognitive impairment (Tijms et al., 2013a, 2014) and related to faster disease progression and cognitive decline in the predementia stage of AD (Dicks et al., 2018; Tijms et al., 2018; Verfaillie et al., 2018). Furthermore, disrupted gray matter network organization has been associated with aggregating amyloid in cognitively normal individuals (ten Kate et al., 2018; Tijms et al., 2016) and before overt atrophy is evident (Voevodskaya et al., 2018).

1.5 ApoE4 impact on the brain networks in MCI and AD

1.5.1 Previous studies of the networks of structural covariance in MCI and AD using graph theory

Table 1 shows preceding studies demonstrating that MCI and AD patients have aberrant structural covariance network topology showing greater segregation and disrupted integration. (Tijms et al., 2013b; Xie and He, 2012). In AD compared to controls, the results indicated a higher characteristic path length, a reduced global efficiency as well as higher local clustering index (He et al., 2008; Lo et al., 2010). Additionally, patients showed a loss of balance between segregation and integration reflected in the small-world attribute and a redistribution of hub regions (Y He et al., 2009; Sanabria-Diaz et al., 2013; Sanz-Arigita et al., 2010; Stam et al., 2009; Supekar et al., 2008; Yao et al., 2010). In particular, MCI's network showed intermediate topological attributes supporting the view of MCI as a transitional stage between normal aging and AD (Dai and He, 2014; Tijms et al., 2013b; Xie and He, 2012).

It could be hypothesized that these network alterations are related to pathological disease features (amyloid-beta (Aβ) plaques and neurofibrillary tangles) in one region of the brain.

It may capture the earliest neurodegenerative changes in MCI, predicting future atrophy in more distant brain areas. In this way, regions that covaried in their cortical thickness e.g., will lose their similarity when one region starts to atrophy, or may show consistent similarity when

both regions atrophy uniformly. Increasing evidence indicates that network topology changes during AD progression (Pereira et al., 2016; Yao et al., 2010) already start at early, preclinical stages (Tijms et al., 2016).

Therefore, brain network measures might have promise as prognostic biomarkers for future cognitive decline in MCI. However, it needs to be noted that no previous studies were exploring the ApoE4-related effects on the structural covariance brain networks in MCI using sMRI. Such analysis could provide important clues into which network topology changes mark the transition to AD and improve our understanding of how the ApoE4 and the disease progression affect the brain networks.

Table 1. Previous studies using sMRI and graph theory approach to explore the Networks of structural covariance in MCI and AD.

Study	N	Network Properties	Main Findings
He et al., 2008	97 NC 92 AD	Cp, Lp, SW, BC, TA, hubs	Cp (AD>NC); Lp (AD>NC) BW (AD<NC); TA (AD>NC) *MCI intermediate topology*
Yao et al., 2010	98 NC 113 MCI 91 AD	Cp, Lp, SW, BC, hubs	Cp (AD>NC), Lp (AD>NC) BW (AD, MCI<NC) *MCI intermediate topology*
Tijms et al., 2013	38 NC 38 AD	Dg, Cp, Lp, SW, BC (regional and global), hubs	Cp (AD<NC); Lp (AD<NC) SW(AD<NC); BC (AD<NC) *MMSE scores associated with Lp in AD*
Li et al., 2012	40 NC 36 sMCI 39 pMCI 37 AD	Cp	Cp (< pMCI in time) Cp< olfactory cortex region in AD *Indicates degenerated wiring efficiency of the brain network due to AD*
Dicks et al., 2018	258 MCI (100 sMCI; 115 pMCI)	Cd, Dg, Cp, Lp, SW, BC, hubs.	SW (pMCI<sMCI) Lower SW associated with cognitve decline. Lower BC correlated with a faster decline in MMSE. *Disrupted network properties were related to worse cognitive impairment.*
Pereira et al., 2016	301 NC 425 MCI (87 eMCI; 71 lMCI; 110 sMCI) 282 AD	Cp, Lp, SW, M, Ts, Cp-n, BC, w-MDg, Pc	Cp (lMCIc, eMCIc, and AD<NC) Ts (patients<NC), M (patients>NC) BC (sMCI, lMCIc, eMCI, AD <NC) M (4 NC, 3 sMCI, lMCIc, and eMCIc ; 5 modules AD) *Prodromal and clinical stages of AD are associated with an abnormal network topology*
Dicks et al., 2020	71 NC 110 pAD	Ns, Cd, Cp, Lp, nCp, nLp, SW	SW (AD<NC) Ns and Cd (AD>NC): associated with progression low Cp and high Lp: associated with early amyloid accumulating. *Gray matter network measures may have use for identifying those individuals with preclinical AD who will show disease progression before overt atrophy*

Legend:sMCI: stable MCI; pMCI: progressive MCI; lMCI: late MCI; eMCI: early MCI; nLp: nodal characteristic ptah length; Cp: clustering index; Lp: characteristic path length; SW: small world; BC: betweenness centrality; TA: target attack; Ns: network size; Cd: connectivity density; Dg: degree; M: modularity; Ts: transitivity; nCP: clustering index nodal; w-MDg: within module degree; Pc: participation coefficient; MMSE: Mini-Mental State Examination.

1.5.2 Previous studies of ApoE4 effects on the brain networks in AD using graph theory.

Despite the interest in assessing the network of structural covariance in MCI, the inclusion of the ApoE4 in previous studies has been scarce to date, limited to healthy aging subjects and AD patients (Brown et al., 2011; Goryawala et al., 2015; Seo et al., 2013; Wang et al., 2015; Yao et al., 2015; Zhao et al., 2012). I summarized the few previous studies' main results in Table 2. It is essential to highlight that there is one used sMRI in a healthy aging sample (Goryawala et al., 2015), while Yao et al. (Yao et al., 2015) included, for the first time, MCI patients to explore the metabolic networks in Carriers and non-Carriers. However, they mixed the healthy, MCI, and AD subjects, challenging interpreting the ApoE4 effects on MCI.

Table 2. Previous studies on the ApoE4-related effects on the brain networks in NC, MCI, and AD using graph theory

Study	Modality	N	Network Properties	Main Findings
Brown et al., 2011	DTI	30 NC non-Carriers 25 NC Carriers	Lc, Gi, SW	mean Lc (Carriers<non-Carriers) SW (Carriers<non-Carriers) loss in MCT (Carriers>non-Carriers) Carriers: negative correlations of age and performance on two episodic memory tasks
Seo et al., 2013	rsFDG-PET	58 NC non-Carriers 28 NC Carriers	Cp, Lp, SW, BC	Cp (Carriers<non-Carriers) Lp (Carriers<non-Carriers) Hubs (Carriers<non-Carriers) BC-Hippocampus (Carriers<non-Carriers) BC- Precuneus (Carriers> non-Carriers) Regional cerebral glucose metabolism (Carriers< non-Carriers)
Goryawala et al., 2015	sMRI	106 NC non-Carriers 41 NC Carriers	Cp, Lp, BC interregional correlations differences	interregional correlation coefficients (Carriers> non-Carriers) (precentral, superior frontal and inferior temporal regions) Cp (Carriers>non-Carriers) Lp (Carriers>non-Carriers) BC (non-Carriers> Carriers) (several regions middle temporal, para-hippocampal gyrus, posterior cingulate and insula)
Yao et al., 2015	rsFDG-PET	NC, MCI, AD mixed in 165 Carriers 165 non-Carriers	Cp, Lp, SW, BC interregional correlations differences	Cp (Carriers<non-Carriers) BC (Carriers<non-Carriers) (left insula, right insula, right anterior cingulate, right paracingulate gyri, left cuneus) Local short distance interregional Correlations (Carriers>non-Carriers) Carriers: disrupted long distance interregional correlations
Wang et al., 2015	rsfMRI	26 AD non-Carriers 16 AD Carriers	Eglob, Eloc, M, Rich-club coefficient, Ns, hubs	Connections number (Carriers<non-Carriers) connectivity weights (Carriers<non-Carriers) Eloc, Eglob, M (Carriers<non-Carriers) DMN connectivity (Carriers<non-Carriers) Carriers impairments on rich-club structures

Zhu et al., 2018	rsfMRI	28 aMCI Carriers 38 aMCI non-Carriers	FCs	ε4-related FCs increases in the right HIP/PHG Carriers: lower or higher FCs between the right HIP/PHG and MPFC or the occipital cortex Carriers: FCs values in the right HIP/PHG and lower HIP/PHG-RSFCs with the bilateral MPFC correlated with the impairment of episodic memory Executive function in the HIP/PHG-FCs with MPFC predicted aMCI-conversion to AD
Li Y et al., 2019	PHF-Tau-PET	MCI and NC 1-non-Carriers- T- (MCI:NC, 54:49) 2-Carriers T- (MCI:NC, 16:18) 3-Carriers T+ (MCI:NC, 18:26) 4-non-Carriers T+ (MCI:NC, 21:23).	Cp, Lp, M, BC	Non-Carriers T− showed significant differences in Cp, Lp, M compared with the other 3 groups. Carriers T+ < Cp Carriers T− < Cp, Lp and Q Non-Carriers T+ < Cp, Lp, M BC showed significant differences in some regions for the Carriers T+ compared with the non-Carriers T− Compared with ApoE4−T− group, the other three groups showed significant regional differences in nodal properties

Legend: MCI: Mild Cognitive Impairment; AD: Alzheimer Disease; NC: healthy controls; aMCI: amnesic Mild Cognitive Impairment; Cp: clustering index; Lp: characteristic path length; SW: small world; BC: betweenness centrality; M: modularity; Ns: nodal strength; Lc: Local interconnectivity; Gi: Global integration; Eglob: global efficiency; Eloc: local efficiency; MTC: mean cortical thickness; FCs: functional connectivity strength; HIP: hippocampus; PHG: parahippocampal gyrus; T+ CSF T-Tau pathology positive; T-: CSF T-Tau pathology negative; DTI: diffusion imaging; rsFDG-PET: resting-state fluorodeoxyglucose Positron emission tomography; rsfMRI: resting-state functional magnetic imaging; PHF-Tau-PET: PHF-Tau Positron Emission Tomography

These findings suggest that the ApoE4 allele modulate the large-scale brain network in AD, indicating disease-related disconnection mechanisms (Delbeuck et al., 2003; Filippi and Agosta, 2011; Yong He et al., 2009). Moreover, they provided new insights into the understanding of AD's biological mechanism that could lead to using a network-based imaging biomarker for disease diagnosis and monitoring.

1.6 Thesis Aims

Based on the evidence above, to my best knowledge, there are no previous studies focused on how ApoE4 affects the topological organization of the covariance brain networks in MCI. Significantly, has still not been explored the interaction effect between ApoE4 and AD progression on these networks. Therefore, the aims of this thesis are the following:

1. To investigate the effect of ApoE4 on the structural covariance brain networks in MCI patients (ApoE4 Carriers versus non-Carriers).

This aim is addressed in *Study 1*. I investigated the ApoE4-related modulation of the topological organization of cortical thickness covariance brain networks in MCI through sMRI using a graph-theory approach. The identification of these subtle alterations at the network level may help detect, at earlier stages, the risk of AD progression associated with the ApoE4.

I examined different features of the structural brain topology:1) regional cortical thickness, 2) global network attributes (clustering index, characteristic path length, local and global efficiency, global connectivity, and homologous region connectivity) 3) nodal properties (normalized betweenness centrality, hubs) 4) network community detection (modularity) and resilience to insults (target attack).

2. To investigate the ApoE4-related changes on the single-subject structural covariance brain network associated with AD progression (stable MCI versus Converters into AD).
3. To examine how the network properties alter with AD biomarkers of $A\beta_{42}$, tau, neurodegeneration, and memory deficits in MCI associated with the ApoE4.

These two aims were tackled in *Study 2*. I analyzed how ApoE4 affects the single-subject gray matter network's in MCI. Moreover, I evaluated the ApoE4 and disease progression interaction effects on these networks' topological properties. Such longitudinal follow-ups are required to reveal changes associated with the genetic risk allele per se and to be able to identify possible network properties alterations related to subsequent progression into AD. Additionally, the ApoE4 modulation on the association between the network topology and other neuropathological AD biomarkers (i.e., CSF $A\beta_{42}$ and total tau levels) were explored.

4. To investigate whether the topological network measures can detect vasodilatory-induced changes in the cerebral blood flow network in MCI.

In this additional research, I investigated whether a network-based approach combined with the graph theory is able to detect cerebrovascular reactivity (CVR) changes in MCI. The findings suggest that this experimental approach is more sensitive to identifying subtle cerebrovascular alterations than the classical experimental designs. Notably, this study paves the way for my next investigation on the ApoE4- cerebrovascular interaction effects on the brain networks during AD progression.

1.7 Thesis Outline

In the previous sections of this *Chapter*, I provide a background of MCI and AD, and brain networks. The first subsection reviews the literature about MCI and AD regarding diagnostic, pathophysiology, and biomarkers. The second subsection is dedicated to describing the ApoE4 as a major genetic risk for AD. The main concepts of the brain network framework and the technical aspects of graph theory to studying the networks of structural covariance in MCI and

AD are presented in the last subsection. Also, a review of previous studies focus on the impact of ApoE4 on the structural covariance brain networks topology in MCI and AD is introduced.

The *Studies 1* and *2*, as well as additional research, are presented in *Chapter 2*. *Study 1* (section 2.1, Annex 6.1) explores the impact of ApoE4 on the brain networks of structural covariance in a cross-sectional MCI sample divided into ApoE4-positive ('Carriers') and ApoE4-negative ('non-Carriers') selected from the Alzheimer Disease Neuroimaging Initiative (ADNI) database. I estimated the cortical thickness from sMRI to calculate the correlation among anatomical regions across subjects and build the cortical thickness covariance networks. At the group level, the topological network properties were described through the graph theory approach.

In *Study 2* (section 2.2, Annex 6.2) I investigated the influence of ApoE4 and the risk of AD progression on the brain network topology in MCI. This study used a single-subject-based approach to construct gray matter networks to investigate whether network properties at baseline predict disease progression. I also explored the association between the network topological properties, AD biomarkers ($A\beta_{42}$, tau), and cognitive measurements.

At the end of this Chapter is enclosed a brief presentation of an additional research study (section 2.3, Annex 6.3) developed during this thesis. This project proposed a new approach to investigate Cerebrovascular reactivity in MCI based on graph theoretical analysis of brain perfusion SPECT data.

The thesis finalizes with a general discussion of my findings, the principal limitations, contributions, and open questions for future work in *Chapter 3.*

2 SUMMARY OF THE RESULTS

2.1 Apolipoprotein E4 effects on Topological Brain Network Organization in Mild Cognitive Impairment

2.1.1 Context

This section is based on the article 'Apolipoprotein E4 effects on Topological Brain Network Organization in Mild Cognitive Impairment', **Gretel Sanabria-Diaz**, Lester Melie-Garcia, Bogdan Draganski, Jean-Francois Demonet, Ferath Kherif. (2021). Scientific Reports, volume 11, 845. https://doi.org/10.1038/s41598-020-80909-7 (Annex 6.1).

2.1.2 Summary of findings

My findings revealed a decrease in global and homologous connectivity strength, clustering index, characteristic path length, local efficiency, modularity, and increased global efficiency in MCI Carriers compared to non-Carriers. MCI Carriers showed lower Normalized Betweenness Centrality (NBC) values in several brain regions. Together they indicate a topological organization more like a random network in this group of patients, a structure previously reported in MCI and AD subjects (Pereira et al., 2016; Tijms et al., 2013a, 2018).

I found a decrease in global connectivity strength- an aggregate measure of the correlation values between all possible pairwise anatomical structures- in MCI Carriers relative to non-Carriers. Previous studies did not report on this network property (Ma et al., 2017; Wang et al., 2017; Yao et al., 2015).

The nodal properties results allowed me to generate hypotheses about the ApoE4 impact on brain network integration and segregation in MCI. My findings showed agreements with previous studies in AD neurodegeneration. The fact that crucial structures like Posterior Cingulate Cortex (PCC) and the Precuneus showed lower NBC values in the Carriers group suggests that regional topological properties may capture disease-related effects that can be further explored in association with the risk of AD progression. Notably, for all detected hubs, regions considered critical for the brain's information flux, lower NBC values were found in Carriers than non-Carriers. Some of these structures belong to the Default Mode Network (DMN) involved in self-referential functions such as episodic memory (Buckner et al., 2008) affected by AD. ApoE4, considered a disrupted metabolic factor (Liu et al., 2013), may contribute to alteration on the DMN activity in MCI, accelerating AD-related pathological mechanisms.

Additionally, I observed a decreased modularity in Carriers as compared with non-Carriers. A less modular network implies fewer connections within modules and more connections to other modules. The increase of interconnectedness between modules can lead to disease pathological markers' rapid spreading and loss of specialization (Salathé and Jones, 2010). Summarizing, these findings concur with the evidence that ApoE4 is associated with an aberrant brain network topology in MCI. On the other hand, the changes were not detectable with the standard univariate approach based on the brain regional cortical thickness.

Reference: *Apolipoprotein E4 effects on Topological Brain Network Organization in Mild Cognitive Impairment*. Author: **Gretel Sanabria-Diaz**, Lester Melie-Garcia, Bogdan Draganski, Jean-Francois Demonet, Ferath Kherif. (2021). Scientific Reports, volume 11, 845. https://doi.org/10.1038/s41598-020-80909-7.

Contribution: elaborated study design, analyzed data, wrote the paper.

Abstract: The Apolipoprotein E isoform E4 (ApoE4) is consistently associated with an elevated risk of developing late-onset Alzheimer's Disease (AD); however, less is known about the potential genetic modulation of the brain networks organization during prodromal stages like Mild Cognitive Impairment (MCI). To investigate this issue during this critical stage, we used a dataset with a cross-sectional sample of 253 MCI patients divided into ApoE4-positive (‘Carriers') and ApoE4-negative ('non-Carriers'). We estimated the cortical thickness (CT) from high-resolution T1-weighted structural magnetic images to calculate the correlation among anatomical regions across subjects and build the CT covariance networks (CT-Nets). The topological properties of CT-Nets were described through the graph theory approach. Specifically, our results showed a significant decrease in characteristic path length, clustering index, local efficiency, global connectivity, modularity, and increased global efficiency for Carriers compared to non-Carriers. Overall, we found that ApoE4 in MCI shaped the topological organization of CT-Nets. Our results suggest that in the MCI stage, the ApoE4 disrupting the CT correlation between regions may be due to adaptive mechanisms to sustain the information transmission across distant brain regions to maintain the cognitive and behavioral abilities before the occurrence of the most severe symptoms.

2.2 Apolipoprotein E allele 4 effects on Single-Subject Gray Matter Networks in Mild Cognitive Impairment

2.2.1 Context

This section is based on the article 'Apolipoprotein E allele 4 effects on Single-Subject Gray Matter Networks in Mild Cognitive Impairment', **Gretel Sanabria-Diaz**, Jean-Francois Demonet, Borja Rodriguez-Herreros, Bogdan Draganski, Ferath Kherif, Lester Melie-Garcia, for the Alzheimer's Disease Neuroimaging Initiative. (2021). NeuroImage: Clinical (under review) (Annex 6.2).

2.2.2 Summary of findings

This study demonstrated the ApoE4 role in disrupting specific parameters of the gray matter network topology. ApoE4 simultaneously affects morphometric, cognitive variables, and CSF variables. Significantly, the rate of change in time of these variables is also affected by the allele. In particular, in Carriers, there is a decreased CSF $A\beta_{42}$ levels, entorhinal cortex atrophy, and increased T-tau and P-tau levels. On the other hand, I uncover specific disruption in topological network properties, morphometric, cognitive, and CSF-derived markers in those MCI patients that will progress to AD. Disease progression conducts more pervasive brain alterations than ApoE4. The clustering index at the regional level showed widespread changes across the brain cortex, driven mostly for the disease, including critical nodes of the DMN related to AD pathology.

I found that the ApoE4 mainly modulated two network properties, clustering index normalized, and sigma. In both cases, MCI Carriers showed higher values than non-Carriers independently of the future disease progression status. These increments (i.e., higher similarity between neighboring nodes) associated with the E4 allele may reflect synchronous atrophy between brain areas, where Carriers will show a more uniform neurodegeneration pattern across the whole gray matter volume.

In particular, the MCI non-Carriers who will progress into AD showed in advance lower clustering index normalized values than those who will remain stable. However, only for MCI Converters, I detected differences associated with the ApoE4. The MCI Carriers Converters showed increased values over those non-Carriers. The rate of change analysis revealed the same patterns as a confirmation of this result's robustness. The findings suggest that the clustering index normalized seems to be a critical network measure to predict disease

progression in MCI. In general, a lower cluster index suggests a topological organization more like a random network.

My study revealed regional normalized clustering index differences between groups driven by the disease progression. These regional differences were widely distributed across the brain with a common denominator: lower values for those MCI converted to AD. It suggests that in MCI, the risk of disease progression is characterized by worse local communication between 'topological neighboring' areas (graph theory concept). These regional changes may be related to AD neuropathological processes that are already operating in this phase, affecting the intracortical gray matter properties similarity.

Interestingly, the CSF $A\beta_{42}$ level was positively associated with the characteristic path length in the Carriers group, while I did not find correlations with P-tau and T-tau. This result agrees with previous studies showing that the E4 allele regulates Aβ aggregation and deposition (for review, see (Liu et al., 2013). Moreover, the positive association between these two measures was confirmed only for the ApoE4 and not for the disease progression factor. These finding suggests that the characteristic path length informs the detrimental E4 allele effects on the amyloid-related pathways in network terms.

Based on these findings, I considered the single subject gray matter network a valid approach that sheds light on the interaction gene-structural covariance. My study provides further information in the current understanding of how ApoE4 -thus far the most important genetic factor known in late-onset AD- influences the brain network topology in MCI subjects.

Reference: *Apolipoprotein E allele 4 effects on Single-Subject Gray Matter Networks in Mild Cognitive Impairment*. Author: **Gretel Sanabria-Diaz**, Jean-Francois Demonet, Borja Rodriguez-Herreros, Bogdan Draganski, Ferath Kherif, Lester Melie-Garcia, for the Alzheimer's Disease Neuroimaging Initiative. (2021). NeuroImage: Clinical (under review)

Contribution: elaborated study design, analyzed data, wrote the paper.

Abstract: There is evidence that gray matter networks are disrupted in Mild Cognitive Impairment (MCI) and associated with cognitive impairment and faster disease progression. However, it remains unknown how these alterations are related to the Apolipoprotein E isoform E4 (ApoE4) presence, the most prominent genetic risk factor for late-onset AD. To investigate this topic, we explore the impact of ApoE4 and the disease progression on the Single-Subject Gray Matter Networks (SSGMNets) using the graph theory approach. Our data sample comprised 200 MCI patients selected from the ADNI database classified in non-Converters and Converters (progressed into AD). Each group included 50 ApoE4-positive (‘Carriers',

ApoE4+) and 50 ApoE4-negative ('non-Carriers', ApoE4-). The SSGMNets were estimated from structural MRI at two-time points: baseline and conversion. We investigated whether altered network topological measures at baseline and their rate of change (RoC) between the two-time points were associated with ApoE4 and disease progression. We also explored the SSGMNets attributes correlation with general cognition score (MMSE), memory (ADNI-MEM), and CSF-derived biomarkers of AD (Aβ42, T-tau, and P-tau). Our results showed that ApoE4 and the disease progression modulated the global network properties independently but not in the RoC. MCI Converters showed a lower clustering index in several regions associated with neurodegeneration in AD. The global network properties were revealed to predict cognitive and memory measures. These findings suggest that SSGMNets might have used in identifying MCI ApoE4 Carriers with a high risk for AD progression.

2.3 Additional Research contributions: Cerebrovascular reactivity effects on the brain network detected by graph theoretical analysis in MCI

2.3.1 Context

This section is based on the article 'Subtle alterations in cerebrovascular reactivity in mild cognitive impairment detected by graph theoretical analysis and not by the standard approach', Sánchez-Catasús, Carlos A, **Sanabria-Diaz, Gretel**, Willemsen, Antoon, Martinez-Montes, Eduardo, Samper-Noa, Juan, Aguila-Ruiz, Angel, Boellaard, Ronald, De Deyn, Peter, Dierckx, Rudi A J O, Melie-Garcia, Lester. (2017). NeuroImage: Clinical, Volume 15, 2017, Pages 151-160. Elsevier BV. ISSN 2213-1582. https://doi.org/10.1016/j.nicl.2017.04.019 (Annex 6.3).

Previous neuroimaging results using the graph theory approach have shown its potential to reveal subtle pathological processes in MCI ((Dai and He, 2014; Tijms et al., 2013b). In principle, this methodology can also be applied to brain perfusion SPECT data to investigate possible subtle network-related Cerebrovascular reactivity (CVR) abnormalities in MCI. Since the regional Cerebral Blood Flux (CBF) is, in most circumstances, tightly coupled to neuronal metabolism, it is assumed that the radiotracer distribution reflects levels of neuronal activity in different brain areas (Devous, 2013; Warwick, 2004). We previously demonstrated this approach's feasibility using brain perfusion SPECT data of healthy control subjects (Melie-Garcia et al., 2013).

2.3.2 Summary of findings

The finding revealed different clustering index and mean strength of association changes in subjects with normal cognition and MCI, while the standard approach did not detect substantial differences. Thus, the results support the concept that multivariate measures (i.e.co-variations) combined with a graph theoretical approach are more sensitive to identifying complex pathological processes, as found in other brain diseases (Bassett et al., 2012; He et al., 2009b). The MCI group showed a decrease in both network measures, suggesting that the cardiovascular reactivity is possibly altered to some extent in MCI stage not detected by the standard analysis. On the other hand, although speculative, the mean strength of association globally increase in the MCI group network in the basal condition might represent an adaptive mechanism in response to pathological processes.

Interestingly, regional clustering index changes overlap to a certain extent with the DMN, which is very active at resting state (for a review (Hafkemeijer et al., 2012)). These nodal alterations could be related to an altered DMN's vascularity based on the two resting states comparisons: without and under the effect of Acetazolamide (ACZ), a vasodilatory challenge. It is known that DMN also overlaps to a certain degree the brain network underlying the episodic memory (Rugg and Vilberg, 2013) that is affected in MCI due to AD (Albert et al., 2011).

Reference: Subtle alterations in cerebrovascular reactivity in mild cognitive impairment detected by theoretical graph analysis and not by the standard approach. Author: Sánchez-Catasús, Carlos A, Sanabria-Diaz, Gretel, Willemsen, Antoon, Martinez-Montes, Eduardo, Samper-Noa, Juan, Aguila-Ruiz, Angel, Boellaard, Ronald, De Deyn, Peter, Dierckx, Rudi A J O, Melie-Garcia, Lester. NeuroImage: Clinical, Volume 15, 2017, Pages 151-160. Elsevier BV. ISSN 2213-1582. https://doi.org/10.1016/j.nicl.2017.04.019

Contribution: contributed to the study design, analyzed the data, provided feedback on data analysis and manuscript preparation/writing, contributed to writing the manuscript.

Abstract: There is growing support that cerebrovascular reactivity (CVR) in response to a vasodilatory challenge, also defined as the cerebrovascular reserve, is reduced in Alzheimer's disease dementia. However, this is less clear in patients with mild cognitive impairment (MCI). The current standard analysis may not reflect subtle abnormalities in CVR. In this study, we aimed to investigate vasodilatory-induced changes in the topology of the cerebral blood flow correlation (CBFcorr) network to study possible network-related CVR abnormalities in MCI.

For this purpose, four CBFcorr networks were constructed: two using CBF SPECT data at baseline and under the vasodilatory challenge of acetazolamide (ACZ), obtained from a group of 26 MCI patients; and two equivalent networks from a group of 26 matched cognitively normal controls. The mean strength of association (SA) and clustering coefficient (C) were used to evaluate ACZ-induced changes on the topology of CBFcorr networks. We found that cognitively normal adults and MCI patients show different patterns of C and SA changes. The observed differences included the medial prefrontal cortices and inferior parietal lobe, which represent areas involved in MCI's cognitive dysfunction. In contrast, no substantial differences were detected by standard CVR analysis. These results suggest that graph theoretical analysis of ACZ-induced changes in the topology of the CBFcorr networks allows the identification of subtle network-related CVR alterations in MCI, which couldn't be detected by the standard approach.

3 DISCUSSION

In this thesis, I assessed for the first time the ApoE4-related effects on the structural covariance brain networks topology in MCI. The findings provide novel experimental evidence regarding the genetic risk impact on the large-scale brain network organization associated with the risk of disease progression and AD biomarkers, which are worth investigating to define intermediate phenotypes in MCI. Additionally, I tested the graph approach potential application to detect cerebrovascular reactivity (CVR) at the network level in MCI patients. This is a previous methodological step for a further study that focuses on the ApoE4- Cerebrovascular interaction effects on the structural and functional covariance brain networks during AD progression.

Few previous studies have found evidence of the E4 allele modulation on the MCI brain networks using graph theory on measures derived from other image modalities (rs-fMRI, FDG-PET, and DWI). However, I consider my approach pertinent based on the following points:

- The network analysis is based on sMRI, which is a powerful imaging technique to study AD. sMRI derived measures have been the most used as a relatively cheap, non-invasive yet powerful biomarker of neuronal loss highly available in current clinical practice and research environments.
- I considered cortical thickness as an appropriate morphometric descriptor that offers unique information about AD. Using graph theory formalism, my previous results demonstrated that the underlying process of complex relations between other brain regions is captured differently by morphometric descriptors like surface area and cortical thickness (Sanabria-Diaz et al., 2010). In particular, cortical thickness has been proposed as a more stable AD diagnosis measure than volume/surface area. The cortical thickness is a direct measure of gray matter atrophy due to the cytoarchitecture feature of the cerebral cortex (Lerch and Evans, 2005; Regeur, 2000; Singh et al., 2006).
- The gray matter volume measure extracted from sMRI has been associated with coordinated growth patterns, functional coactivation, and axonal connectivity (A. Alexander-Bloch et al., 2013; Gong et al., 2012). Previous studies have shown that individual gray matter networks are associated with cognitive impairment (Tijms et al., 2013b, 2014) and related to faster disease progression (Dicks et al., 2018; Verfaillie et al., 2018).
- The patterns of morphological covariance between brain regions can capture early AD-related changes in brain networks. Several studies have found that neurodegenerative

diseases target areas that, in healthy individuals, are particularly highly structurally correlated (Seeley et al., 2009). The regional brain atrophy is linked to the deposition of the AD-related protein amyloid-β. Similar patterns of gray matter loss in brain regions with high structural correlations distinguished cognitively normal young adults genetically at risk of developing AD (Alexander et al., 2012). The atrophy within structural covariance networks highlights their functional significance in AD research and supports a network approach.

- The patterns of morphometric covariations between brain regions are associated with anatomical and functional connectivity. The structural covariance is based on the observation that coordinate variations of brain morphometry occur between functionally- or anatomically-connected areas (Andrews et al., 1997; Lerch et al., 2006; Mechelli et al., 2005). These brain areas correlated in size are often part of systems known to subserve particular behavioral or cognitive functions. As such, the morphometric covariance patterns represent a unique phenomenon. The spatial proximity between brain regions is suggestive of white matter tracts between these regions (Honey et al., 2009; Kaiser et al., 2009; Makris et al., 2006). However, the only whole-brain study comparing white matter connections with cortical thickness covariance between regions on a pair-by-pair basis suggests a substantial but incomplete overlap (30–40%) (Gong et al., 2012). Also, structural covariance between brain regions is indicative of the coupling of their intrinsic activity (A. Alexander-Bloch et al., 2013; Honey et al., 2009; Salvador et al., 2005). Correlations between brain regions in intrinsic brain activity (using rs-fMRI) show striking overlap (but not entirely) with population-based measurements of gray matter covariance between those regions (Kelly et al., 2012; Seeley et al., 2009; Segall et al., 2012). Then, structural covariance connectivity represents processes that are not reduced to anatomical and functional connectivity, making these studies more valuable (for a review, see (A. Alexander-Bloch et al., 2013)).

In the following sections, I summarized the main findings, discuss the results concerning the literature, potential methodological considerations, and possible avenues for future research.

3.1 ApoE4 modifies the structural covariance brain networks topology in MCI

In this first study, I assessed the ApoE4 impact on the structural covariance (i.e.cortical thickness) brain networks topology derived from sMRI using a graph theory approach in MCI. My results showed that one E4 allele's presence is sufficient to affect the brain network

topology in MCI. The findings showed a decrease in characteristic path length, clustering index normalized, local efficiency, global connectivity, modularity, and increased global efficiency for Carriers compared to non-Carriers. These results revealed that multivariate measures (i.e., covariations) combined with a graph theoretical approach are sensitive to identifying complex pathological processes in MCI, as found in other brain diseases. Univariate measures, cortical thickness, in this case, derived from the standard approaches could be insufficient for capturing subtle (early) changes associated with ApoE4.

3.1.1 MCI ApoE4 Carriers present regional network alterations in agreement with previous AD neurodegeneration findings

My results indicated that regional network properties alterations (NBC and hubs) are related to AD neurodegenerative patterns described in previous studies using other neuroimaging techniques. As an example, I found lower NBC values in crucial structures like the posterior cingulate cortex (PCC) in ApoE4 Carriers. The PCC is a key integration node between the medial temporal lobe and medial prefrontal subsystems in the DMN (Buckner et al., 2008; Raichle et al., 2001). In particular, this region has been consistently noted with significant metabolic alterations in AD. It shows very early and comparatively large reductions in cerebral metabolic rate for glucose (Minoshima et al., 1995), and it sits at the convergence point of multiple metabolic covariance networks (Salmon et al., 2009). Notably, patients at genetic risk for AD, such as ApoE4 Carriers, also show similar metabolism differences, implying the disturbances occur early during the disease progression (Reiman et al., 1996).

Another critical structure, the precuneus, was found with lower NBC values in Carriers compared to non-Carriers. Together with the anterior cingulate cortex, the precuneus is among the earliest brain areas showing pathological changes in AD associated with the aggregation of beta amyloid into plaques (Palmqvist et al., 2017; Villain et al., 2012; Villeneuve et al., 2015). This finding suggests that network measures change on these nodes may play a key role in the AD-related pathological process in MCI and can possibly explain the temporo-spatial disconnect between amyloid aggregation and neurodegeneration. Specifically, the precuneus may show very subtle atrophy in response to amyloid aggregation in this phase of the disease, at which point other brain regions are not yet affected by neurodegeneration. These asynchronous atrophy patterns would result in decreased structural covariance between neighboring brain regions and path length alterations, which are captured by the NBC measure. Possibly, the lack of stimulation and/or neurotrophic factors along these connections may then

drive brain atrophy in more distant regions (Salehi et al., 2006; Seeley et al., 2009). However, more research is necessary to determine the neurobiological mechanisms with which regional networks measure change may facilitate neurodegenerative processes and reflect subtle structural alterations in the brain.

Furthermore, together with other areas, it is a binding site of beta-amyloid deposition (Buckner, 2005), possibly due to conducive metabolic conditions and the linkages between synaptic activity and beta-amyloid metabolism (Bero et al., 2011; Cirrito et al., 2008, 2005). Therefore, brain structures such as the PCC and the Precuneus may indicate a particular vulnerability to perturbations of energy metabolism in MCI Carriers. This idea is referred to by Buckner and colleagues (2005) as the 'metabolism hypothesis' (Buckner, 2005). They state that AD takes a foothold earliest in regions of high glycolytic metabolism within the DMN. The implication of the ApoE4 may lie in the well-known toxic roles during AD progression, particularly related to beta-amyloid pathways. In this direction, ApoE4 is recognized as a disrupted metabolic factor (Bero et al., 2011; Liu et al., 2013; Sun et al., 2007), which alters the brain activity patterns and directly modulates the molecular cascades that are relevant to the disease.

Also, in Carriers, lower NBC values were detected in regions that belong to other networks like the Salient Network. Lower NBC values in brain regions that belong to this network may suggest that ApoE4 Carriers had aberrant communication between networks critical for externally oriented cognition compared to non-Carriers. Therefore, a possible hypothesis is that MCI Carriers have altered regulation of control processes that subsequently influence their memory performance. This network operates on identified salience and, as such, includes known sites for sustained attention and working memory (dorsolateral prefrontal cortex, lateral parietal cortex), response selection (dorsomedial frontal), and response suppression (prefrontal cortex) (Curtis and D'Esposito, 2003; Ridderinkhof et al., 2004).

Summarizing, Apoe4-related effects on regional brain network properties seem to agree with previous structural, functional, and metabolic findings in MCI associated with AD progression. The nodal properties might capture additional information related to the E4 allele effects on the brain networks at MCI stages.

3.1.2 ApoE4 affects how the brain networks segregate the information in MCI.

In general, my results showed that brain network segregation is affected in Carriers compared to non-Carriers. Decreasing network segregation is a crucial feature of brain aging (Chan et al., 2014; Geerligs et al., 2014). However, the ApoE4 in MCI may represent an additional factor

that compromises the normal aging process by accelerating it. Multimodal neuroimaging findings may lend support to this possible linkage. Several task-based fMRI studies had revealed less deactivation in the DMN in Carriers than non-Carriers during task performance, implicating a disrupted balance between the DMN and task-positive networks (Lind et al., 2006; Persson et al., 2008). Middle-aged ApoE4 Carriers also showed activation patterns similar to those of the elderly than the non-Carrier during attention and memory tasks (Evans et al., 2014). As a result, Carriers might be more vulnerable to network dysfunctions associated with AD pathology (Fouquet et al., 2014; Kang et al., 2015; Schultz et al., 2017).

The finding seems in agreement with this hypothesis. A lower clustering index, local efficiency, and modularity suggest more disorganized processing between neighboring (topological neighbors, graph theory) brain regions associated with the E4 allele. However, the cortical thickness at the regional level did not show differences between groups. I hypothesized that brain network measures derived from the structural covariance analysis may have applications as an additional surrogate marker to track AD progression in MCI Carriers starting at early stages when atrophy is not yet extensive to show group differences. It holds if we assume that the structural covariance phenomenon indeed results from brain connectivity of some kind, such as white matter connectivity or the functional connectivity of synchronous neuronal activations (for a review, see (A. Alexander-Bloch et al., 2013)). Then I can speculate that the network alterations found in MCI Carriers may indicate ultrastructural brain changes associated with AD and the ApoE4, such as local cell death, reduction of the dendritic extent, and synaptic loss. However, it is challenging to interpret disease-related alterations associated with network measures. Nevertheless, my findings seem to indicate a link between the genetic risk and brain network topological alterations. They suggested that the brain's structural covariance patterns encode different information, which is not captured by other univariate structural measures.

In MCI Carriers, a less segregated brain may facilitate the patterned spreading of AD proteinopathies within this network. Because as the complex network theory implies through different mechanisms, the dysfunction can spread between linked nodes (structural and/or functional connectivity) and trigger a pathological cascade affecting the system when the compensatory mechanisms are overwhelmed. Previous studies in AD suggest a link between brain network connectivity and the spread of pathological markers like beta-amyloid plaques and tau pathology (Liu et al., 2012; Seeley et al., 2009), indicating that this generic network principle applies to AD progression. The network alterations findings agree with the

"disconnection hypothesis" of AD (Buckner et al., 2009; Delbeuck et al., 2003; Reid and Evans, 2013), possibly due to the several toxic effects of E4 allele that ultimately affect the neuronal synaptic communication. Nevertheless, because this study applied a network reconstruction approach that results in one network per group based on cross-sectional results, it remains unclear whether these alterations are associated with the clinical progression and other AD biomarkers at the individual level.

3.1.3. ApoE4 increases the brain network global efficiency, decreased the path length, and increase NBC in temporal areas: compensatory effects or a pleiotropic case?

Together with the evidence mentioned above, we found some indicators suggesting compensatory processes in MCI Carriers, such as increased global efficiency, shorter characteristics path length, and increased NBC in temporal regions. However, previous studies showed that a shorter characteristic path length is associated with more efficient functioning (Li et al., 2009; Van Den Heuvel et al., 2009; Wen et al., 2011), which as an inverse measure, is expressed on higher global network efficiency. A possible explanation of these results is that Carriers have accelerated and more widespread atrophy than non-Carriers; which might lead to more synchronous brain-wide atrophy patterns and thus lower path lengths values.

Why these "better network indicators" were against intuitively found in the ApoE4 Carriers' group? An attractive hypothesis is the ApoE4 description as an example of antagonistic pleiotropy. The concept comes from the evolutionary biology field, and the idea is that specific genes may have a different impact during different life stages. My results suggest that maybe in MCI, the allele somehow confers advantages in brain network functions, meaning an extension of the model proposed by (for review see (Tuminello and Han, 2011)). But, maybe the ApoE4 is not antagonistically pleiotropic but instead interacts with other AD risk factors highly prevalent in MCI (cardiovascular factors) to influence the network topology differentially. As a response, the E4 allele may trigger in advance a complex set of adaptative responses in Carriers compared to non-Carriers to sustain the same behavior. A neural compensation response associated with the ApoE4 has been reported as increase functional brain activity. Simultaneously, this persistent hyperactivation may place neurons under metabolic stress rendering them susceptible to neurodegeneration later on. This seems to be the case of the NBC increases found in MCI ApoE4 Carriers' temporal structures. However, MCI Carriers may exhaust this compensatory process faster, as Ye et al. (2017) showed using functional connectivity (Ye et al., 2017).

3.1.4 Limitations and future perspectives

The main limitation of this study is relative to the sample characteristics and selection process. First, MCI patients exhibit different progressive trajectories, where some ultimately develop AD and others do not. Accordingly, further follow-up longitudinal studies are necessary to examine whether the combination of structural covariance network measures with the ApoE genotype would improve the prediction of the conversion from MCI to AD. Second, the E4 allele dosage effect was not investigated due to insufficient numbers of ApoE4 homozygotes. Future studies, including homozygotic and E2 Carriers, would be essential to expand upon these preliminary findings. Third, the present study applied a cross-sectional design. This approach confuses inter-subject and intra-subject variability (Thompson et al., 2011).

Mostly, MCI represents a heterogeneous entity characterized by differences in cognitive profile and clinical progression (Petersen et al., 2001). Additionally, longitudinal studies are required to determine how ApoE4 affects large-scale network organization across the AD spectrum (preclinical and clinical phases). Finally, a considerable amount of biological variability existed in MCI recruitment based on clinical criteria. This limitation should be overcome by adding neuropathological biomarkers such as Aβ and Tau to better characterize the study groups.

Also, in this research, I did not include the small-world measure in the network analysis. This topological property should be explored in a future study because it is thought to simultaneously reconcile the opposing demands of functional integration and segregation (Tononi et al., 1994)(Tononi et al., 1994). Such a design has been reported affected in various degrees in MCI and AD (Tijms et al., 2013b; Xie and He, 2012).

This network analysis was based on automatic parcellation of human cortical gyri and sulci included in the FreeSurfer package (http://surfer.nmr.mgh.harvard.edu/). In terms of cortical thickness analysis this atlas offers a precise localization of sulco-gyral structures of the human cerebral cortex which is important for the interpretation of structural covariance brain network. The atlas is commonly used for this type of analysis in MCI AD patients. However, other parcellation schemes should be explore to replicate the present results.

3.2 ApoE4-related effects on the structural covariance brain networks are associated with the risk of AD progression and pathological disease markers in MCI

In this second study, my goal was to investigate the ApoE4-related effects on the Single-Subject gray Matter Networks (SSGMNets) in MCI. I hypothesized that the E4 allele is associated with alterations in the brain network topology. Moreover, the ApoE4 and disease

progression affect the network measures related to neuropathological AD biomarkers (i.e., CSF amyloid β42 and total Tau levels). To test this claim, I compared the SSGMNets estimated from sMRI at two-time points. My results indicated that ApoE4 and the disease progression modulated the global network properties independently. MCI Converters showed a lower clustering index normalized in several regions associated with neurodegeneration in AD. The global network properties were revealed to predict cognitive and memory measures. To the best of my knowledge, this study is the first to showed that altered network topological measures at baseline and their rate of change were associated with ApoE4 and disease progression in MCI.

In the following sections, I will discuss these findings in light of the existing literature and critically expose the advantages and the limitations of the present work.

3.2.1 ApoE4 and disease progression modulate the clustering index normalized in MCI

I found differences between groups in the clustering index normalized at baseline. In particular, the MCI non-Carriers who will progress into AD showed in advance lower clustering index normalized values than those who will not progress at the second time point. However, only for MCI Converters, I detected differences associated with the ApoE4. The MCI Carriers Converters showed increased values compare to non-Carriers. The rate of change analysis revealed the same patterns as a confirmation of this result's robustness.

The findings have two main implications 1) The clustering index normalized seems to be a critical network measure to predict disease progression in MCI in the absence of the genetic risk. The change reflects an altered communication between neighboring areas, maybe as a direct consequence of a progressive corticocortical dysconnectivity (Dicks et al., 2018; Pereira et al., 2016; Tijms et al., 2013b). In general, a lower clustering index suggests a topological organization more like a random network. This graph structure has been previously reported in AD subjects and associated with MCI conversion into AD (Pereira et al., 2016; Tijms et al., 2013b, 2018). I suggest future studies concentrate on the clustering index normalized for patient classification based on this result.

2) The ApoE4 effects in MCI Converters seem to be associated with compensatory mechanisms reflected on increased clustering index normalized values. It is suggested that the brain randomly connects different regions, hypothetically, to retrieve the deafferentation-related missing information from wherever it can. In agreement with this idea, previous studies found an increase in activation of task-related regions (Woodard et al., 2009) that are known to be

affected by AD (e.g., posterior cingulate) and frontal areas (for a review, see (Tuminello and Han, 2011)). Other studies reported in ApoE4 Carriers, regardless of diagnosis, enhanced hippocampal activity during encoding in a face-name memory task (Dickerson et al., 2005). A notable trend in previous studies is in E4 Carriers, the high regional activity is beyond those typically involved in early AD (e.g., prefrontal cortex). As several authors have pointed out, Carriers may exhibit decrements in activity in areas initially impacted in AD while continuing to compensate for these alterations with increased activity in regions not initially affected by the disease (Filbey et al., 2010). However, the 'compensatory network effects' found in MCI Carriers seem to be a problem later. As computational studies suggest, too much integration in a system that should be segregated represent a shift in its organization. It reflects a network breakdown that can facilitate the spread of failures, reduce functional specialization, and result in dedifferentiated neural activity (Fornito et al., 2015).

Summarizing, my findings revealed that some network properties changes in MCI Carriers are associated with altered communication between neighboring regions, maybe indicating AD-related pathological markers (i.e., tau-tangles and amyloid-beta plaques depositions). On the other hand, a better global network communication could be considered the expression of compensatory/degeneracy mechanisms to sustain the transmission of the information across distant brain regions. These changes in topological attributes may be considered sensitive markers to detect AD progression.

3.2.2 Subject-based Network properties alterations in MCI ApoE4 Carriers associated with AD-biomarkers.

My study revealed that ApoE4 affects the association between characteristic path length and CSF $A\beta_{42}$ levels in MCI. Following the graph theory concepts, the characteristic path length is related to transferring speed information through the overall network, implying the brain's global efficiency. The finding suggests that in MCI, this process is modulated by the beta-amyloid brain deposition, in turn, affected by the ApoE4. Previous studies have shown that E4 allele correlates with CSF $A\beta_{42}$ levels in AD's preclinical phase (Vemuri et al., 2010) and cognitively normal subjects (Fleisher et al., 2013). In general, there is an agreement in the literature that ApoE4 increases AD's risk by initiating and accelerating Aβ accumulation in the brain.

On the other hand, Carriers exhibited more brain structural disruptions (Brown et al., 2011). Underlying these disconnections results, several reports demonstrated biochemical and brain

structural changes (Bu, 2009) that reduce the fidelity of the communication between brain regions (Greicius et al., 2004), cause neuronal death and white matter degeneration during AD progression (Westlye et al., 2012). I can then speculate that the synergetic interaction of ApoE4 and $A\beta_{42}$ eventually affects the anatomical and functional brain connectivity, reflected on the characteristic path lengths and global efficiency in MCI. In these patients, where epidemiological studies have shown a high risk of conversion and younger age of onset, the ApoE4 allele eventually causes significant network topological changes. It may be due to an inability to compensate for the inefficient neuronal processes that result from synaptic plasticity and neuronal growth (Celone et al., 2006).

3.2.3 Possible biological meaning of regional covariance alterations associated with the ApoE4

Previous studies suggested that the structural covariance brain network disruptions may reflect early neurodegenerative changes that occur in a coordinated way rather than isolation (A. Alexander-Bloch et al., 2013). I can only speculate about the mechanisms that underlie morphological similarities in the cortex, their relationship to connectivity, and alterations under the ApoE4 presence in MCI. It has been consistently demonstrated that ApoE4 is either pathogenic or shows reduced efficiency in multiple brain homeostatic pathways. That includes lipid transport, synaptic integrity, plasticity, glucose metabolism, and cerebrovascular function (Liu et al., 2013; Yamazaki et al., 2019). At a brain macroscale level, all these interactions will be reflected by the structural covariance changes in MCI. One possible explanation for this phenomenon is that the lack of stimulation and/or neurotrophic factors along these connections may drive brain atrophy in more distant regions (Seeley et al., 2009). Specifically, I found a widespread set of brain areas where the clustering index normalized was lower for Carriers than non-Carriers. These findings suggest that in MCI, the synergetic effect of ApoE4 and disease progression induces subtle atrophy in specific regions that may be associated with the beta-amyloid aggregation and tau. Still, at this point, some anatomical areas are not yet affected by neurodegeneration, at least uncaptured by standard measures. However, the atrophy processes at micro and mesoscale would decrease similarity between neighboring brain regions captured by the network analysis.

3.2.4 Limitations and future perspectives

There are several potential limitations to this study. First, only two-time points MRI scans were analyzed. A future investigation related to the ApoE4 effects on the network properties, cognitive decline, and brain atrophy using more time points is necessary. Second, a small group of subjects had CSF measures, which might have affected the correlation analysis accuracy. Third, a gene-dose analysis and susceptibility and protective loci associated with late-onset AD need to be considered in conjunction with ApoE4 for finding possible interaction effects.

Additionally, the MCI diagnosis based on clinical criteria has limited sensitivity and specificity (Nettiksimmons et al., 2014; Wolk et al., 2009). In this study, the ApoE4 effects on gray matter network results are limited by the absence of biomarker-based group analysis. It opens up the possibility that some subjects were misdiagnosed. Future research based on AT (N) biomarkers profiles will show more robust conclusions on the ApoE4 modulation of the network properties.

As a cognitive measure, I used MMSE and ADNI-MEM. They should not be regarded as a detailed neuropsychological assessment. Research is needed to examine whether altered graph properties are related to dysfunction in specific cognitive domains and are more sensitive to detecting decline over time.

Additionally, here I simulated brain insults using targeted removal of nodes based on their NBC values. The negative results obtained could indicate the importance of model attacks based on random nodes and edge elimination. My results suggest that MCI ApoE4 Carriers showed a shift to more network randomization compared to non-Carriers with may be associated with greater resilience to a targeted attack.

In sum, for the first time, I presented evidence that the topological organization of the single-subject gray matter networks is affected by ApoE4 and the disease progression. Also, I found the topological network properties predictive of $A\beta_{42}$, P-tau, T-tau, atrophy, and cognitive impairment in MCI.

3.3 The Cerebrovascular reactivity in MCI is detected by the analysis of covariance and graph theory

The third study demonstrates that brain perfusion SPECT can help clarify essential questions regarding the MCI neuropathological mechanisms. This project is pertinent given our limited understanding of MCI and the low cost of brain perfusion SPECT. We investigated the cerebrovascular reactivity (CVR) in patients with MCI. CVR is also known as the

cerebrovascular reserve. It describes cerebrovascular structures' ability to increase cerebral blood flow (CBF) above a basal condition in response to a vasodilatory challenge. The results indicate that brain perfusion SPECT combined with theoretical graph analysis can reveal network CVR alterations.

3.3.1 Topological measures capture vasodilatory-induced changes in the CBF network in MCI

In MCI, ApoE4 induces progressive cerebrovascular dysfunction through direct signaling and indirectly via modulation of peripheral and central pathways. The E4 allele induced other changes, including reduced cerebral blood flow (CBF), modified neuron-CBF coupling, increased blood-brain barrier leakiness, and cerebral amyloid angiopathy, hemorrhages, and disrupted transport of nutrients and toxins. Considering MCI as a transitional phase between the cognitive changes associated with aging and dementia (Albert et al., 2011; Petersen, 2016), CVR abnormalities will be subtle, partly explaining the ambiguous findings, particularly in MCI patients with a low vascular burden. Furthermore, based on the complexity of the cerebral microvasculature network, the standard analysis of CVR might not reflect subtle alterations. It relies on studying individual regions rather than their interaction.

The results showed that the control and MCI group networks display different topological patterns of CVR changes, especially at the global level. Besides, the observed regional differences included the medial prefrontal cortices and inferior parietal lobe, which represent areas involved in MCI's cognitive dysfunction. The findings also indicate that graph theory analysis identifies network-related CVR alterations in MCI, which could not be detected by the standard approach. Since this study is a group-based network analysis, the topological measures derived from the CBF covariance network cannot be used to support diagnosis and prognosis individually. However, methods to extract the individual patient contribution using a graph network approach have been developed, although not yet applied to SPECT data in MCI.

In summary, this study showed that brain perfusion SPECT combined with theoretical graph analysis is feasible and useful for investigating problems of complex neurological diseases, such as the CVR alterations in MCI. It is a valid approach for future research focus on the ApoE4- Cerebrovascular interactions effects on the structural and functional covariance brain networks in MCI.

3.3.2 Limitations and future perspectives

First, to further clarify some results at the regional level, it may be necessary to increase the number of subjects and/or use a more potent vasodilatory challenge in future studies. Second, research at the individual level to examine the association between network-related CVR alterations and clinical data is essential. Third, longitudinal studies are needed to investigate the CBF network's changes along the continuum from normal aging to AD dementia. Additionally, several limitations are associated with the CBF network's analysis, such as using Pearson's correlation instead of a partial correlation (Melie-Garcia et al., 2013).

Also, we considered that some of the exclusion criterium applied in this study deserve a careful evaluation. In particular the exclusion of MCI patients based on cerebrovascular disorders, carotid stenosis and white matter changes are very challenging criterium as cardiovascular risk factors and AD are closely related. On the other hand, white matter alterations for instance, clearly impact on CVR.

3.4 Methodological remarks and Future Perspectives

3.4.1 Advantages and disadvantages of the graph theory approach to capture ApoE4 related effects on the brain networks

I consider it essential to clarify that the traditional interpretation of networks' properties applied in this thesis cannot reflect real physiological mechanisms in the brain. We need to assume that the neurophysiological interpretation of the obtained results can present difficulties due to the increasing level of conceptual abstraction and steps applied to generate the brain network properties. Graph theory analysis and the derived properties depend, in my case, on covariation in cortical thickness/gray matter volume/CBF between regions. Still, it is not clear the neurobiological basis for the interregional correlations between brain structures. Based on state of the art on the topic, researchers usually do not make straightforward assumptions on the links' nature but rather emphasize mathematical modeling. The literature on morphological connectivity does not always correctly reflect this issue, leading many researchers to believe that mathematically derived connections represent real physiological connections.

My studies assume that any approach investigating genetic risk factors impact on the brain network organization needs to consider pairwise relations between brain regions simultaneously and that graph theory best achieves this goal. Although graphs do not entirely ease deciphering network organization, they can be useful in visualizing the network's structure's essential topological properties. Additionally, the generality of the mathematical

framework of graph theory allows its application in networks derived from various data. Importantly, structural and functional connectivity are mutually interrelated. Morphological connectivity is affected by both functional and anatomical connectivity and captures different information about brain network properties. The graph theory approach summarizes the brain's complex global and regional patterns into biologically meaningful properties.

As models, the graphs theory approach provides a more highly compact description of the network components (Rubinov and Sporns, 2010). The ability to describe multivariate neural processes by looking at their network topology makes graph analysis unique compared to previous univariate methods that look at the activity in single parts of the brain (e.g., power) or bivariate methods looking at pairwise functional connectivity (e.g., cross-correlation).

The network-based measures, in particular clustering index normalized, modularity and sigma, could be considered for potential clinical application in MCI for example to evaluated response to neuromodulation therapies. The network properties may help to track modification on pathological activity within the nervous system in response to therapeutic effect based on a wide spectrum of interventional technologies. Therapies including deep brain stimulation (DBS), intracranial cortical stimulation (ICS), transcranial direct current stimulation (tDCS), and transcranial magnetic stimulation (TMS) have all shown promising results but still their mechanisms of action have not yet been fully elucidated in intermediate stages such as MCI.

On the other hand, the structural covariance brain connectivity analysis using the graph theory approach has some limitations. Here I mentioned those more relevant to this thesis, such as:

- A critical point of difference between structural covariance and other approach is that fMRI and DWI networks can routinely be constructed from measures of inter-regional association or connectivity estimated for an individual image. By contrast, most structural covariance network studies are built from inter-regional correlations estimated across a group of subjects. The group-level analysis limits the opportunity to link structural covariance metrics to inter-individual differences, such as cognitive functions.

- The static nature of the structural covariance analysis. The evidence suggests that brain networks undergo spontaneous reconfigurations at a temporal scale (Calhoun et al., 2014; Chang and Glover, 2010; Park et al., 2012). As such, properties like the modular structure and the hub regions may fluctuate over time. These changes could reflect a dynamic balance between information segregation and integration (Allen et al., 2014; Betzel et al., 2016; Liao et al., 2015). However, the neurophysiological and biochemical mechanisms underlying these dynamic changes and their relationship with cognitive function require further research.

- Additional methodological problems lie in the sMRI analysis in general and structural covariance analysis in particular. Issues like within-scanner subject motion, spatial normalization, and MRI tissue contrast make the reliability and accuracy of the extraction of morphological properties a challenge. The cellular interpretation of MRI-based morphological properties is also non-trivial and challenging to compare across studies. There are methodological hurdles inconclusively assessing the relationship between structural covariance and anatomical and functional connectivity. I believe technological improvements will allow increasingly accurate assessments of these relationships.

3.4.2 Future perspectives

My findings suggest that ApoE4-related disruptions on the structural covariance brain networks play an essential role in MCI and AD progression. Together with other established biomarkers, it may help inform the individual clinical outcome. Still, several questions remain that need to be addressed in futures research. I have shown that structural covariance brain networks (gray matter/cortical thickness) become affected in response to E4 allele in MCI. However, much less is known about the (temporal and/or spatial) relationship between the network's properties and other AD-related processes, such as e.g., tau pathology. For example, it has been suggested that brain connectivity may represent a pathway along which pathological factors may spread (Seeley et al., 2009). It is currently also unclear whether network disruptions based on structural covariance brain patterns initiate other downstream pathological events. Future studies that include longitudinal assessments of network measures and other AD biomarkers should address these questions.

Additionally, it remains largely unclear what the different network measures precisely indicate. In this line, multimodal approaches may also be helpful since ApoE4 effects on brain connectivity can also be measured based on other imaging modalities (e.g., fMRI, DTI). It is still unclear how network measures derived from these different connectivity types are related to each other within individuals, which would help interpret theoretical graph measures. Still, out of these imaging modalities, sMRI is the most robust, the easiest to obtain, and already included in standard dementia workups. As such, biomarkers based on sMRI have the highest potential to be implemented for patient identification in clinical trials.

I showed that in MCI, a more disorganized network configuration is associated with the ApoE4; however, there are currently no cut-off values available. Future studies that combine the ApoE4 genotype from multiple independent cohorts should aim to derive cut-off values for network

measures and assess their accuracy in predicting disease progression on an individual patient level. Also, future studies should specifically investigate the E4 allele effect stratifying the MCI groups based on new biomarkers profiles (e.g AT(N) system) in multiple independent datasets and exclude the possibility that cohort effects drove these effects.

Finally, the results indicate that network measures based on the graph theoretical approach can help identify the risk of disease progression in ApoE4 Carriers and non-Carriers before other measures such as global cortical thickness and grey matter volume. The network's properties seem to offer additional information together with regional atrophy, CSF-derived biomarkers, and cognitive decline, as such, have use to predict and monitor AD progression. The clustering index normalized, sigma, and modularity could be implemented to test treatment effects from this perspective. I envision that brain network topological measures could be the target of neuromodulation treatments (e.g., TMS) and their variation applied on the prediction outcome/progression in MCI.

4 GENERAL CONCLUSIONS

My results suggest that ApoE4 affects the structural covariance brain network topology in MCI, and these changes are related to AD progression and disease biomarkers. I considered that some of these network measures, in particular, clustering index normalized might have applications to predict and monitor MCI patients in the absence of cortical thickness or gray matter volume changes. Here, I demonstrated that ApoE4 and disease progression affect global and regional network properties in different ways. Finally, the studies revealed that independently of the ApoE4, the network properties changes were associated with AD progression and linked to a steeper memory and CSF-derived measures alterations. Together my findings suggest that network measures might contain prognostic information about the future clinical outcome.

In MCI, regional network properties change (betweenness centrality, clustering index normalized, and hubs) associated with the ApoE4 seem to express altered communication between neighboring regions. It may be an early response to AD-related pathological markers (i.e., amyloid-beta plaques depositions). On the other hand, a better global network communication (global efficiency) could be considered the expression of compensatory/degeneracy mechanisms to sustain the transmission of the information across distant brain regions associated with the genetic challenge. These regional changes in topological attributes may be considered sensitive markers to detect early brain network changes related to the disease progression.

The baseline and rate of change results suggest that the clustering index normalized offers consistent information about the risk of AD progression in MCI Carriers and non-Carriers. It could provide additional information to select genetically at-risk individuals for potential prevention opportunities at the earliest AD stages.

Finally, as an additional research contribution, I demonstrated the graph theory approach's feasibility to detect CVR changes in MCI over conventional measures using SPECT data.

5 REFERENCES

Achard, S., Bullmore, E., 2007. Efficiency and cost of economical brain functional networks. PLoS Computational Biology 3, 0174–0183. https://doi.org/10.1371/journal.pcbi.0030017

Achard, S., Salvador, R., Whitcher, B., Suckling, J., Bullmore, E., 2006. A resilient, low-frequency, small-world human brain functional network with highly connected association cortical hubs. The Journal of neuroscience : the official journal of the Society for Neuroscience 26, 63–72. https://doi.org/10.1523/JNEUROSCI.3874-05.2006

Aisen, P.S., Cummings, J., Jack, C.R., Morris, J.C., Sperling, R., Frölich, L., Jones, R.W., Dowsett, S.A., Matthews, B.R., Raskin, J., Scheltens, P., Dubois, B., 2017. On the path to 2025: Understanding the Alzheimer's disease continuum. Alzheimer's Research and Therapy. https://doi.org/10.1186/s13195-017-0283-5

Albert, M.S., DeKosky, S.T., Dickson, D., Dubois, B., Feldman, H.H., Fox, N.C., Gamst, A., Holtzman, D.M., Jagust, W.J., Petersen, R.C., Snyder, P.J., Carrillo, M.C., Thies, B., Phelps, C.H., 2011. The diagnosis of mild cognitive impairment due to Alzheimer's disease: Recommendations from the National Institute on Aging-Alzheimer's Association workgroups on diagnostic guidelines for Alzheimer's disease. Alzheimer's and Dementia 7, 270–279. https://doi.org/10.1016/j.jalz.2011.03.008

Alexander-Bloch, A., Giedd, J.N., Bullmore, E., 2013. Imaging structural co-variance between human brain regions. Nature Reviews Neuroscience 14, 322–336. https://doi.org/10.1038/nrn3465

Alexander-Bloch, A.F., Vertes, P.E., Stidd, R., Lalonde, F., Clasen, L., Rapoport, J., Giedd, J., Bullmore, E.T., Gogtay, N., 2013. The anatomical distance of functional connections predicts brain network topology in health and schizophrenia. Cerebral Cortex 23, 127–138. https://doi.org/10.1093/cercor/bhr388

Alexander, G.E., Bergfield, K.L., Chen, K., Reiman, E.M., Hanson, K.D., Lin, L., Bandy, D., Caselli, R.J., Moeller, J.R., 2012. Gray matter network associated with risk for Alzheimer's disease in young to middle-aged adults. Neurobiology of Aging 33, 2723–2732. https://doi.org/10.1016/j.neurobiolaging.2012.01.014

Allen, E.A., Damaraju, E., Plis, S.M., Erhardt, E.B., Eichele, T., Calhoun, V.D., 2014. Tracking whole-brain connectivity dynamics in the resting state. Cerebral Cortex 24, 663–676. https://doi.org/10.1093/cercor/bhs352

Andrews, T.J., Halpern, S.D., Purves, D., 1997. Correlated size variations in human visual cortex, lateral geniculate nucleus, and optic tract. The Journal of neuroscience : the official journal of the Society for Neuroscience 17, 2859–2868. https://doi.org/Comparative Study Research Support, U.S. Gov't, P.H.S.

Ayton, S., Faux, N.G., Bush, A.I., Neuroimaging, D., 2015. Ferritin levels in the cerebrospinal fluid predict Alzheimer's disease outcomes and are regulated by APOE. Nature Communications 1–9. https://doi.org/10.1038/ncomms7760

Ayton, S., Fazlollahi, A., Bourgeat, P., Raniga, P., Ng, A., Lim, Y.Y., Diouf, I., Farquharson, S., Fripp, J., Ames, D., Doecke, J., Desmond, P., Ordidge, R., Masters, C.L., Rowe, C.C., Maruff, P., Villemagne, V.L., Salvado, O., Bush, A.I., 2017. Cerebral quantitative susceptibility mapping predicts amyloid-β-related cognitive decline. Brain 140, 2112–2119. https://doi.org/10.1093/brain/awx137

Bartzokis, G., 2011. Alzheimer's disease as homeostatic responses to age-related myelin breakdown. Neurobiology of Aging. https://doi.org/10.1016/j.neurobiolaging.2009.08.007

Bartzokis, G., Tishler, T.A., Lu, P.H., Villablanca, P., Altshuler, L.L., Carter, M., Huang, D., Edwards, N., Mintz, J., 2007. Brain ferritin iron may influence age- and gender-related risks of neurodegeneration. Neurobiology of Aging 28, 414–423. https://doi.org/10.1016/j.neurobiolaging.2006.02.005

Bassett, D.S., Bullmore, E., Verchinski, B.A., Mattay, V.S., Weinberger, D.R., Meyer-Lindenberg, A., 2008. Hierarchical organization of human cortical networks in health and schizophrenia. J Neurosci 28, 9239–48. https://doi.org/10.1523/JNEUROSCI.1929-08.2008

Bassett, D.S., Sporns, O., 2017. Network neuroscience. Nature Neuroscience. https://doi.org/10.1038/nn.4502

Batalle, D., Muñoz-Moreno, E., Figueras, F., Bargallo, N., Eixarch, E., Gratacos, E., 2013. Normalization of similarity-based individual brain networks from gray matter MRI and its association with neurodevelopment in infants with intrauterine growth restriction. NeuroImage 83, 901–911. https://doi.org/10.1016/j.neuroimage.2013.07.045

Bekris, L.M., Yu, C.-E., Bird, T.D., Tsuang, D.W., 2010. Review Article: Genetics of Alzheimer Disease. Journal of Geriatric Psychiatry and Neurology 23, 213–227. https://doi.org/10.1177/0891988710383571

Bennett, D.A., Schneider, J.A., Bienias, J.L., Evans, D.A., Wilson, R.S., 2005. Mild cognitive impairment is related to Alzheimer disease pathology and cerebral infarctions. Neurology 64, 834–841. https://doi.org/10.1212/01.WNL.0000152982.47274.9E

Bero, A.W., Yan, P., Roh, J.H., Cirrito, J.R., Stewart, F.R., Raichle, M.E., Lee, J.-M., Holtzman, D.M., 2011. Neuronal activity regulates the regional vulnerability to amyloid-β deposition. Nature Neuroscience 14,

750–756. https://doi.org/10.1038/nn.2801
Bertram, L., Lill, C.M., Tanzi, R.E., 2010. The genetics of alzheimer disease: Back to the future. Neuron 68, 270–281. https://doi.org/10.1016/j.neuron.2010.10.013
Bertram, L., Tanzi, R.E., 2012. The genetics of Alzheimer's disease, in: Progress in Molecular Biology and Translational Science. Elsevier B.V., pp. 79–100. https://doi.org/10.1016/B978-0-12-385883-2.00008-4
Betzel, R.F., Fukushima, M., He, Y., Zuo, X.N., Sporns, O., 2016. Dynamic fluctuations coincide with periods of high and low modularity in resting-state functional brain networks. NeuroImage 127, 287–297. https://doi.org/10.1016/j.neuroimage.2015.12.001
Boccaletti, S., Latora, V., Moreno, Y., Chavez, M., Hwang, D., 2006. Complex networks : Structure and dynamics. Physics Reports 424, 175–308. https://doi.org/10.1016/j.physrep.2005.10.009
Bookheimer, S., Burggren, A., 2009. APOE-4 Genotype and Neurophysiological Vulnerability to Alzheimer's and Cognitive Aging. Annual Review of Clinical Psychology 5, 343–362. https://doi.org/10.1146/annurev.clinpsy.032408.153625
Braak, H., Braak, E., 1997. Frequency of stages of Alzheimer-related lesions in different age categories. Neurobiology of Aging 18, 351–357. https://doi.org/10.1016/S0197-4580(97)00056-0
Braak, H., Braak, E., 1991. Neuropathological stageing of Alzheimer-related changes. Acta Neuropathologica. https://doi.org/10.1007/BF00308809
Braak, H., Del Trecidi, K., 2015. Neuroanatomy and pathology of sporadic Alzheimer's disease. Advances in anatomy, embryology, and cell biology. https://doi.org/10.1007/978-3-319-12679-1
Brandon, J.A., Farmer, B.C., Williams, H.C., Johnson, L.A., 2018. APOE and alzheimer's disease: Neuroimaging of metabolic and cerebrovascular dysfunction. Frontiers in Aging Neuroscience. https://doi.org/10.3389/fnagi.2018.00180
Brier, M.R., Thomas, J.B., Ances, B.M., 2014. Network dysfunction in Alzheimer's disease: refining the disconnection hypothesis. Brain connectivity 4, 299–311. https://doi.org/10.1089/brain.2014.0236
Brown, J.A., Terashima, K.H., Burggren, A.C., Ercoli, L.M., Miller, K.J., Small, G.W., Bookheimer, S.Y., 2011. Brain network local interconnectivity loss in aging APOE-4 allele carriers. Proceedings of the National Academy of Sciences of the United States of America 108, 20760–5. https://doi.org/10.1073/pnas.1109038108
Bu, G., 2009. Apolipoprotein E and its receptors in Alzheimer's disease: pathways, pathogenesis and therapy. Nature Reviews Neuroscience 10, 333–344. https://doi.org/10.1038/nrn2620
Buchhave, P., Minthon, L., Zetterberg, H., Wallin, Å.K., Blennow, K., Hansson, O., 2012. Cerebrospinal fluid levels of β-amyloid 1-42, but not of tau, are fully changed already 5 to 10 years before the onset of Alzheimer dementia. Archives of General Psychiatry 69, 98–106. https://doi.org/10.1001/archgenpsychiatry.2011.155
Buckner, R.L., 2005. Molecular, Structural, and Functional Characterization of Alzheimer's Disease: Evidence for a Relationship between Default Activity, Amyloid, and Memory. Journal of Neuroscience 25, 7709–7717. https://doi.org/10.1523/JNEUROSCI.2177-05.2005
Buckner, R.L., Andrews-Hanna, J.R., Schacter, D.L., 2008. The brain's default network: Anatomy, function, and relevance to disease. Annals of the New York Academy of Sciences 1124, 1–38. https://doi.org/10.1196/annals.1440.011
Buckner, R.L., Sepulcre, J., Talukdar, T., Krienen, F.M., Liu, H., Hedden, T., Andrews-Hanna, J.R., Sperling, R.A., Johnson, K.A., 2009. Cortical Hubs Revealed by Intrinsic Functional Connectivity: Mapping, Assessment of Stability, and Relation to Alzheimer's Disease. Journal of Neuroscience 29, 1860–1873. https://doi.org/10.1523/JNEUROSCI.5062-08.2009
Bullmore, E., Sporns, O., 2009. Complex brain networks: graph theoretical analysis of structural and functional systems. Nature Reviews Neuroscience 10, 186–198. https://doi.org/10.1038/nrn2575
Bullmore, E.T., Woodruff, P.W.R., Wright, I.C., Rabe-Hesketh, S., Howard, R.J., Shuriquie, N., Murray, R.M., 1998. Does dysplasia cause anatomical dysconnectivity in schizophrenia?, in: Schizophrenia Research. Schizophr Res, pp. 127–135. https://doi.org/10.1016/S0920-9964(97)00141-2
Calhoun, V.D., Miller, R., Pearlson, G., Adali, T., 2014. The Chronnectome: Time-Varying Connectivity Networks as the Next Frontier in fMRI Data Discovery. Neuron. https://doi.org/10.1016/j.neuron.2014.10.015
Carrera, E., Tononi, G., 2014. Diaschisis: past, present, future. Brain 137, 2408–2422. https://doi.org/10.1093/brain/awu101
Celone, K.A., Calhoun, V.D., Dickerson, B.C., Atri, A., Chua, E.F., Miller, S.L., DePeau, K., Rentz, D.M., Selkoe, D.J., Blacker, D., Albert, M.S., Sperling, R.A., 2006. Alterations in memory networks in mild cognitive impairment and Alzheimer's disease: An independent component analysis. Journal of Neuroscience 26, 10222–10231. https://doi.org/10.1523/JNEUROSCI.2250-06.2006
Chan, M.Y., Park, D.C., Savalia, N.K., Petersen, S.E., Wig, G.S., 2014. Decreased segregation of brain systems across the healthy adult lifespan. Proceedings of the National Academy of Sciences of the United States of

America 111, E4997–E5006. https://doi.org/10.1073/pnas.1415122111
Chang, C., Glover, G.H., 2010. Time-frequency dynamics of resting-state brain connectivity measured with fMRI. NeuroImage 50, 81–98. https://doi.org/10.1016/j.neuroimage.2009.12.011
Chételat, G., Landeau, B., Eustache, F., Mézenge, F., Viader, F., De La Sayette, V., Desgranges, B., Baron, J.C., 2005. Using voxel-based morphometry to map the structural changes associated with rapid conversion in MCI: A longitudinal MRI study. NeuroImage 27, 934–946. https://doi.org/10.1016/j.neuroimage.2005.05.015
Cirrito, J.R., Kang, J.E., Lee, J., Stewart, F.R., Verges, D.K., Silverio, L.M., Bu, G., Mennerick, S., Holtzman, D.M., 2008. Endocytosis Is Required for Synaptic Activity-Dependent Release of Amyloid-β In Vivo. Neuron 58, 42–51. https://doi.org/10.1016/j.neuron.2008.02.003
Cirrito, J.R., Yamada, K.A., Finn, M.B., Sloviter, R.S., Bales, K.R., May, P.C., Schoepp, D.D., Paul, S.M., Mennerick, S., Holtzman, D.M., 2005. Synaptic activity regulates interstitial fluid amyloid-β levels in vivo. Neuron 48, 913–922. https://doi.org/10.1016/j.neuron.2005.10.028
Corder, E.H., Saunders, A.M., Strittmatter, W.J., Schmechel, D.E., Gaskell, P.C., Small, G.W., Roses, A.D., Haines, J.L., Pericak-Vance, M.A., 1993. Gene dose of apolipoprotein E type 4 allele and the risk of Alzheimer's disease in late onset families. Science 261, 921–923. https://doi.org/10.1126/science.8346443
Cosentino, S., Scarmeas, N., Helzner, E., Glymour, M.M., Brandt, J., Albert, M., Blacker, D., Stern, Y., 2008. APOE epsilon 4 allele predicts faster cognitive decline in mild Alzheimer disease. Neurology 70, 1842–9. https://doi.org/10.1212/01.wnl.0000304038.37421.cc
Craddock, R.C., Jbabdi, S., Yan, C.G., Vogelstein, J.T., Castellanos, F.X., Di Martino, A., Kelly, C., Heberlein, K., Colcombe, S., Milham, M.P., 2013. Imaging human connectomes at the macroscale. Nature Methods. https://doi.org/10.1038/nmeth.2482
Crews, L., Rockenstein, E., Masliah, E., 2010. APP transgenic modeling of Alzheimer's disease: Mechanisms of neurodegeneration and aberrant neurogenesis. Brain Structure and Function. https://doi.org/10.1007/s00429-009-0232-6
Cummings, J.L., Morstorf, T., Zhong, K., 2014. Alzheimer's disease drug-development pipeline: Few candidates, frequent failures. Alzheimer's Research and Therapy 6, 37. https://doi.org/10.1186/alzrt269
Curtis, C.E., D'Esposito, M., 2003. Persistent activity in the prefrontal cortex during working memory. Trends in Cognitive Sciences. https://doi.org/10.1016/S1364-6613(03)00197-9
Dai, Z., He, Y., 2014. Disrupted structural and functional brain connectomes in mild cognitive impairment and Alzheimer's disease. Neuroscience Bulletin 30, 217–232. https://doi.org/10.1007/s12264-013-1421-0
Deco, G., Kringelbach, M.L., 2014. Great expectations: Using whole-brain computational connectomics for understanding neuropsychiatric disorders. Neuron. https://doi.org/10.1016/j.neuron.2014.08.034
Delbeuck, X., Collette, F., Van der Linden, M., 2007. Is Alzheimer's disease a disconnection syndrome?. Evidence from a crossmodal audio-visual illusory experiment. Neuropsychologia 45, 3315–3323. https://doi.org/10.1016/j.neuropsychologia.2007.05.001
Delbeuck, X., Linden, M. Van Der, Collette, F., 2003. Alzheimer's Disease as a Disconnection Syndrome. Neuropsychology review 13, 79–92.
Desikan, R.S., Cabral, H.J., Fischl, B., Guttmann, C.R.G., Blacker, D., Hyman, B.T., Albert, M.S., Killiany, R.J., 2009. Temporoparietal MR imaging measures of atrophy in subjects with mild cognitive impairment that predict subsequent diagnosis of Alzheimer disease. American Journal of Neuroradiology 30, 532–538. https://doi.org/10.3174/ajnr.A1397
Devanand, D.P., Pradhaban, G., Liu, X., Khandji, A., De Santi, S., Segal, S., Rusinek, H., Pelton, G.H., Honig, L.S., Mayeux, R., Stern, Y., Tabert, M.H., De Leon, M.J., 2007. Hippocampal and entorhinal atrophy in mild cognitive impairment: Prediction of Alzheimer disease. Neurology 68, 828–836. https://doi.org/10.1212/01.wnl.0000256697.20968.d7
Devous, M.D., 2013. SPECT functional brain imaging: Instrumentation, radiopharmaceuticals, and technical factors.
Dickerson, B.C., Salat, D.H., Greve, D.N., Chua, E.F., Rand-Giovannetti, E., Rentz, D.M., Bertram, L., Mullin, K., Tanzi, R.E., Blacker, D., Albert, M.S., Sperling, R.A., 2005. Increased hippocampal activation in mild cognitive impairment compared to normal aging and AD. Neurology 65, 404–411. https://doi.org/10.1212/01.wnl.0000171450.97464.49
Dickerson, B.C., Wolk, D.A., 2013. Biomarker-based prediction of progression in MCI: Comparison of AD signature and hippocampal volume with spinal fluid amyloid-β and tau. Frontiers in Aging Neuroscience 5. https://doi.org/10.3389/fnagi.2013.00055
Dicks, E., Tijms, B.M., ten Kate, M., Gouw, A.A., Benedictus, M.R., Teunissen, C.E., Barkhof, F., Scheltens, P., van der Flier, W.M., 2018. Gray matter network measures are associated with cognitive decline in mild cognitive impairment. Neurobiology of Aging 61, 198–206. https://doi.org/10.1016/j.neurobiolaging.2017.09.029
Dicks, E., van der Flier, W.M., Scheltens, P., Barkhof, F., Tijms, B.M., 2020. Single-subject gray matter

networks predict future cortical atrophy in preclinical Alzheimer's disease. Neurobiology of Aging 94, 71–80. https://doi.org/10.1016/j.neurobiolaging.2020.05.008
Drzezga, A., Riemenschneider, M., Strassner, B., Grimmer, T., Peller, M., Knoll, A., Wagenpfeil, S., Minoshima, S., Schwaiger, M., Kurz, A., 2005. Cerebral glucose metabolism in patients with AD and different APOE genotypes. Neurology 64, 102–107. https://doi.org/10.1212/01.WNL.0000148478.39691.D3
Elias-Sonnenschein, L.S., Viechtbauer, W., Ramakers, I.H.G.B., Verhey, F.R.J., Visser, P.J., 2011. Predictive value of APOE-ε4 allele for progression from MCI to AD-type dementia: A meta-analysis. Journal of Neurology, Neurosurgery and Psychiatry 82, 1149–1156. https://doi.org/10.1136/jnnp.2010.231555
Evans, S., Dowell, N.G., Tabet, N., Tofts, P.S., King, S.L., Rusted, J.M., 2014. Cognitive and neural signatures of the APOE E4 allele in mid-aged adults. Neurobiology of Aging 35, 1615–1623. https://doi.org/10.1016/j.neurobiolaging.2014.01.145
Farlow, M.R., He, Y., Tekin, S., Xu, J., Lane, R., Charles, H.C., 2004. Impact of APOE in mild cognitive impairment. Neurology 63, 1898–1901. https://doi.org/10.1212/01.WNL.0000144279.21502.B7
Farrer, L.A., Cupples, L.A., Haines, J.L., Hyman, B., Kukull, W.A., Mayeux, R., Myers, R.H., Pericak-Vance, M.A., Risch, N., van Duijn, C.M., 1997. Effects of age, sex, and ethnicity on the association between apolipoprotein E genotype and Alzheimer disease. A meta-analysis. APOE and Alzheimer Disease Meta Analysis Consortium. JAMA 278, 1349–56.
Fei, M., Jianhua, W., 2013. Apolipoprotein ε4-Allele as a significant risk factor for conversion from mild cognitive impairment to alzheimer's disease: A meta-analysis of prospective studies. Journal of Molecular Neuroscience. https://doi.org/10.1007/s12031-012-9934-y
Filbey, F.M., Chen, G., Sunderland, T., Cohen, R.M., 2010. Failing compensatory mechanisms during working memory in older apolipoprotein E-ε4 healthy adults. Brain Imaging and Behavior 4, 177–188. https://doi.org/10.1007/s11682-010-9097-9
Filippi, M., Agosta, F., 2011. Structural and functional network connectivity breakdown in Alzheimer's disease studied with magnetic resonance imaging techniques. Journal of Alzheimer's Disease 24, 455–474. https://doi.org/10.3233/JAD-2011-101854
Fleisher, A.S., Chen, K., Liu, X., Ayutyanont, N., Roontiva, A., Thiyyagura, P., Protas, H., Joshi, A.D., Sabbagh, M., Sadowsky, C.H., Sperling, R.A., Clark, C.M., Mintun, M.A., Pontecorvo, M.J., Coleman, R.E., Doraiswamy, P.M., Johnson, K.A., Carpenter, A.P., Skovronsky, D.M., Reiman, E.M., 2013. Apolipoprotein E ??4 and age effects on florbetapir positron emission tomography in healthy aging and Alzheimer disease. Neurobiology of Aging 34, 1–12. https://doi.org/10.1016/j.neurobiolaging.2012.04.017
Fleisher, A.S., Sowell, B.B., Taylor, C., Gamst, A.C., Petersen, R.C., Thal, L.J., 2007. Clinical predictors of progression to Alzheimer disease in amnestic mild cognitive impairment. Neurology 68, 1588–1595. https://doi.org/10.1212/01.wnl.0000258542.58725.4c
Forlenza, O. V, Diniz, B.S., Gattaz, W.F., 2010. Diagnosis and biomarkers of predementia in Alzheimer's disease. BMC medicine 8, 89. https://doi.org/10.1186/1741-7015-8-89
Fornito, A., Zalesky, A., Breakspear, M., 2015. The connectomics of brain disorders. Nature Reviews Neuroscience 16, 159–172. https://doi.org/10.1038/nrn3901
Fornito, A., Zalesky, A., Bullmore, E.T., 2016. Fundamentals of Brain Network Analysis, Fundamentals of Brain Network Analysis. Elsevier Inc. https://doi.org/10.1016/C2012-0-06036-X
Fouquet, M., Besson, F.L., Gonneaud, J., La Joie, R., Chételat, G., 2014. Imaging Brain Effects of APOE4 in Cognitively Normal Individuals Across the Lifespan. Neuropsychology Review. https://doi.org/10.1007/s11065-014-9263-8
Friston, K.J., 1994. Functional and effective connectivity in neuroimaging: A synthesis. Human Brain Mapping 2, 56–78. https://doi.org/10.1002/hbm.460020107
Galvin, J.E., Powlishta, K.K., Wilkins, K., McKeel, D.W., Xiong, C., Grant, E., Storandt, M., Morris, J.C., 2005. Predictors of preclinical Alzheimer disease and dementia: A clinicopathologic study. Archives of Neurology 62, 758–765. https://doi.org/10.1001/archneur.62.5.758
Geerligs, L., Maurits, N.M., Renken, R.J., Lorist, M.M., 2014. Reduced specificity of functional connectivity in the aging brain during task performance. Human Brain Mapping 35, 319–330. https://doi.org/10.1002/hbm.22175
Girvan, M., Newman, M.E.J., 2002. Community structure in social and biological networks. Proceedings of the National Academy of Sciences of the United States of America 99, 7821–7826. https://doi.org/10.1073/pnas.122653799
Goldman, J.S., Hahn, S.E., Catania, J.W., Larusse-Eckert, S., Butson, M.B., Rumbaugh, M., Strecker, M.N., Roberts, J.S., Burke, W., Mayeux, R., Bird, T., 2011. Genetic counseling and testing for Alzheimer disease: Joint practice guidelines of the American College of Medical Genetics and the National Society of Genetic Counselors. Genetics in Medicine 13, 597–605.

https://doi.org/10.1097/GIM.0b013e31821d69b8
Gomar, J.J., Bobes-Bascaran, M.T., Conejero-Goldberg, C., Davies, P., Goldberg, T.E., 2011. Utility of combinations of biomarkers, cognitive markers, and risk factors to predict conversion from mild cognitive impairment to Alzheimer disease in patients in the Alzheimer's disease neuroimaging initiative. Archives of General Psychiatry 68, 961–969. https://doi.org/10.1001/archgenpsychiatry.2011.96
Gong, G., He, Y., Chen, Z.J., Evans, A.C., 2012. Convergence and divergence of thickness correlations with diffusion connections across the human cerebral cortex. NeuroImage 59, 1239–1248. https://doi.org/10.1016/j.neuroimage.2011.08.017
Goryawala, M., Duara, R., Loewenstein, D.A., Zhou, Q., Barker, W., 2015. Apolipoprotein-E4 (ApoE4) carriers show altered small-world properties in the default mode network of the brain. Biomedical Physics & Engineering Express 1, 15001. https://doi.org/10.1088/2057-1976/1/1/015001
Gottesman, I.I., Gould, T.D., 2003. The Endophenotype Concept in Psychiatry:\rEtymology and Strategic Intentions. Amercian Journal of Psychiatry 160, 636–645. https://doi.org/10.1176/appi.ajp.160.4.636
Gratton, C., Nomura, E.M., Pérez, F., D'Esposito, M., 2012. Focal brain lesions to critical locations cause widespread disruption of the modular organization of the brain. Journal of Cognitive Neuroscience 24, 1275–1285. https://doi.org/10.1162/jocn_a_00222
Greicius, M.D., Srivastava, G., Reiss, A.L., Menon, V., 2004. Default-mode network activity distinguishes Alzheimer's disease from healthy aging: evidence from functional MRI. Proceedings of the National Academy of Sciences of the United States of America 101, 4637–42. https://doi.org/10.1073/pnas.0308627101
Grundman, M., Petersen, R.C., Ferris, S.H., Thomas, R.G., Aisen, P.S., Bennett, D.A., Foster, N.L., Jack, C.R., Galasko, D.R., Doody, R., Kaye, J., Sano, M., Mohs, R., Gauthier, S., Kim, H.T., Jin, S., Schultz, A.N., Schafer, K., Mulnard, R., van Dyck, C.H., Mintzer, J., Zamrini, E.Y., Cahn-Weiner, D., Thal, L.J., Alzheimer's Disease Cooperative Study, 2004. Mild Cognitive Impairment Can Be Distinguished From Alzheimer Disease and Normal Aging for Clinical Trials. Archives of Neurology 61, 59. https://doi.org/10.1001/archneur.61.1.59
Guerreiro, R., Hardy, J., 2014. Genetics of Alzheimer's Disease. Neurotherapeutics. https://doi.org/10.1007/s13311-014-0295-9
Guimerà, R., Amaral, L.A.N., 2005. Cartography of complex networks: Modules and universal roles. Journal of Statistical Mechanics: Theory and Experiment 2005, 1–13. https://doi.org/10.1088/1742-5468/2005/02/P02001
Haan, M.N., Shemanski, L., Jagust, W.J., Manolio, T.A., Kuller, L., 1999. The role of APOE ε4 in modulating effects of other risk factors for cognitive decline in elderly persons. Journal of the American Medical Association 282, 40–46. https://doi.org/10.1001/jama.282.1.40
Hafkemeijer, A., van der Grond, J., Rombouts, S.A.R.B., 2012. Imaging the default mode network in aging and dementia. Biochimica et Biophysica Acta - Molecular Basis of Disease. https://doi.org/10.1016/j.bbadis.2011.07.008
Hagmann, P., 2005. From diffusion MRI to brain connectomics. https://doi.org/10.5075/EPFL-THESIS-3230
Hänninen, T., Hallikainen, M., Tuomainen, S., Vanhanen, M., Soininen, H., 2002. Prevalence of mild cognitive impairment: a population-based study in elderly subjects. Acta neurologica Scandinavica 106, 148–54.
Hansson, O., Zetterberg, H., Buchhave, P., Londos, E., Blennow, K., Minthon, L., 2006. Association between CSF biomarkers and incipient Alzheimer's disease in patients with mild cognitive impairment: A follow-up study. Lancet Neurology 5, 228–234. https://doi.org/10.1016/S1474-4422(06)70355-6
Hardy, J., 1997. Amyloid, the presenilins and Alzheimer's disease. Trends in Neurosciences. https://doi.org/10.1016/S0166-2236(96)01030-2
Hardy, J.A., Higgins, G.A., 1992. Alzheimer's disease: The amyloid cascade hypothesis. Science. https://doi.org/10.1126/science.1566067
Haxby, J. V., Grady, C.L., Koss, E., Horwitz, B., Heston, L., Schapiro, M., Friedland, R.P., Rapoport, S.I., 1990. Longitudinal Study of Cerebral Metabolic Asymmetries and Associated Neuropsychological Patterns in Early Dementia of the Alzheimer Type. Archives of Neurology 47, 753–760. https://doi.org/10.1001/archneur.1990.00530070043010
He, Y., Chen, Z., Evans, A., 2008. Structural insights into aberrant topological patterns of large-scale cortical networks in Alzheimer's disease. The Journal of neuroscience : the official journal of the Society for Neuroscience 28, 4756–4766. https://doi.org/10.1523/JNEUROSCI.0141-08.2008
He, Y, Chen, Z., Gong, G., Evans, A., 2009. Neuronal networks in Alzheimer's disease. Neuroscientist 15, 333–350. https://doi.org/1073858409334423 [pii]10.1177/1073858409334423
He, Y., Chen, Z.J., Evans, A.C., 2007. Small-world anatomical networks in the human brain revealed by cortical thickness from MRI. Cerebral Cortex 17, 2407–2419. https://doi.org/10.1093/cercor/bhl149
He, Yong, Dagher, A., Chen, Z., Charil, A., Zijdenbos, A., Worsley, K., Evans, A., 2009. Impaired small-world efficiency in structural cortical networks in multiple sclerosis associated with white matter lesion load.

Brain 132, 3366–3379. https://doi.org/10.1093/brain/awp089
Holtzman, D., Herz, J., 2012. Apolipoprotein E and apolipoprotein receptors: normal biology and roles in Alzheimer's disease. Cold Spring Harbor perspectives in Medicin 2, a006312. https://doi.org/10.1101/cshperspect.a006312
Honey, C.J., Sporns, O., Cammoun, L., Gigandet, X., Thiran, J.P., Meuli, R., Hagmann, P., 2009. Predicting human resting-state functional connectivity from structural connectivity. Proceedings of the National Academy of Sciences of the United States of America 106, 2035–2040. https://doi.org/10.1073/pnas.0811168106
Humphries, M.D., Gurney, K., Prescott, T.J., 2006. The brainstem reticular formation is a small-world, not scale-free, network. Proceedings of the Royal Society B: Biological Sciences 273, 503–511. https://doi.org/10.1098/rspb.2005.3354
Hutton, C., De Vita, E., Ashburner, J., Deichmann, R., Turner, R., 2008. Voxel-based cortical thickness measurements in MRI. NeuroImage 40, 1701–1710. https://doi.org/10.1016/j.neuroimage.2008.01.027
Hyman, B.T., Gomez-Isla, T., 1994. Alzheimer's disease is a laminar, regional, and neural system specific disease, not a global brain disease. Neurobiology of Aging. https://doi.org/10.1016/0197-4580(94)90031-0
Hyman, B.T., Phelps, C.H., Beach, T.G., Bigio, E.H., Cairns, N.J., Carrillo, M.C., Dickson, D.W., Duyckaerts, C., Frosch, M.P., Masliah, E., Mirra, S.S., Nelson, P.T., Schneider, J.A., Thal, D.R., Thies, B., Trojanowski, J.Q., Vinters, H. V., Montine, T.J., 2012. National Institute on Aging-Alzheimer's Association guidelines for the neuropathologic assessment of Alzheimer's disease. Alzheimer's and Dementia 8, 1–13. https://doi.org/10.1016/j.jalz.2011.10.007
Iqbal, K., Grundke-Iqbal, I., 2002. Neurofibrillary pathology leads to synaptic loss and not the other way around in Alzheimer disease. Journal of Alzheimer's Disease. https://doi.org/10.3233/JAD-2002-4313
Iturria-Medina, Y., Hachinski, V., Evans, A.C., 2017. The vascular facet of late-onset Alzheimer's disease. Current Opinion in Neurology 30, 623–629. https://doi.org/10.1097/WCO.0000000000000497
Iturria-Medina, Y., Sotero, R.C., Toussaint, P.J., Mateos-Pérez, J.M., Evans, A.C., Weiner, M.W., 2016. Early role of vascular dysregulation on late-onset Alzheimer's disease based on multifactorial data-driven analysis. Nature Communications 7, 11934. https://doi.org/10.1038/ncomms11934
Jack, C.R., Albert, M.S., Knopman, D.S., McKhann, G.M., Sperling, R.A., Carrillo, M.C., Thies, B., Phelps, C.H., 2011. Introduction to the recommendations from the National Institute on Aging-Alzheimer's Association workgroups on diagnostic guidelines for Alzheimer's disease. Alzheimer's and Dementia 7, 257–262. https://doi.org/10.1016/j.jalz.2011.03.004
Jack, C.R., Bennett, D.A., Blennow, K., Carrillo, M.C., Dunn, B., Haeberlein, S.B., Holtzman, D.M., Jagust, W., Jessen, F., Karlawish, J., Liu, E., Molinuevo, J.L., Montine, T., Phelps, C., Rankin, K.P., Rowe, C.C., Scheltens, P., Siemers, E., Snyder, H.M., Sperling, R., Elliott, C., Masliah, E., Ryan, L., Silverberg, N., 2018. NIA-AA Research Framework: Toward a biological definition of Alzheimer's disease. Alzheimer's and Dementia. https://doi.org/10.1016/j.jalz.2018.02.018
Jack, C.R., Knopman, D.S., Jagust, W.J., Petersen, R.C., Weiner, M.W., Aisen, P.S., Shaw, L.M., Vemuri, P., Wiste, H.J., Weigand, S.D., Lesnick, T.G., Pankratz, V.S., Donohue, M.C., Trojanowski, J.Q., Trojanowski, J.Q., 2013. Tracking pathophysiological processes in Alzheimer's disease: an updated hypothetical model of dynamic biomarkers. The Lancet. Neurology 12, 207–16. https://doi.org/10.1016/S1474-4422(12)70291-0
Jack, C.R., Knopman, D.S., Jagust, W.J., Shaw, L.M., Aisen, P.S., Weiner, M.W., Petersen, R.C., Trojanowski, J.Q., 2010. Hypothetical model of dynamic biomarkers of the Alzheimer's pathological cascade. The Lancet Neurology. https://doi.org/10.1016/S1474-4422(09)70299-6
Jack, C.R., Petersen, R.C., Xu, Y.C., O'Brien, P.C., Smith, G.E., Ivnik, R.J., Boeve, B.F., Waring, S.C., Tangalos, E.G., Kokmen, E., 1999. Prediction of AD with MRI-based hippocampal volume in mild cognitive impairment. Neurology 52, 1397–1403. https://doi.org/10.1212/wnl.52.7.1397
Jicha, G.A., Parisi, J.E., Dickson, D.W., Johnson, K., Cha, R., Ivnik, R.J., Tangalos, E.G., Boeve, B.F., Knopman, D.S., Braak, H., Petersen, R.C., 2006. Neuropathologic outcome of mild cognitive impairment following progression to clinical dementia. Archives of Neurology 63, 674–681. https://doi.org/10.1001/archneur.63.5.674
Kaiser, M., Hilgetag, C.C., 2006. Nonoptimal component placement, but short processing paths, due to long-distance projections in neural systems. PLoS Computational Biology 2, 0805–0815. https://doi.org/10.1371/journal.pcbi.0020095
Kaiser, M., Hilgetag, C.C., Van Ooyen, A., 2009. A simple rule for axon outgrowth and synaptic competition generates realistic connection lengths and filling fractions. Cerebral Cortex 19, 3001–3010. https://doi.org/10.1093/cercor/bhp071
Kaiser, M., Martin, R., Andras, P., Young, M.P., 2007. Simulation of robustness against lesions of cortical networks. European Journal of Neuroscience 25, 3185–3192. https://doi.org/10.1111/j.1460-9568.2007.05574.x

Kalmijn, S., Feskens, E.J.M., Launer, L.J., Kromhout, D., 1996. Cerebrovascular disease, the apolipoprotein e4 allele, and cognitive decline in a community-based study of elderly men. Stroke 27, 2230–2235. https://doi.org/10.1161/01.STR.27.12.2230

Kang, J.H., Korecka, M., Figurski, M.J., Toledo, J.B., Blennow, K., Zetterberg, H., Waligorska, T., Brylska, M., Fields, L., Shah, N., Soares, H., Dean, R.A., Vanderstichele, H., Petersen, R.C., Aisen, P.S., Saykin, A.J., Weiner, M.W., Trojanowski, J.Q., Shaw, L.M., 2015. The Alzheimer's Disease Neuroimaging Initiative 2 Biomarker Core: A review of progress and plans. Alzheimer's and Dementia 11, 772–791. https://doi.org/10.1016/j.jalz.2015.05.003

Karch, C.M., Goate, A.M., 2015. Alzheimer's disease risk genes and mechanisms of disease pathogenesis. Biological Psychiatry 77, 43–51. https://doi.org/10.1016/j.biopsych.2014.05.006

Karran, E., Mercken, M., Strooper, B. De, 2011. The amyloid cascade hypothesis for Alzheimer's disease: An appraisal for the development of therapeutics. Nature Reviews Drug Discovery. https://doi.org/10.1038/nrd3505

Kauwe, J.S.K., Wang, J., Mayo, K., Morris, J.C., Fagan, A.M., Holtzman, D.M., Goate, A.M., 2009. Alzheimer's disease risk variants show association with cerebrospinal fluid amyloid beta. neurogenetics 10, 13–17. https://doi.org/10.1007/s10048-008-0150-4

Kelly, C., Biswal, B.B., Craddock, R.C., Castellanos, F.X., Milham, M.P., 2012. Characterizing variation in the functional connectome: Promise and pitfalls. Trends in Cognitive Sciences 16, 181–188. https://doi.org/10.1016/j.tics.2012.02.001

Klupp, E., Förster, S., Grimmer, T., Tahmasian, M., Yakushev, I., Sorg, C., Yousefi, B.H., Drzezga, A., 2014. In Alzheimer's Disease, Hypometabolism in Low-Amyloid Brain Regions May Be a Functional Consequence of Pathologies in Connected Brain Regions. Brain Connectivity 4, 371–383. https://doi.org/10.1089/brain.2013.0212

Landau, S.M., Harvey, D., Madison, C.M., Reiman, E.M., Foster, N.L., Aisen, P.S., Petersen, R.C., Shaw, L.M., Trojanowski, J.Q., Jack, C.R., Weiner, M.W., Jagust, W.J., 2010. Comparing predictors of conversion and decline in mild cognitive impairment. Neurology 75, 230–238. https://doi.org/10.1212/WNL.0b013e3181e8e8b8

Latora, V., Marchiori, M., 2001. Efficient behavior of small-world networks. Physical review letters 87, 198701. https://doi.org/10.1103/PhysRevLett.87.198701

Lerch, J.P., Evans, A.C., 2005. Cortical thickness analysis examined through power analysis and a population simulation. NeuroImage 24, 163–173. https://doi.org/10.1016/j.neuroimage.2004.07.045

Lerch, J.P., Worsley, K., Shaw, W.P., Greenstein, D.K., Lenroot, R.K., Giedd, J., Evans, A.C., 2006. Mapping anatomical correlations across cerebral cortex (MACACC) using cortical thickness from MRI. NeuroImage 31, 993–1003. https://doi.org/10.1016/j.neuroimage.2006.01.042

Li, Y., Liu, Y., Li, J., Qin, W., Li, K., Yu, C., Jiang, T., 2009. Brain anatomical network and intelligence. PLoS Computational Biology 5. https://doi.org/10.1371/journal.pcbi.1000395

Liao, X., Yuan, L., Zhao, T., Dai, Z., Shu, N., Xia, M., Yang, Y., Evans, A., He, Y., 2015. Spontaneous functional network dynamics and associated structural substrates in the human brain. Frontiers in Human Neuroscience 9, 1–17. https://doi.org/10.3389/fnhum.2015.00478

Lind, J., Persson, J., Ingvar, M., Larsson, A., Cruts, M., Van Broeckhoven, C., Adolfsson, R., Bäckman, L., Nilsson, L.-G., Petersson, K.M., Nyberg, L., 2006. Reduced functional brain activity response in cognitively intact apolipoprotein E ε4 carriers. Brain 129, 1240–1248. https://doi.org/10.1093/brain/awl054

Liu, C.-C., Kanekiyo, T., Xu, H., Bu, G., Bu, G., 2013. Apolipoprotein E and Alzheimer disease: risk, mechanisms and therapy. Nature Reviews Neurology 9, 106–118. https://doi.org/10.1038/nrneurol.2012.263

Liu, L., Drouet, V., Wu, J.W., Witter, M.P., Small, S.A., Clelland, C., Duff, K., 2012. Trans-synaptic spread of tau pathology in vivo. PLoS ONE 7, 1–9. https://doi.org/10.1371/journal.pone.0031302

Lo, C., Wang, P., Chou, K., Wang, J., He, Y., Lin, C., 2010. Diffusion Tensor Tractography Reveals Abnormal Topological Organization in Structural Cortical Networks in Alzheimer's Disease -- Lo et al_ 30 (50) 16876 -- Journal of Neuroscience 30, 16876–16885. https://doi.org/10.1523/JNEUROSCI.4136-10.2010

Lopez, O.L., Jagust, W.J., DeKosky, S.T., Becker, J.T., Fitzpatrick, A., Dulberg, C., Breitner, J., Lyketsos, C., Jones, B., Kawas, C., Carlson, M., Kuller, L.H., 2003. Prevalence and classification of mild cognitive impairment in the cardiovascular health study cognition study. Archives of Neurology 60, 1385–1389. https://doi.org/10.1001/archneur.60.10.1385

Ma, C., Wang, J., Zhang, J., Chen, K., Li, X., Shu, N., Chen, Y., Liu, Z., Zhang, Z., 2017. Disrupted Brain Structural Connectivity: Pathological Interactions Between Genetic APOE ε4 Status and Developed MCI Condition. Molecular Neurobiology 54, 6999–7007. https://doi.org/10.1007/s12035-016-0224-5

Mahley, R.W., Huang, Y., 2012. Apolipoprotein E Sets the Stage: Response to Injury Triggers Neuropathology. Neuron 76, 871–885. https://doi.org/10.1016/j.neuron.2012.11.020

Mahley, R.W., Huang, Y., 2009. Alzheimer disease: Multiple causes, multiple effects of apolipoprotein E4, and multiple therapeutic approaches. Annals of Neurology. https://doi.org/10.1002/ana.21736
Mahley, R.W., Weisgraber, K.H., Huang, Y., 2006. Apolipoprotein E4: A causative factor and therapeutic target in neuropathology, including Alzheimer's disease. Proceedings of the National Academy of Sciences 103, 5644–5651. https://doi.org/10.1073/pnas.0600549103
Makris, N., Kaiser, J., Haselgrove, C., Seidman, L.J., Biederman, J., Boriel, D., Valera, E.M., Papadimitriou, G.M., Fischl, B., Caviness, V.S., Kennedy, D.N., 2006. Human cerebral cortex: A system for the integration of volume- and surface-based representations. NeuroImage 33, 139–153. https://doi.org/10.1016/j.neuroimage.2006.04.220
Mandelkow, E.M., Mandelkow, E., 1998. Tau in Alzheimer's disease. Trends in Cell Biology 8, 425–427. https://doi.org/10.1016/S0962-8924(98)01368-3
Markesbery, W.R., Schmitt, F.A., Kryscio, R.J., Davis, D.G., Smith, C.D., Wekstein, D.R., 2006. Neuropathologic substrate of mild cognitive impairment. Archives of Neurology 63, 38–46. https://doi.org/10.1001/archneur.63.1.38
Masters, C.L., Cappai, R., Barnham, K.J., Villemagne, V.L., 2006. Molecular mechanisms for Alzheimer's disease: Implications for neuroimaging and therapeutics. Journal of Neurochemistry. https://doi.org/10.1111/j.1471-4159.2006.03989.x
Matsuzaki, T., Sasaki, K., Tanizaki, Y., Hata, J., Fujimi, K., Matsui, Y., Sekita, A., Suzuki, S.O., Kanba, S., Kiyohara, Y., Iwaki, T., 2010. Insulin resistance is associated with the pathology of Alzheimer disease: The Hisayama study. Neurology 75, 764–770. https://doi.org/10.1212/WNL.0b013e3181eee25f
Mattsson, N., Zetterberg, H., Hansson, O., Andreasen, N., Parnetti, L., Jonsson, M., Herukka, S.K., Van Der Flier, W.M., Blankenstein, M.A., Ewers, M., Rich, K., Kaiser, E., Verbeek, M., Tsolaki, M., Mulugeta, E., Rosén, E., Aarsland, D., Jelle Visser, P., Schröder, J., Marcusson, J., De Leon, M., Hampel, H., Scheltens, P., Pirttilä, T., Wallin, A., Eriksdotter Jönhagen, M., Minthon, L., Winblad, B., Blennow, K., 2009. CSF biomarkers and incipient Alzheimer disease in patients with mild cognitive impairment. JAMA - Journal of the American Medical Association 302, 385–393. https://doi.org/10.1001/jama.2009.1064
McKhann, G., Drachman, D., Folstein, M., Katzman, R., Price, D., Stadlan, E.M., 1984. Clinical diagnosis of alzheimer's disease: Report of the NINCDS-ADRDA work group⋆ under the auspices of department of health and human services task force on alzheimer's disease. Neurology 34, 939–944. https://doi.org/10.1212/wnl.34.7.939
McKhann, G., Knopman, D.S., Chertkow, H., Hymann, B., Jack, C.R., Kawas, C., Klunk, W., Koroshetz, W., Manly, J., Mayeux, R., Mohs, R., Morris, J., Rossor, M., Scheltens, P., Carrillo, M., Weintrub, S., Phelphs, C., 2011. The diagnosis of dementia due to Alzheimer's disease: Recommendations from the National Institute on Aging- Alzheimer's Association workgroups on diagnostic guidelines for Alzheimer's disease. Alzheimers Dementia 7, 263–269. https://doi.org/10.1016/j.jalz.2011.03.005.The
Mechelli, A., Friston, K.J., Frackowiak, R.S., Price, C.J., 2005. Structural Covariance in the Human Cortex. The Journal of neuroscience : the official journal of the Society for Neuroscience 25, 8303–10. https://doi.org/10.1523/JNEUROSCI.0357-05.2005
Melie-Garcia, L., Sanabria-Diaz, G., Sanchez-Catasus, C., 2013. Studying the topological organization of the cerebral blood flow fluctuations in resting state. NeuroImage 64, 173–184. https://doi.org/10.1016/j.neuroimage.2012.08.082
Minoshima, S., Frey, K.A., Koeppe, R.A., Foster, N.L., Kuhl, D.E., 1995. A diagnostic approach in Alzheimer's disease using three-dimensional stereotactic surface projections of fluorine-18-FDG PET. Journal of Nuclear Medicine 36, 1238–1248.
Mishra, S., Blazey, T.M., Holtzman, D.M., Cruchaga, C., Su, Y., Morris, J.C., Benzinger, T.L.S., Gordon, B.A., 2018. Longitudinal brain imaging in preclinical Alzheimer disease: Impact of APOE ϵ4 genotype. Brain 141, 1828–1839. https://doi.org/10.1093/brain/awy103
Mišić, B., Betzel, R.F., de Reus, M.A., van den Heuvel, M.P., Berman, M.G., McIntosh, A.R., Sporns, O., 2016. Network-Level Structure-Function Relationships in Human Neocortex. Cerebral Cortex bhw089. https://doi.org/10.1093/cercor/bhw089
Montine, T.J., Phelps, C.H., Beach, T.G., Bigio, E.H., Cairns, N.J., Dickson, D.W., Duyckaerts, C., Frosch, M.P., Masliah, E., Mirra, S.S., Nelson, P.T., Schneider, J.A., Thal, D.R., Trojanowski, J.Q., Vinters, H. V., Hyman, B.T., 2012. National institute on aging-Alzheimer's association guidelines for the neuropathologic assessment of Alzheimer's disease: A practical approach. Acta Neuropathologica 123, 1–11. https://doi.org/10.1007/s00401-011-0910-3
Mosconi, L., Perani, D., Sorbi, S., Herholz, K., Nacmias, B., Holthoff, V., Salmon, E., Baron, J.-C., De Cristofaro, M.T.R., Padovani, a, Borroni, B., Franceschi, M., Bracco, L., Pupi, a, 2004. MCI conversion to dementia and the APOE genotype: A prediction study with FDG-PET. Neurology 63, 2332–2340. https://doi.org/10.1212/01.WNL.0000147469.18313.3B
Murphy, K.R., Landau, S.M., Choudhury, K.R., Hostage, C.A., Shpanskaya, K.S., Sair, H.I., Petrella, J.R.,

Wong, T.Z., Doraiswamy, P.M., 2013. Mapping the effects of ApoE4, age and cognitive status on 18F-florbetapir PET measured regional cortical patterns of beta-amyloid density and growth. NeuroImage 78, 474–480. https://doi.org/10.1016/j.neuroimage.2013.04.048
Nettiksimmons, J., DeCarli, C., Landau, S., Beckett, L., 2014. Biological heterogeneity in ADNI amnestic mild cognitive impairment. Alzheimer's & dementia : the journal of the Alzheimer's Association 10, 511-521.e1. https://doi.org/10.1016/j.jalz.2013.09.003
Newman, M., 2010. Networks: An Introduction, Networks: An Introduction. Oxford University Press. https://doi.org/10.1093/acprof:oso/9780199206650.001.0001
Palmqvist, S., Schöll, M., Strandberg, O., Mattsson, N., Stomrud, E., Zetterberg, H., Blennow, K., Landau, S., Jagust, W., Hansson, O., 2017. Earliest accumulation of β-amyloid occurs within the default-mode network and concurrently affects brain connectivity. Nature Communications 8, 1–13. https://doi.org/10.1038/s41467-017-01150-x
Park, L.Q., Gross, A.L., McLaren, D.G., Pa, J., Johnson, J.K., Mitchell, M., Manly, J.J., 2012. Confirmatory factor analysis of the ADNI neuropsychological battery. Brain Imaging and Behavior 6, 528–539. https://doi.org/10.1007/s11682-012-9190-3
Peila, R., Rodriguez, B.L., Launer, L.J., 2002. Type 2 diabetes, APOE gene, and the risk for dementia and related pathologies: The Honolulu-Asia Aging Study. Diabetes 51, 1256–1262. https://doi.org/10.2337/diabetes.51.4.1256
Pereira, J.B., Mijalkov, M., Kakaei, E., Mecocci, P., Vellas, B., Tsolaki, M., Kłoszewska, I., Soininen, H., Spenger, C., Lovestone, S., Simmons, A., Wahlund, L.O., Volpe, G., Westman, E., 2016. Disrupted Network Topology in Patients with Stable and Progressive Mild Cognitive Impairment and Alzheimer's Disease. Cerebral Cortex 26, 3476–3493. https://doi.org/10.1093/cercor/bhw128
Persson, J., Lind, J., Larsson, A., Ingvar, M., Sleegers, K., Van Broeckhoven, C., Adolfsson, R., Nilsson, L.G., Nyberg, L., 2008. Altered deactivation in individuals with genetic risk for Alzheimer's disease. Neuropsychologia 46, 1679–1687. https://doi.org/10.1016/j.neuropsychologia.2008.01.026
Petersen, R.C., 2016. Mild cognitive impairment. CONTINUUM Lifelong Learning in Neurology. https://doi.org/10.1212/CON.0000000000000313
Petersen, R.C., 2004. Mild cognitive impairment as a diagnostic entity, in: Journal of Internal Medicine. John Wiley & Sons, Ltd, pp. 183–194. https://doi.org/10.1111/j.1365-2796.2004.01388.x
Petersen, R.C., 2003. Mild Cognitive Impairment: Aging to Alzheimer's Disease.
Petersen, R.C., Doody, R., Kurz, A., Mohs, R.C., Morris, J.C., Rabins, P. V, Ritchie, K., Rossor, M., Thal, L., Winblad, B., 2001. Current concepts in mild cognitive impairment. Archives of neurology 58, 1985–92.
Petersen, R.C., Kokmen, E., Smith, G.E., Waring, S.C., Kurland, L.T., Ivnik, R.J., Tangalos, E.G., Schaid, D.J., Thibodeau, S.N., 1995. Apolipoprotein E Status as a Predictor of the Development of Alzheimer's Disease in Memory-Impaired Individuals. JAMA: The Journal of the American Medical Association 273, 1274–1278. https://doi.org/10.1001/jama.1995.03520400044042
Petersen, R.C., Morris, J.C., 2005. Mild cognitive impairment as a clinical entity and treatment target. Archives of Neurology. https://doi.org/10.1001/archneur.62.7.1160
Petersen, R.C., O'Brien, J., 2006. Mild cognitive impairment should be considered for DSM-V. Journal of Geriatric Psychiatry and Neurology. https://doi.org/10.1177/0891988706291085
Petersen, Ronald C., Smith, G.E., Waring, S.C., Ivnik, R.J., Tangalos, E.G., Kokmen, E., 1999. Mild cognitive impairment: Clinical characterization and outcome. Archives of Neurology 56, 303–308. https://doi.org/10.1001/archneur.56.3.303
Petersen, R C, Smith, G.E., Waring, S.C., Ivnik, R.J., Tangalos, E.G., Kokmen, E., 1999. Mild cognitive impairment: clinical characterization and outcome. Archives of neurology 56, 303–8.
Pievani, M., de Haan, W., Wu, T., Seeley, W.W., Frisoni, G.B., 2011. Functional network disruption in the degenerative dementias. The Lancet Neurology 10, 829–843. https://doi.org/10.1016/S1474-4422(11)70158-2
Plassman, B.L., Langa, K.M., Fisher, G.G., Heeringa, S.G., Weir, D.R., Ofstedal, M.B., Burke, J.R., Hurd, M.D., Potter, G.G., Rodgers, W.L., Steffens, D.C., Willis, R.J., Wallace, R.B., 2007. Prevalence of Dementia in the United States: The Aging, Demographics, and Memory Study. Neuroepidemiology 29, 125–132. https://doi.org/10.1159/000109998
Prestia, A., Caroli, A., Herholz, K., Reiman, E., Chen, K., Jagust, W.J., Frisoni, G.B., Amicucci, G., Archetti, S., Benussi, L., Binetti, G., Bocchio-Chiavetto, L., Bonetti, M., Canu, E., Caobelli, F., Cavedo, E., Chittò, E., Costardi, D., Cotelli, M., Galluzzi, S., Gennarelli, M., Geroldi, C., Ghidoni, R., Giubbini, R., Guerra, U.P., Kuffenschin, G., Lussignoli, G., Moretti, D., Orlandini, A., Paghera, B., Parapini, M., Paternicò, D., Porteri, C., Romano, M., Rosini, S., Scarpazza, C., Villa, I., Zanardini, R., Zanetti, O., 2013. Diagnostic accuracy of markers for prodromal Alzheimer's disease in independent clinical series. Alzheimer's and Dementia 9, 677–686. https://doi.org/10.1016/j.jalz.2012.09.016
Prince, M., Wimo, A., Guerchet, M., Ali, G.C., Wu, Y.-T., Prina, M.A., 2015. World Alzheimer Report 2015 -

The Global Impact of Dementia: An analysis of prevalence, incidence, cost and trends. undefined.
Querbes, O., Aubry, F., Pariente, J., Lotterie, J.-A., Démonet, J.-F., Duret, V., Puel, M., Berry, I., Fort, J.-C., Celsis, P., 2009. Early diagnosis of Alzheimer's disease using cortical thickness: impact of cognitive reserve. Brain : a journal of neurology 132, 2036–47. https://doi.org/10.1093/brain/awp105
Raber, J., Huang, Y., Ashford, J.W., 2004. ApoE genotype accounts for the vast majority of AD risk and AD pathology. Neurobiology of Aging 25, 641–650. https://doi.org/10.1016/j.neurobiolaging.2003.12.023
Raichle, M.E., MacLeod, A.M., Snyder, A.Z., Powers, W.J., Gusnard, D.A., Shulman, G.L., 2001. A default mode of brain function. Proceedings of the National Academy of Sciences of the United States of America 98, 676–82. https://doi.org/10.1073/pnas.98.2.676
Ramakers, I.H.G.B., Visser, P.J., Aalten, P., Bekers, O., Sleegers, K., van Broeckhoven, C.L., Jolles, J., Verhey, F.R.J., 2008. The Association between APOE Genotype and Memory Dysfunction in Subjects with Mild Cognitive Impairment Is Related to Age and Alzheimer Pathology. Dementia and Geriatric Cognitive Disorders 26, 101–108. https://doi.org/10.1159/000144072
Regeur, L., 2000. Increasing loss of brain tissue with increasing dementia: a stereological study of post-mortem brains from elderly females. European Journal of Neurology 7, 47–54. https://doi.org/10.1046/j.1468-1331.2000.00017.x
Reid, A.T., Evans, A.C., 2013. Structural networks in Alzheimer's disease. European Neuropsychopharmacology 23, 63–77. https://doi.org/10.1016/j.euroneuro.2012.11.010
Reiman, E.M., Caselli, R.J., Yun, L.S., Chen, K., Bandy, D., Minoshima, S., Thibodeau, S.N., Osborne, D., 1996. Preclinical evidence of Alzheimer's disease in persons homozygous for the ε4 allele for apolipoprotein E. New England Journal of Medicine 334, 752–758. https://doi.org/10.1056/NEJM199603213341202
Ridderinkhof, K.R., Ullsperger, M., Crone, E.A., Nieuwenhuis, S., 2004. The role of the medial frontal cortex in cognitive control. Science. https://doi.org/10.1126/science.1100301
Rimkus, C.M., Schoonheim, M.M., Steenwijk, M.D., Vrenken, H., Eijlers, A.J., Killestein, J., Wattjes, M.P., Leite, C.C., Barkhof, F., Tijms, B.M., 2019. Gray matter networks and cognitive impairment in multiple sclerosis. Multiple sclerosis (Houndmills, Basingstoke, England) 25, 382–391. https://doi.org/10.1177/1352458517751650
Risacher, S.L., Saykin, A.J., 2013. Neuroimaging and Other Biomarkers for Alzheimer's Disease: The Changing Landscape of Early Detection. https://doi.org/10.1146/annurev-clinpsy-050212-185535
Roses, A.D., 1996. Apolipoprotein E alleles as risk factors in Alzheimer's disease. Annual review of medicine 47, 387–400. https://doi.org/10.1146/annurev.med.47.1.387
Rubinov, M., Sporns, O., 2010. Complex network measures of brain connectivity: Uses and interpretations. NeuroImage 52, 1059–1069. https://doi.org/10.1016/j.neuroimage.2009.10.003
Rugg, M.D., Vilberg, K.L., 2013. Brain networks underlying episodic memory retrieval. Current Opinion in Neurobiology. https://doi.org/10.1016/j.conb.2012.11.005
Rusinek, H., De Santi, S., Frid, D., Tsui, W.H., Tarshish, C.Y., Convit, A., De Leon, M.J., 2003. Regional Brain Atrophy Rate Predicts Future Cognitive Decline: 6-Year Longitudinal MR Imaging Study of Normal Aging. Radiology 229, 691–696. https://doi.org/10.1148/radiol.2293021299
Sabbagh, M.N., Shah, F., Reid, R.T., Sue, L., Connor, D.J., Peterson, L.K.N., Beach, T.G., 2006. Pathologic and nicotinic receptor binding differences between mild cognitive impairment, Alzheimer disease, and normal aging. Archives of Neurology 63, 1771–1776. https://doi.org/10.1001/archneur.63.12.1771
Saito, Y., Murayama, S., 2007. Neuropathology of mild cognitive impairment. Neuropathology 27, 578–584. https://doi.org/10.1111/j.1440-1789.2007.00806.x
Salathé, M., Jones, J.H., 2010. Dynamics and Control of Diseases in Networks with Community Structure. PLoS Computational Biology 6, e1000736. https://doi.org/10.1371/journal.pcbi.1000736
Salehi, A., Delcroix, J.D., Belichenko, P. V., Zhan, K., Wu, C., Valletta, J.S., Takimoto-Kimura, R., Kleschevnikov, A.M., Sambamurti, K., Chung, P.P., Xia, W., Villar, A., Campbell, W.A., Kulnane, L.S., Nixon, R.A., Lamb, B.T., Epstein, C.J., Stokin, G.B., Goldstein, L.S.B., Mobley, W.C., 2006. Increased App Expression in a Mouse Model of Down's Syndrome Disrupts NGF Transport and Causes Cholinergic Neuron Degeneration. Neuron 51, 29–42. https://doi.org/10.1016/j.neuron.2006.05.022
Salmon, E., Kerrouche, N., Perani, D., Lekeu, F., Holthoff, V., Beuthien-Baumann, B., Sorbi, S., Lemaire, C., Collette, F., Herholz, K., 2009. On the multivariate nature of brain metabolic impairment in Alzheimer's disease. Neurobiology of Aging 30, 186–197. https://doi.org/10.1016/j.neurobiolaging.2007.06.010
Salvador, R., Suckling, J., Schwarzbauer, C., Bullmore, E., 2005. Undirected graphs of frequency-dependent functional connectivity in whole brain networks. Philosophical Transactions of the Royal Society B: Biological Sciences 360, 937–946. https://doi.org/10.1098/rstb.2005.1645
Sanabria-Diaz, G., Martínez-Montes, E., Melie-Garcia, L., 2013. Glucose Metabolism during Resting State Reveals Abnormal Brain Networks Organization in the Alzheimer's Disease and Mild Cognitive Impairment. PLoS ONE 8. https://doi.org/10.1371/journal.pone.0068860

Sanabria-Diaz, G., Melie-Garcia, L., Iturria-Medina, Y., Aleman-Gomez, Y., Hernandez-Gonzalez, G., Valdes-Urrutia, L., Galan, L., Valdes-Sosa, P., 2010. Surface area and cortical thickness descriptors reveal different attributes of the structural human brain networks. NeuroImage 50, 1497–1510.

Sánchez-Catasús, C.A., Sanabria-Diaz, G., Willemsen, A., Martinez-Montes, E., Samper-Noa, J., Aguila-Ruiz, A., Boellaard, R., De Deyn, P., Dierckx, R.A.J.O., Melie-Garcia, L., 2017. Subtle alterations in cerebrovascular reactivity in mild cognitive impairment detected by graph theoretical analysis and not by the standard approach. NeuroImage: Clinical 15, 151–160. https://doi.org/10.1016/j.nicl.2017.04.019

Sanz-Arigita, E.J., Schoonheim, M.M., Damoiseaux, J.S., Rombouts, S.A.R.B., Maris, E., Barkhof, F., Scheltens, P., Stam, C.J., 2010. Loss of "Small-World" Networks in Alzheimer's Disease: Graph Analysis of fMRI Resting-State Functional Connectivity. PLoS ONE 5. https://doi.org/10.1371/journal.pone.0013788

Scheltens, P., Blennow, K., Breteler, M.M.B., de Strooper, B., Frisoni, G.B., Salloway, S., Van der Flier, W.M., 2016. Alzheimer's disease. The Lancet. https://doi.org/10.1016/S0140-6736(15)01124-1

Schultz, A.P., Chhatwal, J.P., Hedden, T., Mormino, E.C., Hanseeuw, B.J., Sepulcre, J., Huijbers, W., LaPoint, M., Buckley, R.F., Johnson, K.A., Sperling, R.A., 2017. Phases of Hyperconnectivity and Hypoconnectivity in the Default Mode and Salience Networks Track with Amyloid and Tau in Clinically Normal Individuals. The Journal of neuroscience : the official journal of the Society for Neuroscience 37, 4323–4331. https://doi.org/10.1523/JNEUROSCI.3263-16.2017

Seeley, W.W., Crawford, R.K., Zhou, J., Miller, B.L., Greicius, M.D., 2009. Neurodegenerative Diseases Target Large-Scale Human Brain Networks. Neuron 62, 42–52. https://doi.org/10.1016/j.neuron.2009.03.024

Segall, J.M., Allen, E.A., Jung, R.E., Erhardt, E.B., Arja, S.K., Kiehl, K., Calhoun, V.D., 2012. Correspondence between structure and function in the human brain at rest. Frontiers in Neuroinformatics 6. https://doi.org/10.3389/fninf.2012.00010

Selkoe, D.J., 2002. Alzheimer's disease is a synaptic failure. Science. https://doi.org/10.1126/science.1074069

Seo, E.H., Lee, D.Y., Lee, J., Park, J., Sohn, B.K., Min, Y., Byun, M.S., Choi, H.J., Woo, J.I., 2013. Influence of APOE Genotype on Whole-Brain Functional Networks in Cognitively Normal Elderly. PLoS ONE 8, 2–10. https://doi.org/10.1371/journal.pone.0083205

Serrano-Pozo, A., Frosch, M.P., Masliah, E., Hyman, B.T., 2011. Neuropathological alterations in Alzheimer disease. Cold Spring Harbor Perspectives in Medicine 1, a006189. https://doi.org/10.1101/cshperspect.a006189

Shi, Y., Yamada, K., Liddelow, S.A., Smith, S.T., Zhao, L., Luo, W., Tsai, R.M., Spina, S., Grinberg, L.T., Rojas, J.C., Gallardo, G., Wang, K., Roh, J., Robinson, G., Finn, M.B., Jiang, H., Sullivan, P.M., Baufeld, C., Wood, M.W., Sutphen, C., McCue, L., Xiong, C., Del-Aguila, J.L., Morris, J.C., Cruchaga, C., Fagan, A.M., Miller, B.L., Boxer, A.L., Seeley, W.W., Butovsky, O., Barres, B.A., Paul, S.M., Holtzman, D.M., Holtzman, D.M., 2017. ApoE4 markedly exacerbates tau-mediated neurodegeneration in a mouse model of tauopathy. Nature 549, 523–527. https://doi.org/10.1038/nature24016

Singh, V., Chertkow, H., Lerch, J.P., Evans, A.C., Dorr, A.E., Kabani, N.J., 2006. Spatial patterns of cortical thinning in mild cognitive impairment and Alzheimer's disease. Brain 129, 2885–2893. https://doi.org/10.1093/brain/awl256

Slooter, A.J.C., Cruts, M., Kalmijn, S., Hofman, A., Breteler, M.M.B., Van Broeckhoven, C., Van Duijn, C.M., 1998. Risk estimates of dementia by apolipoprotein E genotypes from a population-based incidence study: The Rotterdam study. Archives of Neurology 55, 964–968. https://doi.org/10.1001/archneur.55.7.964

Small, G.W., Ercoli, L.M., Silverman, D.H.S., Huang, S.C., Komo, S., Bookheimer, S.Y., Lavretsky, H., Miller, K., Siddarth, P., Rasgon, N.L., Mazziotta, J.C., Saxena, S., Wu, H.M., Mega, M.S., Cummings, J.L., Saunders, A.M., Pericak-Vance, M.A., Roses, A.D., Barrio, J.R., Phelps, M.E., 2000. Cerebral metabolic and cognitive decline in persons at genetic risk for Alzheimer's disease. Proceedings of the National Academy of Sciences of the United States of America 97, 6037–6042. https://doi.org/10.1073/pnas.090106797

Sperling, R.A., Aisen, P.S., Beckett, L.A., Bennett, D.A., Craft, S., Fagan, A.M., Iwatsubo, T., Jack, C.R., Kaye, J., Montine, T.J., Park, D.C., Reiman, E.M., Rowe, C.C., Siemers, E., Stern, Y., Yaffe, K., Carrillo, M.C., Thies, B., Morrison-Bogorad, M., Wagster, M. V., Phelps, C.H., 2011. Toward defining the preclinical stages of Alzheimer's disease: Recommendations from the National Institute on Aging-Alzheimer's Association workgroups on diagnostic guidelines for Alzheimer's disease. Alzheimer's and Dementia 7, 280–292. https://doi.org/10.1016/j.jalz.2011.03.003

Sporns, O., 2011. The human connectome: A complex network. Annals of the New York Academy of Sciences. https://doi.org/10.1111/j.1749-6632.2010.05888.x

Sporns, O., Chialvo, D.R., Kaiser, M., Hilgetag, C.C., 2004. Organization, development and function of complex brain networks. Trends in Cognitive Sciences 8, 418–425. https://doi.org/10.1016/j.tics.2004.07.008

Sporns, O., Honey, C.J., Kötter, R., 2007. Identification and Classification of Hubs in Brain Networks. PLoS

ONE 2, e1049. https://doi.org/10.1371/journal.pone.0001049
Sporns, O., Tononi, G., Kötter, R., 2005. The human connectome: A structural description of the human brain. PLoS Computational Biology 1, 0245–0251. https://doi.org/10.1371/journal.pcbi.0010042
Stam, C.J., 2010. Characterization of anatomical and functional connectivity in the brain: A complex networks perspective. International Journal of Psychophysiology 77, 186–194. https://doi.org/10.1016/j.ijpsycho.2010.06.024
Stam, C.J., De Haan, W., Daffertshofer, A., Jones, B.F., Manshanden, I., Van Cappellen Van Walsum, A.M., Montez, T., Verbunt, J.P.A., De Munck, J.C., Van Dijk, B.W., Berendse, H.W., Scheltens, P., 2009. Graph theoretical analysis of magnetoencephalographic functional connectivity in Alzheimer's disease. Brain 132, 213–224. https://doi.org/10.1093/brain/awn262
Sun, Z.-W., Zhu, Y.-X., Liu, H.-Y., Liu, J., Zhu, X.-Q., Zhou, J.-N., Liu, R.-Y., 2007. Decreased cerebral blood flow velocity in apolipoprotein E epsilon4 allele carriers with mild cognitive impairment. European journal of neurology : the official journal of the European Federation of Neurological Societies 14, 150–5. https://doi.org/10.1111/j.1468-1331.2006.01579.x
Supekar, K., Menon, V., Rubin, D., Musen, M., Greicius, M.D., 2008. Network analysis of intrinsic functional brain connectivity in Alzheimer's disease. PLoS Computational Biology 4. https://doi.org/10.1371/journal.pcbi.1000100
Tai, L.M., Thomas, R., Marottoli, F.M., Koster, K.P., Kanekiyo, T., Morris, A.W.J., Bu, G., 2016. The role of APOE in cerebrovascular dysfunction. Acta Neuropathologica. https://doi.org/10.1007/s00401-016-1547-z
ten Kate, M., Visser, P.J., Bakardjian, Hovagim, Barkhof, F., Sikkes, S.A.M., van der Flier, W.M., Scheltens, P., Hampel, Harald, Habert, Marie Odile, Dubois, Bruno, Tijms, B.M., 2018. Gray matter network disruptions and regional amyloid beta in cognitively normal adults. Frontiers in Aging Neuroscience 10. https://doi.org/10.3389/fnagi.2018.00067
Teter, B., Raber, J., Nathan, B., Crutcher, K.A., 2002. The presence of apoE4, not the absence of apoE3, contributes to AD pathology. Journal of Alzheimer's Disease. https://doi.org/10.3233/JAD-2002-4305
Thal, D.R., Capetillo-Zarate, E., Del Tredici, K., Braak, H., 2006. The Development of Amyloid beta Protein Deposits in the Aged Brain. Science of Aging Knowledge Environment 2006, re1–re1. https://doi.org/10.1126/sageke.2006.6.re1
Thompson, W.K., Hallmayer, J., O'Hara, R., 2011. Design Considerations for Characterizing Psychiatric Trajectories Across the Lifespan: Application to Effects of APOE-e4 on Cerebral Cortical Thickness in Alzheimer's Disease. American Journal of Psychiatry 168, 894–903. https://doi.org/10.1176/appi.ajp.2011.10111690
Tijms, B.M., Gouw, A.A., Borta, A., Verfaillie, S., Teunissen, C.E., Scheltens, P., Barkhof, F., Flier, W.M. Van Der, 2018. Gray matter networks and clinical progression in subjects with predementia Alzheimer ' s disease. Neurobiology of Aging 61, 75–81. https://doi.org/10.1016/j.neurobiolaging.2017.09.011
Tijms, B.M., Kate, M. Ten, Wink, A.M., Visser, P.J., Ecay, M., Clerigue, M., Estanga, A., Garcia Sebastian, M., Izagirre, A., Villanua, J., Martinez Lage, P., van der Flier, W.M., Scheltens, P., Sanz Arigita, E., Barkhof, F., 2016. Gray matter network disruptions and amyloid beta in cognitively normal adults. Neurobiology of aging 37, 154–60. https://doi.org/10.1016/j.neurobiolaging.2015.10.015
Tijms, B.M., Möller, C., Vrenken, H., Wink, A.M., de Haan, W., van der Flier, W.M., Stam, C.J., Scheltens, P., Barkhof, F., 2013a. Single-Subject Grey Matter Graphs in Alzheimer's Disease. PLoS ONE 8, e58921. https://doi.org/10.1371/journal.pone.0058921
Tijms, B.M., Seris, P., Willshaw, D.J., Lawrie, S.M., 2012. Similarity-based extraction of individual networks from gray matter MRI scans. Cerebral Cortex 22, 1530–1541. https://doi.org/10.1093/cercor/bhr221
Tijms, B.M., Wink, A.M., de Haan, W., van der Flier, W.M., Stam, C.J., Scheltens, P., Barkhof, F., 2013b. Alzheimer's disease: connecting findings from graph theoretical studies of brain networks. Neurobiology of Aging 34, 2023–2036. https://doi.org/10.1016/j.neurobiolaging.2013.02.020
Tijms, B.M., Yeung, H.M., Sikkes, S.A.M., Möller, C., Smits, L.L., Stam, C.J., Scheltens, P., van der Flier, W.M., Barkhof, F., 2014. Single-Subject Gray Matter Graph Properties and Their Relationship with Cognitive Impairment in Early- and Late-Onset Alzheimer's Disease. Brain Connectivity 4, 337–346. https://doi.org/10.1089/brain.2013.0209
Tiraboschi, P., Hansen, L.A., Masliah, E., Alford, M., Thal, L.J., Corey-Bloom, J., 2004. Impact of APOE genotype on neuropathologic and neurochemical markers of Alzheimer disease. Neurology 62, 1977–83.
Toledo, J.B., Da, X., Weiner, M.W., Wolk, D.A., Xie, S.X., Arnold, S.E., Davatzikos, C., Shaw, L.M., Trojanowski, J.Q., 2014. CSF Apo-E levels associate with cognitive decline and MRI changes. Acta Neuropathologica 127, 621–632. https://doi.org/10.1007/s00401-013-1236-0
Tononi, G., Sporns, O., Edelman, G.M., 1994. A measure for brain complexity: relating functional segregation and integration in the nervous system. Proceedings of the National Academy of Sciences of the United States of America 91, 5033–7.

Trojanowski, J.Q., Lee, V.M.Y., 2000. “Fatal Attractions” of proteins: A comprehensive hypothetical mechanism underlying Alzheimer’s disease and other neurodegenerative disorders, in: Annals of the New York Academy of Sciences. New York Academy of Sciences, pp. 62–67. https://doi.org/10.1111/j.1749-6632.2000.tb05561.x

Tuminello, E.R., Han, S.D., 2011. The Apolipoprotein E Antagonistic Pleiotropy Hypothesis: Review and Recommendations. International Journal of Alzheimer’s Disease 2011, 1–12. https://doi.org/10.4061/2011/726197

Tzourio-Mazoyer, N., Landeau, B., Papathanassiou, D., Crivello, F., Etard, O., Delcroix, N., Mazoyer, B., Joliot, M., 2002. Automated anatomical labeling of activations in SPM using a macroscopic anatomical parcellation of the MNI MRI single-subject brain. NeuroImage 15, 273–289. https://doi.org/10.1006/nimg.2001.0978

Van Den Heuvel, M.P., Stam, C.J., Kahn, R.S., Hulshoff Pol, H.E., 2009. Efficiency of functional brain networks and intellectual performance. Journal of Neuroscience 29, 7619–7624. https://doi.org/10.1523/JNEUROSCI.1443-09.2009

Vemuri, P., Wiste, H.J., Weigand, S.D., Knopman, D.S., Shaw, L.M., Trojanowski, J.Q., Aisen, P.S., Weiner, M., Petersen, R.C., Jack, C.R., Alzheimer’s Disease Neuroimaging Initiative, Initiative, on behalf of the A.D.N., 2010. Effect of apolipoprotein E on biomarkers of amyloid load and neuronal pathology in Alzheimer disease. Annals of neurology 67, 308–16. https://doi.org/10.1002/ana.21953

Verfaillie, S.C.J., Slot, R.E.R., Dicks, E., Prins, N.D., Overbeek, J.M., Teunissen, C.E., Scheltens, P., Barkhof, F., van der Flier, W.M., Tijms, B.M., 2018. A more randomly organized grey matter network is associated with deteriorating language and global cognition in individuals with subjective cognitive decline. Human Brain Mapping 39, 3143–3151. https://doi.org/10.1002/hbm.24065

Vermunt, L., Sikkes, S.A.M., van den Hout, A., Handels, R., Bos, I., van der Flier, W.M., Kern, S., Ousset, Pierre Jean, Maruff, P., Skoog, I., Verhey, F.R.J., Freund-Levi, Y., Tsolaki, Magda, Wallin, Å.K., Olde Rikkert, M., Soininen, H., Spiru, Luisa, Zetterberg, H., Blennow, K., Scheltens, Philip, Muniz-Terrera, G., Visser, P.J., Vellas, B., Reynish, E., Ousset, P. J., Andrieu, S., Burns, A., Pasquier, F., Frisoni, G., Salmon, E., Michel, J.P., Zekry, D.S., Boada, M., Dartigues, J.F., Olde-Rikkert, M.G.M., Rigaud, A.S., Winblad, B., Malick, A., Sinclair, A., Frölich, L., Scheltens, P., Ribera, C., Touchon, J., Robert, P., Salva, A., Waldemar, G., Bullock, R., Tsolaki, M., Rodriguez, G., Spiru, L., Jones, R.W., Stiens, G., Stoppe, G., Eriksdotter Jönhagen, M., Cherubini, A., Lage, P.M., Gomez-Isla, T., Camus, V., Agüera-Morales, E., Lopez, F., Savy, S., Cantet, C., Coley, N., 2019. Duration of preclinical, prodromal, and dementia stages of Alzheimer’s disease in relation to age, sex, and APOE genotype. Alzheimer’s and Dementia 15, 888–898. https://doi.org/10.1016/j.jalz.2019.04.001

Villain, N., Chételat, G., Grassiot, B., Bourgeat, P., Jones, G., Ellis, K.A., Ames, D., Martins, R.N., Eustache, F., Salvado, O., Masters, C.L., Rowe, C.C., Villemagne, V.L., 2012. Regional dynamics of amyloid-β deposition in healthy elderly, mild cognitive impairment and Alzheimer’s disease: a voxelwise PiB–PET longitudinal study. Brain 135, 2126–2139. https://doi.org/10.1093/brain/aws125

Villeneuve, S., Rabinovici, G.D., Cohn-Sheehy, B.I., Madison, C., Ayakta, N., Ghosh, P.M., La Joie, R., Arthur-Bentil, S.K., Vogel, J.W., Marks, S.M., Lehmann, M., Rosen, H.J., Reed, B., Olichney, J., Boxer, A.L., Miller, B.L., Borys, E., Jin, L.-W., Huang, E.J., Grinberg, L.T., DeCarli, C., Seeley, W.W., Jagust, W., 2015. Existing Pittsburgh Compound-B positron emission tomography thresholds are too high: statistical and pathological evaluation. Brain 138, 2020–2033. https://doi.org/10.1093/brain/awv112

Voevodskaya, O., Pereira, J.B., Volpe, G., Lindberg, O., Stomrud, E., van Westen, D., Westman, E., Hansson, O., 2018. Altered structural network organization in cognitively normal individuals with amyloid pathology. Neurobiology of Aging 64, 15–24. https://doi.org/10.1016/j.neurobiolaging.2017.11.014

Vos, S.J.B., van Rossum, I.A., Verhey, F., Knol, D.L., Soininen, H., Wahlund, L.-O., Hampel, H., Tsolaki, M., Minthon, L., Frisoni, G.B., Froelich, L., Nobili, F., van der Flier, W., Blennow, K., Wolz, R., Scheltens, P., Visser, P.J., 2013. Prediction of Alzheimer disease in subjects with amnestic and nonamnestic MCI. Neurology 80, 1124–32. https://doi.org/10.1212/WNL.0b013e318288690c

Wang, J., Wang, X., He, Yi, Yu, X., Wang, H., He, Yong, 2015. Apolipoprotein E4 modulates functional brain connectome in Alzheimer’s disease. Human Brain Mapping 36, 1828–1846. https://doi.org/10.1002/hbm.22740

Wang, Z., Dai, Z., Shu, H., Liao, X., Yue, C., Liu, D., Guo, Q., He, Y., Zhang, Z., 2017. APOE Genotype Effects on Intrinsic Brain Network Connectivity in Patients with Amnestic Mild Cognitive Impairment. Scientific reports 7, 397. https://doi.org/10.1038/s41598-017-00432-0

Ward, R.J., Zucca, F.A., Duyn, J.H., Crichton, R.R., Zecca, L., 2014. The role of iron in brain ageing and neurodegenerative disorders. The Lancet Neurology. https://doi.org/10.1016/S1474-4422(14)70117-6

Warwick, J.M., 2004. Imaging of brain function using SPECT, in: Metabolic Brain Disease. Springer, pp. 113–123. https://doi.org/10.1023/B:MEBR.0000027422.48744.a3

Watts, D.J., Strogatz, S.H., 1998. Collective dynamics of “small-world” networks. Nature 393, 440–2.

https://doi.org/10.1038/30918
Wen, W., He, Y., Sachdev, P., 2011. Structural brain networks and neuropsychiatric disorders. Curr Opin Psychiatry 24, 219–225. https://doi.org/10.1097/YCO.0b013e32834591f8
Westlye, L.T., Reinvang, I., Rootwelt, H., Espeseth, T., 2012. Effects of APOE on brain white matter microstructure in healthy adults. Neurology 1961–1969. https://doi.org/10.1212/WNL.0b013e3182735c9c
Winblad, B., Palmer, K., Kivipelto, M., Jelic, V., Fratiglioni, L., Wahlund, L.O., Nordberg, A., Bäckman, L., Albert, M., Almkvist, O., Arai, H., Basun, H., Blennow, K., De Leon, M., Decarli, C., Erkinjuntti, T., Giacobini, E., Graff, C., Hardy, J., Jack, C., Jorm, A., Ritchie, K., Van Duijn, C., Visser, P., Petersen, R.C., 2004. Mild cognitive impairment - Beyond controversies, towards a consensus: Report of the International Working Group on Mild Cognitive Impairment, in: Journal of Internal Medicine. J Intern Med, pp. 240–246. https://doi.org/10.1111/j.1365-2796.2004.01380.x
Wolk, D.A., Price, J.C., Saxton, J.A., Snitz, B.E., James, J.A., Lopez, O.L., Aizenstein, H.J., Cohen, A.D., Weissfeld, L.A., Mathis, C.A., Klunk, W.E., DeKoskym, S.T., 2009. Amyloid imaging in mild cognitive impairment subtypes. Annals of Neurology 65, 557–568. https://doi.org/10.1002/ana.21598
Woodard, J.L., Seidenberg, M., Nielson, K.A., Antuono, P., Guidotti, L., Durgerian, S., Zhang, Q., Lancaster, M., Hantke, N., Butts, A., Rao, S.M., 2009. Semantic memory activation in amnestic mild cognitive impairment. Brain 132, 2068–2078. https://doi.org/10.1093/brain/awp157
Wright, I.C., Sharma, T., Ellison, Z.R., McGuire, P.K., Friston, K.J., Brammer, M.J., Murray, R.M., Bullmore, E.T., 1999. Supra-regional brain systems and the neuropathology of schizophrenia. Cerebral Cortex 9, 366–378. https://doi.org/10.1093/cercor/9.4.366
Xie, T., He, Y., 2012. Mapping the Alzheimer's Brain with Connectomics. Frontiers in Psychiatry 2, 1–14. https://doi.org/10.3389/fpsyt.2011.00077
Yamazaki, Y., Painter, M.M., Bu, G., Kanekiyo, T., 2016. Apolipoprotein E as a Therapeutic Target in Alzheimer's Disease: A Review of Basic Research and Clinical Evidence. CNS Drugs 30, 773–789. https://doi.org/10.1007/s40263-016-0361-4
Yamazaki, Y., Zhao, N., Caulfield, T.R., Liu, C.C., Bu, G., 2019. Apolipoprotein E and Alzheimer disease: pathobiology and targeting strategies. Nature Reviews Neurology. https://doi.org/10.1038/s41582-019-0228-7
Yao, Z., Hu, B., Zheng, J., Zheng, W., Chen, X., Gao, X., Xie, Y., Fang, L., 2015. A FDG-PET study of metabolic networks in apolipoprotein E ε4 allele carriers. PLoS ONE 10, 1–16. https://doi.org/10.1371/journal.pone.0132300
Yao, Z., Zhang, Y., Lin, L., Zhou, Y., Xu, C., Jiang, T., Initiative, the A.D.N., 2010. Abnormal Cortical Networks in Mild Cognitive Impairment and Alzheimer's Disease. PLoS Computational Biology 6, e1001006. https://doi.org/10.1371/journal.pcbi.1001006
Ye, Q., Su, F., Shu, H., Gong, L., Xie, C., Zhang, Z., Bai, F., 2017. The apolipoprotein E gene affects the three-year trajectories of compensatory neural processes in the left-lateralized hippocampal network. Brain Imaging and Behavior 11, 1446–1458. https://doi.org/10.1007/s11682-016-9623-5
Zhao, X., Liu, Y., Wang, X., Liu, B., Xi, Q., Guo, Q., Jiang, H., Jiang, T., Wang, P., 2012. Disrupted Small-World Brain Networks in Moderate Alzheimer's Disease: A Resting-State fMRI Study. PLoS ONE 7, e33540. https://doi.org/10.1371/journal.pone.0033540
Zielinski, B.A., Gennatas, E.D., Zhou, J., Seeley, W.W., 2010. Network-level structural covariance in the developing brain. Proceedings of the National Academy of Sciences of the United States of America 107, 18191–18196. https://doi.org/10.1073/pnas.1003109107

6 ARTICLES

6.1 Apolipoprotein E4 effects on Topological Brain Network Organization in Mild Cognitive Impairment

scientific reports

Check for updates

OPEN

Apolipoprotein E4 effects on topological brain network organization in mild cognitive impairment

Gretel Sanabria-Diaz[1]✉, Lester Melie-Garcia[1], Bogdan Draganski[1], Jean-Francois Demonet[2] & Ferath Kherif[1]

The Apolipoprotein E isoform E4 (ApoE4) is consistently associated with an elevated risk of developing late-onset Alzheimer's Disease (AD); however, less is known about the potential genetic modulation of the brain networks organization during prodromal stages like Mild Cognitive Impairment (MCI). To investigate this issue during this critical stage, we used a dataset with a cross-sectional sample of 253 MCI patients divided into ApoE4-positive ('Carriers') and ApoE4-negative ('non-Carriers'). We estimated the cortical thickness (CT) from high-resolution T1-weighted structural magnetic images to calculate the correlation among anatomical regions across subjects and build the CT covariance networks (*CT-Nets*). The topological properties of *CT-Nets* were described through the graph theory approach. Specifically, our results showed a significant decrease in characteristic path length, clustering-index, local efficiency, global connectivity, modularity, and increased global efficiency for Carriers compared to non-Carriers. Overall, we found that ApoE4 in MCI shaped the topological organization of *CT-Nets*. Our results suggest that in the MCI stage, the ApoE4 disrupting the CT correlation between regions may be due to adaptive mechanisms to sustain the information transmission across distant brain regions to maintain the cognitive and behavioral abilities before the occurrence of the most severe symptoms.

Late-onset Alzheimer's Disease (AD) is a degenerative brain disease and the most common form of dementia in late-life, affecting millions of people worldwide[1]. Because of the lack of treatment, identifying causal risk factors at the early stages is paramount in clinical investigation. Most of the research is focusing its attention on the Mild Cognitive Impairment (MCI) stage. MCI is considered an intermediate phase between normal aging and AD. It is mainly characterized by a decline in cognitive abilities that do not interfere with daily functioning[2]. These patients are at increased risk of developing AD or another dementia[1]. Epidemiological research suggests an estimated 40% to 60% of MCI individuals aged 58 years and older have underlying AD pathology[3,4].

Nevertheless, MCI does not always lead to dementia; some patients remain stable or revert to a normal state while other progress to different brain pathologies. This clinical variability is based on the interplay between physiological, environmental, and genetic factors as part of the disease multifactorial etiology[5,6]. In those MCI cases destined to evolve to Alzheimer's Disease, this "window" is an opportunity to develop biomarkers that help to identify etiology and predict progression.

Our study is motivated by the fact that the Apolipoprotein E isoform E4 (ApoE4) is the best-established genetic risk factor for AD[7]. Among MCI ApoE4 Carriers, previous studies have reported an increased risk of developing AD, a younger mean age of onset and more rapid cognitive decline than non-Carriers[8]. Likewise, in MCI, the prevalence of this genotype is substantially higher than in control individuals[9]. The ApoE4 mechanisms in AD's pathogenesis are not entirely understood but have been related to amyloid-β-dependent and independent pathways[10]. Although the amount of evidence linking ApoE4 with cognitive deficits, morphological, structural, and functional brain alterations during AD progression[11,12] at this point, it is still unclear how this genetic risk factor impairs the brain networks organization.

Our study's second motivation is based on previous research supporting the idea of AD being a disconnection syndrome, which disrupts higher-order neuronal networks[13]. In this context, using a network-based approach

[1]Laboratoire de Recherche en Neuroimagerie (LREN), Département des neurosciences cliniques, Centre Hospitalier Universitaire Vaudois (CHUV), Mont Paisible 16, 1011 Lausanne, Switzerland. [2]Leenaards Memory Center, Lausanne University Hospital (CHUV), Lausanne, Switzerland. ✉email: gretels.sanabria@gmail.com

is critical to understand brain alterations and cognitive deficits during the disease progression. One feasible mathematical approach to elucidate the AD impact on brain networks is the graph formalism[14]. In graph theory terms, our brain is studied as a model to describe some essential elements -nodes- (brain regions) and the relationship between them (edges). Afterward, the brain complex covariance patterns are translated into global and regional graph metrics[15]. During the last decade, the graph analysis has been applied to characterize the brain structural covariance in AD and MCI[16]. It is based on the phenomenon that regions correlated in morphometric descriptors (i.e., cortical thickness) are often part of the same brain system that subserve specific behavioral and cognitive functions[17]. The mechanisms underlying these coordinated patterns seem to be related to mutually trophic effects, common pathological vulnerabilities, and genetic factors[16].

Following this modeling approach, studies using different neuroimaging modalities have shown aberrant brain network properties in AD, MCI, and preclinical states[18]. They revealed disease-related network alterations such as a loss of balance between segregation and integration of information (small-world attribute) and redistribution of regions considered central for the information flux over the network (hub regions)[19–23]. Additionally, Alzheimer's patients show decreased long-distance-interhemispheric correlations- and increased correlations between brain regions targeted by the disease[18,19,23]. These disruptions could reflect that the whole-brain network is more segregated and less integrated during AD progression than in healthy individuals. Despite such findings, the ApoE4 risk factor's inclusion has been scarce and limited mostly to healthy aging subjects and AD patients[24–28].

There is only a handful of investigations on the ApoE4 effects on topological brain networks organizations in MCI. Two studies using resting-state Functional Magnetic Imaging (rs-fMRI) and diffusion weight imaging (DWI) compared MCI Carrier and non-Carriers groups[29,30]. In both cases, the network analysis showed specific aberrant patterns in MCI Carriers. Yao and colleagues[31] reported for the first time differences between Carriers and non-Carriers based on metabolic covariance networks using Fluorodeoxyglucose Positron Emission Tomography (FDG-PET). Carriers were found to have lower clustering index and disruptive long-distance interregional correlations.

Nevertheless, ApoE4-related effects on the structural covariance network topology have not yet been fully explored in MCI. Such work is necessary to clarify how the genetic risks mediate and constrain the covariance patterns and the phenotypic expression in MCI. The identification of these subtle alterations at the network level may help detect, at earlier stages, the risk of AD progression in MCI ApoE4 Carriers compared to other disease-related markers like atrophy.

Precisely, we focus on the ApoE4-related modulation of the topological organization of cortical thickness covariance brain networks in MCI through structural MRI (sMRI) and graph-theory approach. We examine different features of the structural brain topology: (1) regional cortical thickness, (2) global network attributes (clustering index, characteristic path length, local and global efficiency, global connectivity, and homologous region connectivity) (3) nodal properties (normalized betweenness centrality, hubs) (4) network community detection (modularity) and resilience to insults (target attack). We hypothesize that ApoE4 is related to both local and global network properties changes in MCI.

Materials and methods

Subjects. Data used in the preparation of this article were obtained from the Alzheimer's Disease Neuroimaging Initiative (ADNI) database (adni.loni.usc.edu). The ADNI was launched in 2003 as a public–private partnership, led by Principal Investigator Michael W. Weiner, MD. ADNI's primary objective has been to test whether serial magnetic resonance imaging, positron emission tomography, other biological markers, and clinical and neuropsychological assessment can be combined to measure the progression of MCI and early Alzheimer's Disease. For up-to-date information about ADNI, including Police and Procedures, see www.adni-info.org.

In the present study, 253 MCI participants with baseline T1-weighted structural magnetic resonance images were selected and downloaded from the USC's Laboratory of Neuroimaging ADNI (http://www.loni.ucla.edu/ADNI/).

The inclusion criteria were as follows: Mini-Mental-State-Examination (MMSE) scores between 24 and 30 (inclusive), a memory complaint, objective memory loss measured by education adjusted scores on the Wechsler Memory Scale Logical Memory II, a Clinical Dementia Rating (CDR) of 0.5, and absence of significant levels of impairment in other cognitive domains, essentially preserved activities of daily living and an absence of dementia.

Exclusion criteria included: (1) the presence of a major depressive disorder or significant symptoms of depression; (2) modified Hachinski ischemia score greater than 5; (3) significant neurological or psychiatric illness; (4) use of antidepressant drugs with anticholinergic side effects; (5) high dose of neuroleptics, chronic sedatives, hypnotics, antiparkinsonian medication, and use of narcotic analgesics. Detail about inclusion/exclusion criterium can be found in http://adni.loni.usc.edu/wp-content/themes/freshnewa-dev-v2/clinical/ADNI-1_Protocol.pdf)[32].

The MCI group was stratified into those with one ApoE4 allele (Carriers) and those without (non-Carriers). ApoE genotyping details can be accessed at http://adni.loni.usc.edu/data-samples/clinical-data/[33]. Participants with one or more E2 allele(s) were excluded from this study due to the allele's possible protective effects[34].

The subjects also met the following criteria: anatomical study acquired in a 1.5 T MRI-scanner, right-handedness, high sMRI image quality. For biomarker's measurements (Cerebrospinal fluid) characteristics, see Supplementary Information.

Ethical statements. As per ADNI protocols, all procedures performed in studies involving human participants were under the institutional national research committee's ethical standards and the 1964 Helsinki declaration and its later amendments or comparable ethical standards. More details can be found at adni.loni.

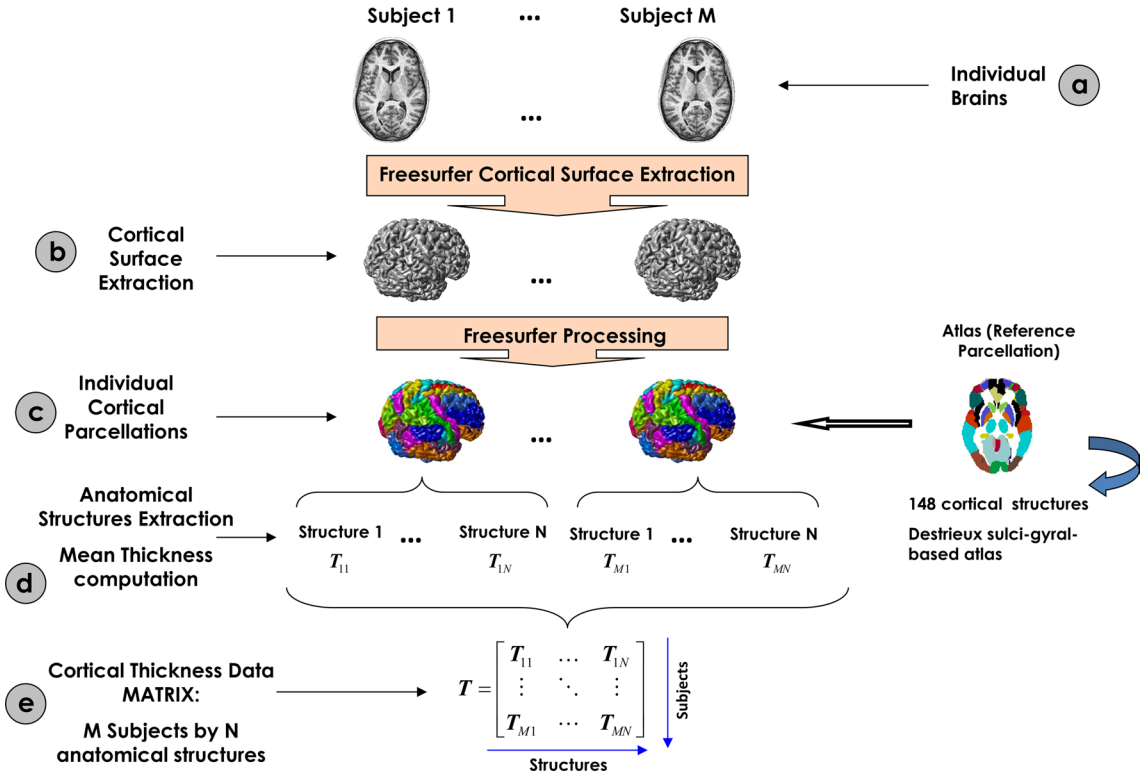

Figure 1. Flowchart of the cortical thickness matrix construction. (**a**) Representation of the M individual anatomic MRI images. (**b**) During FreeSurfer processing, the cortical surface of the M subjects was extracted. (**c**) Using the FreeSurfer toolbox, the cortical surfaces were labeled using a reference atlas. (**d**) The cortical thickness for each structure was calculated as the mean thickness of all vertices defined as belongs to that structure. (**e**) All mean thickness values for all structures and subjects were organized in an array denoted by T of M rows by N columns.

usc.edu. Participants were studied under ADNI protocols approved by the Institutional Review Board (IRB) at each recruitment site, and written informed consent was obtained from all subjects prior to enrollment. A listing of sites with named Site Investigators can be found online at http://adni.loni.usc.edu/wp-content/themes/freshnews-dev-v2/documents/policy/ADNI_Acknowledgement_List%205-29-18.pdf.

Data acquisition and preprocessing. Preprocessed versions of the 253 baselines T1-weighted MRI scans were downloaded. Further details are available in the ADNI-MRI technical procedures manual (http://adni.loni.usc.edu/methods/documents/MRI protocols). Preprocessing steps can be found elsewhere[35–37].

Computation of mean cortical thickness matrices. Cortical reconstruction and volumetric segmentation were performed using the *Freesurfer* analysis software suite with default settings (http://adni.loni.usc.edu/methods/documents/MRI protocols). The technical details of these procedures have been previously described[38]. *FreeSurfer* provides the cerebral cortex's parcellation based on Destrieux sulci-gyral-based atlas[39] and the mean cortical thickness for each cortical structure. We used these outputs to construct our data matrices for each group. The number of rows corresponds to the number of subjects, while the number of columns corresponds to the number of structures (Fig. 1).

Cortical thickness network construction. We defined a connection as statistical associations in cortical thickness between each pair of brain regions for a parcellation scheme of N = 148 anatomical structures (subcortical gray nuclei were excluded) (Supplementary Table S1 online). The synchronized covariations in cortical thickness between two regions were computed using Pearson's correlation coefficient across subjects. Thus, the interregional correlation matrix (N × N, N is the number of brain regions) of such connections was obtained using all pairs of anatomical structures. Self-connections were excluded implying zeros in the diagonal of the symmetric matrix. It is essential to point out that a partial correlation analysis could not be used in our case because the sample size was not large enough for a robust estimation of this measure.

Before the correlation analysis, a linear regression was performed at every region to remove the effects of age, gender, age-gender interaction, and cerebral mean cortical thickness.

In the next step, we obtained for each MCI group Nboot = 2000 bootstrap samples of the connectivity matrix by selecting a random subset of subjects with replacement using the classical bootstrapping procedure described in[40].

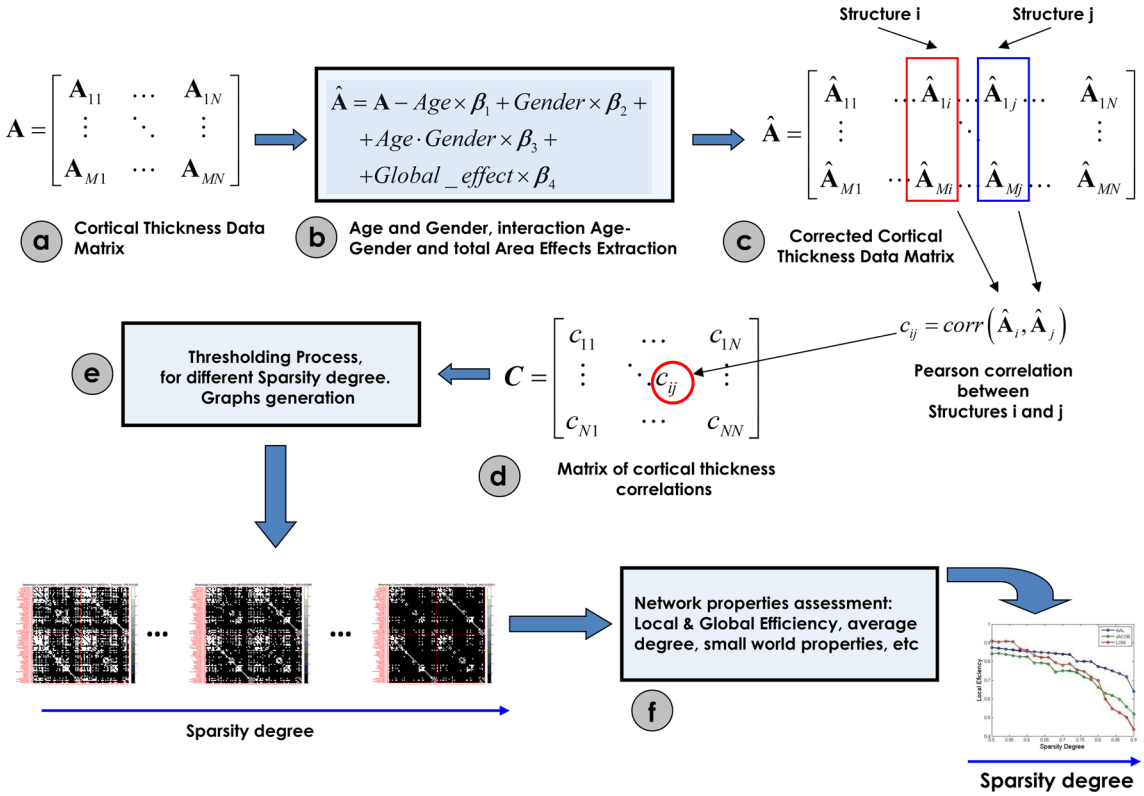

Figure 2. Steps for assessing the networks of cortical thickness covariance. (**a**) Matrix of the morphometric descriptor (cortical thickness) for the Destrieux parcellation. (**b**) The data matrix was substituted by residuals of the linear regression to subtract effects of age, gender, interaction age–gender, and the global effect (global mean cortical thickness) represented in (**c**). (**d**) Correlation matrix representing the concurrent changes among all pairs of anatomical structures. (**e**) The thresholding process for different sparsity levels to generate binary graphs. (**f**) Assessment of the network properties for all binary graphs obtained in (**e**).

The connectivity matrices obtained from bootstrapping were thresholded to create sparse binary graphs. We explored the Network Properties of the graphs over a range of sparsity degrees varied from 0.5 to 0.9 in steps of 0.02[41]. This range of sparsity degree has been indicated in previous studies to be optimal[42,43]. Similarly to other papers, only the positive correlation values are used to define the connectivity matrices. This choice is based on the lack of a clear physiological justification for negative correlations and the possible contamination by spurious negative correlation as a side effect of regressing out global effects in the preprocessing step (Fig. 2).

Network properties analysis, graph theory approach. In general, a complex network can be represented as a graph G = [N, K], the components of this system are called nodes (N), and the relations or connections between them are called edges (K)[44]. The nodes are the anatomical regions, and the edges are the correlations in cortical thickness across subjects between pairs of these brain regions. It is important to note here that this is a mathematically derived network whose connections do not necessarily constitute brain functional or physiological mechanisms directly. However, these networks are based on structural data. Therefore, they indirectly reflect the underlying mechanism, allowing us at the same time to use them and their properties as possible biomarkers of the differences between normal and pathological brain states.

In particular, we analyzed the following global network attributes: clustering index[45], characteristic path length[44,45], local and global efficiency[46], global connectivity, and homologous regions connectivity[47]. To describe the network's nodal properties, we computed the normalized betweenness centrality (NBC)[19,23] measure to identify the network hubs. We also performed a modularity analysis representing a network with densely interconnected nodes and relatively few connections between nodes in different modules[48]. It is a reflection of the natural segregation within a network[49–51]. Additionally, we carried out a 'Targeted-Attack' study to evaluate the cortical thickness covariance network's resilience when the most critical regions (hubs) are virtually attacked. Definitions for these measures within the traditional interpretation of complex networks framework[52] can be found in Supplementary Information and Table S2 online.

Methodology for studying differences in regional cortical thickness. Cortical vertex-wise regression analyses were performed using the SurfStat MATLAB toolbox (http://www.math.mcgill.ca/keith/surfstat). Age, gender, and mean cortical thickness (CT) were statistically controlled. The statistical significance of the t-statistic maps for cortical thickness differences was corrected for multiple comparisons using Random Field

	MCI		
	Carriers	Non-carriers	Statistics
N	126	127	–
Gender (M/F)	80/46	88/39	$p = 0.33^{\&}$
Age (y)	74.17 (6.91)	76 (7.97)	$U(6542) = -2.51, p = 0.01^{+}$
Age range	56.8–88.9	54.6–89.8	–
Education (y)	15.63 (3.03)	15.61 (3.38)	$U(7878) = -2.21, p = 0.83^{+}$
MMSE	26.97 (1.85)	27.17 (1.83)	$U(7492) = -0.87, p = 0.38^{+}$
Mean cortical thickness (mm)	2.23 (0.12)	2.23 (0.14)	$U(7902) = -0.17, p = 0.86^{+}$

Table 1. Demographics and neuropsychological variables for MCI groups. Age, Education, MMSE, and Mean cortical thickness values are represented by means and standard deviations. Gender (M/F) is represented by the number of subjects. Significant set at $p < 0.05$. The superscripts "&" represents χ^2 test; "+" represents the Mann–Whitney U test. Key: *MCI* mild cognitive impairment; Carriers: *ApoE4*-positive; non-Carriers: *ApoE4*-negative; *M* male; *F* female; *y* years; *MMSE* mini-mental state examination.

Theory (RFT) to avoid false positives when more than 80,000 tests were performed[53]. RFT identifies statistically significant "clusters" of vertices and vertex "peaks". Cluster p-values show regions of connected vertices with p-values below 0.001 in clusters whose extent is significant at $p < 0.05$, i.e., a collection of connected vertices with $p < 0.001$ that was unlikely to occur by chance.

Statistical methods to study ApoE4 modulation of global network properties. Network properties (NP) of the cortical thickness correlation matrices were computed for each sparsity degree values and different bootstrap samples in each MCI group. Thus, we had a set of Nboot = 2000 NP curves for each network property. The area under the curve (AUC) was computed for each network attribute to contrast the global behavior of these attributes[54]. The NP curves' monotonic changes make AUC a suitable descriptor of the networks' global performance.

We followed three main steps to examine differences in global network properties between groups: (1) construction of the empirical bootstrapped distribution of differences by subtracting the corresponding bootstrap samples between groups; (2) definition of the statistical significance level: a 95 percent confidence interval (CI) (biased corrected percentile bootstrap CI)[55] of the distribution of the empirical difference is estimated; (3) Hypothesis testing: a significant difference between groups is accepted if CI does not contain zero, no significant difference is considered otherwise. A p-value associated with each hypothesis test is also reported.

Methodology to explore nodal betweenness centrality (NBC) differences between groups. For each bootstrap sample of the cortical thickness connectivity matrix, the NBC was computed at every single sparsity degree. Previously to this process, the largest component[54] of all bootstrap samples of the cortical thickness covariation matrices were calculated. The minimum sparsity degree for the largest connected components (equal to the number of structures) was used as an upper limit of the sparsity degree range. This step guarantees that all nodal NBCs come from fully connected cortical thickness networks. Similarly to global network properties, we take the AUC and follow the three main steps to examine differences between groups for each anatomical structure. To control for multiple comparisons (across the number of structures), we applied the False Discovery Rate (FDR) correction.

Hubs were selected as those with mean NBC superior to 1.5, similar to[41].

Construction of the Cortical Thickness Network and computation of network metrics were performed using the MorphoConnect toolbox[56] and subroutines of the Brain Connectivity Toolbox[52] (https://sites.google.com/site/bctnet/). The figures were created using the BrainNet Viewer package[57] (http://www.nitrc.org/projects/bnv) and the Gephi package[58] (https://gephi.org/).

Results

Demographic and neuropsychological variables. There were no significant differences in gender, education, MMSE scores, and mean cortical thickness between groups (Table 1). However, the age was significantly different between MCI Carriers compared to non-Carriers ($U(6542) = -2.51$, $p = 0.01$). The MCI Carriers group was younger than non-Carriers on the diagnosis age (74.17 vs. 76). This result agrees with previous studies were ApoE4 had been associated with a younger age of onset[59].

ApoE4-related changes in regional cortical thickness. Differences in cortical thickness between MCI Carriers and non-Carriers were not statistically significant after FDR correction (Supplementary Fig. S1 online). However, percent difference maps show trends for a reduced thickness bilaterally in the anterior temporal lobe and frontal lobe regions in the Carriers group compared with non-Carriers. The non-Carriers group tended to lower cortical thickness values in left posterior parietal areas, the precuneus, posterior cingulate gyrus, and frontal pole. For a list of clusters, see Supplementary Table S3 online.

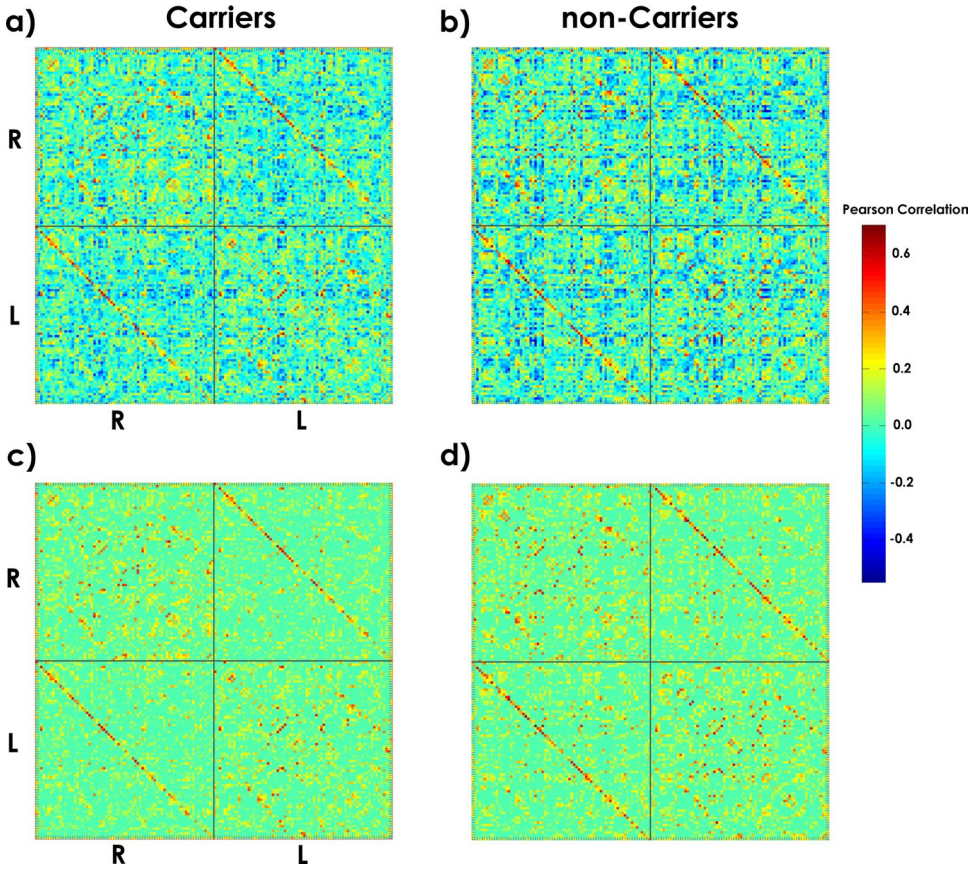

Figure 3. Cortical thickness correlation matrices for each group. (**a**) and (**b**) display matrices with positive and negative correlation values. (**c**) and (**d**) represent matrices with positive correlation values. The strength of the connection is indicated by the color bar. The 'R-'R' and 'L-'L' quadrants represent the intra-hemispheric cortical thickness correlations in the right and left hemispheres. The 'R-'L' and 'L-'R' quadrants depict the inter-hemispheric interactions. The diagonal of the 'L'-'R' quadrant shows the correlations in cortical thickness between homologous structures across hemispheres.

ApoE4 modulates the global network properties. Figure 3 shows the cortical thickness matrices for negative (Fig. 3a,b) and positive correlation values (Fig. 3c,d) for each group. Only matrices with positive values were used for the subsequent analysis.

Figure 4 shows the changes in global network properties for both groups across various densities thresholds (0.5 to 0.9). The two networks exhibit differences in clustering index, characteristic path length, local and global efficiency, global connectivity, homologous regions connectivity, and modularity. The Target Attack simulation was not significantly different between groups ($p > 0.05$) for the whole range of densities values (Table 2).

The comparison of the global network properties based on the AUC values revealed in MCI Carriers as compared with non-Carriers a decrease in clustering index, characteristic path length, local efficiency, homologous regions connectivity, global connectivity strength, and modularity. In contrast, the MCI Carriers group exhibited higher global efficiency (Fig. 5). The results of the statistical analysis, including confidence intervals, can be found in Table 2.

Group-based differences in normalized betweenness centrality (NBC). We also studied the effects of ApoE4 on the Normalized Betweenness Centrality (NBC), a regional network property. The AUC analysis showed 11 regions with NBC differences between groups after FDR correction ($p < 0.05$) (Fig. 6). The full list of structures and the statistical analysis results (including confidence intervals) can be found in Supplementary Table S4 online. NBC regional differences between groups comprise mainly occipital-temporal brain areas followed by limbic and frontal regions. Compared with non-Carriers, Carriers showed lower NBC for all brain regions except for the right lingual gyrus, left inferior temporal sulcus, right medial occipitotemporal sulcus (collateral sulcus), and lingual sulcus.

ApoE4 modifies the brain network hubs. We also studied the effects on the hubs of the cortical thickness covariance network due to the presence of ApoE4. There were identified 24 hubs in each group (Fig. 7). The detailed list of structures and its NBC values were tabulated in Supplementary Table S5 online. We identify 11 common hubs to both groups (Fig. 7, yellow structures), including limbic (bilateral anterior part of the cingulate

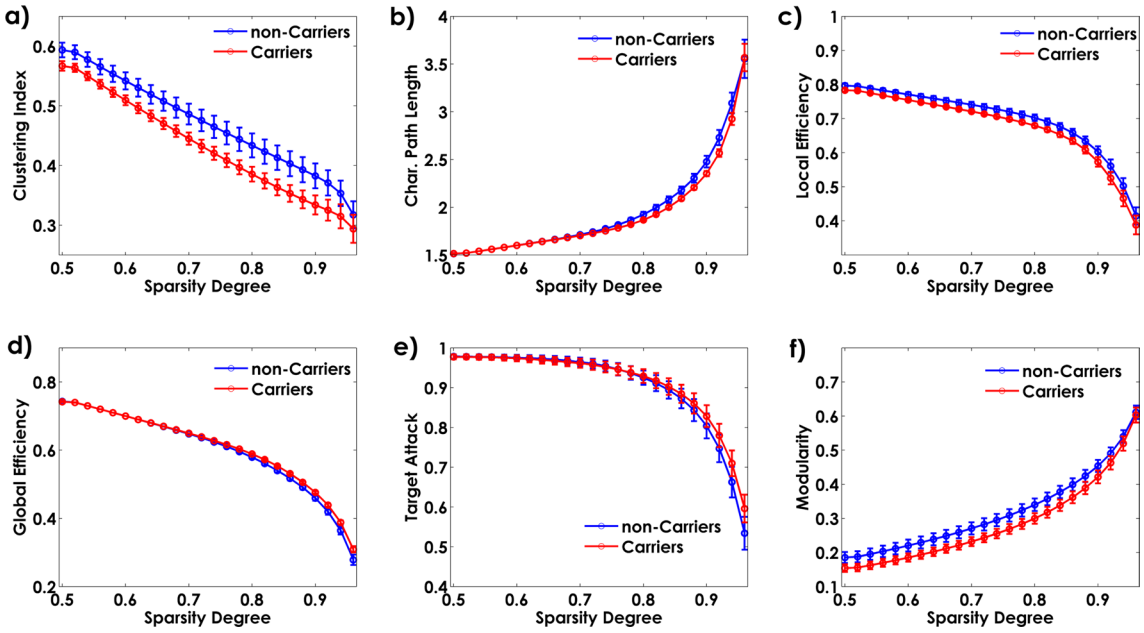

Figure 4. Global network properties as a function of sparsity degrees.

Network property	Carriers	Non-carriers	Confidence interval (95%)	p-value
Clustering index	7.92 (0.2)	8.57 (0.3)	[− 1.62, − 0.61]	**$0.04*10^{-4}$**
Characteristic path length	28.74 (0.06)	29.04 (0.15)	[− 0.88, − 0.28]	**$0.03*10^{-3}$**
Target attack	16.24 (0.09)	16.25 (0.09)	[− 0.12, 0.42]	0.67
Local efficiency	12.39 (0.08)	12.70 (0.13)	[− 0.78, − 0.32]	**$0.09*10^{-4}$**
Global efficiency	11.24 (0.01)	11.19 (0.03)	[0.04, 0.14]	**$0.06*10^{-3}$**
Global connectivity	0.06 (0.01)	0.07 (0.01)	[− 0.01, − 0.001]	**0.04**
Homologous regions connectivity	0.36 (0.01)	0.4 (0.01)	[− 0.08, − 0.01]	**0.02**
Modularity	3.83 (0.20)	4.45 (0.28)	[− 1.61, − 0.29]	**0.02**

Table 2. Network properties differences between groups. Network properties in each group are represented by the mean and standard deviations: mean (s.d). In bold, the significance differences, those confidence intervals that do not contain zero.

gyrus and sulcus, left posterior-dorsal part of the cingulate gyrus), insular (bilateral posterior ramus of the lateral sulcus, anterior segment of the circular sulcus of the insula), frontal (central operculum and sulci), temporal (superior temporal sulcus) and temporal-occipital and parietal-occipital regions (parieto-occipital sulcus, anterior transverse collateral sulcus).

Compared to non-Carriers, where hubs comprised mainly parietal-occipital-temporal areas, in the Carriers group were localized predominantly in frontal and parietal-occipital-temporal regions. Hub regions found only in Carriers, including the posterior-dorsal part of the cingulate gyrus, inferior occipital gyrus and sulcus, superior temporal and orbital gyrus. Areas identified as hubs in the non-Carriers comprised the lingual aspect of the medial occipitotemporal gyrus, supramarginal gyrus, and subcallosal gyrus.

ApoE4-related change of the cortical thickness network modularity. Modularity estimation was performed on the groups averaged connectivity matrix using Newman's metric. The resulting analysis (Fig. 8) divided the 148 cortical nodes into five modules for MCI Carriers and three modules in the non-Carriers group.

The modules are represented on a circular graph layout, where the nodes are placed in circles if they belong to the same module. Three communities defined the non-Carriers modularity with similar region numbers (community 1: N = 41, community 2: N = 59, and community 3: N = 48). Each module included a distributed set of regions. However, the analysis per lobule showed an anterior community based mainly in the frontal areas, a central module with similar frontal, parietal and occipital regions, and a posterior module integrated by temporal and temporal-occipital areas. On the other hand, Carriers showed more segregated modularity based on 5 communities with two large modules (community 2: N = 33 and community 3: N = 39) and three smaller ones (community 1: N = 30, community 4: N = 22, and community 5: N = 24). In this group, the community composition was more diverse as compared with non-Carriers. However, we were able to identify that the modules showed a specific pattern of regions summarized as follows: community (1) temporal-occipital, community (2)

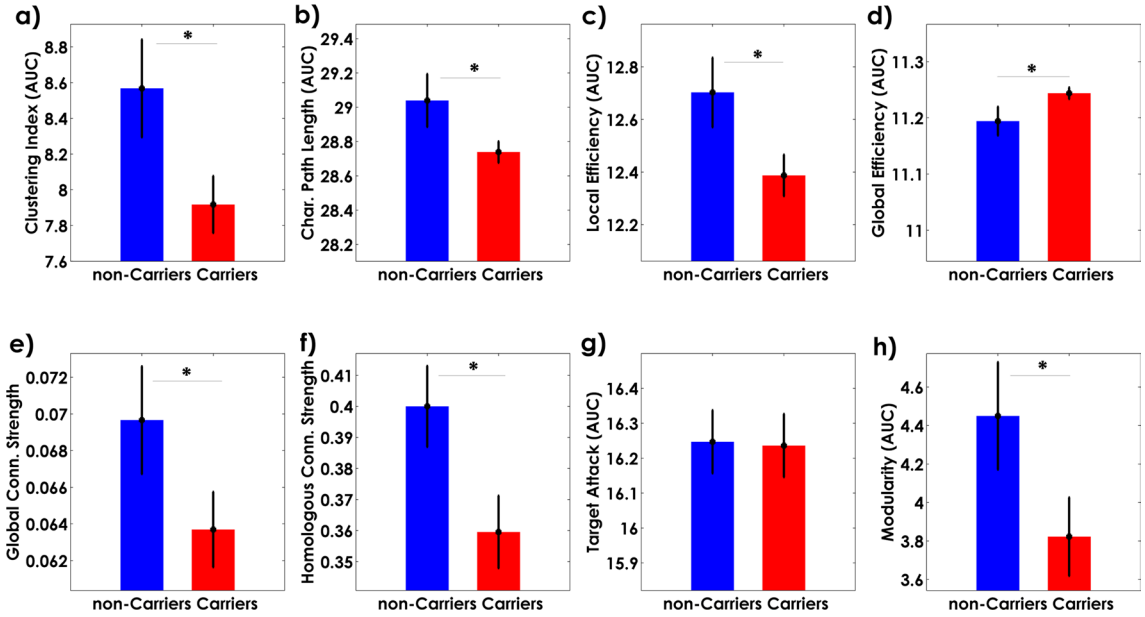

Figure 5. The area under the curves (AUC) of the cortical thickness covariance global properties. The bar heights represent the mean of the network properties, and the error bars are their standard deviation.

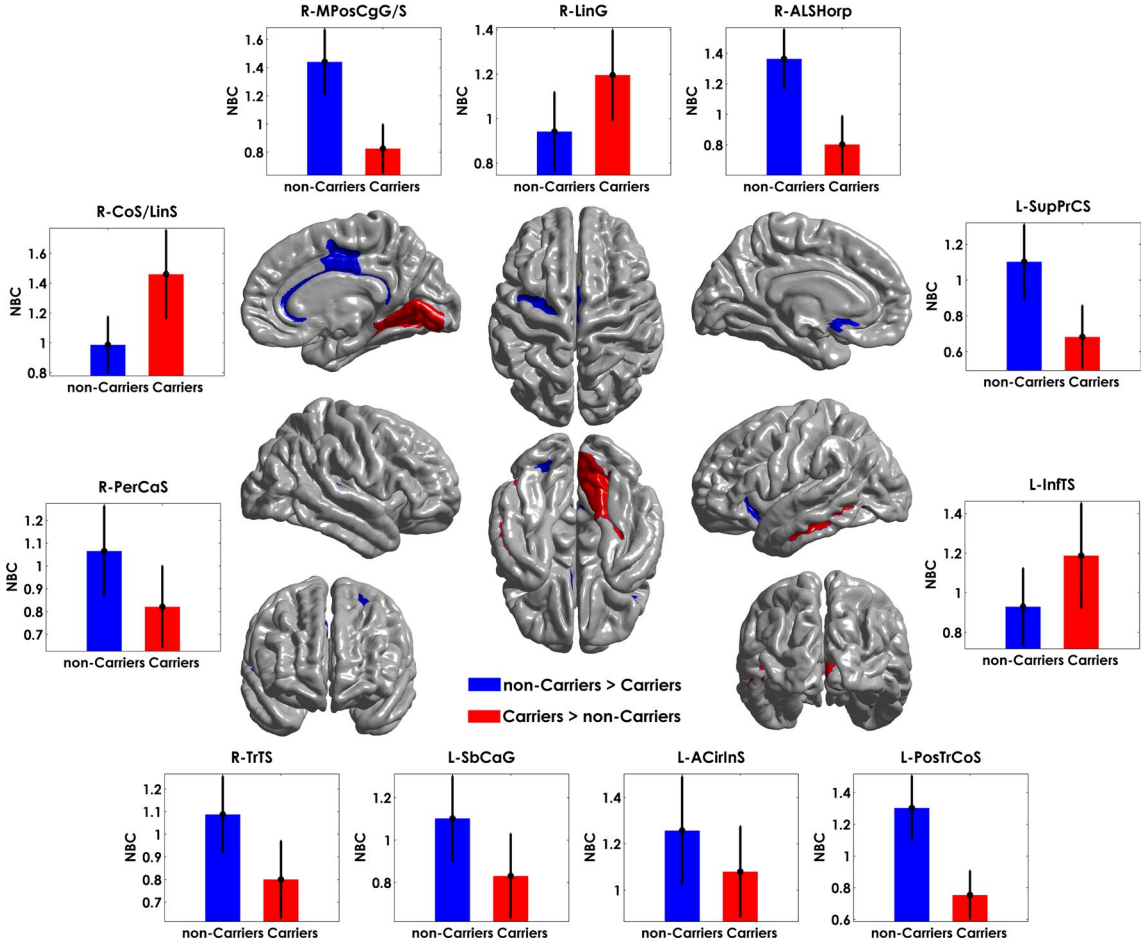

Figure 6. Significant differences between groups based on NBC. The bar heights represent the mean NBC values for each group, and the error bars the standard deviations. R: right hemisphere, L: left hemisphere. The regions were mapped onto the cortical surfaces using the BrainNet Viewer package (http://www.nitrc.org/projects/bnv).

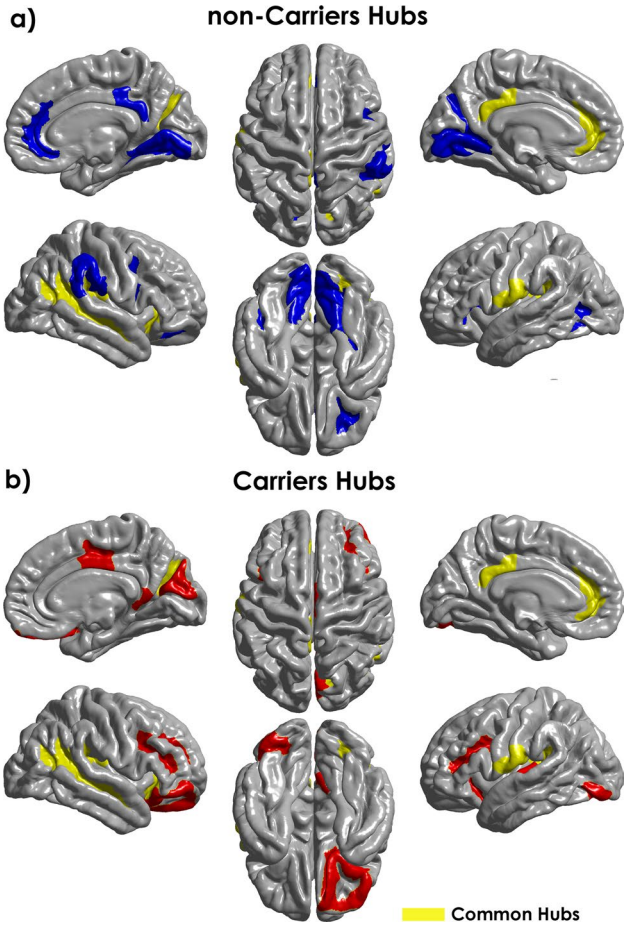

Figure 7. Hubs regions in MCI Carriers and non-Carriers based on the Normalized Betweenness Centrality (NBC). The blue regions represent hubs in the Carriers and the red ones the non-Carriers. In yellow are represent hubs common to both groups. The NBC values were mapped onto the cortical surfaces using the BrainNet Viewer package (http://www.nitrc.org/projects/bnv).

frontoparietal, community (3) parietal-occipital, community (4) insula, community (5) frontal regions. For a complete list of regions per module in each group, see Supplementary Table S6 online.

It is worth noting that modules 2 and 3 in Carriers are assigned to the second module in non-Carriers and modules 4 and 5 to module 3, suggesting a low level of segregation for non-Carriers. The sub-modules combine to form predominantly anterior–posterior large communities.

Discussion

We investigated for the first time the cortical thickness structural covariance networks in ApoE4 Carriers and non-Carriers groups to assess the effect of genetic risk on large-scale network topology in MCI. Few previous studies have found evidence of the ApoE4 modulation on the MCI brain network topology using graph theory based on physiological variables derived from other image modalities (rs-fMRI, FDG-PET, and DWI). However, our approach is timely based on the following points:

(1) As a morphometric descriptor, cortical thickness offers unique information about morphological covariance patterns between brain regions compared to other cortical measures[41].
(2) Structural covariance analysis is attractive because of the wide availability (in clinical and research settings) of high-quality sMRI scans compared with other modalities. Additionally, the cortical thickness derived from sMRI has proved consistent across scanner systems and field strengths[60].
(3) It has been shown that anatomical covariance patterns are related to functional and anatomical connectivity. However, comparing these connectivity measures has demonstrated that brain structural covariance networks capture complementary information of the same physiological processes[16,61].
(4) Graph theory provides a unique description of the multivariate neural process by looking at their local and global connectivity topology.
(5) Unlike the previous studies[29–31], we introduced the modularity and target attack analyses providing further information about the topological organization of the structural covariance networks in MCI.

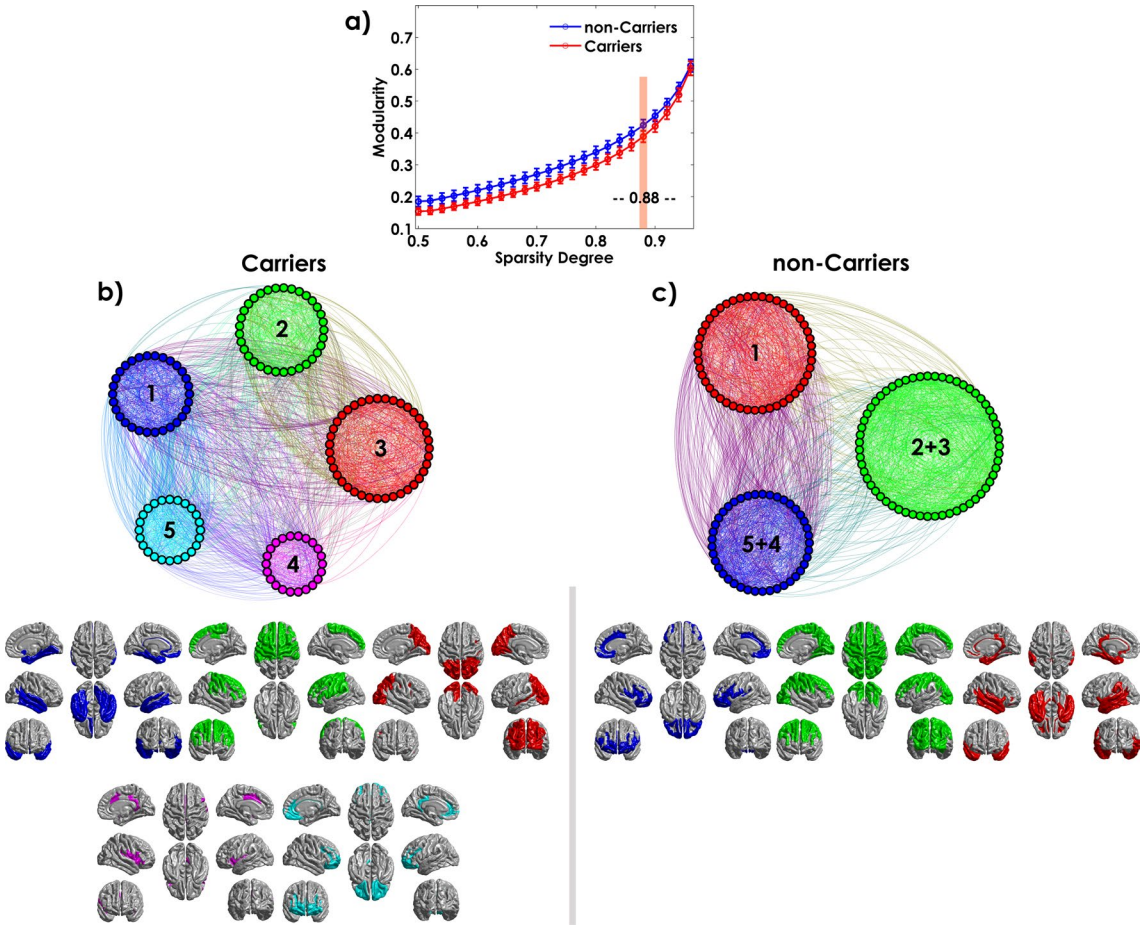

Figure 8. Module distributions for both Carriers and non-Carriers groups estimated using Newman's spectral community detection algorithm at sparsity degree 0.88. The circular representation of the modules was based on the Gephi package (https://gephi.org/). Inferior panels show the cortical surface mapping of the modules in both Carriers and non-Carriers groups using the BrainNet Viewer package (http://www.nitrc.org/projects/bnv). Each color represents those regions that belong to a specific module.

Summarizing, our research presents novel experimental evidence regarding the ApoE4 effects on the brain network topology, which are worth investigating to define intermediate phenotypes in MCI.

In general, our findings revealed a decrease in global and homologous connectivity strength, clustering index, characteristic path length, local efficiency, modularity, and an increase of global efficiency in MCI Carriers compared to non-Carriers. MCI carriers showed lower values of NBC in several brain regions. Together, these findings concur with the evidence that ApoE4 is associated with an aberrant brain network topology in MCI. On the other hand, the changes are not detectable with the standard univariate approach based on the cortical thickness's differences. Our results support the concept that multivariate measures (i.e., covariations) combined with a graph theoretical approach are more sensitive to identifying complex pathological processes, as found in other brain diseases. Univariate measures derived from the standard methods could be insufficient for capturing subtle (early) abnormal changes.

Some of these results deserve more attention and will be discussed in the following.

In particular, we observed a decrease in the clustering coefficient index in MCI Carriers relative to non-Carriers, indicating lower local cortical thickness correlations. This finding suggests a topological organization more like a random network in this group of patients, a structure previously reported in AD subjects[18,62,63]. Moreover, it has been demonstrated an association between longitudinal decreases of the clustering index and risk of MCI conversion into AD[63]. Previous studies showed no differences between groups or reported similar results[29,31]. The disagreement between investigations could be related to several factors like group composition, sample size, different neuroimaging modalities, and atlas parcellation.

In the current study, we also observed a shorter characteristic path length associated with the presence of the ApoE4, indicating that fewer steps are required to carry on the information across remote brain regions[64]. A similar result was found in previous research in cognitively normal elderly ApoE4 Carriers[26] using FDG-PET. A compensatory mechanism for early local pathological events seems a plausible hypothesis when the clustering index decreases in the presence of shorter characteristic path length. Also, the ApoE4 allele has been proposed as an example of antagonistic pleiotropy[65]. The concept means that ApoE4 may offer benefits during early and

middle age and promote better compensatory mechanisms during early disease phases like MCI that can be captured using a complex network approach.

Like in the clustering index, one previous study reported no differences between groups in characteristic path length[31]. However, our results seem to be more reliable since Yao et al. (2015) gathered the MCI, AD, and healthy controls to form the Carriers and non-Carriers groups, making it challenging to disentangle group differences[31].

Our analysis also showed a decrease in global connectivity strength- an aggregate measure of the correlation values between all possible pairwise anatomical structures- in MCI Carriers relative to non-Carriers. Previous studies did not report on this network property[29–31]. This finding may indicate that mechanisms underlying cortical thickness are differentially coordinated across this group of patients. Another possibility is that ApoE4 increases the interindividual differences between regional cortical thicknesses in Carriers. It may be due to less cortical thickness coordinated patterns concerning the homogeneity effects created by putative compensatory and shared brain region vulnerability associated with the aging processes and interactions with the MCI stage.

The nodal properties results allowed us to generate hypotheses about the ApoE4 impact on brain network integration and segregation in MCI. Similar to previous studies, we found the opposite effects of the ApoE4 genotype on nodal centrality[30,31]. There is probably more than one cause for these alterations, which makes disease-related changes in structural covariance challenging to interpret. A regional lower NBC may be suggestive of dysconnectivity due to a localized degeneration. By contrast, an increase may indicate over connectivity or synchronized cortical thickness loss in several areas targeted by the same neurodegenerative process. Most brain regions reported here are different from previous studies[30,31] based on other neurophysiological variables. It is indicative that the networks of cortical thickness covariance capture supplementary information of the anatomical brain organization. Other factors could also be playing a role like sample characteristics and different statistical approaches.

Our findings showed agreements with previous studies in AD neurodegeneration. The fact that crucial structures like Posterior Cingulate Cortex (PCC) showed lower NBC values in the Carriers group suggests that regional topological properties may capture disease-related effects that can be further explored in association with the risk of AD progression. We identified between-group differences in NBC across different lobes, consistent with previous findings[26,30]. Several regions in the Limbic and Frontal cortex decreased centrality in Carriers as compared with non-Carriers. Notably, for all detected hubs, NBC was lower in Carriers than non-Carriers. Some of these structures were: cingulate gyrus, middle occipital gyrus, occipital pole, superior frontal sulci, and orbital gyrus. It is important to note that several of these regions are part of the Default Mode Network (DMN). As is recognized, the DMN is involved in self-referential functions such as episodic memory[66] affected by AD. In this network, the PCC is a key integration node between the medial temporal lobe and medial prefrontal subsystems[66,67]. Previous studies reported in the DMN (including PCC) high glycolytic metabolism, enhancing abnormal amyloid deposition aggregation[68,69]. ApoE4, as a disrupted metabolic factor[10], may alter the DMN resting-state activity and ultimately bringing atrophy in MCI ApoE4 Carriers, accelerating AD pathology early during the disease course.

Lower NBC values were also found in regions that belong to the Saliente Network (i.e.insula). This network operates on identified salience and, as such, includes known sites for sustained attention and working memory (dorsolateral prefrontal cortex, lateral parietal cortex), response selection (dorsomedial frontal), and response suppression (prefrontal cortex)[70–72]. Our findings may suggest that ApoE4 Carriers have altered regulation of control processes that subsequently influence memory performance.

To the best of our knowledge, we reported, for the first time, a modularity analysis of the structural covariance network in MCI. We observed a decreased modularity in Carriers as compared with non-Carriers. A less modular network implies fewer connections within modules and more connections to other modules. In graph theory terms, Carriers shows better cost-efficiency wiring regarding the physical volume occupied, conduction delay, and metabolic cost. On the other hand, the increase of interconnectedness between modules can lead to the rapid spreading of disease pathological markers (neurodegenerative process) and loss of specialization[73]. In many networks, as in our case, modularity and global efficiency are inversely related, as a highly modular topology could require long communication paths to integrate information across the network.

In addition to these differences, the module size and composition also change associated with the ApoE4. This analysis revealed in Carriers a spatial rearrangement of these communities. They include sets of brain regions that are anatomically proximal, and they mainly belong to the same lobule. However, in non-Carriers, the module's compositions are more distributed across the cortex. We identified anterior-medial-posterior network modularity mainly formed by frontal, frontal-parietal, and temporal-occipital modules. This modular topology has been described previously in resting-state networks in normal aging. It evidences the brain network evolves from a preferentially local connectivity pattern to a more distant and functionally community structure[74]. Further longitudinal studies on modularity patterns differences between Carriers and non-Carriers could offer an exciting opportunity to distinguish those MCI patients at high risk of AD progression.

In conclusion, our study applies the graph theory to assess the ApoE4-related changes on global and local network topology in MCI based on the concurrent variations of the cortical thickness across anatomical structures. Our findings showed that some network properties changes in MCI Carriers seem to be associated with altered communication between neighboring regions. It may be an early response to AD-related pathological markers (i.e., tau-tangles and amyloid-beta plaques depositions). On the other hand, a better global network communication could be considered the expression of compensatory/degeneracy mechanisms to sustain the transmission of the information across distant brain regions associated with the genetic challenge. These changes in topological attributes may be considered sensitive markers to detect early brain network changes related to the disease progression.

The methodological approach used in this study has several limitations. The structural covariance analysis has a static nature. Evidence suggests that the brain undergoes spontaneous reconfiguration at a temporal scale[75],

as such properties like modular structure and hub may fluctuate over time. A quantitative comparison of the network topological attributes between studies is difficult. These properties' values depend on experimental parameters like brain parcellation, nodes-edge definitions, and sample size[76]. Despite providing useful information, structural covariance analysis is a group approach. It does not allow individual analysis and statistical associations between topological network attributes and clinical/cognitive measures.

Other aspects need to be addressed in future investigations. (1) MCI patients exhibit different progression trajectories that we did not consider here; accordingly, further follow-up longitudinal studies are warranted to examine the interaction between network properties, disease progression, and ApoE4 (2) The inclusion of healthy elderly sample, as well as AD patients, would help to fully characterize the ApoE4 effect on the brain network properties across the disease spectrum (4) This study did not investigate whether the ApoE4-related impact on the brain network topology is mediated by pathological disease markers like beta-amyloid and tau deposition. Further investigations on this topic will clarify the underlying mechanisms associated with the brain network properties changes. Despite these limitations, our study sheds light on the structural connectomics of MCI associated with the ApoE4. We considered a complex network analysis with the genetic risk factors inclusion, a valuable approach to understanding the AD spectrum, which could improve the personalized medicine perspective.

Data availability

Data used in the preparation of this article were obtained from the Alzheimer's Disease Neuroimaging Initiative (ADNI) database (adni.loni.usc.edu). ADNI database is publicly accessible from adni.loni.usc.edu upon request. ADNI's primary goal has been to test whether serial MRI, PET, other biological markers, and clinical and neuropsychological assessment can be combined to measure the progression of mild cognitive impairment and early Alzheimer's Disease. The Principal Investigator of ADNI is Michael W. Weiner, MD (email: Michael.Weiner@ucsf.edu).

Received: 12 June 2020; Accepted: 30 December 2020
Published online: 12 January 2021

References

1. 2020 Alzheimer's disease facts and figures. *Alzheimer's Dementia* **16**, 391–460 (2020)
2. Albert, M. S. *et al.* The diagnosis of mild cognitive impairment due to Alzheimer's disease: Recommendations from the National Institute on Aging-Alzheimer's Association workgroups on diagnostic guidelines for Alzheimer's disease. *Alzheimer's Dementia* **7**, 270–279 (2011).
3. Jansen, W. J. *et al.* Prevalence of cerebral amyloid pathology in persons without dementia: A meta-analysis. *JAMA* **313**, 1924–1938 (2015).
4. Mueller, S. G. *et al.* Ways toward an early diagnosis in Alzheimer's disease: The Alzheimer's Disease Neuroimaging Initiative (ADNI). *Alzheimer's Dementia* **1**, 55–66 (2005).
5. Gao, W. *et al.* Intersubject variability of and genetic effects on the Brain's functional connectivity during infancy. *J. Neurosci.* **34**, 11288–11296 (2014).
6. Petersen, R. C. Mild cognitive impairment: Transition between aging and Alzheimer's disease. *Neurologia (Barcelona, Spain)* **15**, 93–101 (2000).
7. Rao, A. T., Degnan, A. J. & Levy, L. M. Genetics of Alzheimer disease. *AJNR Am. J. Neuroradiol.* **35**, 457–458 (2014).
8. Farlow, M. R. *et al.* Impact of APOE in mild cognitive impairment. *Neurology* **63**, 1898–1901 (2004).
9. Norberg, J. *et al.* Regional differences in effects of APOE ε4 on cognitive impairment in non-demented subjects. *Dement. Geriatr. Cogn. Disord.* **32**, 135–142 (2011).
10. Liu, C.-C., Liu, C.-C., Kanekiyo, T., Xu, H. & Bu, G. Apolipoprotein E and Alzheimer disease: Risk, mechanisms and therapy. *Nat. Rev. Neurol.* **9**, 106–118 (2013).
11. Liu, Y., Cai, Z.-L., Xue, S., Zhou, X. & Wu, F. Proxies of cognitive reserve and their effects on neuropsychological performance in patients with mild cognitive impairment. *J. Clin. Neurosci.* **20**, 548–553 (2013).
12. Cherbuin, N., Leach, L. S., Christensen, H. & Anstey, K. J. Neuroimaging and APOE genotype: A systematic qualitative review. *Dement. Geriatr. Cogn. Disord.* **24**, 348–362 (2007).
13. Delbeuck, X., Van der Linden, M. & Collette, F. Alzheimer' disease as a disconnection syndrome?. *Neuropsychol. Rev.* **13**, 79–92 (2003).
14. Xie, T. & He, Y. Mapping the Alzheimer's brain with connectomics. *Front. Psychiatry* **2**, 1–14 (2012).
15. Bullmore, E. T. & Bassett, D. S. Brain Graphs: Graphical models of the human brain connectome. *Annu. Rev. Clin. Psychol.* **7**, 113–140 (2011).
16. Alexander-Bloch, A., Giedd, J. N. & Bullmore, E. Imaging structural co-variance between human brain regions. *Nat. Rev. Neurosci.* **14**, 322–336 (2013).
17. Lerch, J. P. *et al.* Mapping anatomical correlations across cerebral cortex (MACACC) using cortical thickness from MRI. *NeuroImage* **31**, 993–1003 (2006).
18. Tijms, B. M. *et al.* Alzheimer's disease: Connecting findings from graph theoretical studies of brain networks. *Neurobiol. Aging* **34**, 2023–2036 (2013).
19. He, Y., Chen, Z. & Evans, A. Structural insights into aberrant topological patterns of large-scale cortical networks in Alzheimer's disease. *J. Neurosci.* **28**, 4756–4766 (2008).
20. Lo, C.-Y. *et al.* Diffusion tensor tractography reveals abnormal topological organization in structural cortical networks in Alzheimer's disease. *J. Neurosci.* **30**, 16876–16885 (2010).
21. Stam, C. J., Jones, B. F., Nolte, G., Breakspear, M. & Scheltens, P. Small-world networks and functional connectivity in Alzheimer's disease. *Cereb. Cortex* **17**, 92–99 (2007).
22. Supekar, K., Menon, V., Rubin, D., Musen, M. & Greicius, M. D. Network analysis of intrinsic functional brain connectivity in Alzheimer's disease. *PLoS Comput. Biol.* **4**, e1000100 (2008).
23. Sanabria-Diaz, G., Martínez-Montes, E. & Melie-Garcia, L. Glucose metabolism during resting state reveals abnormal brain networks organization in the Alzheimer's disease and mild cognitive impairment. *PLoS ONE* **8**, e68860 (2013).
24. Brown, J. A. *et al.* Brain network local interconnectivity loss in aging APOE-4 allele carriers. *Proc. Natl. Acad. Sci. USA* **108**, 20760–20765 (2011).
25. Goryawala, M., Duara, R., Loewenstein, D. A., Zhou, Q. & Barker, W. Apolipoprotein-E4 (ApoE4) carriers show altered small-world properties in the default mode network of the brain. *Biomed. Phys. Eng. Express* **1**, 15001 (2015).

26. Seo, E. H. *et al.* Influence of APOE genotype on whole-brain functional networks in cognitively normal elderly. *PLoS ONE* **8**, 2–10 (2013).
27. Wang, J., Wang, X., He, Y., Yu, X. & Wang, H. Apolipoprotein E e 4 modulates functional brain connectome in Alzheimer's disease. *Hum. Brain Mapp.* **36**, 1828–1846 (2015).
28. Zhao, X. *et al.* Disrupted small-world brain networks in moderate Alzheimer's disease: A resting-state fMRI study. *PLoS ONE* **7**, e99540 (2012).
29. Ma, C. *et al.* Disrupted brain structural connectivity: Pathological interactions between genetic APOE ε4 status and developed MCI condition. *Mol. Neurobiol.* **54**, 6999–7007 (2017).
30. Wang, Z. *et al.* APOE genotype effects on intrinsic brain network connectivity in patients with amnestic mild cognitive impairment. *Sci. Rep.* **7**, 397 (2017).
31. Yao, Z. *et al.* A FDG-PET study of metabolic networks in apolipoprotein E ε4 allele carriers. *PLoS ONE* **10**, 1–16 (2015).
32. Petersen, R. C. *et al.* Alzheimer's Disease Neuroimaging Initiative (ADNI): Clinical characterization. *Neurology* **74**, 201–209 (2010).
33. Saykin, A. J. *et al.* Alzheimer's disease neuroimaging initiative biomarkers as quantitative phenotypes: Genetics core aims, progress, and plans. *Alzheimer's Dementia* **6**, 265–273 (2010).
34. Serrano-Pozo, A., Qian, J., Monsell, S. E., Betensky, R. A. & Hyman, B. T. APOEε2 is associated with milder clinical and pathological Alzheimer disease. *Ann. Neurol.* **77**, 917–929 (2015).
35. Jovicich, J. *et al.* Reliability in multi-site structural MRI studies: Effects of gradient non-linearity correction on phantom and human data. *NeuroImage* **30**, 436–443 (2006).
36. Fornito, A. *et al.* Variability of the paracingulate sulcus and morphometry of the medial frontal cortex: Associations with cortical thickness, surface area, volume, and sulcal depth. *Hum. Brain Mapp.* **29**, 222–236 (2008).
37. Sled, J. G., Zijdenbos, A. P. & Evans, A. C. A nonparametric method for automatic correction of intensity nonuniformity in MRI data. *IEEE Trans. Med. Imaging* **17**, 87–97 (1998).
38. Fischl, B. *et al.* Automatically parcellating the human cerebral cortex. *Cereb. Cortex* **14**, 11–22 (2004).
39. Destrieux, C., Fischl, B., Dale, A. & Halgren, E. Automatic parcellation of human cortical gyri and sulci using standard anatomical nomenclature. *NeuroImage* **53**, 1–15 (2010).
40. Efron, B. & Tibshirani, R. *An Introduction to the Bootstrap* (Chapman & Hall, New York, 1994).
41. Sanabria-Diaz, G. *et al.* Surface area and cortical thickness descriptors reveal different attributes of the structural human brain networks. *NeuroImage* **50**, 1497–1510 (2010).
42. He, Y., Chen, Z. J. & Evans, A. C. Small-world anatomical networks in the human brain revealed by cortical thickness from MRI. *Cereb. Cortex* **17**, 2407–2419 (2007).
43. Achard, S. & Bullmore, E. Efficiency and cost of economical brain functional networks. *PLoS Comput. Biol.* **3**, 0174–0183 (2007).
44. Boccaletti, S., Latora, V., Moreno, Y., Chavez, M. & Hwang, D. Complex networks: Structure and dynamics. *Phys. Rep.* **424**, 175–308 (2006).
45. Watts, D. J. & Strogatz, S. H. Collective dynamics of 'small-world' networks. *Nature* **393**, 440–442 (1998).
46. Latora, V. & Marchiori, M. Efficient behavior of small-world networks. *Phys. Rev. Lett.* **87**, 198701 (2001).
47. Freeman, L. C. A set of measures of centrality based on betweenness. *Sociometry* **40**, 35 (1977).
48. Castellano, C., Cecconi, F., Loreto, V., Parisi, D. & Radicchi, F. Self-contained algorithms to detect communities in networks. *Eur. Phys. J. B* **38**, 311–319 (2004).
49. Newman, M. & Girvan, M. Finding and evaluating community structure in networks. *Phys. Rev. E* **69**, 26113 (2004).
50. Buldú, J. M. *et al.* Reorganization of functional networks in mild cognitive impairment. *PLoS ONE* **6**, 1–8 (2011).
51. Daianu, M. *et al.* In *Algebraic Connectivity of Brain Networks Shows Patterns of Segregation Leading to Reduced Network Robustness in Alzheimer's Disease BT*: *Computational Diffusion MRI* (eds O'Donnell, L. *et al.*) 55–64 (Springer International Publishing, Berlin, 2014).
52. Rubinov, M. & Sporns, O. Complex network measures of brain connectivity: Uses and interpretations. *NeuroImage* **52**, 1059–1069 (2010).
53. Chung, M. K. *et al.* Cortical thickness analysis in autism with heat kernel smoothing. *NeuroImage* **25**, 1256–1265 (2005).
54. He, Y. *et al.* Impaired small-world efficiency in structural cortical networks in multiple sclerosis associated with white matter lesion load. *Brain* **132**, 3366–3379 (2009).
55. Efron, B. *The Jackknife, the Bootstrap and Other Resampling Plans* (Society for Industrial and Applied Mathematics, Philadelphia, 1982).
56. Melie-Garcia, L., Sanabria-Diaz, G., Iturria-Medina, Y., Alemán-Gómez, Y. MorphoConnect: toolbox for studying structural brain networks using morphometric descriptors. In *16th Annual Meeting of the Organization for Human Brain Mapping* (2010).
57. Xia, M., Wang, J. & He, Y. BrainNet viewer: A network visualization tool for human brain connectomics. *PLoS ONE* **8**, e68910 (2013).
58. Bastian, M., Heymann, S. & Jacomy, M. Gephi : An open source software for exploring and manipulating networks visualization and exploration of large graphs. *Icwsm* **8**, 361–362 (2009).
59. Verghese, P. B., Castellano, J. M. & Holtzman, D. M. Apolipoprotein E in Alzheimer's disease and other neurological disorders. *Lancet Neurol* **10**, 241–252 (2011).
60. Dickerson, B. C. *et al.* Detection of cortical thickness correlates of cognitive performance: Reliability across MRI scan sessions, scanners, and field strengths. *NeuroImage* **39**, 10–18 (2008).
61. Gong, G., He, Y., Chen, Z. J. & Evans, A. C. Convergence and divergence of thickness correlations with diffusion connections across the human cerebral cortex. *NeuroImage* **59**, 1239–1248 (2012).
62. Tijms, B. M. *et al.* Gray matter networks and clinical progression in subjects with predementia Alzheimer ' s disease. *Neurobiol. Aging* **61**, 75–81 (2018).
63. Pereira, J. B. *et al.* Disrupted network topology in patients with stable and progressive mild cognitive impairment and Alzheimer's disease. *Cereb. Cortex* **26**, 3476–3493 (2016).
64. Sporns, O. & Zwi, J. D. *The Small World of the Cerebral Cortex* 145–162 (Springer, Berlin, 2004).
65. Tuminello, E. R. & Han, S. D. The Apolipoprotein E antagonistic pleiotropy hypothesis: Review and recommendations. *Int. J. Alzheimer's Dis.* **2011**, 1–12 (2011).
66. Buckner, R. L., Andrews-Hanna, J. R. & Schacter, D. L. The brain's default network: Anatomy, function, and relevance to disease. *Ann. N. Y. Acad. Sci.* **1124**, 1–38 (2008).
67. Raichle, M. E. *et al.* A default mode of brain function. *Proc. Natl. Acad. Sci. USA* **98**, 676–682 (2001).
68. Bero, A. W. *et al.* Neuronal activity regulates the regional vulnerability to amyloid-β deposition. *Nat. Neurosci.* **14**, 750–756 (2011).
69. Sun, Z.-W. *et al.* Decreased cerebral blood flow velocity in apolipoprotein E epsilon4 allele carriers with mild cognitive impairment. *Eur. J. Neurol.* **14**, 150–155 (2007).
70. Curtis, C. E. & D'Esposito, M. Persistent activity in the prefrontal cortex during working memory. *Trends Cogn. Sci.* **7**, 415–423 (2003).
71. Lau, H. C., Rogers, R. D. & Passingham, R. E. On measuring the perceived onsets of spontaneous actions. *J. Neurosci.* **26**, 7265–7271 (2006).
72. Ridderinkhof, K. R., Ullsperger, M., Crone, E. A. & Nieuwenhuis, S. The role of the medial frontal cortex in cognitive control. *Science* **306**, 443–447 (2004).

73. Salathé, M. & Jones, J. H. Dynamics and control of diseases in networks with community structure. *PLoS Comput. Biol.* **6**, e1000736 (2010).
74. Fair, D. A. *et al.* The maturing architecture of the brain's default network. *Proc. Natl. Acad. Sci. USA* **105**, 4028–4032 (2008).
75. Calhoun, V. D., Miller, R., Pearlson, G. & Adali, T. The chronnectome: Time-varying connectivity networks as the next frontier in fMRI data discovery. *Neuron* **84**, 262–274 (2014).
76. Zalesky, A., Fornito, A. & Bullmore, E. T. Network-based statistic: Identifying differences in brain networks. *NeuroImage* **53**, 1197–1207 (2010).

Acknowledgements

The investigators within the ADNI contributed to the design and implementation of ADNI and/or provided data but did not participate in the analysis or writing of this report. A complete listing of ADNI investigators and affiliations can be found at http://adni.loni.usc.edu/wp-content/uploads/how_to_apply/ADNI_Acknowledgement_List.pdf. ADNI was launched in 2003 as a public-private partnership led by Principal Investigator Michael W. Weiner, MD. ADNI is funded by the National Institute on Aging, the National Institute of Biomedical Imaging and Bioengineering, and through generous contributions from the following: AbbVie, 'Alzheimer's Association; 'Alzheimer's Drug Discovery Foundation; Araclon Biotech; BioClinica, Inc.; Biogen; Bristol-Myers Squibb Company; CereSpir, Inc.; Cogstate; Eisai Inc.; Elan Pharmaceuticals, Inc.; Eli Lilly and Company; EuroImmun; F. Hoffmann-La Roche Ltd and its affiliated company Genentech, Inc.; Fujirebio; GE Healthcare; IXICO Ltd.; Janssen Alzheimer Immunotherapy Research & Development, LLC.; Johnson & Johnson Pharmaceutical Research & Development LLC.; Lumosity; Lundbeck; Merck & Co., Inc.; Meso Scale Diagnostics, LLC.; NeuroRx Research; Neurotrack Technologies; Novartis Pharmaceuticals Corporation; Pfizer Inc.; Piramal Imaging; Servier; Takeda Pharmaceutical Company; and Transition Therapeutics. The Canadian Institutes of Health Research is providing funds to support ADNI clinical sites in Canada. Private sector contributions are facilitated by the Foundation for the National Institutes of Health (www.fnih.org). The grantee organization is the Northern California Institute for Research and Education, and the study is coordinated by the 'Alzheimer's Therapeutic Research Institute at the University of Southern California. ADNI data are disseminated by the Laboratory for Neuro Imaging at the University of Southern California. This study was funded by Janssen Prevention Centre, http://www.janssen.com/janssen-prevention-center. FK and GS received funding from the European Union Seventh Framework Programme (FP7/2007–2013) under grant agreement No 604102 and the European 'Union's Horizon 2020 research and innovation programme under grant agreement No 720270 (HBP SGA1) and the MORPHEMIC Grant (ID: 871643). BD is supported by the Swiss National Science Foundation (NCCR Synapsy, project grants Nr. 32003B_135679, 32003B_159780, and CRSK-3_190185) and the Leenaards Foundation. LREN is very grateful to Roger De Spoelberch and Partridge Foundations for their generous financial support. The authors thank Dr. Borja Rodriguez Herreros and Maya Jastrzębowska for their contributions to this paper's revision.

Author contributions

G.S.D. conceived and designed the experiment. A.D.N.I. acquired the data. L.M.G. implemented the programming codes. G.S.D. and L.M.G. analyzed the data. G.S.D. wrote the main manuscript. K.F., J.F.D., and L.M.G. provided feedback on data analysis and manuscript preparation/writing. G.S.D. and L.M.G. prepared the figures. K.F. and J.F.D. supervised the project. J.F.D. and B.D. provided feedback on the discussion section. All authors contributed to constructive discussions regarding the interpretation of the results.

Competing interests

The authors declare no competing interests.

Additional information

Supplementary Information The online version contains supplementary material available at https://doi.org/10.1038/s41598-020-80909-7.

Correspondence and requests for materials should be addressed to G.S.-D.

Reprints and permissions information is available at www.nature.com/reprints.

Publisher's note Springer Nature remains neutral with regard to jurisdictional claims in published maps and institutional affiliations.

Title: Apolipoprotein E4 effects on Topological Brain Network Organization in Mild Cognitive Impairment

Authors: Gretel Sanabria-Diaz, Lester Melie-Garcia, Bogdan Draganski, Jean-Francois Demonet, Ferath Kherif

Supplementary Information

Supplementary Table S1. List of anatomical structures

Code	Atlas Name	Structure Full name	Structure Short Name	Lobe
1	G and S frontomargin	Fronto-marginal gyrus (of Wernicke) and sulcus	FMarG.S	F
2	G and S occipital inf	Inferior occipital gyrus (O3) and sulcus	InfOcG.S	T -O
3	G and S paracentral	Paracentral lobule and sulcus	PaCL.S	F-P
4	G and S subcentral	Subcentral gyrus (central operculum) and sulci	SbCG.S	F
5	G and S transv frontopo	Transverse frontopolar gyri and sulci	TrFPoG.S	F
6	G and S cingul Ant	Anterior part of the cingulate gyrus and sulcus (ACC)	ACgG.S	L
7	G and S cingul Mid Ant	Middle-anterior part of the cingulate gyrus and sulcus (aMCC)	MACgG.S	L
8	G and S cingul Mid Post	Middle-posterior part of the cingulate gyrus and sulcus (pMCC)	MPosCgG.S	L
9	G cingul Post dorsal	Posterior-dorsal part of the cingulate gyrus (dPCC)	PosDCgG	L
10	G cingul Post ventral	Posterior-ventral part of the cingulate gyrus (vPCC, isthmus of the cingulate gyrus)	PosVCgG	L
11	G cuneus	Cuneus (O6)	Cun	O
12	G front inf Opercular	Opercular part of the inferior frontal gyrus	InfFGOpp	F
13	G front inf Orbital	Orbital part of the inferior frontal gyrus	InfFGOrp	F
14	G front inf Triangul	Triangular part of the inferior frontal gyrus	InfFGTrip	F
15	G front middle	Middle frontal gyrus (F2)	MFG	F
16	G front sup	Superior frontal gyrus (F1)	SupFG	F
17	G Ins lg and S cent ins	Long insular gyrus and central sulcus of the insula	LoInG.CInS	I
18	G insular short	Short insular gyri	ShoInG	I
19	G occipital middle	Middle occipital gyrus (O2, lateral occipital gyrus)	MOcG	O
20	G occipital sup	Superior occipital gyrus (O1)	SupOcG	O
21	G oc temp lat fusifor	Lateral occipito-temporal gyrus (fusiform gyrus, O4-T4)	FuG	T-O
22	G oc temp med Lingual	Lingual gyrus, lingual part of the medial occipito-temporal gyrus, (O5)	LinG	O-T

23	G oc temp med Parahip	Parahippocampal gyrus, parahippocampal part of the medial occipito-temporal gyrus, (T5)	PaHipG	O-T
24	G orbital	Orbital gyri	OrG	F
25	G pariet inf Angular	Angular gyrus	AngG	P
26	G pariet inf Supramar	Supramarginal gyrus	SuMarG	P
27	G parietal sup	Superior parietal lobule (lateral part of P1)	SupPL	P
28	G postcentral	Postcentral gyrus	PosCG	P
29	G precentral	Precentral gyrus	PrCG	F
30	G precuneus	Precuneus (medial part of P1)	PrCun	P
31	G rectus	Straight gyrus, Gyrus rectus	RG	F
32	G subcallosal	Subcallosal area, subcallosal gyrus	SbCaG	L
33	G temp sup G T transv	Anterior transverse temporal gyrus (of Heschl)	HG	T
34	G temp sup Lateral	Lateral aspect of the superior temporal gyrus	SupTGLp	T
35	G temp sup Plan polar	Planum polare of the superior temporal gyrus	PoPI	T
36	G temp sup Plan tempo	Planum temporale or temporal plane of the superior temporal gyrus	TPI	T
37	G temporal inf	Inferior temporal gyrus (T3)	InfTG	O-T
38	G temporal middle	Middle temporal gyrus (T2)	MTG	T
39	Lat Fis ant Horizont	Horizontal ramus of the anterior segment of the lateral sulcus (or fissure)	ALSHorp	F
40	Lat Fis ant Vertical	Vertical ramus of the anterior segment of the lateral sulcus (or fissure)	ALSVerp	F
41	Lat Fis post	Posterior ramus (or segment) of the lateral sulcus (or fissure)	PosLS	I
42	Pole occipital	Occipital pole	OcPo	T-O
43	Pole temporal	Temporal pole	TPo	T-O
44	S calcarine	Calcarine sulcus	CcS	O
45	S central	Central sulcus (Rolando's fissure)	CS	F
46	S cingul Marginalis	Marginal branch (or part) of the cingulate sulcus	CgSMarp	F
47	S circular insula ant	Anterior segment of the circular sulcus of the insula	ACirInS	I
48	S circular insula inf	Inferior segment of the circular sulcus of the insula	InfCirInS	I
49	S circular insula sup	Superior segment of the circular sulcus of the insula	SupCirInS	I
50	S collat transv ant	Anterior transverse collateral sulcus	ATrCoS	O-T
51	S collat transv post	Posterior transverse collateral sulcus	PosTrCoS	O-T
52	S front inf	Inferior frontal sulcus	InfFS	F
53	S front middle	Middle frontal sulcus	MFS	F
54	S front sup	Superior frontal sulcus	SupFS	F
55	S interm prim Jensen	Sulcus intermedius primus (of Jensen)	JS	P
56	S intrapariet and P tra	Intraparietal sulcus (interparietal sulcus) and transverse parietal sulci	IntPS.TrPS	P
57	S oc middle and Lunatus	Middle occipital sulcus and lunatus sulcus	MOcS.LuS	O
58	S oc sup and transversa	Superior occipital sulcus and transverse occipital sulcus	SupOcS.TrOcS	O
59	S occipital ant	Anterior occipital sulcus and preoccipital notch (temporo-occipital incisure)	AOcS	T-O
60	S oc temp lat	Lateral occipito-temporal sulcus	LOcTS	O-T
61	S oc temp med and	Medial occipito-temporal sulcus (collateral	CoS.LinS	O-T

	Lingu	sulcus) and lingual sulcus		
62	S orbital lateral	Lateral orbital sulcus	LOrS	F
63	S orbital med olfact	Medial orbital sulcus (olfactory sulcus)	MedOrS	F
64	S orbital H Shaped	Orbital sulci (H-shaped sulci)	OrS	F
65	S parieto occipital	Parieto-occipital sulcus (or fissure)	POcS	P-O
66	S pericallosal	Pericallosal sulcus (S of corpus callosum)	PerCaS	L
67	S postcentral	Postcentral sulcus	PosCS	P
68	S precentral inf part	Inferior part of the precentral sulcus	InfPrCS	F
69	S precentral sup part	Superior part of the precentral sulcus	SupPrCS	F
70	S suborbital	Suborbital sulcus (sulcus rostrales, supraorbital sulcus)	SbOrS	F
71	S subparietal	Subparietal sulcus	SbPS	P
72	S temporal inf	Inferior temporal sulcus	InfTS	T-O
73	S temporal sup	Superior temporal sulcus (parallel sulcus)	SupTS	T
74	S temporal transverse	Transverse temporal sulcus	TrTS	T

The regions are listed following the anatomical brain atlas described in Destrieux et al. (2010). The subcortical regions were not included. The short names, as well as the full structure names, are specified. The lobe to which the structure belongs is also included. L: Limbic; I: Insula; P: Parietal; O: Occipital; F: Frontal; T: Temporal. G: gyri; S: sulcus.

Supplementary Table S2. Network properties definition and interpretation.

Network Property	Definition	Interpretation
Measures of functional brain segregation *Functional segregation: the ability for specialized processing to occur within densely interconnected groups of brain regions*		
Clustering index	. Nodes are considered neighbors when a connection between them exists, which is not reduced to a physical neighborhood concept.	In anatomical networks, the clusters suggest the potential for functional segregation, while the presence of clusters in functional networks suggests an organization of statistical dependencies indicative of segregated neural processing.
Modularity	Many complex networks, like the brain, consisting of several modules. Modules are derived from a decomposition of the network into subcomponents that are internally strongly coupled but externally only weakly correlated. Each module contains several densely interconnected nodes (brain regions).	Dense connectivity within modules allows brain regions within each module to interact with one another easily. In contrast, sparser connectivity between modules allows each set of brain regions to be relatively independent of one another (specialized functions). Diminished connectivity between communities can result in loss of essential interactions or even disconnection of an entire community. On the other hand, excessive connectivity between modules may result in loss of compartmentalization or specialization of this brain region group.
	It is the average efficiency of the local	This measure reveals how much the

Local Efficiency	subgraphs	brain as a system is fault-tolerant, showing how efficient the communication is among the first neighbors of a node (brain region) when it is removed.
Measures of functional brain integration *Functional integration: is the ability to combine specialized information from distributed brain regions rapidly*		
Characteristic path length	The path length is the minimum number of edges that must be traversed to go from one node (brain region) to another. It is a measure of the typical separation between two brain regions. The average shortest path length between all pairs of nodes in the the network is known as the characteristic path length of the network. Connection lengths are typically dimensionless and do not represent spatial or metric distance.	Lengths of paths consequently estimate the potential for functional integration between brain regions. Shorter paths are implying a more substantial potential for integration between brain regions. Paths in functional/morphological networks represent statistical associations and may not correspond to information flow on anatomical connections. In this case, paths are less straightforward to interpret in terms of brain functions.
Global efficiency	It is the average inverse of the shortest path length.	The global efficiency es primarily affected by the shorth path length, represents a superior measure of integration.
Global connectivity	It summarizes the interregional correlations coefficients between all possible pairs of nodes (brain regions). Describes the degree to which nodes are connected in a network. It can be quantified based on network metrics such as the relative density, the shortest path, or the diameter of the network.	Previous studies have found strong correlations between regions with no direct structural (white matter tracts) connection. The total interregional morphometric correlations could capture all indirect structural correlations between two brain regions facilitated by a third party, from which diverse factors such as pathologic changes to the connectivity patterns could be detected.
Normalized betweenness centrality	The centrality of a node (brain region) measures how many of the shortest paths between all other brain regions pairs in the network pass through it. Bridging nodes that connect disparate parts of the network have a high betweenness centrality.	A node (brain region) with high centrality is thus crucial to efficient communication. It is based on the idea that central nodes participate in many short paths within a network, and consequently, act as essential controls of information flow. Their loss is particularly disruptive to the brain network. Several regions in the frontal and parietal cortex have high centrality in the human brain, particularly the posterior cingulate and precuneus. These are areas of the brain defined as transmodal or heteromodal. They are involved in integrating processing across several cognitive modalities. Some of these regions overlap with the DMN, while others coincide with the frontoparietal system.
	Hubs are nodes with a high degree or	Hubs often interact with many other

Hubs	high centrality. Measures of node centrality assess the importance of individual nodes. The hubs of the network are the regions with high values of NBC.	areas, facilitate functional integration, and play a vital role in the brain network resilience to insult. Hubs are a cost-efficient solution to increase network efficiency to support cognitive processes without requiring many metabolically expensive connections. Hubs are suggested to be essential for cognition because they are located along the shortest paths in the network, and therefore are likely to play a critical role in distributed patterns of communication. This location is evident both by their high degree and by their tendency to connect, forming a core or "rich-club" that boosts inter-hub communication's robustness and promotes efficient communication across the brain. Damage to brain hubs is expected to have critical consequences for cognitive function in terms of the severity and pervasiveness of cognitive deficits.
Measures of network resilience *Reflects the brain network vulnerability to insults*		
Targeted Attack	The importance of an individual node to network efficiency can be assessed by deleting it and estimating the the efficiency of the 'lesioned' network. It is an indirect measure of resilience that reflects network vulnerability to insult. Complex networks like the brain are highly vulnerable to disruptions of the central node (hubs).	Robustness refers either to the network's structural integrity following the deletion of nodes or edges or to the effects of perturbations on local or global network states. Direct measures of network resilience generally test the network before and after a presumed insult by computationally simulated targeted removal of nodes and links. The effects of such lesions on the brain network may then be quantified by characterizing changes in the resulting brain connectivity.

Sample Biomarkers Characteristics

Cerebrospinal fluid (CSF) samples at baseline were collected from 192 MCI subjects as part of the ADNI-1 protocol. The overlap between this sample and the one selected for the present study corresponds to 132 subjects (67 MCI-Carriers and 65 MCI non-Carriers). For details about CSF samples and methods see UPENN CSF Biomarkers Elecsys [ADNI1,GO,2].csv and UPENN CSF Biomarkers Elecsys METHODS [ADNI1,GO,2] (PDF) at https://ida.loni.usc.edu/pages/access/studyData

MCI groups characterization based on ADNI1 CSF biomarker measurements (Aβ (1-42), tTau, and pTau) at baseline

Biomarkers	**MCI-Carriers** (N,67)	**MCI non-Carriers** (N, 65)
Aβ(1-42)*	710.88 (398.26)	1068.54 (528.09)
tTau*	335.79 (125.94)	276.52 (109.45)
pTau*	35.77 (16.90)	26.05 (11.93)

Values are represented by the mean (pg/mL) and the Standard deviations (SD). N: number of subjects; MCI: Mild Cognitive Impairment; Carriers: *ApoE4*-positive; non-Carriers: *ApoE4*-negative; Aβ(1-42): β-Amyloid (1-42); tTau: Total-Tau; pTau: Phospho-Tau. The superscript "*" represents significant T-test for independent samples set at $p<0.05$

MCI groups characterization as biomarker positive and negative based on Aβ (1-42), tTau and pTau

	Group			
	MCI-Carriers		**MCI non-Carriers**	
Biomaker	BM+	BM-	BM+	BM-
Aβ(1-42)	56 (83.9)	11(16.4)	30 (46.1)	35 (53.8)
pTau	45 (67.2)	22 (32.8)	24 (36.9)	41 (63)
tTau	41 (61.2)	26 (38.8)	22 (33.8)	43 (66.1)
***pTau*/ Aβ(1-42)**	55 (82)	12 (17.9)	29 (44.6)	36 (55.2)
***tTau*/ Aβ(1-42)**	56 (83.6)	11 (16.4)	28 (43)	37 (56.9)

Values are represented by the number of subjects (%). The positive (+) and negative (-) status are based on PET-optimized cut-offs for Aβ(1-42), pTau/Aβ(1-42) and tTau/Aβ(1-42). CSF, cerebrospinal fluid; BM, biomarker; Aβ(1-42): β-Amyloid (1-42); tTau: Total-Tau; pTau: Phospho-Tau; MCI, mild cognitive impairment. For biomarkers, cut-offs description, see Hansson et al. (2018).

CSF Biomarkers groups characterization. The Amyloid plaque burden +/- represented by Aβ (1-42) and Tau pathology represented by tTau+ or -

Biomaker	**MCI-Carriers**	**MCI non-carriers**
Aβ(1-42)+/ tTau +	37 (55.2%)	5 (7.5%)
Aβ(1-42)+/ tTau -	19 (28.4%)	25 (37.3%)
Aβ(1-42)-/ tTau +	4 (5.9%)	17 (25.6%)
Aβ(1-42)-/ tTau -	7(10.5%)	18 (26.9%)

Values are represented by the number of subjects (%). The positive (+) and negative (-) status are based on PET-optimized cut-offs for Aβ(1-42), pTau/Aβ(1-42) and tTau/Aβ(1-42). CSF, cerebrospinal fluid; Aβ(1-42): β-Amyloid

(1-42); tTau: Total-Tau; pTau: Phospho-Tau; MCI, mild cognitive impairment. For biomarkers, cut-offs description, see Hansson et al. (2018).

Graph Theory Metrics

The following group theoretical metrics were computed in the present study:

Clustering index (C). The clustering index of a node 'i' is defined as the number of existing connections between the node's neighbors divided by all possible connections. It is a measure of the inherent tendency to cluster nodes into strictly connected neighborhoods. Nodes are considered neighbors when a connection between them exists, which is not reduced to a physical neighborhood concept. The clustering index for the whole graph G is defined as the average clustering around each node:

$$C = \frac{1}{N}\sum_{i \in G} C_i \tag{1}$$

Represent the number of nodes. Clearly, $0 < C < 1$; and $C = 1$ if and only if the network is fully connected, that is, each node is connected to all other nodes.

Characteristic path length (L). The characteristic path length L of the graph G is the smallest number of connections required to connect one node to another, averaged over all pairs of nodes. It is a measure of the typical separation between two nodes (structures) i and j $\left(\forall i, j \in N\right)$, and it is defined as the mean of geodesic lengths d_{ij} over all pairs of nodes.

$$L = \frac{1}{N\left(N-1\right)}\sum_{\substack{i,\, j \in G \\ i \neq j}} d_{ij} \tag{2}$$

In the unweighted network context, the geodesic length d_{ij} is defined as the number of edges along the shortest path connecting nodes i and j.

Nodal efficiency (E_{glob}, E_{loc}). The concept of efficiency has also been expressed in terms of information flow. That is, small-world networks are very efficient in terms of global and local communication and they are defined to have high global E_{glob} and local E_{loc} efficiency. The global E_{glob} of a graph G is expressed as:

$$E_{glob} = \frac{1}{N(N-1)} \sum_{\substack{i,j \in G \\ i \neq j}} \frac{1}{d_{ij}} \tag{3}$$

This measure reflects how efficiently the information can be exchanged over the network, considering a parallel system in which each node sends information concurrently through the network. On the other hand, the E_{loc} of G is defined as the average efficiency of the local subgraphs:

$$E_{loc} = \frac{1}{N} \sum_{i \in G} E_{glob}(G_i) \tag{4}$$

Where G_i is the subgraph of the neighbors of '*i*'. This measure reveals how much the system is fault-tolerant, showing how efficient the communication is among the first neighbors of *i* when it is removed. As above, nodes are considered neighbors when a connection between them exists, which is not reduced to a physical neighborhood concept.

Global and Homologous regional connectivity. We assessed the global connectivity and homologous region connectivity. First, the absolute correlation coefficient values were converted to z using Fisher's r-to-z transformation, followed by taking the mean and transforming back to correlations through the inverse Fisher's z-to-r transformation. All anatomical regions were used to estimate the global connectivity, whereas only the correlation values between homologous regions were used in the mean homologous region connectivity.

Nodal centrality: normalized betweenness centrality (NBC). The 'betweenness centrality' B_i of a node *i* is defined as the number of shortest paths between any two nodes that run through node *i*. We measured the normalized betweenness centrality as $b_i = B_i / \langle B \rangle$, where $\langle B \rangle$ was the average betweenness of the network. b_i is a global centrality measure that captures a node's influence over information flow between other nodes in the network. In our case, betweenness centrality b_i could be used to reflect the effects of ApoE4 on the global roles of regions in the cortical thickness covariance networks. Hubs were selected as those with b_i superior to 1.5, similar to previous investigations.

Modularity. A complex network module is a subset of nodes that are densely connected within the modules but sparsely connected between the modules. Here we have adopted Newman's metric as a modularity measure to compare our results with previous studies that used this method in other neuroimaging modalities.

Targeted Attack: Methodology to study the robustness of the cortical thickness covariance network

We calculated a surrogate measure of the resilience of the cortical thickness covariance network against a targeted attack. In a simulated targeted attack study, network hubs are removed one by one in order of betweenness centrality (NBC). Each time a node was removed from the network, the largest connected component's size was recomputed. We defined the robustness parameter as the AUC showing the relative largest connected component's size versus the number of nodes removed[94]. Robust networks retain large connected components even when several nodes have been knocked out, represented by a large AUC. As before, we repeated this procedure for all bootstrapped connectivity matrices and sparsity degrees. The same statistical procedure used for

evaluating the ApoE4 effect of global network properties was applied to explore network robustness differences between groups.

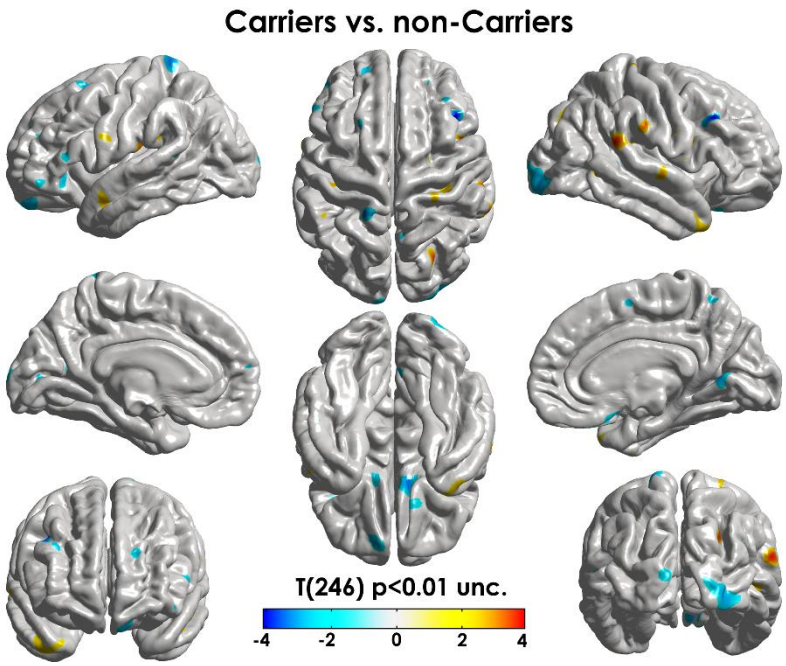

Fig S1. Spatially distributed differences in cortical thickness between MCI Carriers and non-Carriers (p<.01, uncorrected). Relative deficits in Carriers compared with non-Carriers are displayed in red/yellow, while excesses are shown in blue/cyan. Surfaces are presented in lateral, medial, and frontal views for the left and right pial (outer) surface. After Random-field theory-based cluster-corrected (q<.05) there were no clusters of significant differences between groups.

Supplementary Table S3. Cortical thickness cluster differences between MCI Carriers vs non-Carriers for p<0.01 (uncorrected)

Structure Name	t-Student	p-value
rh G front middle	-4.10	3E-05
rh S front inf	-4.00	4E-05
rh S precentral-inf-part	3.92	6E-05
rh G pariet inf-Supramar	3.75	1E-04
lh S oc-temp med and Lingual	3.69	1E-04
rh G occipital sup	3.61	2E-04
rh S orbital med-olfact	-3.40	4E-04
lh G and S paracentral	-3.39	4E-04
rh Medial wall	-3.37	4E-04
rh G rectus	-3.37	4E-04
lh G and S subcentral	3.35	5E-04
lh G pariet inf-Supramar	3.34	5E-04
lh G parietal sup	-3.26	6E-04

rh G oc-temp med-Lingual	-3.18	8E-04
rh S oc sup and transversal	3.10	1E-03
rh Pole occipital	-3.09	1E-03
lh G front sup	-3.05	1E-03
lh S front sup	-3.05	1E-03
lh Lat Fis-post	3.02	1E-03
rh G temp sup-Lateral	2.98	2E-03
rh S intrapariet and P trans	2.98	2E-03
lh G orbital	-2.95	2E-03
rh S postcentral	2.94	2E-03
rh S interm prim-Jensen	2.92	2E-03
rh G front sup	-2.92	2E-03
rh G postcentral	2.92	2E-03
rh G and S cingul-Mid-Post	-2.90	2E-03
rh S central	2.90	2E-03
lh S central	2.87	2E-03
lh Lat Fis-ant-Horizont	-2.86	2E-03
rh G and S occipital inf	-2.86	2E-03
rh S circular insula sup	2.86	2E-03
rh S front middle	-2.84	2E-03
rh G occipital middle	-2.84	2E-03
rh S temporal inf	2.83	3E-03
rh G precuneus	-2.83	3E-03
lh G temp sup-Lateral	2.83	3E-03
lh G precentral	2.82	3E-03
lh S orbital med-olfact	-2.79	3E-03
rh G temporal middle	2.78	3E-03
rh G subcallosal	-2.77	3E-03
lh Medial wall	-2.77	3E-03
lh G front inf-Orbital	-2.76	3E-03
lh G front middle	-2.75	3E-03
lh G front inf-Triangul	-2.73	3E-03
rh G front inf-Opercular	2.70	4E-03
lh Pole occipital	-2.68	4E-03
rh Lat Fis-post	2.66	4E-03
rh Pole temporal	2.66	4E-03
lh S calcarine	-2.64	4E-03
lh S temporal sup	-2.60	5E-03
rh S temporal sup	2.59	5E-03
rh S precentral-sup-part	2.56	6E-03
lh G cuneus	-2.54	6E-03
rh G orbital	-2.53	6E-03
rh G precentral	2.53	6E-03
lh S orbital lateral	-2.52	6E-03
lh S front middle	-2.52	6E-03
rh G temp sup-Plan tempo	2.47	7E-03
lh Lat Fis-ant-Vertical	-2.44	8E-03
lh G temporal middle	2.41	8E-03
lh S parieto occipital	-2.40	8E-03
lh G postcentral	-2.37	9E-03

lh G occipital sup	-2.37	9E-03
rh S front sup	-2.35	1E-02
lh G temporal inf	-2.35	1E-02
lh G occipital middle	-2.35	1E-02
rh G and S subcentral	2.34	1E-02
rh G pariet inf-Angular	-2.34	1E-02
lh G precuneus	2.33	1E-02
lh S circular insula ant	-2.32	1E-02
rh G temp sup-Plan polar	2.30	1E-02
lh G insular short	-2.30	1E-02
lh S intrapariet and P trans	-2.30	1E-02
lh G rectus	-2.30	1E-02
lh S postcentral	2.29	1E-02
lh G oc-temp med-Lingual	-2.28	1E-02
rh G parietal sup	-2.27	1E-02
lh S oc middle and Lunatus	-2.26	1E-02
rh G and S cingul-Mid-Ant	-2.25	1E-02
rh S pericallosal	2.25	1E-02
rh G and S paracentral	-2.24	1E-02
rh S subparietal	-2.23	1E-02
rh S parieto occipital	-2.22	1E-02
rh S cingul-Marginalis	-2.21	1E-02
rh S calcarine	-2.21	1E-02
rh G oc-temp med-Parahip	2.21	1E-02
lh G pariet inf-Angular	-2.20	1E-02
rh S orbital-H Shaped	-2.18	2E-02
rh S occipital ant	2.17	2E-02
rh G cingul-Post-dorsal	2.17	2E-02
lh G oc-temp med-Parahip	-2.14	2E-02
lh G and S cingul-Mid-Post	2.13	2E-02
rh G front inf-Triangul	-2.13	2E-02
lh S circular insula sup	2.11	2E-02
rh Lat Fis-ant-Vertical	-2.09	2E-02
lh S suborbital	-2.08	2E-02
rh S circular insula inf	2.08	2E-02
rh G cingul-Post-ventral	2.08	2E-02
lh G temp sup-G T transv	2.06	2E-02
rh G and S transv frontopol	-2.05	2E-02
rh G Ins lg and S cent ins	2.05	2E-02
lh S circular insula inf	2.03	2E-02
rh S temporal transverse	2.02	2E-02
rh G temporal inf	-2.02	2E-02
rh G temp sup-G T transv	2.01	2E-02
lh S oc-temp lat	2.00	2E-02
lh S collat transv post	-1.99	2E-02
lh G temp sup-Plan tempo	1.97	2E-02
lh G Ins lg and S cent ins	-1.96	3E-02
lh S pericallosal	-1.93	3E-02
lh S front inf	1.93	3E-02
lh S precentral-inf-part	-1.92	3E-02

lh G and S frontomargin	-1.92	3E-02
lh G and S transv frontopol	-1.90	3E-02
rh S collat transv ant	1.88	3E-02
lh G and S cingul-Ant	-1.88	3E-02
lh G and S occipital inf	-1.88	3E-02
lh G front inf-Opercular	-1.86	3E-02
lh G and S cingul-Mid-Ant	-1.85	3E-02
lh S oc sup and transversal	-1.84	3E-02
rh S suborbital	-1.83	3E-02
lh S orbital-H Shaped	-1.81	4E-02
rh S oc middle and Lunatus	-1.76	4E-02
rh G cuneus	-1.75	4E-02
lh S temporal inf	1.74	4E-02
lh S temporal transverse	1.73	4E-02
rh S oc-temp med and Lingual	1.72	4E-02
lh S occipital ant	1.71	4E-02
lh S precentral-sup-part	1.69	5E-02
rh S oc-temp lat	-1.67	5E-02
lh S interm prim-Jensen	1.65	5E-02

Supplementary Table S4. Significant differences in NBC between MCI Carriers and non-Carriers groups (FDR-corrected). Values represent the NBC mean and standard deviation (s.d). NBC: Normalize Betweenness Centrality.

Structure	Carriers NBC (s.d)	non-Carriers NBC (s.d)	p-value
Rh G and S cingul-Mid-Post	0.82 (0.17)	1.44 (0.23)	$1.2*10^{-9}$
Rh G oc-temp med-Lingual	1.19 (0.20)	0.94 (0.18)	0.02
Rh Lat Fis-ant-Horizont	0.80 (0.18)	1.36 (0.19)	$0.009*10^{-5}$
Rh S oc-temp med and Lingual	1.46 (0.29)	0.99 (0.19)	0.02
Rh S pericallosal	0.82 (0.18)	1.06 (0.20)	$0.008*10^{-5}$
Rh S temporal transverse	0.80 (0.17)	1.09 (0.17)	$0.007*10^{-3}$
Lh G subcallosal	0.83 (0.20)	1.10 (0.20)	0.04
Lh S circular insula ant	1.08 (0.19)	1.28 (0.23)	0.02
Lh S collat transv post	0.75 (0.15)	1.30 (0.20)	$2.3*10^{-11}$
Lh S precentral-sup-part	0.68 (0.17)	1.10 (0.21)	$0.05*10^{-3}$
Lh S temporal inf	1.19 (0.26)	0.93 (0.19)	0.02

Supplementary Table S5. Hubs regions for Carriers and non-Carriers listing by the descending order of the normalized betweenness centrality in each group

Carriers Hubs	NBC	non-Carriers Hubs	NBC
Rh S temporal sup	**2.73**	**Rh G and S cingul-Ant**	**2.69**
Rh G and S cingul-Mid-Post	**2.40**	**Rh S parieto occipital**	**2.59**
Rh G cingul-Post-ventral	**2.23**	**Lh S parieto occipital**	**2.26**
Rh Lat Fis-ant-Horizont	**2.02**	**Lh S oc-temp lat**	**2.15**
Lh S collat transv post	**1.81**	**Rh S oc-temp med and Lingual**	**1.99**
Lh G and S occipital inf	**1.70**	**Lh G oc-temp med-Lingual**	**1.78**
Lh S circular insula ant	**1.65**	**Rh G pariet inf-Supramar**	**1.78**
Lh G and S subcentral	**1.59**	**Lh S circular insula sup**	**1.73**
Rh S collat transv post	**1.50**	**Lh Lat Fis-ant-Horizont**	**1.69**
Rh G cuneus	1.47	**Rh Lat_Fis-post**	**1.68**
Lh G and S cingul-Ant	1.41	**Lh G and S subcentral**	**1.58**
Rh S front inf	1.35	**Rh S circular insula ant**	**1.57**
Rh G orbital	1.35	**Lh G and S cingul-Ant**	**1.55**
Rh S circular insula inf	1.28	Rh S temporal sup	1.33
Lh G cingul-Post-dorsal	1.19	Lh S occipital _ant	1.31
Rh S orbital med-olfact	1.17	Lh Lat Fis-post	1.22
Lh G temp sup-G T- transv	1.12	Lh S calcarine	1.20
Rh S circular insula ant	1.11	Rh G cingul-Post-dorsal	1.13
Rh S parieto occipital	1.08	Rh S interm prim-Jensen	1.10
Lh S temporal transverse	1.07	Rh G oc-temp med-Lingual	1.07
Lh S front inf	1.04	Rh S orbital-H Shaped	1.07
Lh Lat Fis-post	1.04	Lh G cingul-Post-dorsal	1.03
Rh S front middle	1.03	Rh S collat transv post	1.02
Rh Lat Fis-post	1.03	Rh S precentral-inf-part	1.00

Values represent the regional NBC means. Regions considered hubs per group if NBC>1. In bold hub regions with the higher NBC values (NBC>1.5). NBC: Normalize Betweenness Centrality.

Supplementary Table S6. List of brain regions module composition per group

Structure Full name	Atlas Name	Carriers	non-Carriers
Fronto-marginal gyrus (of Wernicke) and sulcus	G and S frontomargin	V	I

Inferior occipital gyrus (O3) and sulcus	G and S occipital inf	III	II
Paracentral lobule and sulcus	G and S paracentral	II	II
Subcentral gyrus (central operculum) and sulci	G and S subcentral	II (L), IV (R)	I
Transverse frontopolar gyri and sulci	G and S transv frontopo	V	I
Anterior part of the cingulate gyrus and sulcus (ACC)	G and S cingul Ant	V	I
Middle-anterior part of the cingulate gyrus and sulcus (aMCC)	G and S cingul Mid Ant	IV	I
Middle-posterior part of the cingulate gyrus and sulcus (pMCC)	G and S cingul Mid Post	II (L), IV (Ll)	I
Posterior-dorsal part of the cingulate gyrus (dPCC)	G cingul Post dorsal	IV (R), V (L)	III
Posterior-ventral part of the cingulate gyrus (vPCC, isthmus of the cingulate gyrus)	G cingul Post ventral	IV (R), V (L)	III
Cuneus (O6)	G cuneus	III	II
Opercular part of the inferior frontal gyrus	G front inf Opercular	II (L), IV (R)	I
Orbital part of the inferior frontal gyrus	G front inf Orbital	II (L), IV (R)	I
Triangular part of the inferior frontal gyrus	G front inf Triangul	II	I
Middle frontal gyrus (F2)	G front middle	II	II
Superior frontal gyrus (F1)	G front sup	II	II
Long insular gyrus and central sulcus of the insula	G Ins lg and S cent ins	IV	III
Short insular gyri	G insular short	IV	III
Middle occipital gyrus (O2, lateral occipital gyrus)	G occipital middle	III	II
Superior occipital gyrus (O1)	G occipital sup	III	II
Lateral occipito-temporal gyrus (fusiform gyrus, O4-T4)	G oc temp lat fusifor	I	II (R), III (L)
Lingual gyrus, lingual part of the medial occipito-temporal gyrus, (O5)	G oc temp med Lingual	I (R), III (L)	II
Parahippocampal gyrus, parahippocampal part of the medial occipito-temporal gyrus, (T5)	G oc temp med Parahip	I	III
Orbital gyri	G orbital	V	I
Angular gyrus	G pariet inf Angular	III	II
Supramarginal gyrus	G pariet inf Supramar	II	II (R), III (L)
Superior parietal lobule (lateral part of P1)	G parietal sup	III	II
Postcentral gyrus	G postcentral	II	II
Precentral gyrus	G precentral	II	II
Precuneus (medial part of P1)	G precuneus	III	II
Straight gyrus, Gyrus rectus	G rectus	I (L), V (R)	I
Subcallosal area, subcallosal gyrus	G subcallosal	I	I (R), III (L)
Anterior transverse temporal gyrus (of Heschl)	G temp sup G T transv	II	I
Lateral aspect of the superior temporal gyrus	G temp sup Lateral	I	III
Planum polare of the superior temporal gyrus	G temp sup Plan polar	I	III
Planum temporale or temporal plane of the superior temporal gyrus	G temp sup Plan tempo	II	III
Inferior temporal gyrus (T3)	G temporal inf	I	III
Middle temporal gyrus (T2)	G temporal middle	I	III
Horizontal ramus of the anterior segment of the lateral sulcus (or fissure)	Lat Fis ant Horizont	IV (L), V (R)	I
Vertical ramus of the anterior segment of the lateral sulcus (or fissure)	Lat Fis ant Vertical	II (L), IV (L)	I
Posterior ramus (or segment) of the lateral sulcus (or fissure)	Lat Fis post	II (L), IV (R)	I (L), III (R)

Occipital pole	Pole occipital	III	II
Temporal pole	Pole temporal	I	III
Calcarine sulcus	S calcarine	III	II
Central sulcus (Rolando's fissure)	S central	II	II
Marginal branch (or part) of the cingulate sulcus	S cingul Marginalis	II (R), III (L)	II
Anterior segment of the circular sulcus of the insula	S circular insula ant	IV	I
Inferior segment of the circular sulcus of the insula	S circular insula inf	IV	III
Superior segment of the circular sulcus of the insula	S circular insula sup	IV	III
Anterior transverse collateral sulcus	S collat transv ant	I	III
Posterior transverse collateral sulcus	S collat transv post	III	II
Inferior frontal sulcus	S front inf	V	I
Middle frontal sulcus	S front middle	V	I
Superior frontal sulcus	S front sup	II	II
Sulcus intermedius primus (of Jensen)	S interm prim Jensen	III	II
Intraparietal sulcus (interparietal sulcus) and transverse parietal sulci	S intrapariet and P tra	III	II
Middle occipital sulcus and lunatus sulcus	S oc middle and Lunatus	III	II
Superior occipital sulcus and transverse occipital sulcus	S oc sup and transversa	III	II
Anterior occipital sulcus and preoccipital notch (temporo-occipital incisure)	S occipital ant	III	II
Lateral occipito-temporal sulcus	S oc temp lat	I	III
Medial occipito-temporal sulcus (collateral sulcus) and lingual sulcus	S oc temp med and Lingu	I	III
Lateral orbital sulcus	S orbital lateral	V	I (L), III (R)
Medial orbital sulcus (olfactory sulcus)	S orbital med olfact	I (L), V (R)	III
Orbital sulci (H-shaped sulci)	S orbital H Shaped	V	III
Parieto-occipital sulcus (or fissure)	S parieto occipital	III	II
Pericallosal sulcus (S of corpus callosum)	S pericallosal	I (L), V (R)	III
Postcentral sulcus	S postcentral	III	II
Inferior part of the precentral sulcus	S precentral inf part	II (L) , III (R)	I (L), II (R)
Superior part of the precentral sulcus	S precentral sup part	II	II
Suborbital sulcus (sulcus rostrales, supraorbital sulcus)	S suborbital	V	I (L), III (R)
Subparietal sulcus	S subparietal	III	II
Inferior temporal sulcus	S temporal inf	I	III
Superior temporal sulcus (parallel sulcus)	S temporal sup	I (R), III (L)	III
Transverse temporal sulcus	S temporal transverse	I, IV (L)	I

In each structure, the module is identified with roman numbers. R: right hemisphere, L: left hemisphere. G: gyri; S: sulcus.

6.2 Apolipoprotein E allele 4 effects on Single-Subject Gray Matter Networks in Mild Cognitive Impairment

NeuroImage: Clinical

Apolipoprotein E allele 4 effects on Single-Subject Gray Matter Networks in Mild Cognitive Impairment

--Manuscript Draft--

Manuscript Number:	
Article Type:	Regular Article
Section/Category:	Dementia
Keywords:	Mild Cognitive Impairment; Alzheimer Disease; gray matter networks; single-subject gray matter networks; graph theory; MCI
Corresponding Author:	Gretel Sanabria-Diaz SWITZERLAND
First Author:	Gretel Sanabria-Diaz
Order of Authors:	Gretel Sanabria-Diaz
	Jean-Francois Demonet
	Borja Rodriguez-Herreros
	Bogdan Draganski
	Ferath Kherif
	Lester Melie-Garcia
Abstract:	There is evidence that gray matter networks are disrupted in Mild Cognitive Impairment (MCI) and associated with cognitive impairment and faster disease progression. However, it remains unknown how these alterations are related to the presence of Apolipoprotein E isoform E4 (ApoE4), the most prominent genetic risk factor for late-onset Alzheimer's disease (AD). To investigate this topic at the individual level, we explore the impact of ApoE4 and the disease progression on the Single-Subject Gray Matter Networks (SSGMNets) using the graph theory approach. Our data sample comprised 200 MCI patients selected from the ADNI database, classified as non-Converters and Converters (will progress into AD). Each group included 50 ApoE4 - positive ('Carriers', ApoE4+) and 50 ApoE4 - negative ('non-Carriers', ApoE4-). The SSGMNets were estimated from structural MRIs at two-time points: baseline and conversion. We investigated whether altered network topological measures at baseline and their rate of change (RoC) between baseline and conversion time points were associated with ApoE4 and disease progression. We also explored the correlation of SSGMNets attributes with general cognition score (MMSE), memory (ADNI-MEM), and CSF-derived biomarkers of AD (Aβ42, T-tau, and P-tau). Our results showed that ApoE4 and the disease progression modulated the global topological network properties independently but not in their RoC. MCI converters showed a lower clustering index in several regions associated with neurodegeneration in AD. The SSGMNets' topological organization was revealed to be able to predict cognitive and memory measures. The findings, presented here, suggest that SSGMNets could indeed be used to identify MCI ApoE4 Carriers with a high risk for AD progression.
Suggested Reviewers:	

Apolipoprotein E allele 4 effects on Single-Subject Gray Matter Networks in Mild Cognitive Impairment

Gretel Sanabria-Diaz [a,b+], Jean-Francois Demonet [c], Borja Rodriguez-Herreros [d], Bogdan Draganski [a,e] Ferath Kherif [a&], Lester Melie-Garcia [f,g&], for the Alzheimer's Disease Neuroimaging Initiative[*]

[a]*LREN, Department of Clinical Neurosciences, Lausanne University Hospital (CHUV), Rue du Bugnon 46, Mont Paisible 16,1011 Lausanne, Vaud, Switzerland.*

[b]*Faculté de biologie et de médecine (FMB), Université de Lausanne (UNIL), Rue du Bugnon 21, 1011 Lausanne, Switzerland*

[c]*Leenaards Memory Center, Lausanne University Hospital (CHUV), Rue du Bugnon 21, Mont Paisible 16,1011 Lausanne, Switzerland*

[d]*Cantonal Autism Center, University of Lausanne. University Hospital Lausanne. Av. de Beaumont 23, 1011 Lausanne, Switzerland*

[e]*Max-Planck-Institute for Human Cognitive and Brain Sciences, Postfach 500355, D-04303, Leipzig, Germany*

[f]*Applied Signal Processing Group (ASPG), Swiss Federal Institute of Technology Lausanne (EPFL), Route Cantonale, 1015. Lausanne, Switzerland*

[g]*Translational Imaging in Neurology Group (ThINk), Department of Biomedical Engineering, University of Basel and University Hospital Basel, Gewerbestrasse 14, 4123 Allschwil. Basel, Switzerland*

[&]*These authors contributed equally*

[+]Correspondence author:

Gretel Sanabria-Diaz

Laboratoire de recherche en neuroimagerie (LREN), Département des neurosciences cliniques, Centre Hospitalier Universitaire Vaudois (CHUV), Mont Paisible 16, 1011 Lausanne, Switzerland. Phone: +41 21 314 9593. Fax: +41 21 314 1256

E-mail address: gretels.sanabria@gmail.com

Gretel Sanabria-Diaz: gretels.sanabria@gmail.com
Bogdan Draganski: bogdan.draganski@gmail.com
Jean-Francois Demonet: jf.demonet@gmail.com
Borja Rodriguez-Herreros: borja.rodriguez84@gmail.com
Ferath Kherif: Ferath.Kherif@chuv.ch
Lester Melie-Garcia: lester.melie@gmail.com, lester.meliegarcia@unibas.ch

*Data used in preparation of this article were obtained from the Alzheimer's Disease Neuroimaging Initiative (ADNI) database (adni.loni.usc.edu). As such, the investigators within the ADNI contributed to the design and implementation of ADNI and/or provided data but did not participate in analysis or writing of this report. A complete listing of ADNI investigators can be found at:
http://adni.loni.usc.edu/wp-content/uploads/how_to_apply/ADNI_Acknowledgement_List.pdf

Running title: *ApoE4 effects on brain networks in MCI*

Abstract

There is evidence that gray matter networks are disrupted in Mild Cognitive Impairment (MCI) and associated with cognitive impairment and faster disease progression. However, it remains unknown how these alterations are related to the presence of Apolipoprotein E isoform E4 (ApoE4), the most prominent genetic risk factor for late-onset Alzheimer's disease (AD). To investigate this topic at the individual level, we explore the impact of ApoE4 and the disease progression on the Single-Subject Gray Matter Networks (*SSGMNets*) using the graph theory approach. Our data sample comprised 200 MCI patients selected from the ADNI database, classified as non-Converters and Converters (will progress into AD). Each group included 50 ApoE4-positive ('Carriers', ApoE4+) and 50 ApoE4-negative ('non-Carriers', ApoE4-). The *SSGMNets* were estimated from structural MRIs at two-time points: baseline and conversion. We investigated whether altered network topological measures at baseline and their rate of change (RoC) between baseline and conversion time points were associated with ApoE4 and disease progression. We also explored the correlation of *SSGMNets* attributes with general cognition score (MMSE), memory (ADNI-MEM), and CSF-derived biomarkers of AD (Aβ42, T-tau, and P-tau). Our results showed that ApoE4 and the disease progression modulated the global topological network properties independently but not in their RoC. MCI converters showed a lower clustering index in several regions associated with neurodegeneration in AD. The *SSGMNets'* topological organization was revealed to be able to predict cognitive and memory measures. The findings presented here suggest that *SSGMNets* could indeed be used to identify MCI ApoE4 Carriers with a high risk for AD progression.

Keywords: Mild Cognitive Impairment; Alzheimer Disease; gray matter networks; single-subject gray matter networks; graph theory.

1. Introduction

Late-Onset Alzheimer's Disease (LOAD) is the most common cause of dementia, accounting for 60% to 80% of cases (Hardy, 1997). However, there are no disease-modifying treatments and clinical drug trials have a high failure rate (Cummings et al., 2014). The postulate for this result is that AD brain pathology begins years before the cognitive decline. Consequently, in recent years, research has moved toward the study of the earliest clinical signs of neurodegeneration that are likely to evolve to AD. In this effort, a particular interest has been dedicated to Mild cognitive impairment (MCI) as a transitional phase between the cognitive changes associated with aging and early AD (Petersen, 2004; Petersen et al., 2001). It is a window in which it may be possible to intervene and modulate the disease progression (Albert et al., 2011; Gauthier et al., 2006; Mueller et al., 2005; Petersen et al., 1999).

However, MCI is especially challenging because of the considerable variability in terms of individual clinical outcomes (Jack et al., 2013; Scheltens, 2013), dependent on multiple genetic and environmental risk factors involved in AD pathogenesis (Collie and Maruff, 2000; Petersen, 2000). In terms of genetic markers, the best-established genetic risk factor for AD is the Apolipoprotein E (ApoE) ε4 allele (ApoE4) (for reviews, Bekris et al., 2010; Bookheimer and Burggren, 2009; Liu et al., 2013). While there are evidence linking ApoE4 to cognitive deficits, morphological, structural, and functional brain alterations during AD progression (Cherbuin et al., 2007; Chia-Chan Liu et al., 2013), at this point, it is still unclear how this genetic risk factor affects the organization of brain networks.

One viable mathematical approach to elucidate the ApoE4 impact on MCI brain networks is graph formalism (Boccaletti et al., 2006). In graph theory, our brain is studied as a model composed of some basic elements -nodes- (brain regions) and their relationship (edges); and the brain's complex co-variance patterns are translated into global and regional graph metrics

(Bullmore and Bassett, 2011). During the o past decade, graph analysis has already been applied to study the structural co-variance networks in AD and MCI (Alexander-Bloch et al., 2013). It is based on the phenomenon that regions that are correlated in morphometric descriptors (e.g., cortical thickness) are highly probable to be part of the same brain system underlying particular behavioral and cognitive functions (Lerch et al., 2006).

Using graph theory formalism, previous studies found evidence of the ApoE4-related modulation on healthy aging, MCI, and the AD co-variance brain network based on physiological variables derived from different image modalities (rsFMRI, FDG-PET, and DWI) (Brown et al., 2011; Giau et al., 2015; Goryawala et al., 2015; Li et al., 2019; Sanabria-Diaz et al., 2021; Seo et al., 2013; Wang et al., 2015; Yao et al., 2015; Zhu et al., 2018). Their findings propose a link between the possession of ApoE4 and brain network organization abnormalities in AD, suggesting disease-related disconnection mechanisms (Delbeuck et al., 2003; Filippi and Agosta, 2011; He et al., 2009). Moreover, these studies have provided new insights into the understanding of the biological mechanism of AD. They could lead to the use of a network-based imaging biomarker for MCI diagnosis and monitoring.

Nevertheless, it is essential to highlight that the inclusion of MCI is only reported by one previous study conducted by Yao et al. (Yao et al., 2015). Yet, in this case, the sample design makes the interpretation of the MCI brain network topology challenging as the groups (NC, MCI, and AD) were pulled together to conform the Carriers and non-Carriers samples. Additionally, only one study used data from structural Magnetic Resonance Imaging (sMRI) to construct the brain network structural co-variance, in this case, applied to a healthy aging sample (Goryawala et al., 2015). sMRI is an attractive technique because of the wide availability in clinical and research settings and its high anatomical resolution compared with other neuroimaging modalities (i.e PET).

Recently our group published the first study about the ApoE4-related effects on the structural co-variance brain network topology in MCI (Sanabria-Diaz et al., 2021). We found that the E4 allele shaped the topological organization of cortical thickness networks in this phase. Our results revealed several network measures alterations in MCI Carriers (ApoE4-positive) compared to non-Carriers, such as a decrease in global and homologous connectivity strength, clustering index, characteristic path length, local efficiency, modularity, and an increase of global efficiency. In general, they support an aberrant network topology associated with the genetic risk, which was not detectable with a standards univariate approach.

However, this study has main limitations 1) we applied a group-based graph analysis that generated one correlation matrix per group. This method did not allow us to establish associations between the network properties changes and other AD biomarkers (i.e., CSF Aβ42, tau, hippocampal atrophy) at the individual level. In our opinion, it is a critical aspect to gain insight into the biological meaning of the structural co-variance network alterations. Second, the study was based on a cross-sectional design where information about the final clinical outcome was not included. As MCI is highly heterogenic in terms of prognosis, the progression into AD is essential to control confounding effects and relate the ApoE4 to the brain network topological alterations. Finally, ApoE4 and AD progression's interaction effects were not analyzed, making it challenging to disentangle each factor's implication on the results.

In the recent past, the group-based graph analysis limitation has been overcome by a methodology that constructs single-subject brain networks from the native gray matter segmentation space (Dicks et al., 2018, 2020; Tijms et al., 2012, 2013a, 2014, 2018). This method accounts for the similarity in gray matter structure between brain areas measured with sMRI (Mechelli et al., 2005; Tijms et al., 2012). These co-variance patterns have been

associated with coordinated growth trajectories of gray matter during development, functional co-activation, and axonal connectivity (Alexander-Bloch et al., 2013; Gong et al., 2012).

Few prior studies applied this approach to explore *Single-Subject Gray Matter Networks* (*SSGMNets*) in AD and MCI (Dicks et al., 2018, 2020; Tijms et al., 2013a, 2016, 2018). These studies showed that the more network topology randomness, the worse cognitive impairment level in AD patients (Tijms et al., 2013a, 2014). Additionally, in preclinical phases, the network measures changes predicted hippocampal atrophy rate and faster atrophy in other areas associated with AD progression (Dicks et al., 2020). In MCI, the network measures showed sensitivity to initial structural alterations related to amyloid deposition (Tijms et al., 2018). The network properties alteration revealed a relation with cognitive impairment and a faster decline in almost all cognitive domains (Dicks et al., 2018).

Despite these preceding findings, we are unaware of any studies that focused on how ApoE4 affects *SSGMNets* in MCI. Moreover, no neuroimaging study has so far explored the interaction between ApoE4 and disease progression on these networks' topological properties in MCI. Such longitudinal follow-ups are required to reveal changes associated with the genetic risk allele per se and to be able to identify possible network properties alterations related to subsequent progression into AD. Additionally, the ApoE4 modulation on the association between the network topology and other neuropathological AD biomarkers (e.g., CSF amyloid β 42 (Aβ42) and total tau levels) in MCI is still unexplored.

This paper precisely addresses these crucial questions and provides experimental evidence of MCI pathological processes, which may help implement future strategies to prevent or delay the progression into AD.

2. Materials and Methods

2.1 Participants

Data used in the preparation of this article were obtained from the Alzheimer's Disease Neuroimaging Initiative (ADNI) database (http://adni.loni.usc.edu). The ADNI was launched in 2003 as a public-private partnership, led by Principal Investigator Michael W. Weiner, MD. The primary goal of ADNI has been to test whether serial magnetic resonance imaging (MRI), positron emission tomography (PET), other biological markers, and clinical and neuropsychological assessment can be combined to measure the progression of mild cognitive impairment and early Alzheimer's disease. ADNI was approved by the institutional review board of all participating institutions, and written informed consent was obtained from all participants at each site. For up-to-date information, see www.adni-info.org. Full details of subject recruitment, biomarkers as quantitative phenotypes, MRI scanning protocols, and data pre-processing were published elsewhere (C. R. J. Jack et al., 2010; Mueller et al., 2005; Saykin et al., 2010) (http://www.loni.ucla.edu/ADNI/), and only a brief account is given here.

We selected participants with a clinical diagnosis of late amnesic MCI who had completed at least two visits and fulfilled ADNI I inclusion/exclusion criteria (http://adni.loni.usc.edu/wp-content/uploads/ 2010/09/ADNI_GeneralProceduresManual.pdf.). Details of the diagnostic protocol have been previously described in (Aisen et al., 2015; Petersen et al., 2010). Briefly, the inclusion criteria for MCI were as follows: Mini-Mental-State-Examination (MMSE) scores between 24 and 30 (inclusive), a memory complaint, objective memory loss measured by education adjusted scores on the Wechsler Memory Scale Logical Memory II (Aisen et al., 2015; Petersen et al., 2010), a Clinical Dementia Rating (CDR) of 0.5, and absence of

significant levels of impairment in other cognitive domains, essentially preserved activities of daily living and a lack of dementia.

Exclusion criteria included: 1) the presence of a major depressive disorder or significant symptoms of depression; 2) modified Hachinski ischemia score greater than five; 3) significant neurological or psychiatric illness; 4) use of antidepressant drugs with anticholinergic side effects; 5) high dose of neuroleptics, chronic sedatives, hypnotics, antiparkinsonian medication, and use of narcotic analgesics. Details about the criteria can be found in http://adni.loni.usc.edu/wp-content/themes/freshnewa-dev-v2/clinical/ADNI-1_Protocol.pdf) (Petersen et al., 2010).

We stratified the MCI group into those with only one ApoE4 allele (ApoE4+, Carriers) and those without (ApoE4-, non-Carriers).

We excluded homozygotic subjects as well as participants with an E2 allele due to the possible protective effects (Serrano-Pozo et al., 2015). ApoE genotyping was performed at the time of participant enrollment and included in the ADNI-I database. The samples were sent to the ADNI Biomarker Core at the University of Pennsylvania within 24 hours of collection for analysis. ApoE genotyping details can be accessed at http://adni.loni.usc.edu/data-samples/clinical-data/ (Saykin et al., 2010). For genotyping methods see www.ADNI.org.

Following the aforementioned criterium we selected from the ADNI I database a sample of 200 late MCI participants subdivided into 100 late MCI non-Converters and 100 Converters to AD (Tables 1 and Table S2). Each subgroup was subdivided into 50 Carriers (ApoE4+) and 50 non-Carriers' (ApoE4-) patients. The final number of subjects in each subgroup (50) was determined by a lower number of patients classified as stable MCI ApoE4 Carriers, the similarity between groups in general demographic variables (age, gender, education level), genotype and clinical inclusion criterium and MRI technical requirements.

Table 1. Demographics and Clinical Characteristics of the MCI non-Converters and Converters. MMSE, Gray matter Volume, normalized Gray matter volume, CDR were found differences between groups (in bold), specifically in MCI that converted to AD in the second diagnosis time.

	MCI non-Converters				**MCI Converters**			
	Diagnosis Time 1 (MCI)		Diagnosis Time 2 (MCI)		Diagnosis Time 1 (MCI)		Diagnosis Time 2 (AD)	
	Carriers	non-Carriers	Carriers	non-Carriers	Carriers	non-Carriers	Carriers	non-Carriers
# of Participant	50	50	50	50	50	50	50	50
males/ females	34/16	36/14	34/16	36/14	37/13	36/14	37/13	36/14
Age, years	74.76 (7.12)	76.33 (7.85)	77.06 (7.04)	77.71 (7.92)	74.18 (6.74)	75.71 (8.52)	77.47 (7.12)	78.71 (8.84)
Education, years	15.76 (2.99)	15.68 (2.86)	15.76 (2.99)	15.68 (2.86)	16.66 (2.49)	16.50 (2.57)	16.66 (2.49)	16.50 (2.57)
Average MMSE	**27.46 (1.85)**	**27.76 (1.67)**	**27.40 (1.68)**	**27.80 (1.85)**	**27.10 (1.46)**	**26.60 (1.69)**	**21.34 (3.71)**	**23.06 (3.87)**
CDR 0.5	**50**	**50**	**50**	**50**	**50**	**50**	**15**	**20**
CDR 1	na	na	na	na	na	na	**28**	**23**
CDR 2	na	na	na	na	na	na	**7**	**7**
TIV	1592.3 (167.2)	1591.6 (174.1)	1569.8 (202.9)	1584.6 (198.9)	1602.2 (192.7)	1591.7 (177.5)	1602.3 (192.5)	1577.2 (196.7)
Gray matter volume	**608.5 (63.8)**	**598.2 (70.11)**	**585.3 (79.98)**	**585.2 (85.38)**	**593.6 (82.25)**	**575.9 (58.97)**	**561.6 (81.57)**	**541.9 (86.71)**
Normalized Gray matter volume	**0.40 (0.04)**	**0.39 (0.04)**	**0.39 (0.04)**	**0.38 (0.05)**	**0.39 (0.04)**	**0.38 (0.03)**	**0.38 (0.04)**	**0.36 (0.05)**
Network size	7486.68 (651.8)	7420.5 (649.10)	7339.72 (855.47)	7392.02 (664.41)	7420.86 (792.77)	7404.6 (681.54)	7287.72 (810.93)	7226.92 (918.19)

Data are presented as number or mean and standard deviations (SD). MMSE is Mini-mental state examination, mm3: cubic millimeter, MCI is Mild Cognitive Impairment, CDR is Clinical Dementia Rate, TIV is total intracranial volume, na is not applicable.

2.2 Cognitive and biomarker measures

We used a composite score for memory (ADNI-MEM) using data from the ADNI neuropsychological battery. The ADNI-MEM description can be found in (Crane et al., 2012). The authors described the composite score as an empirically derived memory measure that includes items from four memory tests available within the ADNI test battery, including the ADAS-Cog, the Rey Auditory Verbal Learning Test (RAVLT) (Rey, 1958), Logical Memory

from the Wechsler Memory Scale (Wechsler, 1945), and the word list from the Mini-Mental State Examination (Folstein et al., 1975). ADNI-MEM has been validated in published papers (Folstein et al., 1975; C. R. Jack et al., 2010; Jack and Holtzman, 2013). The ADNI-MEM scores for each ADNI participant at each study visit are reported in the UWNPSYCHSUM file. More details about the cognitive tests can be found at ADNI website (http://adni.loni.usc.edu/methods/documents/) under clinical protocols. The individual cognitive measurements downloaded from the ADNI website (https://ida.loni.usc.edu/pages/access/studyData.jsp?categoryId=12&subCategoryId=36) and the composite ADNI-MEM method information can be found at (UW - Neuropsych Summary Scores Methods.pdf).

2.3 Biomarker measurements in CSF: Aβ42, P-tau, T-tau.

In the present study, we used the CSF core biomarkers measurements for AD performed with the Elecsys® total-tau CSF, the Elecsys® Phospho-Tau (181P) CSF, and the Elecsys® β-amyloid (1–42) CSF immunoassays on a Cobas E 601 instruments (Hansson O et al., 2018; Bittner et al., 2016). The data is available in the 'UPENNBIOMK9.csv' file at the ADNI database (downloaded on May 11th, 2019). The analyzed measuring ranges of these assays are the following: 80 to 1300 pg/ml for total-Tau CSF, 8 to 120 pg/ml for Phospho-Tau (181P) CSF, and 200 to 1700 pg/ml for Elecsys® β-Amyloid (1-42) CSF immunoassays. The CSF biomarkers have been shown to predict cognitive decline and progression to dementia in patients with MCI (Hansson et al., 2018; Shaw et al., 2009).

Details about CSF biomarker group classification based on the A/T/N scheme (Jack CR et al., 2016) are described in Supplementary Table S3.

2.4 MRI acquisition and pre-processing

Pre-processed versions of the 400 T1-weighted MRI scans were downloaded from LONI Image Data Archive. Further details are available in the ADNI-MRI technical procedures manual (ADNI-MRICore, 2005). Further details are available in the ADNI-MRI technical procedures manual (http://adni.loni.usc.edu/methods/documents/MRI protocols). Pre-processing steps can be found elsewhere (Fornito et al., 2008; Jovicich et al., 2006; Sled et al., 1998). Images were pre-processed using Statistical Parametric Mapping software version 12 (SPM12) (https://www.fil.ion.ucl.ac.uk/spm/software/spm12/). First, the structural T1 weighted images are segmented into gray matter, white matter, and cerebrospinal fluid tissue classes using default settings. Next, 114 gray matter regions were parcellated based on Neuromorphometrics atlas using the Neuromorphometrics toolbox (Full list of structures listed in Supplementary Materials Table S1) (unpublished, Prof. John Ashburner personal communication) (http://www.Neuromorphometrics.com/) to obtain individual anatomical atlases. This atlas has proved to show high sensitivity detecting age modulation on the networks of myelin co-variance topological features (Melie-Garcia et al., 2018). The scans from subjects ranging in age from 5 to 96 have been painstakingly labeled and double-checked by experts using two protocols that precisely define neuroanatomical region boundaries. Unlike an atlas of a single subject, this data provides an indication of the variation of the living human brain.

The Total intracranial volume (TIV) was computed as the sum of gray and white matter and cerebrospinal fluid volumes in cm^3. Normalized gray matter volume is defined as the ratio between gray matter volume and TIV.

The native T1-weighted images were re-oriented to the canonical MNI space of the SPM12 'avg305T1' template using a rigid-body transformation and resliced to a voxel size 2×2×2 mm. Both transformations were applied to the native space gray matter segmented images and

individual atlases using trilinear and nearest-neighbor interpolations, respectively. These pre-preprocessing steps help to standardize voxel sizes and reduce dimensionality.

2.5 Single Subject Gray Matter Networks and it's Topological Properties

2.5.1 Extraction of Single Subject Gray Matter Networks.

Single Subject Gray Matter Networks (*SSGMNets*) were extracted from transformed gray matter segmentation using a method developed and published by Tijms et al. 2012 (https://github.com/bettytijms/Single_Subject_Gray_Matter_Networks; (Tijms et al., 2012)). This toolbox was implemented in MATLAB programming language (http://www.mathworks.com).

Briefly, to extract *SSGMNets*, each individual's gray matter segmentation is parcellated into multiple small cubes of 3 x 3 x 3 = 27 voxels each. These non-overlapping cubes serve as the 'nodes' in the network, thereby using geometrical information and gray matter density values (i.e., from the tissue segmentation) in the voxels. Their 'connection' refers to 'edges' indicating statistically similar gray matter morphology of two cubes as determined by calculating the Pearson's correlation. Notably, the term 'connection' in this methodology should not be confused with anatomical connections (axonal connections). The cortex is a curved object, and hence two similar cubes could be at an angle to each other, incorrectly decreasing similarity values (Tijms et al., 2012). Therefore, each seed node was rotated by an angle θ with multiples of 45 degrees and reflected over all axes to identify the target node's maximal similarity value. Nodes with zero variance in their gray matter density values were excluded (average across all subjects <0.01%) since, in this case, the correlation coefficient is undefined (Tijms et al., 2012). All pairwise correlations are entries in a matrix denominated 'connectivity' or 'adjacency matrix' in graph theory terms. The presence or absence of connections between nodes is

determined according to an individualized threshold with a random permutation method that ensures a maximum of 5% spurious connections for each *SSGMNets* (Tijms et al., 2012).

A correction for multiple comparisons was applied using the False Discovery Rate (FDR) to determine a corrected-threshold (FDR-threshold) (Benjamini and Hochberg, 1995; Benjamini and Yekutieli, 2001). The FDR-threshold was applied to binarize the *SSGMNet.* An edge (element of the connectivity matrix) indicated by '1' occurs when a correlation is higher than the FDR-threshold. On the contrary, the absence of an edge is represented by 0 while the correlation is lower than FDR-threshold.

2.5.2 Network properties computation: graph theory approach

Formally, a complex network can be represented as a graph G=[N, K], the components of this system are called nodes (N), and K refers to the relations or connections between them are called edges (Boccaletti et al., 2006). In our case, the nodes are the cubes defined over the individual's gray matter segmentation, and the edges are derived from the statistical similarity in gray matter morphology between pairs of cubes (i.e., nodes).

Technically, we used the following global network attributes to characterize the *SSGMNet* topological organization. The attributes include the clustering coefficient (Clux) (i.e., the level of interconnectedness between the neighbors of a node), the characteristic path length (CharPath) (i.e., the minimum number of edges between any pair of nodes), the normalized clustering index (Clux-Normalized), the normalized characteristic path length (CharPath-Normalized), and global efficiency (Eglobal) (i.e., how efficiently the information can be exchanged over the network). The global connectivity (GConnect) is defined as the mean correlation of all the connectivity matrix elements.

To estimate Clux-Normalized (gamma) and CharPath-Normalized (lambda), we first constructed 20 randomized reference networks matching the original ones in size and degree distribution. The Clux and CharPath mean over the 20 random networks are calculated and denoted as Clux_rand and CharPath_rand. So, Clux-Normalized and CharPath-Normalized are defined as the ratios: Clux-Normalized = Clux/Clux_rand and CharPath-Normalized = CharPath/CharPath_rand (Humphries and Gurney, 2008; Maslov and Sneppen, 2002; Watts and Strogatz, 1998). The small world (sigma) attribute is computed as the ratio between Clux-Normalized and CharPath-Normalized.

We estimated the normalized clustering index attribute for each node to describe the network's nodal properties and summarized it at each of 114 anatomical structures defined in the Neuromorphometric atlas.

We define the sparsity of the networks as the density of the connection within the connectivity matrix. This measure was calculated as the percentage number of existing edges respect the maximum number of possible edges (N x (N – 1), where N is the number of nodes).

All network measures were computed with functions from the Brain Connectivity Toolbox (www.brain-connectivity-toolbox.net). More information about the graph network topological properties definition and meaning can be found elsewhere (Rubinov and Sporns, 2010).

2.6 Rate of change analysis

We also were interested in evaluating the impact of ApoE4 and progression factors on the Rate of Change (RoC) of the *SSGMNets* topological properties, morphometric, psychological, and CSF variables. RoC provides information about how fast the variables change linearly with time. If a variable Y is defined in two-time points t1, t2 as Y(t1) and Y(t2), RoC is estimated as follows: $RoC=\Delta Y/\Delta t$ where $\Delta t = t2 - t1$ and $\Delta Y= Y(t2)-Y(t1)$. Also, RoC normalizes the

variable's change between two-time points by the elapsed time. This time normalization step is necessary when subjects have different Δt between baseline and second visit time.

2.7 Statistical analysis

We checked the normal distributions of all variables using Kolmogorov–Smirnov tests and visual inspection of the histograms. To test a significant separation from the normality of the variables' distributions, the Lilliefors tests were applied. The Log-transformation successfully rendered the data normal in some variables. For other variables that remain not normal, a rank transformation was applied instead to conform to the use of parametric statistical models (Conover and Iman, 1981). Comparisons of clinical and demographic variables between groups were performed with Analysis of Variance (ANOVA), Kruskal-Wallis, or Chi-square tests where appropriate.

Baseline network topological measures were compared between groups with Analysis of Covariance statistical models (ANCOVA) to estimate the two main effects ApoE4 status (Carriers vs. non-Carriers) and disease progression (Converters vs. non-Converters) and the interaction term ApoE4*progression. The additional covariates were age, gender, educational level, MRI magnetic field strength, handedness, and gray matter volume. We checked whether the dependent variable's variance is equal between the groups by performing Levene's test of equal variances. If significant differences were found (all $p>0.05$), either a 'rank' or a 'log10' transformation was applied to the dependent variable. Additionally, we used a Games-Howell method when equal group/level variances are not assumed and posthoc comparisons with Tukey's or Bonferroni corrections to adjust for multiple comparisons. These statistical verifications are essential to ensure the dependent variable transformations' reliability and results' validity using parametric models.

As reported previously, the size, degree, and connectivity density might influence other network properties (van Wijk et al., 2010; Zalesky et al., 2010). Therefore, we first tested group effects for these network properties defining size, connectivity density, and average degree. For those significant, these properties were added as additional covariates (Dicks et al., 2018; Tijms et al., 2013a)

ANCOVA analysis was performed for the normalized clustering index at each brain region defined in the Neuromorphometric atlas. We also included the regional gray matter volume and nodal degree as additional covariates. False discovery rate (FDR) correction was used to adjust for multiple comparisons by the number of structures.

The association of network properties with psychological (ADNI-MEM, MMSE) and CSF variables (Aβ42, T-tau, and P-tau) were assessed using a partial correlation model. The method allows calculating the linear partial correlation between our variables of interest adjusting for different covariates. Our covariates were: age, gender, educational level, and TIV. Where appropriate, we adjust for multiple comparisons using FDR correction.

To find statistical differences between partial correlation coefficients, we first applied the Fisher's Z transform z=ln((1+r)/(1-r))/2 for each correlation coefficient. After, we used the Z-test correcting for degrees of freedom as follows: Z = (z1-z2)/sqrt (1/(n1-q-3) + 1/(n2-q-3)) (Afifi et al., 2003) (assuming standard normal distribution under the null hypothesis of no difference in 'mean' partial correlations); where 'z1' and 'z2' are the two transformed partial correlations, 'n1' and 'n2' are sample sizes, and 'q' is the number of covariates involved in the partial correlation computation.

The statistical analysis was performed using the JASP software (https://jasp-stats.org/). For the partial correlation analysis, we used MATLAB software ('*partialcorri.m*' function) (https://www.mathworks.com/).

3 Results

3.1 Sample Description statistics

The groups did not significantly differ in age, gender, education, or network size (number of nodes) at time points 1 and 2 (see Table 1). All *SSGMNets* followed a small-world topology and did not exhibit disconnected nodes.

3.2 Baseline effects of ApoE4 and disease progression on the network properties

All groups showed a small-world architecture (i.e., $\sigma > 1$). We found significant group differences in disease progression and ApoE4 factors in the ANCOVA analysis after correcting for multiple hypotheses.

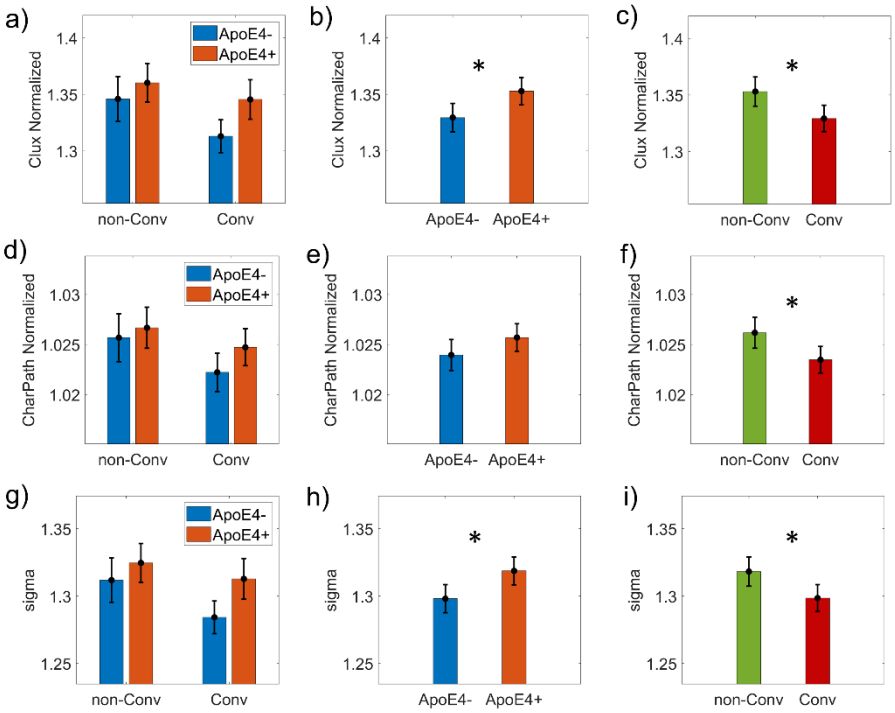

Figure 1. ANCOVA results for Network topological attributes. It is represented the bar plots of Clustering index normalized (Clux-Normalized), Characteristic path length normalized (CharPath-Normalized), and sigma. The first column of graphs (panels a), d) and g)) shows the groups subdivided into non-Converters (non-Conv), Converters (Conv), and Carriers (ApoE4+), non-Carriers (ApoE4-). The second column (panels b), e) and h)) shows the results of the ApoE4 main effect comparing ApoE4+ versus ApoE4-. The third column (panels c), f) and i)) shows the disease progression's results as comparing non-Converters (non-Conv) versus Converters (Conv). Asterisks indicate statistically significant differences. The bars' height represents the mean, and the error bars the 95% confidence interval (CI).

MCI Converters showed lower values in all network properties than non-Converters (Figure 1, panels c), f), i)). We did not find ApoE4*disease progression interaction effects. More details about these results can be found in Table S4, Supplementary Material.

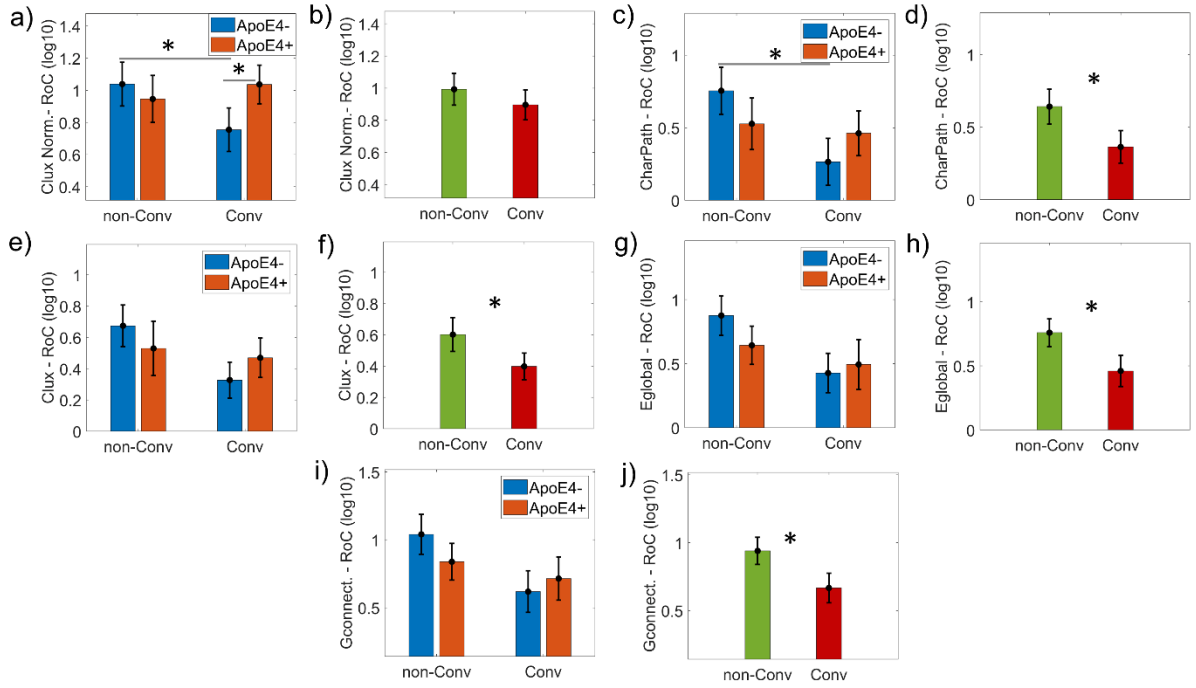

Figure 2. ANCOVA results for the Rate of Change (RoC) of the Network topological attributes. It is represented the bar plots of Clustering index normalized (Clux Normalized), Characteristic path length (CharPath), Clustering index (Clux), global efficiency (Eglobal), and Global connectivity (Gconnect). Panels a), c), e), g) and i) show the groups subdivided into non-Converters (non-Conv), Converters (Conv), and Carriers (ApoE4+), non-Carriers (ApoE4-). Panels b), d), f), h) and j) represent the disease progression's main effect results as comparing non-Converters (non-Conv) versus Converters (Conv). 'Clux Normalized' and 'CharPath' showed an interaction effect ApoE4*disease progression. All topological network attributes depicted a significant disease progression effect. A log10 transformation was applied to all variables to meet the equal group variances condition in the parametric ANCOVA statistical design. Asterisks indicate statistically significant differences (p-corrected<0.05). The bars' height represents the mean, and the error bars the 95% confidence interval (CI).

3.3 ApoE4 and disease progression effects on the network properties rate of change

We found differences (Figure 2) in the rate of change (RoC) related to progression factor in Clux *($F(1,190)= 5.273$, $p=0.023$, $\omega^2 =0.021$)*, CharPath *($F(1,190)= 10.378$, $p=0.002$, $\omega^2 =0.044$)*, GConnect *($F(1,190)= 10.153$, $p=0.002$, $\omega^2 =0.043$)* and Eglobal *($F(1,190)= 10.712$, $p=0.001$, $\omega^2 =0.046$).* The ApoE4*disease progression interaction effect was found in Clux-Normalized *($F(1,190)= 7.414$, $p=0.007$, $\omega^2 =0.031$)* and CharPath *($F(1,190)= 5.566$, $p=0.019$,*

ω^2 *=0.222)* Figure 2, panels a) and c). The highest interaction size effect was found in the CharPath (*size-effect* ω^2 *=0.222)*. Interestingly, the post hoc analysis shows that only in the non-Carriers group, non-Converters showed higher Clux-Normalized and CharPath RoC than Converters. On the other hand, in the Converters group, the Carriers depicted significantly more Clux-Normalized as compared with non-Carriers. The ApoE4 effects, as a global factor, were not present in this analysis. Details about this analysis can be found in Supplementary Material Table S6.

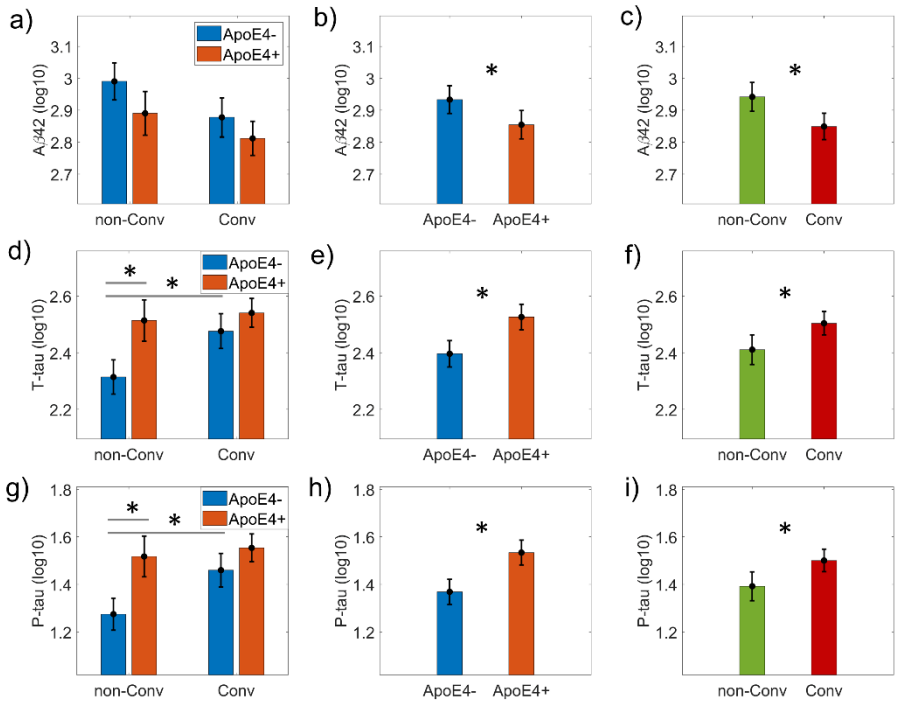

Figure 3. ANCOVA results for Cerebrospinal Fluid (CSF) variables. Bar plots for Aβ42, T-tau, and P-tau variables. The first column of graphs (panels a), d) and g)) shows the groups subdivided into non-Converters (non-Conv), Converters (Conv), and ApoE4+, ApoE4-. The second column (panels b), e) and h)) represents the ApoE4 main effect results comparing ApoE4+ versus ApoE4-. The third column (panels c), f) and i)) shows the disease progression's results as comparing non-Converters (non-Conv) versus Converters (Conv). The CSF measures were log10 transformed to meet the equal group variances condition in the parametric ANCOVA statistical design. Asterisks indicate statistically significant differences (p-corrected<0.05). The bars' height represents the mean, and the error bars the 95% confidence interval (CI).

3.4 Effects of ApoE4 and disease progression on cognitive, morphometric, and CSF-derived measures in baseline

Figures 3 and 4 show the ANCOVA results for the baseline groups' differences in cognitive, regional gray matter volume, and CSF biomarkers.

The CSF-derived measures (Aβ42, T-tau and P-tau) showed significantly group differences in the ANCOVA analysis for ApoE4, disease progression and the ApoE4*disease progression interaction.

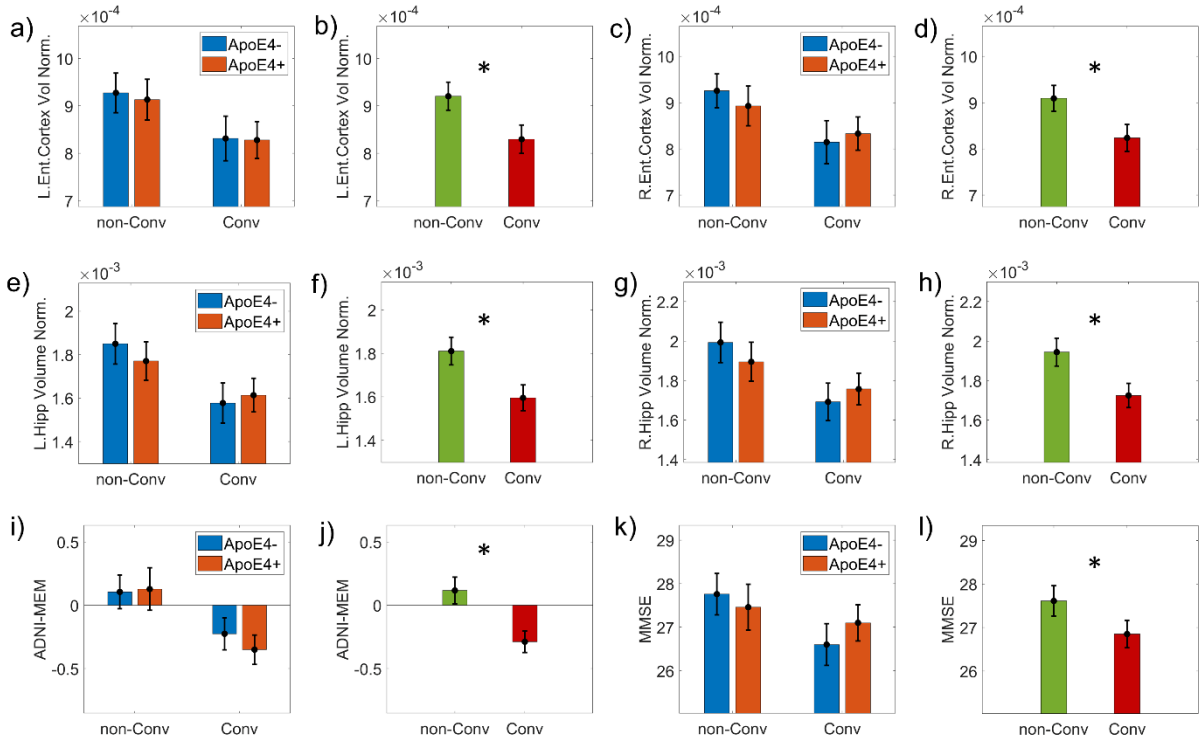

Figure 4. ANCOVA results for the volumetric and cognitive variables. The volumetric variables were: normalized volume of the left Entorhinal cortex (L.Ent.Cortex Vol Norm.) (panels a) and b)), and right Entorhinal cortex (R.Ent.Cortex Vol Norm.) (panels c) and d)); the normalized volume of the left Hippocampus (L.Hipp Volume Norm.) (panels e) and f)), and right Hippocampus (R.Hipp Volume Norm.) (panels g) and h)). The cognitive variables are ADNI-MEM (panels i) and j)) and Mini-Mental score (MMSE) (panels k) and l). For all variables, a bar plot with the groups subdivided in non-Converters (non-Conv), Converters (Conv), and ApoE4+, ApoE4- are shown. All variables showed a significant disease progression main effect as comparing non-Converters (non-Conv) versus Converters (Conv) (see Materials and Methods section). Asterisks indicate statistically significant differences (p-corrected<0.05). The bars' height represents the mean, and the error bars the 95% confidence interval (CI).

The results revealed an ApoE4 effect on Aβ42 *($F(1,118)= 7.365$, $p=0.008$; $\omega^2 =0.047$)*; T-tau *($F(1,118)= 17.734$, $p=0.001$, $\omega^2 =0.110$)* and P-tau *($F(1,118)= 21.739$, $p=0.001$, $\omega^2 =0.133$)*. The MCI Carriers' group exhibited lower CSF Aβ42 levels and higher T-tau and P-tau compared to non-Carriers at baseline.

For the disease progression factor all measures were significantly different between Converters and non-Converters (Aβ42: *$F(1,118)= 9.905$, $p=0.002$, $\omega^2 =0.065$; T*-tau: *$F(1,118)= 9.473$, $p=0.003$, $\omega^2 =0.056$); P*-tau: *($F(1,118)= 9.924$, $p=0.002$, $\omega^2 =0.057$).*

The ApoE4*disease progression interaction was found only in Tau measures (T-tau: *$F(1,118)= 4.899$, $p=0.029$, $\omega^2 =0.026$;* P-tau: *$F(1,118)= 4.522$, $p=0.036$, $\omega^2 =0.023$).* The post hoc analysis showed significant differences between Converters and non-Converters in the non-Carriers group and between Carriers and non-Carriers in the non-Converters group. Interestingly we did not find significant differences for MCI Carriers associated with disease progression (see Supplementary Material Table S4).

We found significant effects associated with disease progression in MMSE *($F(1,194)= 14.133$, $p=0.001$, $\omega^2 =0.058$)* and ADNI-MEM *($F(1,194)= 43.209$, $p=0.001$, $\omega^2 =0.166$)*. The test scores showed significant differences between Converters and non-Converters in the non-Carriers group (see Supplementary Material Table S4). ADNI-MEM also captured this difference for the Carrier's group. Finally, the left and right hippocampus and entorhinal gray matter volume normalized revealed differences between non-Converters and Converters (*R.Hipp*: *($F(1,191)= 25.482$, $p=0.001$, $\omega^2 =0.091$; L.Hipp: ($F(1,191)= 28.141$, $p=0.001$, $\omega^2 =0.099$; R.EC: ($F(1,191)= 17.803$, $p=0.001$, $\omega^2 =0.069$; L.EC: $F(1,191)= 17.537$, $p=0.001$, $\omega^2 =0.070$)* (Supplementary Material Table S4). However, both right hemisphere regions, showed differences associated with disease progression for non-Carrier's group. In the left hemisphere significant differences were also found for Carriers.

The highest size effects associated with ApoE4 was found for P-tau (ω^2 =0.13) and T-tau (ω^2 =0.11). The ADNI-MEM showed the maximum size effect associated with the disease progression (ω^2 =0.166).

The post hoc testing results (p-value corrected by Bonferroni) for all variables with statistically significant differences can be found in Supplementary Material Table S4.

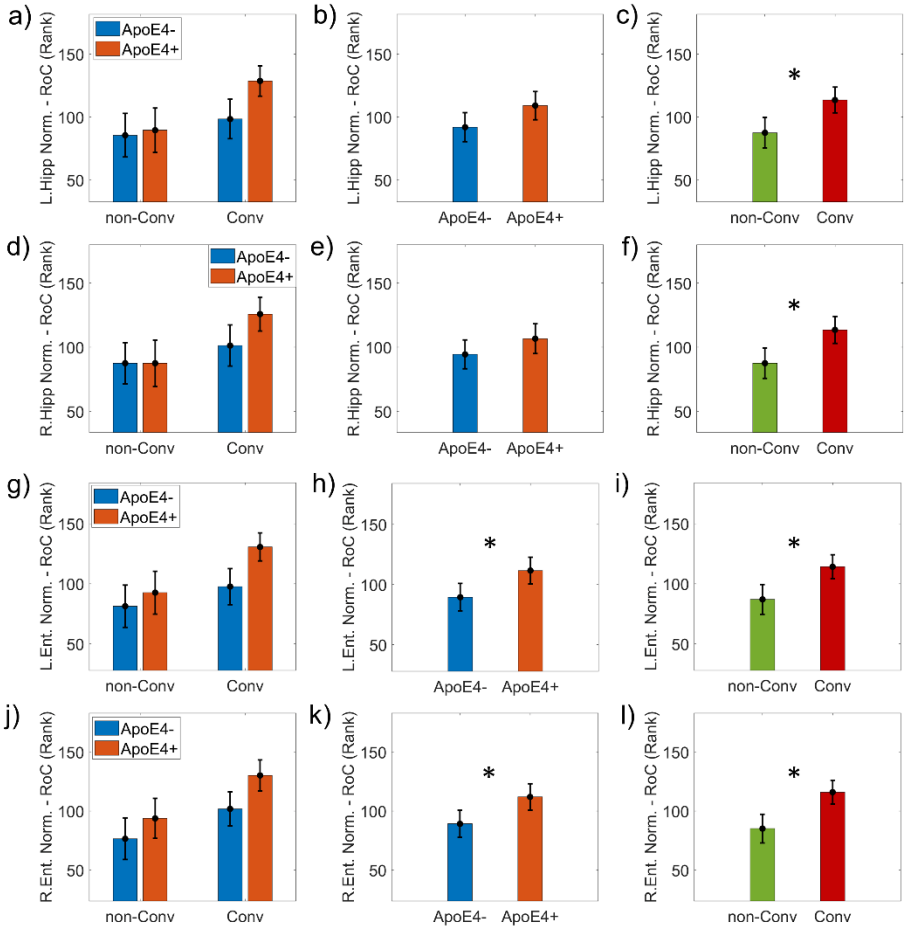

Figure 5. ANCOVA results for the Rate of Change (RoC) of the volumetric measures. It is represented the bar plots of the normalized volume of the left Hippocampus (L.Hipp Volume Norm.) (panels a), b) and c)), right Hippocampus (R.Hipp Volume Norm.) (panels d), e) and f)) and the normalized volume of the left Entorhinal cortex (L.Ent.Cortex Vol Norm.) (panels g), h) and i)), and right Entorhinal cortex (R.Ent.Cortex Vol Norm.) (panels j), k) and l)). The first column of graphs shows the groups subdivided into non-Converters (non-Conv), Converters (Conv), and APOE4+, APOE4-. The second column shows the results of the APOE4 main effect comparing APOE4+ versus APOE4-. The third column shows the disease progression's main effect as comparing non-Converters (non-Conv) versus Converters (Conv). 'L.Ent.Cortex Vol Norm.' and 'R.Ent.Cortex Vol Norm.' showed a significant APOE4 effect. A 'rank' transformation was applied to meet the equal group variances condition in the parametric ANCOVA statistical design. Asterisks indicate statistically significant differences (p-corrected<0.05). The bars' height represents the mean, and the error bars the 95% confidence interval (CI).

3.5 ApoE4 and disease progression effects on the rate of change of cognitive and morphometric variables

The normalized volume in left and right entorhinal cortex showed groups significant differences associated with the disease progression ($F(1,191)= 10.869$, $p<0.00$, $\omega^2 =0.046$; $F(1,191)= 14.823$, $p<0.001$, $\omega^2 =0.064$) as well as in the right and left hippocampus ($F(1,191)= 9.573$, $p=0.002$, $\omega^2 =0.041$; $F(1,191)= 9.271$, $p=0.003$, $\omega^2 =0.039$) (see Figure 5).

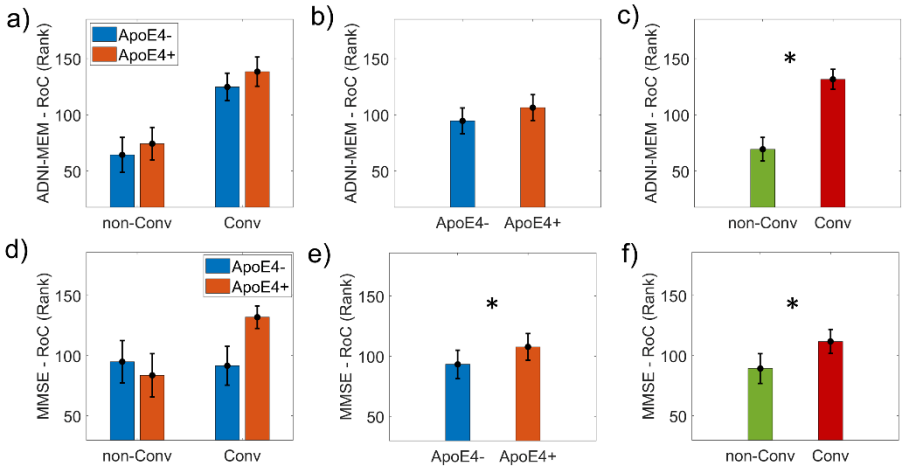

Figure 6. ANCOVA results for the Rate of Change (RoC) of cognitive variables. It is represented the bar plots of the cognitive variables are ADNI-MEM (panels a), b) and c)) and Mini-Mental score (MMSE) (panels c), d) and e)). The first column of graphs shows the groups subdivided into non-Converters (non-Conv), Converters (Conv), and APOE4+, APOE4-. The second column shows the results of the APOE4 main effect comparing APOE4+ versus APOE4-. The third column represents the disease progression's main effect, comparing non-Converters (non-Conv) versus Converters (Conv). Both variables showed a significant disease progression effect. MMSE also showed a significant APOE4 effect (panel e)). A 'rank' transformation was applied to meet the equal group variances condition in the parametric ANCOVA statistical design. Asterisks indicate statistically significant differences (p-corrected<0.05). The bars' height represents the mean, and the error bars the 95% confidence interval (CI).

We found an ApoE4-related effect on the rate of change of MMSE ($F(1,194)= 62.744$, $p<0.001$, $\omega^2 =0.015$), the left and right entorhinal cortex normalized volume ($F(1,191)= 8.236$, $p=0.007$, $\omega^2 =0.034$; $F(1,191)= 8.616$, $p=0.004$, $\omega^2 =0.064$). The MMSE and ADNI-MEM rate of change were also affected by the disease progression ($F(1,194)= 62.744$, $p<.001$, $\omega^2 =0.231$; $F(1,194)= 77.778$, $p<.001$, $\omega^2 =0.278$) (see Figure 6).

The ApoE4 highest size effect was found for the right entorhinal cortex (ω^2 =0.06). The MMSE (ω^2 =0.231), ADNI-MEM (ω^2 =*0.278)*, and right entorhinal cortex *(ω^2 =0.06)* showed the maximum size effects associated with the disease progression. The results of the posthoc comparison can be found in Supplementary Material Table S6.

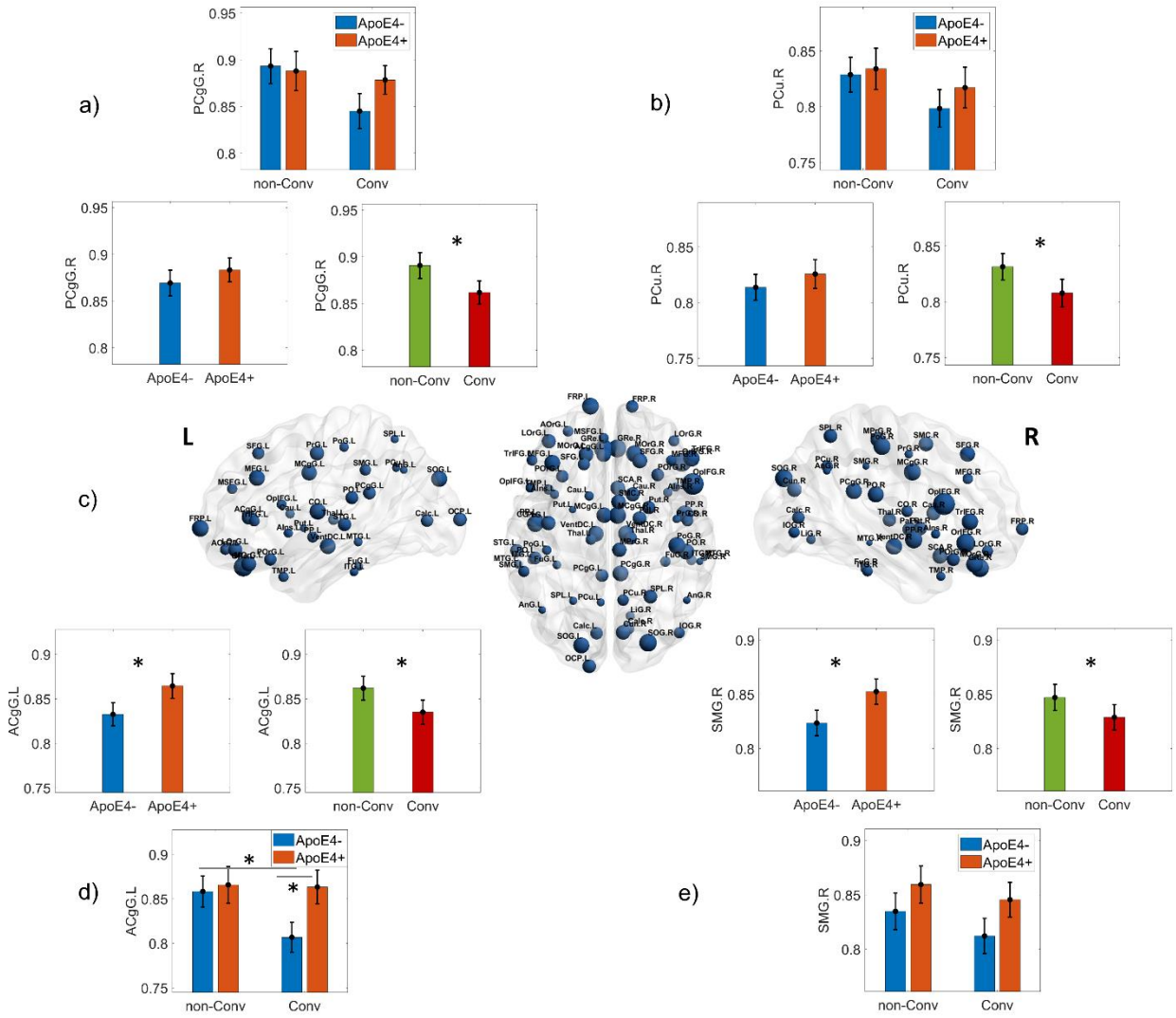

Figure 7. ANCOVA results for the nodal normalized clustering index (nodal Clux Normalized) topological measure. All structures represented as spheres in panel c) were those with significant p-values (FDR corrected multiple comparisons) for the disease progression main effect (Converters versus non-Converters). The larger the sphere diameter, the larger the difference between groups. The panels a) and b) represent the results for the right Posterior Cingulate gyrus (PCgG.R) and the right Precuneus (PCu.R), respectively. Panel d) and e) show the left Anterior Cingulate gyrus (ACgG.L) and right Supramarginal gyrus (SMG.R), respectively. These structures showed differences in ApoE4 main effect (p uncorrected). The ACgG.L also shows an interaction effect of APOE-disease progression. Asterisks indicate statistically significant differences for p-corrected<0.05 (FDR) except for panel d) and e) p-uncorrected<0.01. The bars' height represents the mean, and the error bars the 95% confidence interval (CI).

3.6 ApoE4 and disease progression-related changes on regional normalized clustering index

As the network Clux-Normalized showed significant group differences associated with the ApoE4 and disease progression factors and its RoC, we studied the origin of these differences at the regional level.

The normalized clustering index is commonly used as an indicator of functional segregation and, as such, suggests the role of a particular region on specialized processing that occurs within densely interconnected groups of brain regions.

We found 13 regions with differences between Carriers and non-Carriers (p-uncorrected<0.01) (Supplementary Material Table S8). However, only the right supramarginal gyrus - PCgG.R - (p_{FDR}=0.043) and the left anterior cingulate gyrus - ACgG.L - (p_{FDR}=0.015) survived multiple comparison correction. Both showed higher Clux-Normalized values for Carriers compared to non-Carriers.

For the disease progression effect, 75 regional ANCOVAs were significantly different between groups, after FDR correction for multiple comparisons (Supplementary Material Table S9). Figure 7 shows the spatial distribution of regional normalized clustering index group differences. The MCI that will progress into AD showed lower Clux-Normalized for all regions than those that will not. Some of these regions were: right fusiform gyrus (p_{FDR} =0.006), right and left middle frontal gyrus (p_{FDR} =0.002; p_{FDR} =0.0001), right and left posterior cingulate cortex (p_{FDR} =0.002; p_{FDR} =0.005), right precuneus (p_{FDR} =0.006), right and left superior frontal gyrus (p_{FDR} =0.0001; p_{FDR} =0.001) and left supramarginal gyrus (p_{FDR} =0.005). For details of regional groups' mean and confident intervals, see Supplementary Material Table S9.

The left anterior cingulate gyrus (ACgG.L) showed significant interaction effects ApoE4*disease progression but for p-uncorrected<0.01.

3.7 ApoE4 and disease progression effects on the association between network properties and cognitive and CSF variables

We further scrutinized the relationships between network measures, memory deficit measured with ADNI-MEM, cognitive decline evaluated with MMSE (available for all subjects), as well as CSF Aβ42, T-tau, and P-tau levels.

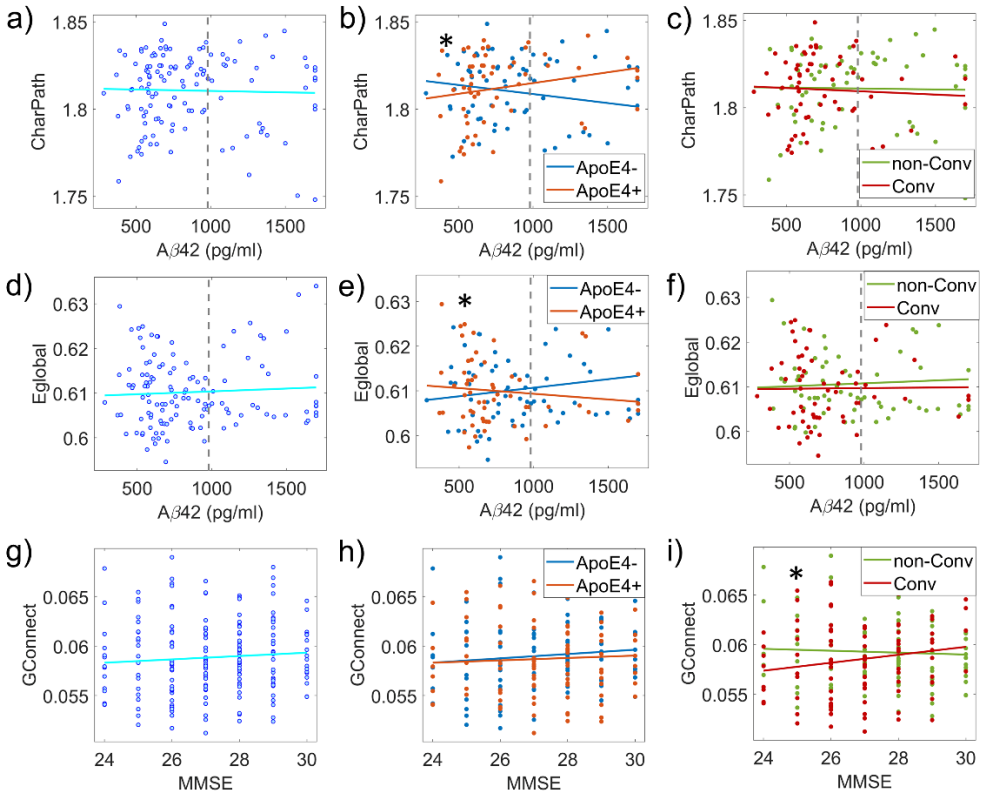

Figure 8. Differences in the correlation between Network topological attributes and cognitive and CSF variables: APOE4 and disease progression effects. Significant differences between APOE4+ versus APOE4- in the correlation of the variables Characteristic path length (CharPath) (panel b) and Global Efficiency (Eglobal) (panel e)) with Aβ42. Global connectivity (GConnect) correlation with MMSE is different between Converters (Conv) and non-Converters (non-Cov) (panel i)). Gray dotted lines in Aβ42 plots denote this parameter's normality limit (980 pg/ml). Asterisks indicate statistically significant differences ($p<0.05$).

The analysis pulling together all groups and at individual groups showed several associations between the network properties and other measures (Supplementary Material Tables from S10, S11, S12, S13, and S14).The Clux-Normalized was related to ADNI-MEM using all subjects ($r=0.206$, $p=0.003$) and with Carriers ($r=0.225$, $p=0.03$) and non-Carriers ($r=0.234$, $p=0.021$)

groups separated. The clustering index correlated with ADNI-MEM in general (r=0.259, p=0.0002, N=200 subjects), non-Converters (r=0.249, p=0.014, N=100), as well as with MMSE in the non-Carriers (r=0.217, p=0.033, N=100). Also, clustering index showed a correlation with ADNI-MEM in non-Carriers group (r=0.388, $p=8.97*10^{-5}$, N=100) and not in Carriers.

We found the normalized characteristic path length (CharPath-Normalized) to correlate in general with ADNI-MEM (r=0.246, p=0.0005, N=200). In Carriers, CharPath-Normalized was associated with ADNI-MEM (r=0.297, p=0.003) and in non-Carriers (r=0.232, p=0.023) as well. Finally, CharPath-Normalized show significant correlations with MMSE in non-Carriers (r=0.148, p=0.038) and with Aβ42 in Carriers (r=0.283, p=0.039).

The global connectivity showed association with ADNI-MEM in general (r=0.162, p=0.024), non-Converters (r=0.24, p=0.016) and non-Carriers (r=0.287, p=0.004) groups. Finally, in non-Converters, we found an association between global efficiency and ADNI-MEM (r=0.209, p=0.04). The CSF Tau measures did not reveal associations with the network properties.

For ApoE4, we found significant differences in the correlations between the characteristic path length and Aβ42 levels (Carriers r=0.229, non-Carriers r=-0.171, z-stats=2.158, p=0.03). Also in global efficiency we obtained the same effect (Carriers r=-0.16, non-Carriers r=0.20, z-stats=-2.00, p=0.044).

The correlation between global connectivity and MMSE was different between Converters and non-Converters (Converters r=0.2, non-Converters r=-0.08, z-stats=2.01, p=0.04). The correlation between network properties with ADNI-MEM and CSF tau measures did not reveal significant differences between Converters versus non-Converters and Carriers versus non-Carriers.

4 Discussion

The present study shows that *SSGMNet* is affected independently by ApoE4 and disease progression in late-MCI. The topological network alterations indicate a shift towards a random organization, more in Carriers than non-Carriers. Our findings reveal the intricate relationship between the *SSGMNet* attributes and ApoE4 genotype, suggesting modulated effects by independent processes associated with disease progression.

The main results of this research can be summarized as follows: 1) At baseline (all subjects classified as MCI) the ApoE4 and the future progression to AD status modulate topological network properties differently; 2) the Rate of Change (RoC) of characteristic path length and Clux-Normalized were affected by ApoE4 and disease progression status interaction; 3) The Clux-Normalized values were lower in MCI who will progress into AD compared to those who will not; 4) Clux-Normalized decreased in several regions belonging to the Default Mode Network (DMN) in MCI Converters respect to non-Converters; 5) ApoE4 and disease progression affect the association between specific topological network features and CSF Aβ42; and MMSE variables.

The present results are in line with the idea that disruptions in gray matter networks start years before dementia unfolds and, as such, may be sensitive to the concurrent changes in structural integrity across the brain in MCI. The baseline and RoC analysis findings underline the importance of considering cross-sectional and longitudinal approaches, as they could provide complementary information. Some of these findings deserve more attention and will be discussed in the following subsections.

ApoE4 and progression to AD status impairs the SSGMNet topology in MCI

Our results revealed that the ApoE4 mainly modulated two network properties, Normalized clustering index, and sigma. In both attributes, higher values in MCI Carriers were found than non-Carriers independently of the disease progression status. These increments (e.g., higher similarity between neighboring nodes) associated with the E4 allele may reflect synchronous atrophy between brain areas, whereas Carriers show a more uniform neurodegeneration pattern across the brain. This finding seems to contradict previous studies reporting lower clustering index in MCI Carriers (Li et al., 2019; Sanabria-Diaz et al., 2021). The source of this variability may be primarily related to a different network methodology, morphometric descriptors, group selection, and sample size, among other factors.

Additionally, the higher values of small-worldness in Carriers as indicative of a more random network organization, which has often been reported in AD and MCI (Dicks et al., 2018; Tijms et al., 2013a; Yao et al., 2010). The disease progression also modulated the sigma property, with lower values in Converters compared to non-Converters. This association has been demonstrated in previous longitudinal and cross-sectional studies in MCI (Friedman et al., 2014).

Independent of the ApoE4 factor, we found that those MCI who will progress into AD have lower normalized characteristic path length. It suggests a more random network, consequently reducing the potential for functional integration between brain regions. This effect potentially reflects the interplay between synchronous atrophy over time (Tijms et al., 2018) and regional adaptative/maladaptive mechanisms (Fornito et al., 2015).

Additionally, only the CSF measures were modified by the E4 allele at baseline. Our results in Carriers confirm previous findings where ApoE4 status was associated with brain amyloid accumulation and lower CSF Aβ42 as well as higher tau levels in MCI (Hashimoto et al., 2012;

Chia-Chen Liu et al., 2013; Risacher et al., 2013). Yet, the impact of the disease progression status at baseline was captured by the hippocampus, entorhinal volumes and ADNI-MEM composite score. The MCI Converter groups showed higher volume loss in both structures and lower scores on the memory test than the non-Converters. Both measures have been previously associated with MCI progression into AD (Crane et al., 2012; Farlow et al., 2004; Giorgio et al., 2020; C. R. Jack et al., 2010; Jack et al., 2013, 2004).

Compared to our previous paper (Sanabria-Diaz et al., 2021), there are several differences. Contrary to the mentioned study, we also classified MCI patients at baseline based on the clinical progression (non-Converters versus Converter into AD). Second, the evaluation of the network measures is different between studies. We found the Clux-Normalized more sensitive to detect ApoE4 effects, a network attribute that was not explored in the previous work. Each research used a different morphometric descriptor (cortical thickness versus grey matter density). Based on a prior study from our group, it is known that morphometric descriptors capture distinct properties of the interaction between brain structures (Sanabria-Diaz et al., 2010). Importantly, we explore the modulation on the time Rate of Change (RoC) of network attributes, CSF biomarkers, and cognitive measures in the same MCI cohort. This relevant contribution is missing in our previous paper.

ApoE4 genotype differentially modulates the rate of change of SSGMNet properties and other AD-related biomarkers

Our study revealed that the RoC of characteristic path length and Normalized clustering index were affected by the interaction between ApoE4 and disease progression status. The effect was driven by the non-Carrier's group, were patients who will later on progress into AD showed the steepest decline compared to those that will not convert to AD. This result may help to establish

which network properties changes are associated with AD progression in MCI non-Carriers. It supports the hypothesis that a higher rate of decreasing over time in both metrics in MCI is associated with an AD progression. In particular, a previous study in non-demented subjects (amyloid positive) showed an association between clinical progression over time and lowered normalized clustering index values (Tijms et al., 2016). Also, RoC results indicated that the gray matter networks seem to move towards a random network organization, which has been previously reported for AD subjects by other studies (Pereira et al., 2016; Phillips et al., 2015; Tijms et al., 2013a, 2014).

Interestingly, none of the network measures's RoC is affected by ApoE4 as a global ANOVA effect, although several were sensitive to the disease progression. Longitudinally, the main differences associated with the clinical progression were found to have a steeper decrease in cluster index normalized, characteristic path length, global connectivity, and global efficiency in Converters. Altogether these findings suggest brain connectivity alterations (for a review, see (Tijms et al., 2013b)). They may reflect a reduced ability to integrate information across distributed brain regions and altered communication between neighboring areas (Dicks et al., 2018; Pereira et al., 2016).

Additionally, we found an independent effect of the E4 allele on the entorhinal cortex rate of atrophy. The Carriers showed a higher RoC in this structure volume compared to non-Carriers. Specifically, a previous study using ADNI database confirms an association between E4 allele and a more significant increase in atrophy rate in the hippocampus and entorhinal cortex in MCI Carriers' Converters (Hostage et al., 2014; Risacher et al., 2010). In our study, the steeper atrophy in these regions in MCI Converters confirms the most extensive effects described in areas previously demonstrated to display significant atrophy in AD. Nevertheless, this analysis

revealed the importance of monitoring the entorhinal cortex volume in MCI since it is affected independently by ApoE4 and disease progression.

A faster cognitive decline associated with ApoE4 was also captured by MMSE. Our result suggests that this test score, used in clinical and research settings to measure cognitive impairment, is modulated by the ApoE4. Based on this finding, we considered incorporating the subject E4 allele information for MCI cognitive characterization a valuable research strategy, especially in clinical trials. On the other hand, independently of ApoE4, the RoC for ADNI-MEM total score revealed faster memory decline for those who progressed into AD. ADNI-MEM has been considered in a previous study using the ADNI database, as the most discriminative cognitive feature for classifying stable versus progressive MCI (Giorgio et al., 2020).

ApoE4 and disease progression modulate the regional Normalized Clustering index in MCI

Our study found regional normalized clustering index differences between groups mostly driven by the disease progression. These regional differences were widely distributed across the brain with a common denominator: lower Clux-Normalized values for those MCI that will convert to AD. It suggests that in MCI, the risk of disease progression is characterized by worse local communication between 'topological neighboring' areas (graph theory concept). The fact that all identified regions showed a lower clustering index normalized in MCI Converters may be related to AD neuropathological processes that are already operating in this phase, which in turn affect the intracortical gray matter properties similarity.

It has been previously described that intracortical morphometric similarity is related to coordinated changes of cortical structures (for a review, see (Alexander-Bloch et al., 2013)). This hypothesis may explain why several regions with lower values in MCI Converters belong

to the default-mode network (DMN), including the posterior cingulate cortex, precuneus, temporal and prefrontal areas (Greicius et al. 2004). This finding agrees with our previous study, where several regions belonging to the DMN showed nodal alteration associated with the ApoE4 (Sanabria-Diaz et al., 2021). However, many of them diverge between studies probably related to several methodological differences (i.e., parcellation schemes and sample size).

Our findings support the idea that a continuous DMN activity increases the metabolism-dependent cascade conducive to AD (Buckner et al., 2009, 2005; Raichle, 2006). In this regard, as part of the DMN, memory systems may be preferentially affected because it plays a central role in the resting state activity (Buckner et al., 2005).

In addition to this hyper functional-activation hypothesis, the regional clustering alterations may arise due to axonal connectivity. For example, we found lower values in the posterior cingulate cortex and the precuneus for those MCI who will progress into AD. Both structures have been reported in previous network studies in MCI and AD at a group and individual-based level (Dicks et al., 2018; He et al., 2008; Pereira et al., 2016; Tijms et al., 2014, 2013a; Yao et al., 2010). Moreover, the posterior cingulate cortex constitutes a central node in the DMN. This structure has reciprocal connections to the medial temporal lobe structures (i.e., entorhinal cortex, parahippocampal gyrus, precuneus, orbitofrontal cortex) affected during AD progression. Along with the precuneus, the posterior cingulate cortex has a role in episodic memory retrieval (Maddock et al., 2001; Nielsen et al., 2005), working memory (Kozlovskiy et al., 2012), and it has been implicated in several intrinsic control networks (Leech et al., 2012).

These results support the hypothesis that in MCI, regional network alterations are associated with network degeneration. There are several mechanisms suggested by which it occurs: 1)

Selective neuronal vulnerability that may affect functional circuits (Hyman et al., 1984), inducing compensatory strategies at the network level (Palop et al., 2007, 2006); 2) Retrograde axonal transport deficits that result in axonal degeneration (Salehi et al., 2006); 3) Prion disease mechanism where misfolded disease proteins may propagate throughout brain circuits (Scott et al., 2013).

ApoE4 and disease progression effects on the association between network properties, cognitive and CSF-derived measures

Additionally, the present study investigated the associations between the network topological properties, memory, general cognition, and CSF-derived measures. We studied the general correlation between these variables and, separately, the influence of ApoE4 and disease progression factors. We found that in MCI, several network properties showed a positive correlation with memory functions evaluated using ADNI-MEM. Our findings agree with a recent MCI study in which the gray matter network properties showed the strongest associations with a decline in global cognition and memory (Dicks et al., 2018). The correlation with ADNI-MEM is consistent with the memory domain being among the first cognitive functions affected in the amnesic MCI subtype (Jack et al., 2013). A practical implication of this finding is the possible use of the network measures to monitor new therapies' efficiency in clinical trials in MCI patients.

Interestingly, the CSF Aβ42 level was positively associated with the characteristic path length in the Carriers group, while we did not find correlations with P-tau and T-tau. This result agrees with previous studies showing that the E4 allele modulates the brain Aβ aggregation and deposition (for review, see (Chia-Chen Liu et al., 2013)). Moreover, the positive association between these two measures was confirmed only for ApoE4 and not for the disease progression

factor. Our finding suggests that the characteristic path length informs the detrimental E4 allele effects on the amyloid-related pathways in network terms. We hypothesized that synaptic dysfunction due to increased AD-related brain pathology (amyloid aggregation, tau) renders gray matter morphology more dissimilar at a regional level, resulting in differences between Carriers and non-Carriers.

Finally, the CSF P-tau and T-tau levels were not associated with the network topology either for ApoE4 or disease progression factors. This finding may suggest that the network attributes are not sensitive to Tau levels changes and/or may reflect a different neurodegenerative mechanism. Consistent with this explanation, a previous study found gray matter network measures contained predictive information in addition to total CSF Tau levels (Tijms et al., 2018).

Limitations and Future Considerations

There are several potential limitations to this study that should be considered. First, two-time points MRI scans were analyzed in the current study. Future investigation on the ApoE4-related effects on the network properties, longitudinal cognitive decline, and brain atrophy is necessary. Second, a small sample of subjects had CSF measures, which might have affected the accuracy of the association analysis. Third, this study was specifically limited to those subjects who were already clinically diagnosed with amnesic MCI. Thus, our study may not be generalizable to other clinical studies or populations. Further studies are needed to support the present findings with larger sample sizes.

A gene-dose analysis as well as susceptibility and protective loci associated with late-onset AD need to be considered in conjunction to ApoE4 for studying possible interaction effects. Another potential limitation is that our study included an average period of 3 years between

the two visits (time points). Hence, some patients in the non-Converter MCI group could progress to dementia later on. Yet, we demonstrated the impact of the E4 allele on the RoC of structural gray matter networks alongside the cross-sectional results. To the best of our knowledge, this has not been studied before and warrants further investigation of how gray matter network integrity changes over time in MCI.

Future research is needed to examine whether altered graph properties are related to a particular cognitive domain and are more sensitive to predict cognitive decline. The graphs' diagnostic potential should be further investigated using classification algorithms and state of the art machine learning algorithms.

It remains an open question how the brain structural co-variance connectivity is related to anatomical and functional connectivity and how this relationship changes during AD progression. Future multimodal neuroimaging studies are required to answer this question. A strength of the current approach is that we illustrated the network properties affected by ApoE4 and disease progression and their relation to inter-individual differences in other biomarkers in MCI, suggesting that they encode additional relevant information.

5 Conclusions

This paper demonstrated the role of ApoE4 in disrupting specific parameters of the gray matter network topology. ApoE4 simultaneously affects morphometric, cognitive variables, as well as CSF variables. Significantly, the time RoC of these variables is also affected by the allele. In particular, in Carriers, there are a decreased CSF Aβ42 levels, increased entorhinal cortex atrophy and increased T-tau and P-tau levels. We also discovered specific disruption in topological network properties, morphometric, cognitive, and CSF-derived markers in those MCI patients that will progress to AD. Disease progression conducts more pervasive brain

alterations than ApoE4. The clustering index normalized at the regional level showed widespread changes across the brain cortex, driven mostly by the disease progression, overlapping with the critical nodes of the DMN related to AD pathology.

Based on these findings, we considered the *SSGMNets* as a valid approach to sheds light on the cognition-gene-structural co-variance interaction. This is a potentially significant development because it could find use in MCI biomarkers research and may even offer clinical value. The study further provides information to advance the current understanding of how ApoE4 -which is far the most important genetic factor known in late-onset AD- influences brain network topology in MCI subjects. Examining ApoE4 with factors such as the risk of AD progression, as we have demonstrated, may be crucial in building classification models in an attempt to measure subtle network changes in MCI.

Declarations of interest

The authors declare no competing interests.

Role of the funding source

FK and GS received funding from the European Union Seventh Framework Programme (FP7/2007–2013) under grant agreement No 604102 and the European 'Union's Horizon 2020 research and innovation programme and the MORPHEMIC Grant (ID: 871643).

BD is supported by the Swiss National Science Foundation (NCCR Synapsy, project grants Nr. 32003B_135679, 32003B_159780, and CRSK-3_190185) and the Leenaards Foundation. LREN is very grateful to Roger De Spoelberch and Partridge Foundations for their generous financial support.

Credit authorship contribution statement

Gretel Sanabria Diaz: Conceptualization, Data curation, Methodology, Visualization, Writing-original draft **Jean-Francois Demonet**: Supervision, Writing-original manuscript draft **Borja Rodriguez-Herreros**: Formal analysis, Writing-original draft **Bogdan Draganski**: Supervision, Writing-original manuscript draft **Ferath Kherif**: Methodology, Supervision, Writing-original manuscript draft **Lester Melie Garcia**: Conceptualization, Formal analysis, Methodology, Software, Supervision, Visualization, Writing-original draft.

Acknowledgments

Data collection and sharing for this project was funded by the Alzheimer's Disease Neuroimaging Initiative (ADNI) (National Institutes of Health Grant U01 AG024904) and DOD ADNI (Department of Defense award number W81XWH-12-2-0012). ADNI is funded by the National Institute on Aging, the National Institute of Biomedical Imaging and Bioengineering, and through generous contributions from the following: AbbVie, Alzheimer's Association; Alzheimer's Drug Discovery Foundation; Araclon Biotech; BioClinica, Inc.; Biogen; Bristol-Myers Squibb Company; CereSpir, Inc.; Cogstate; Eisai Inc.; Elan Pharmaceuticals, Inc.; Eli Lilly and Company; EuroImmun; F. Hoffmann-La Roche Ltd and its affiliated company Genentech, Inc.; Fujirebio; GE Healthcare; IXICO Ltd.; Janssen Alzheimer Immunotherapy Research & Development, LLC.; Johnson & Johnson Pharmaceutical Research & Development LLC.; Lumosity; Lundbeck; Merck & Co., Inc.; Meso Scale Diagnostics, LLC.; NeuroRx Research; Neurotrack Technologies; Novartis Pharmaceuticals Corporation; Pfizer Inc.; Piramal Imaging; Servier; Takeda Pharmaceutical Company; and Transition Therapeutics. The Canadian Institutes of Health Research is

providing funds to support ADNI clinical sites in Canada. Private sector contributions are facilitated by the Foundation for the National Institutes of Health (www.fnih.org). The grantee organization is the Northern California Institute for Research and Education, and the study is coordinated by the Alzheimer's Therapeutic Research Institute at the University of Southern California. ADNI data are disseminated by the Laboratory for Neuro Imaging at the University of Southern California.

We thank Dr. Betty Tijms and Dr. Ellen Dicks (Amsterdam University Medical Center) for helping us in the use of the Single Subject Gray matter network analysis Toolbox.

References

Afifi, A., Clark, V.A., May, S., 2003. Computer-Aided Multivariate Analysis (4th ed.). https://doi.org/10.1177/0146621605284351

Aisen, P.S., Petersen, R.C., Donohue, M., Weiner, M.W., 2015. Alzheimer's Disease Neuroimaging Initiative 2 Clinical Core: Progress and plans. Alzheimer's and Dementia 11, 734–739. https://doi.org/10.1016/j.jalz.2015.05.005

Albert, M.S., DeKosky, S.T., Dickson, D., Dubois, B., Feldman, H.H., Fox, N.C., Gamst, A., Holtzman, D.M., Jagust, W.J., Petersen, R.C., Snyder, P.J., Carrillo, M.C., Thies, B., Phelps, C.H., 2011. The diagnosis of mild cognitive impairment due to Alzheimer's disease: Recommendations from the National Institute on Aging-Alzheimer's Association workgroups on diagnostic guidelines for Alzheimer's disease. Alzheimer's and Dementia 7, 270–279. https://doi.org/10.1016/j.jalz.2011.03.008

Alexander-Bloch, A., Giedd, J.N., Bullmore, E., 2013. Imaging structural co-variance between human brain regions. Nature Reviews Neuroscience 14, 322–336. https://doi.org/10.1038/nrn3465

Bekris, L.M., Yu, C.-E., Bird, T.D., Tsuang, D.W., 2010. Genetics of Alzheimer disease. Journal of geriatric psychiatry and neurology 23, 213–27. https://doi.org/10.1177/0891988710383571

Benjamini, Y., Hochberg, Y., 1995. Controlling the False Discovery Rate: A Practical and Powerful Approach to Multiple Testing, Source: Journal of the Royal Statistical Society. Series B (Methodological).

Benjamini, Y., Yekutieli, D., 2001. The control of the false discovery rate in multiple testing under dependency. Annals of Statistics 29, 1165–1188. https://doi.org/10.1214/aos/1013699998

Boccaletti, S., Latora, V., Moreno, Y., Chavez, M., Hwang, D., 2006. Complex networks : Structure and dynamics. Physics Reports 424, 175–308. https://doi.org/10.1016/j.physrep.2005.10.009

Bookheimer, S., Burggren, A., 2009. APOE-4 genotype and neurophysiological vulnerability

to Alzheimer's and cognitive aging. Annual review of clinical psychology 5, 343–62. https://doi.org/10.1146/annurev.clinpsy.032408.153625

Brown, J.A., Terashima, K.H., Burggren, A.C., Ercoli, L.M., Miller, K.J., Small, G.W., Bookheimer, S.Y., 2011. Brain network local interconnectivity loss in aging APOE-4 allele carriers. Proceedings of the National Academy of Sciences of the United States of America 108, 20760–5. https://doi.org/10.1073/pnas.1109038108

Buckner, R.L., Sepulcre, J., Talukdar, T., Krienen, F.M., Liu, H., Hedden, T., Andrews-Hanna, J.R., Sperling, R.A., Johnson, K.A., 2009. Cortical Hubs Revealed by Intrinsic Functional Connectivity: Mapping, Assessment of Stability, and Relation to Alzheimer's Disease. Journal of Neuroscience 29, 1860–1873. https://doi.org/10.1523/JNEUROSCI.5062-08.2009

Buckner, R.L., Snyder, A.Z., Shannon, B.J., LaRossa, G., Sachs, R., Fotenos, A.F., Sheline, Y.I., Klunk, W.E., Mathis, C.A., Morris, J.C., Mintun, M.A., 2005. Molecular, structural, and functional characterization of Alzheimer's disease: Evidence for a relationship between default activity, amyloid, and memory. Journal of Neuroscience 25, 7709–7717. https://doi.org/10.1523/JNEUROSCI.2177-05.2005

Bullmore, E.T., Bassett, D.S., 2011. Brain Graphs: Graphical Models of the Human Brain Connectome. Annual Review of Clinical Psychology 7, 113–140. https://doi.org/10.1146/annurev-clinpsy-040510-143934

Cherbuin, N., Leach, L.S., Christensen, H., Anstey, K.J., 2007. Neuroimaging and APOE genotype: A systematic qualitative review. Dementia and Geriatric Cognitive Disorders 24, 348–362. https://doi.org/10.1159/000109150

Collie, A., Maruff, P., 2000. The neuropsychology of preclinical Alzheimer's disease and mild cognitive impairment. Neuroscience and Biobehavioral Reviews. https://doi.org/10.1016/S0149-7634(00)00012-9

Conover, W.J., Iman, R.L., 1981. Rank Transformations as a Bridge Between Parametric and Nonparametric Statistics. The American Statistician 35, 124. https://doi.org/10.2307/2683975

Crane, P.K., Carle, A., Gibbons, L.E., Insel, P., Mackin, R.S., Gross, A., Jones, R.N., Mukherjee, S., Curtis, S.M., Harvey, D., Weiner, M., Mungas, D., 2012. Development and assessment of a composite score for memory in the Alzheimer's Disease Neuroimaging Initiative (ADNI). Brain Imaging and Behavior 6, 502–516. https://doi.org/10.1007/s11682-012-9186-z

Cummings, J.L., Morstorf, T., Zhong, K., 2014. Alzheimer's disease drug-development pipeline: Few candidates, frequent failures. Alzheimer's Research and Therapy 6. https://doi.org/10.1186/alzrt269

Delbeuck, X., Linden, M. Van der, Collette, F., 2003. Alzheimer' Disease as a Disconnection Syndrome? Neuropsychology Review 13, 79–92. https://doi.org/10.1023/A:1023832305702

Dicks, E., Tijms, B.M., ten Kate, M., Gouw, A.A., Benedictus, M.R., Teunissen, C.E., Barkhof, F., Scheltens, P., van der Flier, W.M., 2018. Gray matter network measures are associated with cognitive decline in mild cognitive impairment. Neurobiology of Aging 61, 198–206. https://doi.org/10.1016/j.neurobiolaging.2017.09.029

Dicks, E., van der Flier, W.M., Scheltens, P., Barkhof, F., Tijms, B.M., 2020. Single-subject gray matter networks predict future cortical atrophy in preclinical Alzheimer's disease. Neurobiology of Aging 94, 71–80. https://doi.org/10.1016/j.neurobiolaging.2020.05.008

Farlow, M.R., He, Y., Tekin, S., Xu, J., Lane, R., Charles, H.C., 2004. Impact of APOE in mild

cognitive impairment. Neurology 63, 1898–901. https://doi.org/10.1212/01.WNL.0000144279.21502.B7

Filippi, M., Agosta, F., 2011. Structural and functional network connectivity breakdown in Alzheimer's disease studied with magnetic resonance imaging techniques. Journal of Alzheimer's Disease 24, 455–474. https://doi.org/10.3233/JAD-2011-101854

Folstein, M.F., Folstein, S.E., McHugh, P.R., 1975. "Mini-mental state". A practical method for grading the cognitive state of patients for the clinician. Journal of Psychiatric Research 12, 189–198. https://doi.org/10.1016/0022-3956(75)90026-6

Fornito, A., Wood, S.J., Whittle, S., Fuller, J., Adamson, C., Saling, M.M., Velakoulis, D., Pantelis, C., Y??cel, M., 2008. Variability of the paracingulate sulcus and morphometry of the medial frontal cortex: Associations with cortical thickness, surface area, volume, and sulcal depth. Human Brain Mapping 29, 222–236. https://doi.org/10.1002/hbm.20381

Fornito, A., Zalesky, A., Breakspear, M., 2015. The connectomics of brain disorders. Nature Reviews Neuroscience 16, 159–172. https://doi.org/10.1038/nrn3901

Friedman, E.J., Young, K., Asif, D., Jutla, I., Liang, M., Wilson, S., Landsberg, A., Schuff, N., 2014. Directed Progression Brain Networks in Alzheimer's Disease: Properties and Classification. Brain connectivity 4, 384–393. https://doi.org/10.1089/brain.2014.0235

Gauthier, S., Reisberg, B., Zaudig, M., Petersen, R.C., Ritchie, K., Broich, K., Belleville, S., Brodaty, H., Bennett, D., Chertkow, H., Cummings, J.L., de Leon, M., Feldman, H., Ganguli, M., Hampel, H., Scheltens, P., Tierney, M.C., Whitehouse, P., Winblad, B., International Psychogeriatric Association Expert Conference on mild cognitive impairment, 2006. Mild cognitive impairment. The Lancet 367, 1262–1270. https://doi.org/10.1016/S0140-6736(06)68542-5

Giau, V. Van, Bagyinszky, E., An, S.S.A., Kim, S., 2015. Role of apolipoprotein E in neurodegenerative diseases. Neuropsychiatric disease and treatment 11, 1723–37. https://doi.org/10.2147/NDT.S84266

Giorgio, J., Landau, S.M., Jagust, W.J., Tino, P., Kourtzi, Z., 2020. Modelling prognostic trajectories of cognitive decline due to Alzheimer's disease. NeuroImage: Clinical 26, 102199. https://doi.org/10.1016/j.nicl.2020.102199

Gong, G., He, Y., Chen, Z.J., Evans, A.C., 2012. Convergence and divergence of thickness correlations with diffusion connections across the human cerebral cortex. NeuroImage 59, 1239–1248. https://doi.org/10.1016/j.neuroimage.2011.08.017

Goryawala, M., Duara, R., Loewenstein, D.A., Zhou, Q., Barker, W., 2015. Apolipoprotein-E4 (ApoE4) carriers show altered small-world properties in the default mode network of the brain. Biomedical Physics & Engineering Express 1, 15001. https://doi.org/10.1088/2057-1976/1/1/015001

Hansson, O., Seibyl, J., Stomrud, E., Zetterberg, H., Trojanowski, J.Q., Bittner, T., Lifke, V., Corradini, V., Eichenlaub, U., Batrla, R., Buck, K., Zink, K., Rabe, C., Blennow, K., Shaw, L.M., 2018. CSF biomarkers of Alzheimer's disease concord with amyloid-β PET and predict clinical progression: A study of fully automated immunoassays in BioFINDER and ADNI cohorts. Alzheimer's & Dementia 14, 1470–1481. https://doi.org/10.1016/j.jalz.2018.01.010

Hardy, J., 1997. Amyloid, the presenilins and Alzheimer's disease. Trends in Neurosciences. https://doi.org/10.1016/S0166-2236(96)01030-2

Hashimoto, T., Serrano-Pozo, A., Hori, Y., Adams, K.W., Takeda, S., Banerji, A.O., Mitani, A., Joyner, D., Thyssen, D.H., Bacskai, B.J., Frosch, M.P., Spires-Jones, T.L., Finn, M.B., Holtzman, D.M., Hyman, B.T., 2012. Apolipoprotein E, Especially Apolipoprotein E4,

Increases the Oligomerization of Amyloid Peptide. Journal of Neuroscience 32, 15181–15192. https://doi.org/10.1523/JNEUROSCI.1542-12.2012

He, Y., Chen, Z., Evans, A., 2008. Structural insights into aberrant topological patterns of large-scale cortical networks in Alzheimer's disease. The Journal of neuroscience : the official journal of the Society for Neuroscience 28, 4756–4766. https://doi.org/10.1523/JNEUROSCI.0141-08.2008

He, Y., Wang, J., Wang, L., Chen, Z.J., Yan, C., Yang, H., Tang, H., Zhu, C., Gong, Q., Zang, Y., Evans, A.C., 2009. Uncovering intrinsic modular organization of spontaneous brain activity in humans. PLoS ONE 4, 23–25. https://doi.org/10.1371/journal.pone.0005226

Hostage, C.A., Choudhury, K.R., Doraiswamy, P.M., Petrella, J.R., 2014. Mapping the Effect of the Apolipoprotein E Genotype on 4-Year Atrophy Rates in an Alzheimer Disease – related Brain. Radiology 271, 211–219. https://doi.org/10.1148/radiol.13131041

Humphries, M.D., Gurney, K., 2008. Network 'Small-World-Ness': A Quantitative Method for Determining Canonical Network Equivalence. PLoS ONE 3, e0002051. https://doi.org/10.1371/journal.pone.0002051

Hyman, B.T., Van Hoesen, G.W., Damasio, A.R., Barnes, C.L., 1984. Alzheimer's disease: Cell-specific pathology isolates the hippocampal formation. Science 225, 1168–1170. https://doi.org/10.1126/science.6474172

Jack, C.R., Holtzman, D.M., 2013. Biomarker Modeling of Alzheimer's Disease. Neuron 80, 1347–1358. https://doi.org/10.1016/j.neuron.2013.12.003

Jack, C.R., Knopman, D.S., Jagust, W.J., Petersen, R.C., Weiner, M.W., Aisen, P.S., Shaw, L.M., Vemuri, P., Wiste, H.J., Weigand, S.D., Lesnick, T.G., Pankratz, V.S., Donohue, M.C., Trojanowski, J.Q., Trojanowski, J.Q., 2013. Tracking pathophysiological processes in Alzheimer's disease: an updated hypothetical model of dynamic biomarkers. The Lancet. Neurology 12, 207–16. https://doi.org/10.1016/S1474-4422(12)70291-0

Jack, C.R., Knopman, D.S., Jagust, W.J., Shaw, L.M., Aisen, P.S., Weiner, M.W., Petersen, R.C., Trojanowski, J.Q., 2010. Hypothetical model of dynamic biomarkers of the Alzheimer's pathological cascade. The Lancet Neurology. https://doi.org/10.1016/S1474-4422(09)70299-6

Jack, C.R., Shiung, M.M., Gunter, J.L., O'Brien, P.C., Weigand, S.D., Knopman, D.S., Boeve, B.F., Ivnik, R.J., Smith, G.E., Cha, R.H., Tangalos, E.G., Petersen, R.C., 2004. Comparison of different MRI brain athrophy rate measures with clinical disease progression in AD. Neurology 62, 591–600. https://doi.org/10.1212/01.WNL.0000110315.26026.EF

Jack, C.R.J., Bernstein, M. a, Borowski, B.J., Gunter, J.L., Fox, N.C., Thompson, P.M., Schuff, N., Krueger, G., Killiany, R.J., Decarli, C.S., Dale, A.M., Carmichael, O.W., Tosun, D., Weiner, M.W., Jack Jr, C.R., 2010. Update on the magnetic resonance imaging core of the Alzheimer's disease neuroimaging initiative. Alzheimer's & dementia: the journal of the Alzheimer's Association 6, 212–220. https://doi.org/10.1016/j.jalz.2010.03.004

Jovicich, J., Czanner, S., Greve, D., Haley, E., Van Der Kouwe, A., Gollub, R., Kennedy, D., Schmitt, F., Brown, G., MacFall, J., Fischl, B., Dale, A., 2006. Reliability in multi-site structural MRI studies: Effects of gradient non-linearity correction on phantom and human data. NeuroImage 30, 436–443. https://doi.org/10.1016/j.neuroimage.2005.09.046

Kozlovskiy, S.A., Vartanov, A. V., Nikonova, E.Y., Pyasik, M.M., Velichkovsky, B.M., 2012. The cingulate cortex and human memory processes. Psychology in Russia: State of the Art 231–243. https://doi.org/10.11621/pir.2012.0014

Leech, R., Braga, R., Sharp, D.J., 2012. Echoes of the brain within the posterior cingulate

cortex. Journal of Neuroscience 32, 215–222. https://doi.org/10.1523/JNEUROSCI.3689-11.2012

Lerch, J.P., Worsley, K., Shaw, W.P., Greenstein, D.K., Lenroot, R.K., Giedd, J., Evans, A.C., 2006. Mapping anatomical correlations across cerebral cortex (MACACC) using cortical thickness from MRI. NeuroImage 31, 993–1003. https://doi.org/10.1016/j.neuroimage.2006.01.042

Li, Y., Yao, Z., Yu, Y., Fu, Y., Zou, Y., Hu, B., 2019. The influence of cerebrospinal fluid abnormalities and ApoE 4 on PHF-tau protein: Evidence from voxel analysis and graph theory. Frontiers in Aging Neuroscience 10. https://doi.org/10.3389/fnagi.2019.00208

Liu, Chia-Chan, Kanekiyo, T., Xu, H., Bu, G., Bu, G., 2013. Apolipoprotein E and Alzheimer disease: risk, mechanisms and therapy. Nature Reviews Neurology 9, 106–118. https://doi.org/10.1038/nrneurol.2012.263

Liu, Chia-Chen, Liu, Chia-Chan, Kanekiyo, T., Xu, H., Bu, G., 2013. Apolipoprotein E and Alzheimer disease: risk, mechanisms and therapy. Nature reviews. Neurology 9, 106–18. https://doi.org/10.1038/nrneurol.2012.263

Maddock, R.J., Garrett, A.S., Buonocore, M.H., 2001. Remembering familiar people: The posterior cingulate cortex and autobiographical memory retrieval. Neuroscience 104, 667–676. https://doi.org/10.1016/S0306-4522(01)00108-7

Maslov, S., Sneppen, K., 2002. Specificity and stability in topology of protein networks. Science 296, 910–913. https://doi.org/10.1126/science.1065103

Mechelli, A., Friston, K.J., Frackowiak, R.S., Price, C.J., 2005. Structural Covariance in the Human Cortex. The Journal of neuroscience : the official journal of the Society for Neuroscience 25, 8303–10. https://doi.org/10.1523/JNEUROSCI.0357-05.2005

Melie-Garcia, L., Slater, D., Ruef, A., Sanabria-Diaz, G., Preisig, M., Kherif, F., Draganski, B., Lutti, A., 2018. Networks of myelin covariance. Human Brain Mapping 39, 1532–1554. https://doi.org/10.1002/hbm.23929

Mueller, S.G., Weiner, M.W., Thal, L.J., Petersen, R.C., Jack, C.R., Jagust, W., Trojanowski, J.Q., Toga, A.W., Beckett, L., 2005. Ways toward an early diagnosis in Alzheimer's disease: the Alzheimer's Disease Neuroimaging Initiative (ADNI). Alzheimer's & dementia : the journal of the Alzheimer's Association 1, 55–66. https://doi.org/10.1016/j.jalz.2005.06.003

Nielsen, F.Å., Balslev, D., Hansen, L.K., 2005. Mining the posterior cingulate: Segregation between memory and pain components. NeuroImage 27, 520–532. https://doi.org/10.1016/j.neuroimage.2005.04.034

Palop, J.J., Chin, J., Mucke, L., 2006. A network dysfunction perspective on neurodegenerative diseases. Nature 443, 768–773. https://doi.org/10.1038/nature05289

Palop, J.J., Chin, J., Roberson, E.D., Wang, J., Thwin, M.T., Bien-Ly, N., Yoo, J., Ho, K.O., Yu, G.Q., Kreitzer, A., Finkbeiner, S., Noebels, J.L., Mucke, L., 2007. Aberrant Excitatory Neuronal Activity and Compensatory Remodeling of Inhibitory Hippocampal Circuits in Mouse Models of Alzheimer's Disease. Neuron 55, 697–711. https://doi.org/10.1016/j.neuron.2007.07.025

Pereira, J.B., Mijalkov, M., Kakaei, E., Mecocci, P., Vellas, B., Tsolaki, M., Kłoszewska, I., Soininen, H., Spenger, C., Lovestone, S., Simmons, A., Wahlund, L.O., Volpe, G., Westman, E., 2016. Disrupted Network Topology in Patients with Stable and Progressive Mild Cognitive Impairment and Alzheimer's Disease. Cerebral Cortex 26, 3476–3493. https://doi.org/10.1093/cercor/bhw128

Petersen, R.C., 2004. Mild cognitive impairment as a diagnostic entity, in: Journal of Internal

Medicine. John Wiley & Sons, Ltd, pp. 183–194. https://doi.org/10.1111/j.1365-2796.2004.01388.x

Petersen, R.C., 2000. Mild cognitive impairment: transition between aging and Alzheimer's disease. Neurologia (Barcelona, Spain) 15, 93–101.

Petersen, R.C., Aisen, P.S., Beckett, L.A., Donohue, M.C., Gamst, A.C., Harvey, D.J., Jack, C.R., Jagust, W.J., Shaw, L.M., Toga, A.W., Trojanowski, J.Q., Weiner, M.W., 2010. Alzheimer's Disease Neuroimaging Initiative (ADNI): Clinical characterization. Neurology 74, 201–209. https://doi.org/10.1212/WNL.0b013e3181cb3e25

Petersen, R.C., Doody, R., Kurz, A., Mohs, R.C., Morris, J.C., Rabins, P. V, Ritchie, K., Rossor, M., Thal, L., Winblad, B., 2001. Current concepts in mild cognitive impairment. Archives of neurology 58, 1985–92.

Petersen, R.C., Smith, G.E., Waring, S.C., Ivnik, R.J., Tangalos, E.G., Kokmen, E., 1999. Mild cognitive impairment: Clinical characterization and outcome. Archives of Neurology 56, 303–308. https://doi.org/10.1001/archneur.56.3.303

Phillips, D.J., McGlaughlin, A., Ruth, D., Jager, L.R., Soldan, A., 2015. Graph theoretic analysis of structural connectivity across the spectrum of Alzheimer's disease: The importance of graph creation methods. NeuroImage: Clinical 7, 377–390. https://doi.org/10.1016/j.nicl.2015.01.007

Raichle, M.E., 2006. The Brain ' s Dark Energy. Science 314, 1249–1250. https://doi.org/10.1126/science.

Rey, A., 1958. L'examen Clinique en Psychologie. Presses Universitaires de France, Paris.

Risacher, S.L., Kim, S., Shen, L., Nho, K., Foroud, T., Green, R.C., Petersen, R.C., Jack, C.R., Aisen, P.S., Koeppe, R.A., Jagust, W.J., Shaw, L.M., Trojanowski, J.Q., Weiner, M.W., Saykin, A.J., 2013. The role of apolipoprotein E (APOE) genotype in early mild cognitive impairment (E-MCI). Frontiers in Aging Neuroscience 5, 1–12. https://doi.org/10.3389/fnagi.2013.00011

Risacher, S.L., Shen, L., West, J.D., Kim, S., McDonald, B.C., Beckett, L.A., Harvey, D.J., Jack, C.R., Weiner, M.W., Saykin, A.J., Alzheimer's Disease Neuroimaging Initiative (ADNI), 2010. Longitudinal MRI atrophy biomarkers: relationship to conversion in the ADNI cohort. Neurobiology of aging 31, 1401–18. https://doi.org/10.1016/j.neurobiolaging.2010.04.029

Rubinov, M., Sporns, O., 2010. Complex network measures of brain connectivity: Uses and interpretations. NeuroImage 52, 1059–1069. https://doi.org/10.1016/j.neuroimage.2009.10.003

Salehi, A., Delcroix, J.D., Belichenko, P. V., Zhan, K., Wu, C., Valletta, J.S., Takimoto-Kimura, R., Kleschevnikov, A.M., Sambamurti, K., Chung, P.P., Xia, W., Villar, A., Campbell, W.A., Kulnane, L.S., Nixon, R.A., Lamb, B.T., Epstein, C.J., Stokin, G.B., Goldstein, L.S.B., Mobley, W.C., 2006. Increased App Expression in a Mouse Model of Down's Syndrome Disrupts NGF Transport and Causes Cholinergic Neuron Degeneration. Neuron 51, 29–42. https://doi.org/10.1016/j.neuron.2006.05.022

Sanabria-Diaz, G., Melie-Garcia, L., Draganski, B., Demonet, J.-F., Kherif, F., 2021. Apolipoprotein E4 effects on topological brain network organization in mild cognitive impairment. Scientific Reports 11, 845. https://doi.org/10.1038/s41598-020-80909-7

Sanabria-Diaz, G., Melie-Garcia, L., Iturria-Medina, Y., Aleman-Gomez, Y., Hernandez-Gonzalez, G., Valdes-Urrutia, L., Galan, L., Valdes-Sosa, P., 2010. Surface area and cortical thickness descriptors reveal different attributes of the structural human brain networks. NeuroImage 50, 1497–1510.

Saykin, A.J., Shen, L., Foroud, T.M., Potkin, S.G., Swaminathan, S., Kim, S., Risacher, S.L., Nho, K., Huentelman, M.J., Craig, D.W., Thompson, P.M., Stein, J.L., Moore, J.H., Farrer, L.A., Green, R.C., Bertram, L., Jack, C.R., Weiner, M.W., 2010. Alzheimer's Disease Neuroimaging Initiative biomarkers as quantitative phenotypes: Genetics core aims, progress, and plans. Alzheimer's and Dementia 6, 265–273. https://doi.org/10.1016/j.jalz.2010.03.013

Scheltens, P., 2013. Dementia: Mild cognitive impairment - Amyloid and beyond. Nature Reviews Neurology 9. https://doi.org/10.1038/nrneurol.2013.147

Scott, J.R., Davies, D., Fraser, H., 2013. Scrapie in the central nervous system: neuroanatomical spread of infection and Sinc control of pathogenesis.

Seo, E.H., Lee, D.Y., Lee, J., Park, J., Sohn, B.K., Min, Y., Byun, M.S., Choi, H.J., Woo, J.I., 2013. Influence of APOE Genotype on Whole-Brain Functional Networks in Cognitively Normal Elderly. PLoS ONE 8, 2–10. https://doi.org/10.1371/journal.pone.0083205

Serrano-Pozo, A., Qian, J., Monsell, S.E., Betensky, R.A., Hyman, B.T., 2015. *APOE* ε2 is associated with milder clinical and pathological Alzheimer disease. Annals of Neurology 77, 917–929. https://doi.org/10.1002/ana.24369

Shaw, L.M., Vanderstichele, H., Knapik-Czajka, M., Clark, C.M., Aisen, P.S., Petersen, R.C., Blennow, K., Soares, H., Simon, A., Lewczuk, P., Dean, R., Siemers, E., Potter, W., Lee, V.M.Y., Trojanowski, J.Q., 2009. Cerebrospinal fluid biomarker signature in alzheimer's disease neuroimaging initiative subjects. Annals of Neurology 65, 403–413. https://doi.org/10.1002/ana.21610

Sled, J.G., Zijdenbos, A.P., Evans, A.C., 1998. A nonparametric method for automatic correction of intensity nonuniformity in MRI data. IEEE transactions on medical imaging 17, 87–97. https://doi.org/10.1109/42.668698

Tijms, B.M., Kate, M. Ten, Wink, A.M., Visser, P.J., Ecay, M., Clerigue, M., Estanga, A., Garcia Sebastian, M., Izagirre, A., Villanua, J., Martinez Lage, P., van der Flier, W.M., Scheltens, P., Sanz Arigita, E., Barkhof, F., 2016. Gray matter network disruptions and amyloid beta in cognitively normal adults. Neurobiology of aging 37, 154–60. https://doi.org/10.1016/j.neurobiolaging.2015.10.015

Tijms, B.M., Möller, C., Vrenken, H., Wink, A.M., de Haan, W., van der Flier, W.M., Stam, C.J., Scheltens, P., Barkhof, F., 2013a. Single-Subject Grey Matter Graphs in Alzheimer's Disease. PLoS ONE 8, e58921. https://doi.org/10.1371/journal.pone.0058921

Tijms, B.M., Seris, P., Willshaw, D.J., Lawrie, S.M., 2012. Similarity-based extraction of individual networks from gray matter MRI scans. Cerebral Cortex 22, 1530–1541. https://doi.org/10.1093/cercor/bhr221

Tijms, B.M., ten Kate, M., Gouw, A.A., Borta, A., Verfaillie, S., Teunissen, C.E., Scheltens, P., Barkhof, F., van der Flier, W.M., 2018. Gray matter networks and clinical progression in subjects with predementia Alzheimer's disease. Neurobiology of Aging 61, 75–81. https://doi.org/10.1016/j.neurobiolaging.2017.09.011

Tijms, B.M., Wink, A.M., de Haan, W., van der Flier, W.M., Stam, C.J., Scheltens, P., Barkhof, F., 2013b. Alzheimer's disease: connecting findings from graph theoretical studies of brain networks. Neurobiology of Aging 34, 2023–2036. https://doi.org/10.1016/j.neurobiolaging.2013.02.020

Tijms, B.M., Yeung, H.M., Sikkes, S.A.M., Möller, C., Smits, L.L., Stam, C.J., Scheltens, P., van der Flier, W.M., Barkhof, F., 2014. Single-Subject Gray Matter Graph Properties and Their Relationship with Cognitive Impairment in Early- and Late-Onset Alzheimer's Disease. Brain Connectivity 4, 337–346. https://doi.org/10.1089/brain.2013.0209

van Wijk, B.C.M., Stam, C.J., Daffertshofer, A., 2010. Comparing Brain Networks of Different Size and Connectivity Density Using Graph Theory. PLoS ONE 5, e13701. https://doi.org/10.1371/journal.pone.0013701

Wang, J., Wang, X., He, Yi, Yu, X., Wang, H., He, Yong, 2015. Apolipoprotein E ε4 modulates functional brain connectome in Alzheimer's disease. Human Brain Mapping 36, 1828–1846. https://doi.org/10.1002/hbm.22740

Watts, D.J., Strogatz, S.H., 1998. Collective dynamics of "small-world" networks. Nature 393, 440–2. https://doi.org/10.1038/30918

Wechsler, D., 1945. A Standardized Memory Scale for Clinical Use. Journal of Psychology: Interdisciplinary and Applied 19, 87–95. https://doi.org/10.1080/00223980.1945.9917223

Yao, Z., Hu, B., Zheng, J., Zheng, W., Chen, X., Gao, X., Xie, Y., Fang, L., 2015. A FDG-PET Study of Metabolic Networks in Apolipoprotein E ε4 Allele Carriers. PLOS ONE 10, e0132300. https://doi.org/10.1371/journal.pone.0132300

Yao, Z., Zhang, Y., Lin, L., Zhou, Y., Xu, C., Jiang, T., 2010. Abnormal Cortical Networks in Mild Cognitive Impairment and Alzheimer's Disease. PLoS Computational Biology 6. https://doi.org/10.1371/journal.pcbi.1001006

Zalesky, A., Fornito, A., Harding, I.H., Cocchi, L., Y??cel, M., Pantelis, C., Bullmore, E.T., 2010. Whole-brain anatomical networks: Does the choice of nodes matter? NeuroImage 50, 970–983. https://doi.org/10.1016/j.neuroimage.2009.12.027

Zhu, L., Shu, H., Liu, D., Guo, Q., Wang, Z., Zhang, Z., 2018. Apolipoprotein E ε4 specifically modulates the hippocampus functional connectivity network in patients with amnestic mild cognitive impairment. Frontiers in Aging Neuroscience 10. https://doi.org/10.3389/fnagi.2018.00289

Apolipoprotein E allele 4 effects on Single-Subject Gray Matter Networks in Mild Cognitive Impairment

Gretel Sanabria-Diaz, Jean-Francois Demonet, Borja Rodriguez-Herreros, Bogdan Draganski Ferath Kherif, Lester Melie-Garcia, for the Alzheimer's Disease Neuroimaging Initiative

Supplementary Material

Table S1. List of gray matter structures defined in the Neuromorphometrics atlas.

Structure Name	Abbreviated Name Left	Abbreviated Name Right
Accumbens Area	Accum.R	Accum.L
Amygdala	Amyg.R	Amyg.L
Caudate	Cau.R	Cau.L
Hippocampus	Hip.R	Hip.L.L
Pallidum	Pal.R	Pal.L
Putamen	Put.R	Put.L
Thalamus Proper	Thal.R	Thal.L
Ventral DC	VentDC.R	VentDC.L
Anterior cingulate gyrus	ACgG.R	ACgG.L
Anterior insula	AIns.R	AIns.L
Anterior orbital gyrus	AOrG.R	AOrG.L
Angular gyrus	AnG.R	AnG.L
Calcarine cortex	Calc.R	Calc.L
Central operculum	CO.R	CO.L
Cuneus	Cun.R	Cun.L
Entorhinal area	Ent.R	Ent.L
Frontal operculum	FO.R	FO.L
Frontal pole	FRP.R	FRP.L
Fusiform gyrus	FuG.R	FuG.L
Gyrus rectus	GRe.R	GRe.L
Inferior occipital gyrus	IOG.R	IOG.L
Inferior temporal gyrus	ITG.R	ITG.L
Lingual gyrus	LiG.R	LiG.L
Lateral orbital gyrus	LOrG.R	LOrG.L
Middle cingulate gyrus	MCgG.R	MCgG.L
Medial frontal cortex	MFC.R	MFC.L
Middle frontal gyrus	MFG.R	MFG.L
Middle occipital gyrus	MOG.R	MOG.L
Medial orbital gyrus	MOrG.R	MOrG.L
Postcentral gyrus medial segment	MPoG.R	MPoG.L

Precentral gyrus medial segment	MPrG.R	MPrG.L
Superior frontal gyrus medial segment	MSFG.R	MSFG.L
Middle temporal gyrus	MTG.R	MTG.L
Occipital pole	OCP.R	OCP.L
Occipital fusiform gyrus	OFuG.R	OFuG.L
Opercular part of the inferior frontal gyrus	OpIFG.R	OpIFG.L
Orbital part of the inferior frontal gyrus	OrIFG.R	OrIFG.L
Posterior cingulate gyrus	PCgG.R	PCgG.L
Precuneus	PCu.R	PCu.L
Parahippocampal gyrus	PHG.R	PHG.L
Posterior insula	PIns.R	PIns.L
Parietal operculum	PO.R	PO.L
Postcentral gyrus	PoG.R	PoG.L
Posterior orbital gyrus	POrG.R	POrG.L
Planum polare	PP.R	PP.L
Precentral gyrus	PrG.R	PrG.L
Planum temporale	PT.R	PT.L
Subcallosal area	SCA.R	SCA.L
Superior frontal gyrus	SFG.R	SFG.L
Supplementary motor cortex	SMC.R	SMC.L
Supramarginal gyrus	SMG.R	SMG.L
Superior occipital gyrus	SOG.R	SOG.L
Superior parietal lobule	SPL.R	SPL.L
Superior temporal gyrus	STG.R	STG.L
Temporal pole	TMP.R	TMP.L
Triangular part of the inferior frontal gyrus	TrIFG.R	TrIFG.L
Transverse temporal gyrus	TTG.R	TTG.L

Table S2. Cognitive, CSF, and morphometric measures characteristics of the MCI groups.

	MCI-Non-Converters				**MCI Converters**					
	Diagnosis Time 1 (MCI)		Diagnosis Time 2 (stable MCI)		Diagnosis Time 1 (MCI)		Diagnosis Time 2 (AD)		Post Hoc Test	
	carriers	non-carriers	carriers	non-carriers	carriers	non-carriers	carriers	non-carriers	Time 1	Time 2
# of Participant	50	50	50	50	50	50	50	50	na	na
ADNI-MEM	0.128 (0.590)	0.105 (0.467)	0.090 (0.611)	0.205 (0.653)	-0.351 (0.409)	-0.226 (0.444)	-1.189 (0.698)	-0.809 (0.568)	$2,3^{***}$ $4,5^{**}$	1^{*} 2,3,4,5 ***
R. Hipp volume, mm^3	2.890 (0.508)	3.006 (0.512)	2.678 (0.597)	2.864 (0.638)	2.669 (0.462)	2.558 (0.497)	2.257 (0.533)	2.249 (0.597)	$3,4^{**}$ 5^{***}	$3,4^{**}$ 5^{***}
L. Hipp volume, mm^3	2.701 (0.453)	2.791 (0.465)	2.488 (0.497)	2.655 (0.586)	2.448 (0.438)	2.385 (0.493)	2.027 (0.458)	2.084 (0.573)	2^{*} $3,4^{**}$ 5^{***}	2^{*} $3,4^{**}$ 5^{***}
R. E.C volume, mm^3	1.363 (1.367)	1.398 (0.197)	1.268 (0.258)	1.357 (0.245)	1.268 (0.219)	1.233 (0.248)	1.080 (0.256)	1.099 (0.297)	2^{*} 5^{***}	2^{*} 5^{***}
L.E.C volume, mm^3	1.395 (0.231)	1.400 (0.219)	1.293 (0.238)	1.354 (0.255)	1.258 (0.231)	1.257 (0.255)	1.065 (0.242)	1.125 (0.293)	2^{*} 5^{***}	2^{*} 5^{***}
CSF test participant (BM+: $A\beta_{42}$, P-tau, T-tau)	31 (22,23,21)	33 (17,10,7)	na	na	26 (25,23,20)	34 (25,23,22)	na	na	Time 1	Time 2
CSF $A\beta_{42,}$ pg/ml	853.387 (396.721)	1045.530 (377.282)	na	na	681.200 (248.598)	817.279 (342.995)	na	na	3^{***}	na
CSF P-tau, pg/ml	37.707 (20.390)	20.744 (9.983)	na	na	37.716 (12.372)	31.820 (13.991)	na	na	$3,6^{***}$ 5^{**}	na
CSF T-tau, pg/ml	360.155 (161.852)	222.791 (94.803)	na	na	361.515 (104.888)	323.006 (125.550)	na	na	$3,6^{***}$ 5^{*}	na

Legend: Aβ42: Amyloid-beta 42, P-tau: phosphorylated tau, T-tau: total tau, Hipp: hippocampus, E.C: entorhinal cortex, L: left, R: right, mm3: millimeter, pg/ml : picogram/milliliter, CSF : cefaloraquidic liquid, BM+ : biomarker positive.

Note. For ANOVA, p-value and confidence intervals adjusted using the Tukey method. For Kruskal-Wallis test, we applied the Games-Howell method, where equal group/level variances are not assumed. The p-values are corrected with the Tukey method. *p < .05; ** p < .01, ***p<0.001. Post hoc contrasts : [1]Converter carriers - Converter non-carriers ; [2]Converter carriers - non-Converter carriers ; [3]Converter carriers - non-Converter non-carriers; [4]Converter non-carriers - non-Converter carriers; [5]Converter non-carriers - non-Converter non-carriers ; [6]Non-converter carriers - non-Converter non-carriers

Table S3. MCI classification based on the ATN system.

We assigned "A+" to those individuals that had a CSF Aβ1-42< 980 pg/ml, "T+" to those individuals with P-tau > 24 pg/ml and "N+" to those individuals with T-tau > 266 pg/ml. Because a number of ATN profiles contained very few participants, we also clustered the 8 biomarker profiles into three categories. The A–T–N– profile was labeled as the "normal AD biomarker" category (green shadow). We clustered the remaining A– (A–T–N+, A–T+N–, and A–T+N+) as "non-AD related pathology" (grey shadow), and we clustered all A+ (A+T–N–, A+T–N+, A+T+N–, A+T+N+) as "Alzheimer Disease-related pathology" (orange shadow).

ATN classification	**Groups**				
	Converters non-Carriers	Converters Carriers	Non-converters Carriers	Non-converters non-Carriers	Total
A-T-N-	3	1	4	13	21
A-T-N+	1	0	0	1	2
A-T+N-	1	0	0	0	1
A-T+N+	4	0	5	3	12
A+T-N-	7	3	4	11	25
A+T-N+	1	2	2	2	7
A+T+N-	0	0	0	0	0
A+T+N+	17	20	16	4	57
Total	34	26	31	33	

Legend: ATN: AD-related biomarkers system. It is divided into three binary categories based on the nature of the underlying pathophysiology. Biomarkers of fibrillary Aβ deposition (A+) are retention on amyloid (PET or CSF Aβ). Biomarkers of tau pathology (neurofibrillary tangles) (CSF phosphorylated tau (p-tau) and tau PET). Biomarkers of AD-like neurodegeneration or neuronal injury (CSF total tau (t-tau), [^{18}F]-fluorodeoxyglucose (FDG)-PET, sMRI) in regions characteristic of AD.

Table S4. ANCOVA significant results at baseline.

Factors	Variables	95% CI for Mean Difference		SE	df	t	p	Cohen's d
		Lower	Upper					
ApoE4 (non-Carriers vs. Carriers)	Aβ42 (log10)	-0.144	-0.023	0.031	118	-2.714	0.008	-0.480
	T-tau (log10)	0.070	0.194	0.031	118	4.211	<.001	0.731
	P-tau (log10)	0.096	0.239	0.036	118	4.662	<.001	0.809
	Clux-Normalized	$8.2*10^{-4}$	0.028	0.007	190	2.091	0.038	0.233
	Sigma	0.001	0.024	0.006	190	2.178	0.031	0.242
Disease Progression (Converter vs. non-Converter)	Aβ42 (log10)	0.036	0.157	0.031	118	3.147	0.002	0.561
	T-tau (log10)	-0.158	-0.034	0.031	118	-3.078	0.003	-0.516
	P-tau (log10)	-0.184	-0.042	0.036	118	-3.150	0.002	-0.521
	Clux-Normalized	0.002	0.030	0.007	190	2.248	0.026	2.248
	CharPath-Normalized	$3.2*10^{-4}$	0.004	$9.02*10^{-4}$	190	2.330	0.021	0.289
	Sigma	0.001	0.025	0.006	190	2.149	0.033	0.244
	MMSE	0.415	1.331	0.232	194	3.759	<.001	0.520
	ADNI-MEM	0.309	0.573	0.067	194	6.573	<.001	0.914
	L.Hipp	$1.37*10^{-4}$	$2.9*10^{-4}$	$4.01*10^{-4}$	191	5.305	<.001	0.687
	R.Hipp	$1.3*10^{-4}$	$3.03*10^{-4}$	$4.32*10^{-4}$	191	5.048	<.001	0.655
	L.E.C	$4.5*10^{-5}$	$1.27*10^{-4}$	$2.06*10^{-4}$	191	4.188	<.001	0.577
	R.E.C	$4.3*10^{-5}$	$1.18*10^{-4}$	$1.9*10^{-5}$	191	4.219	<.001	0.565

Legend: Aβ42: Amyloid-beta 42, P-tau: phosphorylated Tau, T-tau: total Tau, Hipp: hippocampus, E.C: entorhinal cortex, MMSE: Mini-mental state examination, ADNI-MEM: Alzheimer Disease Neuroimaging Initiative composite score for memory, L: left, R: right; log10: logarithmic transformation. SE: the standard error of the estimated mean; df: the degrees of freedom of the model; t: the value of the t-statistic; p: probability values are corrected by Bonferroni. Cohen's d: size effect, it is not corrected for multiple comparisons.

Table S5. ApoE4*disease progression ANCOVA significant interaction effects for T-tau at baseline

Measure	Group Contrast	Mean difference	95% CI for Mean Difference		SE	t	p
			Lower	Upper			
T-tau	Converter non-Carrier vs. non-Converter non-Carriers	-0.273	-0.532	-0.015	0.100	-2.738	0.041
	Converter non-Carriers vs. Converter Carriers	-0.286	-0.535	-0.038	0.096	-2.986	0.019
P-tau	Converter non-Carriers vs. non-Converter non-Carriers	0.189	0.062	0.315	0.049	3.891	< .001
	non-Converter Carriers vs. Converter Carriers	-0.280	-0.416	-0.145	0.052	-5.383	< .001
	non-Converter non-Carriers vs. non-converter Carriers	-0.244	-0.373	-0.114	0.050	-4.905	< .001

Legend: P-tau: phosphorylated tau, T-tau: total Tau. SE: the standard error of the estimated mean; t: value of the t-statistics.
Note. p-values and confidence intervals adjusted for comparing a family of 4 estimates (confidence intervals corrected using the Tukey method). p-values corrected by Bonferroni.

Table S6. ApoE4 and disease progression ANCOVA significant results for the Rate of Change (RoC).

Factors	Measure	95% CI for Mean Difference		SE	df	t	p	Cohen's d
		Lower	Upper					
ApoE4 (Carriers vs non-Carriers)	MMSE (rank)	-28.990	-1.951	7.108	194	-2.247	0.026	-0.278
	R.EC Norm (rank)	-39.043	-7.659	7.955	191	-2.935	0.004	-0.483
	R.EC Norm (rank)	-38.629	-7.158	7.977	191	-2.870	0.005	-0.487
Disease Progression (Converter vs non-Converter)	MMSE (rank)	42.612	70.867	7.163	194	7.921	<.001	1.119
	ADNI-MEM (rank)	48.063	75.752	7.020	194	8.819	<.001	1.267
	R.Hipp Norm (rank)	9.134	41.260	8.144	191	3.094	0.002	0.446
	L.Hipp Norm (rank)	8.706	40.733	8.118	191	3.045	0.003	0.437
	R.EC Norm (rank)	15.031	46.611	8.005	191	3.650	<.001	0.524
	L.EC Norm (rank)	10.631	42.298	8.027	191	3.297	0.001	0.473
	Clux (log10)	0.023	0.307	0.072	190	2.296	0.023	0.337
	CharPath (log10)	0.107	0.446	0.086	190	3.221	0.002	0.473
	GConnect (log10)	0.094	0.399	0.077	190	3.186	0.002	0.468
	Eglobal (log10)	0.112	0.450	0.086	190	3.273	0.001	0.484

Legend: Hipp: hippocampus, E.C: entorhinal cortex, MMSE: Mini-mental state examination, ADNI-MEM: Alzheimer Disease Neuroimaging Initiative composite score for memory, L: left, R: right, log10: logarithm transformation, rank: rank transformation. SE: the standard error of the estimated mean; df: the degrees of freedom of the model; t: the value of the t-statistic; p: probability values are corrected by Bonferroni. Cohen's d: size effect, it is not corrected for multiple comparisons.

Table S7. ApoE4*disease progression significant interaction effects for the variables rate of change

Measure	Group Contrast	Mean difference	95% CI for Mean Difference		SE	t	p
			Lower	Upper			
Clux (log10)	Converter non-Carriers vs. non-Converter non-Carriers	-0.474	-0.788	-0.159	0.121	-3.901	< .001
CharPath-Normalized	Converter Carriers vs. non-Converter non-Carriers	-0.273	-0.532	-0.015	0.100	-2.738	0.041
	Converter non-Carriers vs. Converter Carriers	-0.286	-0.535	-0.038	0.096	-2.986	0.019

Legend: CharPath-Normalized: Normalized Characteristic path length, Clux: clustering index, log10: logarithm transformation, SE: the standard error of the estimated mean; t: value of the t-statistics.

Note. p-values and confidence intervals adjusted for comparing a family of 4 estimates (confidence intervals corrected using the Tukey method). p-values corrected by Bonferroni.

Table S8. ANCOVA significant results for ApoE4 main effect for nodal Normalized Clustering index (Nodal Clux-Normalized). Highlighted in red are the Right supramarginal gyrus (SMG.R) (p-corrected = 0.042, p-uncorrected=0.0005) and Left ACgG anterior cingulate gyrus (ACgG.L) (p-corrected = 0.015, p-uncorrected=0.00061) that show significant differences after FDR correction for multiple comparisons. The rest of the reported p-values are uncorrected p<0.01.

Structure Names	Structures Short name	ApoE4- Mean	ApoE4- 95% Conf. Interval size	ApoE4+ Mean	ApoE4+ 95% Conf. Interval	Uncorrected p<0.01
Right LiG lingual gyrus	LiG.R	0.78	0.055	0.80	0.062	0.009
Right OFuG occipital fusiform gyrus	OFuG.R	0.79	0.063	0.81	0.067	0.007
Right PoG postcentral gyrus	PoG.R	0.80	0.052	0.82	0.052	0.008
Right PT planum temporale	PT.R	0.78	0.065	0.80	0.078	0.005
Right SMG supramarginal gyrus	SMG.R	0.82	0.059	0.85	0.058	0.0005
Right SOG superior occipital gyrus	SOG.R	0.82	0.066	0.84	0.073	0.0037
Right SPL superior parietal lobule	SPL.R	0.80	0.061	0.82	0.059	0.0086
Right TTG transverse temporal gyrus	TTG.R	0.81	0.082	0.85	0.083	0.0030
Left ACgG anterior cingulate gyrus	ACgG.L	0.83	0.065	0.86	0.069	0.00061
Left AnG angular gyrus	AnG.L	0.80	0.058	0.82	0.065	0.0030
Left LiG lingual gyrus	LiG.L	0.78	0.059	0.80	0.063	0.0071
Left MSFG superior frontal gyrus medial segment	MSFG.L	0.84	0.059	0.86	0.066	0.0091
Left SPL superior parietal lobule	SPL.L	0.81	0.059	0.83	0.056	0.0027

Table S9. ANCOVA significant results for disease progression main effects for nodal Normalized Clustering index (Nodal Clux-Normalized). The reported p-values are FDR corrected for multiple comparisons.

Structure Names	Structures Short name	non-Conv. Mean	non-Conv. 95 % Conf. Interval	Conv. Mean	Conv. 95% Conf. Interval	Corrected p value (FDR)
Right Caudate	Cau.R	0.91	0.066	0.88	0.061	0.015
Right Pallidum	Pal.R	0.99	0.076	0.96	0.076	0.029
Right Putamen	Put.R	0.89	0.054	0.87	0.059	0.012
Right Thalamus Proper	Thal.R	0.93	0.047	0.91	0.050	0.005
Right Ventral DC	VentDC.R	0.95	0.070	0.92	0.062	0.012
Right AIns anterior insula	AIns.R	0.87	0.059	0.85	0.054	0.023
Right AnG angular gyrus	AnG.R	0.83	0.054	0.81	0.061	0.037
Right Calc calcarine cortex	Calc.R	0.77	0.073	0.75	0.073	0.031
Right CO central operculum	CO.R	0.84	0.069	0.82	0.057	0.023
Right Cun cuneus	Cun.R	0.80	0.062	0.77	0.062	0.012
Right FRP frontal pole	FRP.R	0.90	0.066	0.87	0.070	0.024
Right FuG fusiform gyrus	FuG.R	0.82	0.056	0.80	0.058	0.019
Right GRe gyrus rectus	GRe.R	0.85	0.080	0.82	0.068	0.015
Right IOG inferior occipital gyrus	IOG.R	0.87	0.067	0.84	0.061	0.024
Right ITG inferior temporal gyrus	ITG.R	0.87	0.056	0.85	0.058	0.019
Right LiG lingual gyrus	LiG.R	0.80	0.063	0.78	0.055	0.025
Right LOrG lateral orbital gyrus	LOrG.R	0.87	0.070	0.84	0.067	0.031
Right MCgG middle cingulate gyrus	MCgG.R	0.89	0.066	0.86	0.062	0.012
Right MFG middle frontal gyrus	MFG.R	0.84	0.049	0.82	0.054	0.012

Right MOrG medial orbital gyrus	MOrG.R	0.87	0.061	0.84	0.067	0.012
Right MPrG precentral gyrus medial segment	MPrG.R	0.85	0.076	0.82	0.073	0.023
Right MTG middle temporal gyrus	MTG.R	0.84	0.050	0.82	0.056	0.037
Right OpIFG opercular part of the inferior frontal	OpIFG.R	0.84	0.068	0.81	0.058	0.004
Right OrIFG orbital part of the inferior frontal gyrus	OrIFG.R	0.86	0.072	0.82	0.081	0.015
Right PCgG posterior cingulate gyrus	PCgG.R	0.89	0.069	0.86	0.062	0.012
Right PCu precuneus	PCu.R	0.83	0.059	0.80	0.062	0.019
Right PO parietal operculum	PO.R	0.85	0.080	0.82	0.073	0.022
Right PoG postcentral gyrus	PoG.R	0.83	0.049	0.80	0.052	0.004
Right POrG posterior orbital gyrus	POrG.R	0.86	0.068	0.84	0.065	0.022
Right PP planum polare	PP.R	0.84	0.076	0.81	0.072	0.015
Right PrG precentral gyrus	PrG.R	0.87	0.059	0.85	0.058	0.031
Right SCA subcallosal area	SCA.R	0.86	0.079	0.83	0.082	0.031
Right SFG superior frontal gyrus	SFG.R	0.88	0.049	0.85	0.054	0.005
Right SMC supplementary motor cortex	SMC.R	0.87	0.071	0.84	0.061	0.015
Right SMG supramarginal gyrus	SMG.R	0.84	0.060	0.82	0.058	0.042
Right SOG superior occipital gyrus	SOG.R	0.85	0.070	0.82	0.068	0.012
Right SPL superior parietal lobule	SPL.R	0.83	0.059	0.80	0.060	0.012
Right TMP temporal pole	TMP.R	0.88	0.051	0.86	0.058	0.023
Right TrIFG triangular part of the inferior frontal	TrIFG.R	0.86	0.062	0.83	0.067	0.012
Left Caudate	Cau.L	0.90	0.067	0.88	0.066	0.040
Left Putamen	Put.L	0.88	0.054	0.86	0.055	0.031
Left Thalamus Proper	Thal.L	0.94	0.053	0.92	0.050	0.012
Left Ventral DC	VentDC.L	0.93	0.066	0.90	0.067	0.012
Left ACgG anterior cingulate gyrus	ACgG.L	0.86	0.067	0.83	0.068	0.015
Left AIns anterior insula	AIns.L	0.88	0.060	0.86	0.058	0.026
Left AOrG anterior orbital gyrus	AOrG.L	0.85	0.073	0.82	0.068	0.039
Left AnG angular gyrus	AnG.L	0.82	0.063	0.80	0.062	0.046
Left Calc calcarine cortex	Calc.L	0.77	0.070	0.75	0.069	0.025
Left CO central operculum	CO.L	0.85	0.069	0.82	0.063	0.012
Left FRP frontal pole	FRP.L	0.90	0.071	0.87	0.066	0.012
Left FuG fusiform gyrus	FuG.L	0.81	0.054	0.79	0.059	0.025
Left GRe gyrus rectus	GRe.L	0.83	0.082	0.80	0.064	0.012
Left ITG inferior temporal gyrus	ITG.L	0.87	0.053	0.85	0.054	0.022
Left LOrG lateral orbital gyrus	LOrG.L	0.87	0.076	0.85	0.067	0.022
Left MCgG middle cingulate gyrus	MCgG.L	0.86	0.062	0.83	0.069	0.013
Left MFG middle frontal gyrus	MFG.L	0.85	0.053	0.82	0.053	0.005
Left MOrG medial orbital gyrus	MOrG.L	0.88	0.069	0.85	0.066	0.015
Left MSFG superior frontal gyrus medial segment	MSFG.L	0.86	0.062	0.84	0.064	0.025
Left MTG middle temporal gyrus	MTG.L	0.84	0.055	0.82	0.055	0.023
Left OCP occipital pole	OCP.L	0.85	0.069	0.82	0.072	0.023
Left OpIFG opercular part of the inferior frontal	OpIFG.L	0.83	0.064	0.81	0.072	0.041
Left PCgG posterior cingulate gyrus	PCgG.L	0.87	0.065	0.84	0.061	0.018
Left PCu precuneus	PCu.L	0.81	0.056	0.80	0.059	0.031
Left PO parietal operculum	PO.L	0.84	0.072	0.81	0.070	0.025
Left PoG postcentral gyrus	PoG.L	0.83	0.052	0.81	0.056	0.019
Left POrG posterior orbital gyrus	POrG.L	0.85	0.066	0.82	0.063	0.021
Left PP planum polare	PP.L	0.82	0.069	0.80	0.068	0.031
Left PrG precentral gyrus	PrG.L	0.87	0.061	0.84	0.052	0.012
Left SFG superior frontal gyrus	SFG.L	0.88	0.049	0.85	0.056	0.012
Left SMG supramarginal gyrus	SMG.L	0.85	0.060	0.83	0.058	0.019
Left SOG superior occipital gyrus	SOG.L	0.83	0.075	0.80	0.073	0.019
Left SPL superior parietal lobule	SPL.L	0.83	0.056	0.81	0.059	0.029
Left STG superior temporal gyrus	STG.L	0.83	0.058	0.80	0.066	0.015
Left TMP temporal pole	TMP.L	0.88	0.054	0.85	0.055	0.016
Left TrIFG triangular part of the inferior frontal gyrus	TrIFG.L	0.87	0.069	0.85	0.068	0.034

Table S10. Correlation between network topological attributes and MMSE taking all data sample and dividing groups into Converts and non-Converters and APOE4+, APOE4-. The significant values are represented in red.

Topological Variables	General Corr.	p - General Corr.	Conv. Corr.	p – Conv. Corr.	non-Conv. Corr.	p – non-Conv. Corr.	APOE4+ Corr.	p – APOE4+ Corr.	APOE4- Corr.	p - APOE4- Corr.
Clux Normalized	0.12	0.094	0.007	0.94	0.095	0.35	0.09	0.36	0.15	0.12
Clux	0.12	0.070	-0.05	0.62	0.18	0.064	0.04	0.69	0.21	0.03
CharPathL Normalized	0.14	0.038	0.105	0.30	0.068	0.50	0.15	0.12	0.14	0.16
CharPathL	0.014	0.84	0.095	0.35	-0.11	0.25	0.05	0.57	-0.02	0.82
Global Connectivity	0.081	0.25	-0.086	0.40	0.203	0.046	0.005	0.96	0.15	0.13
Eglobal	0.042	0.55	-0.092	0.37	0.17	0.09	-0.02	0.83	0.10	0.32

Table S11. Correlation between network topological attributes and ADNI-MEM taking all data sample and dividing groups into Converts and non-Converters and APOE4+, APOE4-. The significant values are represented in red.

Topological Variables	General Corr.	p - General Corr.	Conv. Corr.	p – Conv. Corr.	non-Conv. Corr.	p - non-Conv. Corr.	APOE4+ Corr.	p – APOE4+ Corr.	APOE4- Corr.	p - APOE4- Corr.
Clux Normalized	**0.206**	**0.003**	0.09	0.37	0.071	0.48	**0.22**	**0.030**	**0.234**	**0.021**
Clux	**0.26**	**$2*10^{-4}$**	0.12	0.22	**0.25**	**0.014**	0.13	0.176	**0.388**	**$8.97*10^{-5}$**
CharPathL Normalized	**0.246**	**$5*10^{-4}$**	0.17	0.08	0.072	0.48	**0.29**	**0.003**	**0.232**	**0.022**
CharPathL	0.019	0.785	0.07	0.49	-0.145	0.15	0.12	0.243	-0.061	0.55
Global Connectivity	**0.162**	**0.023**	0.040	0.69	**0.24**	**0.016**	0.03	0.705	**0.287**	**0.004**
Eglobal	0.087	0.22	-0.007	0.93	0.20	0.040	-0.02	0.785	0.198	0.051

Table S12. Correlation between network topological attributes and CSF measure Aβ42 taking all data sample and dividing groups into Converts and non-Converters and APOE4+, APOE4-. The significant values are represented in red.

Topological Variables	General Corr.	p - General Corr.	Conv. Corr.	p – Conv. Corr.	non-Conv. Corr.	p - non-Conv. Corr.	APOE4+ Corr.	p – APOE4+ Corr.	APOE4- Corr.	p - APOE4- Corr.
Clux Normalized	0.08	0.36	0.035	0.78	-0.053	0.69	0.25	0.06	0.006	0.95
Clux	0.07	0.41	0.053	0.68	-0.031	0.81	-0.03	0.81	0.15	0.21
CharPathL Normalized	0.10	0.27	0.033	0.80	-0.009	0.94	0.28	0.039	-0.03	0.75
CharPathL	0.006	0.94	-0.02	0.84	-0.014	0.91	0.22	0.09	-0.17	0.18
Global Connectivity	0.069	0.45	0.065	0.61	0.012	0.92	-0.11	0.41	0.21	0.08
Eglobal	0.038	0.67	0.049	0.70	0.013	0.91	-0.16	0.22	0.20	0.10

Table S13. Correlation between network topological attributes and CSF measure Tau taking all data sample and dividing groups into Converts and non-Converters and APOE4+, APOE4-. The significant values are represented in red.

Topological Variables	General Corr.	p - General Corr.	Conv. Corr.	p – Conv. Corr.	non-Conv. Corr.	p – non-Conv. Corr.	APOE4 + Corr.	p – APOE4 + Corr.	APOE4 -Corr.	p - APOE4 -Corr.
Clux Normalized	-0.06	0.51	-0.08	0.52	0.12	0.37	-0.11	0.39	-0.14	0.25
Clux	-0.005	0.95	0.05	0.66	0.02	0.87	-0.02	0.88	-0.037	0.76
CharPathL Normalized	-0.05	0.56	-0.06	0.63	0.15	0.26	-0.05	0.72	-0.10	0.40
CharPathL	-0.03	0.72	-0.08	0.54	0.10	0.42	-0.005	0.96	-0.06	0.60
Global Connectivity	0.005	0.95	0.07	0.57	-0.04	0.76	-0.029	0.83	0.01	0.93
Eglobal	0.017	0.84	0.07	0.54	-0.07	0.60	-0.015	0.91	0.03	0.78

Table S14. Correlation between network topological attributes and CSF measure pTau taking all data sample and dividing groups into Converts and non-Converters and APOE4+, APOE4-. The significant values are represented in red.

Topological Variables	General Corr.	p - General Corr.	Conv. Corr.	p – Conv. Corr.	non-Conv. Corr.	p – non-Conv. Corr.	APOE4 + Corr.	p – APOE4+ Corr.	APOE4- Corr.	p - APOE4 -Corr.
Clux Normalized	-0.04	0.63	-0.08	0.50	0.16	0.22	-0.13	0.34	-0.11	0.361
Clux	-0.01	0.89	0.03	0.81	0.027	0.83	-0.02	0.88	-0.045	0.72
CharPathL Normalized	-0.04	0.61	-0.06	0.60	0.17	0.20	-0.07	0.58	-0.077	0.54
CharPathL	-0.02	0.82	-0.06	0.61	0.12	0.37	-0.026	0.85	-0.034	0.78
Global Connectivity	-0.007	0.93	0.04	0.71	-0.04	0.73	-0.02	0.88	-0.012	0.92
Eglobal	0.004	0.96	0.05	0.65	-0.07	0.56	-0.0009	0.99	0.0076	0.95

Table S15. Statistical differences APOE4+ vs. APOE4- and Converters (Conv) vs. non-Converters (non-Conv) in the linear correlation between topological network attributes and MMSE. The topological network attributes are: Clustering index normalized (Clux Normalized), Clustering index (Clux), Characteristic path length Normalized (CharPathL Normalized), Global connectivity, and global efficiency (Eglobal). The significant values are represented in red.

Topological Variables	Conv. Corr.	non-Conv. Corr.	Z-Stats (Conv. vs. non-Conv.)	p (Conv. vs. non-Conv.)	APOE4+ Corr.	APOE4- Corr.	Z-Stats (APOE4+ vs. APOE4-)	p (APOE4+ vs. APOE4-)
Clux Normalized	0.095	0.007	0.607	0.54	0.094	0.15	-0.457	0.64
Clux	0.189	-0.05	1.67	0.09	0.040	0.21	-1.243	0.21
CharPathL Normalized	0.068	0.105	-0.25	0.79	0.15	0.14	0.101	0.91
CharPathL	-0.11	0.095	-1.46	0.14	0.05	-0.02	0.559	0.57
Global Connectivity	**0.20**	**-0.08**	**2.01**	**0.04**	0.005	0.15	-1.033	0.30
Eglobal	0.17	-0.09	1.84	0.065	-0.022	0.10	-0.856	0.39

Legend: **Conv. Corr** : Converters group partial correlation coefficient; **non-Conv. Corr**: non-Converters group partial correlation coefficient; **Z-Stats (Conv. vs. non-Conv.)**: Z-stats Converters vs. non-Converters correlation coefficients; **p (Conv. vs. non-Conv.)**: p-value of the Z-stats Converters vs. non-Converters; **APOE4+ Corr.** : APOE4+ group partial correlation coefficient; **APOE4- Corr.** : APOE4- group partial correlation coefficient; **Z-Stats (APOE4+ vs. APOE4-)** Z-stats APOE4+ vs. APOE4- correlation coefficients; **p (APOE4+ vs. APOE4-)** p-value of the Z-Stats (APOE4+ vs. APOE4-).

Table S16. Statistical differences APOE4+ vs. APOE4- and Converters (Conv) vs. non-Converters (non-Conv) in the linear correlation between topological network attributes and ADNI-MEM. The topological network attributes are: Clustering index normalized (Clux Normalized), Clustering index (Clux), Characteristic path length Normalized (CharPathL Normalized), Global connectivity, and global efficiency (Eglobal). The significant values are represented in red.

Topological Variables	Conv. Corr.	non-Conv. Corr.	Z-Stats (Conv. vs. non-Conv.)	p (Conv. vs. non-Conv.)	APOE4+ Corr.	APOE4- Corr.	Z-Stats (APOE4+ vs. APOE4-)	p (APOE4+ vs. APOE4-)
Clux Normalized	0.071	0.09	-0.143	0.88	0.22	0.23	-0.08	0.93
Clux	0.25	0.12	0.88	0.37	0.14	0.39	-1.85	0.063
CharPathL Normalized	0.072	0.17	-0.71	0.47	0.29	0.23	0.48	0.63
CharPathL	-0.14	0.07	-1.49	0.13	0.12	-0.06	1.25	0.20
Global Connectivity	0.24	0.04	1.43	0.15	0.039	0.29	-1.76	0.078
Eglobal	0.20	-0.007	1.51	0.12	-0.028	0.199	-1.58	0.11

Legend: **Conv. Corr** : Converters group partial correlation coefficient; **non-Conv. Corr**: non-Converters group partial correlation coefficient; **Z-Stats (Conv. vs. non-Conv.)**: Z-stats Converters vs. non-Converters correlation coefficients; **p (Conv. vs. non-Conv.)**: p-value of the Z-stats Converters vs. non-Converters; **APOE4+ Corr.** : APOE4+ group partial correlation coefficient; **APOE4- Corr.** : APOE4- group partial correlation coefficient; **Z-Stats (APOE4+ vs. APOE4-)** Z-stats APOE4+ vs. APOE4- correlation coefficients; **p (APOE4+ vs. APOE4-)** p-value of the Z-Stats (APOE4+ vs. APOE4-).

Table S17. Statistical differences APOE4+ vs. APOE4- and Converters (Conv) vs. non-Converters (non-Conv) in the linear correlation between topological network attributes and CSF measure Aβ42. The topological network attributes are: Clustering index normalized (Clux Normalized), Clustering index (Clux), Characteristic path length Normalized (CharPathL Normalized), Global connectivity, and global efficiency (Eglobal). The significant values are represented in red.

Topological Variables	Conv. Corr.	non-Conv. Corr.	Z-Stats (Conv. vs. non-Conv.)	p (Conv. vs. non-Conv.)	APOE4+ Corr.	APOE4- Corr.	Z-Stats (APOE4+ vs. APOE4-)	p (APOE4+ vs. APOE4-)
Clux Normalized	-0.05	0.035	-0.47	0.63	0.25	0.006	1.34	0.17
Clux	-0.03	0.053	-0.45	0.65	-0.03	0.158	-1.02	0.30
CharPathL Normalized	-0.009	0.033	-0.22	0.81	0.28	-0.039	1.76	0.078
CharPathL	-0.014	-0.02	0.057	0.95	**0.229**	**-0.171**	**2.15**	**0.03**
Global Connectivity	0.012	0.06	-0.28	0.77	-0.11	0.216	-1.77	0.07
Eglobal	0.013	0.04	-0.18	0.85	**-0.16**	**0.20**	**-2.00**	**0.044**

Legend: **Conv. Corr** : Converters group partial correlation coefficient; **non-Conv. Corr**: non-Converters group partial correlation coefficient; **Z-Stats (Conv. vs. non-Conv.)**: Z-stats Converters vs. non-Converters correlation coefficients; **p (Conv. vs. non-Conv.)**: p-value of the Z-stats Converters vs. non-Converters; **APOE4+ Corr.** : APOE4+ group partial correlation coefficient; **APOE4- Corr.** : APOE4- group partial correlation coefficient; **Z-Stats (APOE4+ vs. APOE4-)** Z-stats APOE4+ vs. APOE4- correlation coefficients; **p (APOE4+ vs. APOE4-)** p-value of the Z-Stats (APOE4+ vs. APOE4-).

Table S18. Statistical differences APOE4+ vs. APOE4- and Converters (Conv) vs. non-Converters (non-Conv) in the linear correlation between topological network attributes and CSF measure T-tau. The topological network attributes are: Clustering index normalized (Clux Normalized), Clustering index (Clux), Characteristic path length Normalized (CharPathL Normalized), Global connectivity, and global efficiency (Eglobal). The significant values are represented in red.

Topological Variables	Conv. Corr.	non-Conv. Corr.	Z-Stats (Conv. vs. non-Conv.)	p (Conv. vs. non-Conv.)	APOE4+ Corr.	APOE4- Corr.	Z-Stats (APOE4+ vs. APOE4-)	p (APOE4+ vs. APOE4-)
Clux Normalized	0.12	-0.08	1.09	0.27	-0.11	-0.14	0.14	0.88
Clux	0.02	0.05	-0.18	0.85	-0.02	-0.037	0.09	0.92
CharPathL Normalized	0.15	-0.06	1.15	0.24	-0.05	-0.10	0.30	0.75
CharPathL	0.10	-0.08	1.006	0.31	-0.005	-0.066	0.32	0.74
Global Connectivity	-0.041	0.07	-0.61	0.53	-0.029	0.010	-0.21	0.83
Eglobal	-0.07	0.07	-0.79	0.42	-0.015	0.035	-0.27	0.78

Legend: **Conv. Corr** : Converters group partial correlation coefficient; **non-Conv. Corr**: non-Converters group partial correlation coefficient; **Z-Stats (Conv. vs. non-Conv.)**: Z-stats Converters vs. non-Converters correlation coefficients; **p (Conv. vs. non-Conv.)**: p-value of the Z-stats Converters vs. non-Converters; **APOE4+ Corr.** : APOE4+ group partial correlation coefficient; **APOE4- Corr.** : APOE4- group partial correlation coefficient; **Z-Stats (APOE4+ vs. APOE4-)** Z-stats APOE4+ vs. APOE4- correlation coefficients; **p (APOE4+ vs. APOE4-)** p-value of the Z-Stats (APOE4+ vs. APOE4-).

Table S19. Statistical differences APOE4+ vs. APOE4- and Converters (Conv) vs. non-Converters (non-Conv) in the linear correlation between topological network attributes and CSF measure P-tau. The topological network attributes are: Clustering index normalized (Clux Normalized), Clustering index (Clux), Characteristic path length Normalized (CharPathL Normalized), Global connectivity, and global efficiency (Eglobal). The significant values are represented in red.

Topological Variables	Conv. Corr.	non-Conv. Corr.	Z-Stats (Conv. vs. non-Conv.)	p (Conv. vs. non-Conv.)	APOE4+ Corr.	APOE4- Corr.	Z-Stats (APOE4+ vs. APOE4-)	p (APOE4+ vs. APOE4-)
Clux Normalized	0.16	-0.087	1.34	0.178	-0.13	-0.11	-0.07	0.93
Clux	0.027	0.030	-0.01	0.99	-0.02	-0.04	0.13	0.89
CharPathL Normalized	0.17	-0.067	1.29	0.19	-0.07	-0.07	0.004	0.99
CharPathL	0.12	-0.066	1.003	0.31	-0.02	-0.03	0.04	0.96
Global Connectivity	-0.04	0.048	-0.50	0.61	-0.02	-0.01	-0.04	0.96
Eglobal	-0.07	0.058	-0.73	0.46	-0.00091	0.007	-0.04	0.96

Legend: **Conv. Corr** : Converters group partial correlation coefficient; **non-Conv. Corr**: non-Converters group partial correlation coefficient; **Z-Stats (Conv. vs. non-Conv.)**: Z-stats Converters vs. non-Converters correlation coefficients; **p (Conv. vs. non-Conv.)**: p-value of the Z-stats Converters vs. non-Converters; **APOE4+ Corr.** : APOE4+ group partial correlation coefficient; **APOE4- Corr.** : APOE4- group partial correlation coefficient; **Z-Stats (APOE4+ vs. APOE4-)** Z-stats APOE4+ vs. APOE4- correlation coefficients; **p (APOE4+ vs. APOE4-)** p-value of the Z-Stats (APOE4+ vs. APOE4-).

6.3 Subtle alterations in cerebrovascular reactivity in mild cognitive impairment detected by graph theoretical analysis and not by the standard approach

NeuroImage: Clinical 15 (2017) 151–160

Contents lists available at ScienceDirect

NeuroImage: Clinical

journal homepage: www.elsevier.com/locate/ynicl

Subtle alterations in cerebrovascular reactivity in mild cognitive impairment detected by graph theoretical analysis and not by the standard approach

Carlos A. Sánchez-Catasús[a,b,*], Gretel Sanabria-Diaz[c,d], Antoon Willemsen[a], Eduardo Martinez-Montes[d], Juan Samper-Noa[d,e], Angel Aguila-Ruiz[b], Ronald Boellaard[a], Peter P. De Deyn[f], Rudi A.J.O. Dierckx[a], Lester Melie-Garcia[c,d]

[a] Department of Nuclear Medicine and Molecular Imaging, University of Groningen, University Medical Center Groningen, The Netherlands
[b] Department of Nuclear Medicine, Center for Neurological Restoration (CIREN), Havana, Cuba
[c] Laboratoire de Recherche en Neuroimagerie (LREN), Centre Hospitalier Universitaire Vaudois (CHUV), Lausanne, Switzerland
[d] Neuroinformatics Department, Cuban Neuroscience Center, Havana, Cuba
[e] Hospital Carlos J. Finlay, Havana, Cuba
[f] Department of Neurology and Alzheimer Research Center, University of Groningen, University Medical Center Groningen, The Netherlands

ARTICLE INFO

Keywords:
Graph theoretical
Cerebrovascular reactivity
Mild cognitive impairment

ABSTRACT

There is growing support that cerebrovascular reactivity (CVR) in response to a vasodilatory challenge, also defined as the cerebrovascular reserve, is reduced in Alzheimer's disease dementia. However, this is less clear in patients with mild cognitive impairment (MCI). The current standard analysis may not reflect subtle abnormalities in CVR. In this study, we aimed to investigate vasodilatory-induced changes in the topology of the cerebral blood flow correlation (CBF_{corr}) network to study possible network-related CVR abnormalities in MCI. For this purpose, four CBF_{corr} networks were constructed: two using CBF SPECT data at baseline and under the vasodilatory challenge of acetazolamide (ACZ), obtained from a group of 26 MCI patients; and two equivalent networks from a group of 26 matched cognitively normal controls. The mean strength of association (*SA*) and clustering coefficient (*C*) were used to evaluate ACZ-induced changes on the topology of CBF_{corr} networks. We found that cognitively normal adults and MCI patients show different patterns of *C* and *SA* changes. The observed differences included the medial prefrontal cortices and inferior parietal lobe, which represent areas involved in MCI's cognitive dysfunction. In contrast, no substantial differences were detected by standard CVR analysis. These results suggest that graph theoretical analysis of ACZ-induced changes in the topology of the CBF_{corr} networks allows the identification of subtle network-related CVR alterations in MCI, which couldn't be detected by the standard approach.

1. Introduction

There is increasing evidence that patients with Alzheimer's disease (AD) dementia have decreased cerebrovascular reactivity (CVR) in response to a vasodilatory challenge, also defined as the cerebrovascular reserve (Glodzik et al., 2013, for a review). However, this is less clear in patients during the prodromal mild cognitive impairment (MCI) stage of AD. Some studies show a decrease (Richiardi et al., 2014; Glodzik et al., 2011; Cantin et al., 2011; Zavoreo et al., 2010), while others do not (Shim et al., 2015; Fromm et al., 2013; Anzola et al., 2011). This issue is becoming important in AD research because it could have implications for early diagnosis and treatment of AD. Early CVR abnormalities, especially at the microvascular level, affect the neurovascular coupling and consequently the neural activation (Pillai and Mikulis, 2015), which in turn alters the brain's functional integrity (Iadecola, 2004).

MCI due to AD is the transition from normal cognition to dementia (Albert et al., 2011). Accordingly, CVR abnormalities would be subtle or borderline which may partly explain ambiguous findings, particularly in MCI patients with a low vascular burden. Furthermore, considering the complexity of the cerebral microvasculature network the standard analysis of CVR might not reflect subtle network-related alterations since it relies on the analysis of individual regions (or the whole brain) rather than on the interaction between them.

Recently, graph theoretical analysis of large-scale structural MRI (sMRI) correlation networks has shown its potential to reveal subtle network-related pathological processes in MCI (Tijms et al., 2013; He et al., 2009a, for reviews). We previously demonstrated that the

* Corresponding author at: University Medical Center Groningen, Department of Nuclear Medicine and Molecular Imaging. Hanzeplein 1, 9713 GZ Groningen, The Netherlands.
E-mail address: c.a.sanchez.catasus@umcg.nl (C.A. Sánchez-Catasús).

http://dx.doi.org/10.1016/j.nicl.2017.04.019
Received 1 September 2016; Received in revised form 10 March 2017; Accepted 19 April 2017
Available online 25 April 2017

cerebral blood flow correlation (CBF_{corr}) network, based on CBF SPECT data, shows a non-random topological organization (Melie-García et al., 2013). The same topological organization had been previously observed in sMRI correlation (Alexander-Bloch et al., 2013, for a review) and fiber tractography networks (Iturria-Medina et al., 2008). Therefore, we speculate that graph theoretical analysis can also be applied to CBF SPECT data to detect possible subtle network-related CVR abnormalities in MCI.

Here, we constructed four CBF_{corr} networks: two using CBF SPECT data at baseline and under the vasodilatory challenge of acetazolamide (ACZ), obtained from a group of relatively young MCI patients with limited vascular risk factors; and two equivalent networks using a group of matched cognitive normal controls. ACZ is a reproducible, simple, and a safe vasodilatory stimulus (Vagal et al., 2009, for a review).

Graph metrics based on the concepts of the mean strength of association (*SA*) (Bullmore and Bassett, 2011) and clustering coefficient (*C*) (Watts and Strogatz, 1998) were used to evaluate ACZ-induced changes on the topology of the CBF_{corr} networks. The *SA* for a particular brain region (node) measures the correlation's mean (co-variation's mean) with the rest of the network; while *C* measures local connectivity (i.e. how well neighbors of a node are connected).

Hence, using graph theoretical analysis, our aim was to investigate ACZ-induced changes in the topology of the CBF_{corr} network to study possible network-related CVR abnormalities in MCI. We also investigated CVR by the standard approach in the same groups of subjects for comparing with graph theoretical analysis findings.

2. Methods

2.1. Subjects

Twenty-six MCI patients and twenty-six clinically healthy control volunteers were studied, selected from one hundred subjects recruited over a two-year period and a one-year follow-up and based on the inclusion and exclusion criteria detailed below. The Ethics Committee of the Center for Neurological Restoration of Havana, Cuba, approved the study. All participating subjects gave written informed consent according to the Helsinki Declaration. Table 1 summarizes sociodemographic and clinical characteristics of the MCI and control groups.

All subjects were screened for a complete medical history, routine blood tests, cranial MRI, neuropsychological testing and neurological/psychiatric examinations. Subjects were clinically diagnosed as MCI using the criteria based on the Clinical Dementia Rating Scale (CDR) (Morris, 1993). According to these criteria, subjects were classified as MCI with CDR = 0.5; while normal cognitive subjects with CDR = 0. All of MCI subjects maintained independence in their daily living. In addition to the Mini-Mental State Examination (MMSE), specific mnemonic and non-mnemonic cognitive tests were also performed for all subjects to further characterize cognitive function (Supplementary Table S1).

Table 1
Sociodemographic and clinical features of control and MCI groups.

	Control (N = 26)	MCI (N = 26)	p-value
Age (years)	60.9 ± 7.3	64.7 ± 6.9	0.06[a]
Gender (female/male)	13/13	14/12	0.78[b]
Education (years)	13.6 ± 3.9	11.8 ± 4.6	0.13[a]
MMSE	29.3 ± 1.1	26.9 ± 1.24	10^{-6}[a]
Hypertension	27%	35%	0.55[b]
Hyperlipidemia	19%	23%	0.73[b]
Diabetes	15%	15%	1[b]
Smoking	27%	19%	0.51[b]

Data shown as mean ± SD or percent of subjects.
[a] Student *t*-tests for independent samples.
[b] Chi-square test.

The inclusion criteria were: 1) MCI patients with memory complaints as the main cognitive symptom, which worsened over a period of one year; 2) subjects (patients and controls) with limited (and treated) vascular risk factors, based upon clinical examination, blood tests and magnetic resonance angiography (MRA) findings; 3) subjects without significant depression, according to the Hamilton Depression Scale (score < 8) (Hamilton, 1960); 4) no prior or current treatment with anti-acetylcholinesterase agents; and 5) right-handedness.

The exclusion criteria were: 1) significant medical problems (i.e. serious cardiac disease, poorly controlled diabetes or hypertension; severe inflammatory, thyroid, renal, hepatic or other chronic diseases); 2) cerebrovascular disorders (i.e. transient ischemic attack or cerebral infarction), moderate and severe carotid stenosis by MRA findings, large white matter changes on MRI (based on T2 and FLAIR sequences), hydrocephalus or intracranial mass; 3) history of traumatic brain injury, migraine or another neurological disease; and 4) psychiatric disorder, substance abuse or dependence.

2.2. CBF SPECT imaging under the acetazolamide challenge

CBF SPECT imaging was carried out by a double-head rectangular gamma camera (Sopha Medical Vision, France) equipped with ultra-high-resolution fan beam collimators. More about the acquisition and reconstruction parameters, including corrections for attenuation and partial volume effect (PVE) due to atrophy, are described in our preceding article (Melie-García et al., 2013). A two-day protocol was used for CBF SPECT imaging at baseline (basal SPECT) and under the ACZ challenge (ACZ SPECT).

Absolute measurement is necessary to quantify (optimally) the CBF response to the vasodilatory stimulus (Boles Ponto et al., 2004). Therefore, global CBF at basal condition ($gCBF_{Basal}$) and under ACZ ($gCBF_{ACZ}$) was determined in absolute units (mL/min/100 g) by spectral analysis of non-invasive radionuclide angiographies (Takasawa et al., 2002). The radionuclide angiography was performed before SPECT acquisition, for both basal and ACZ conditions. Briefly, a radionuclide angiography of the head and chest was performed after injection of 555 MBq of technetium-99-ethyl cysteinate dimer (ECD) into the antecubital vein of the right arm under resting condition (supine, eyes open, dimly lit quiet room) to estimate $gCBF_{Basal.}$ The same procedure was repeated to estimate $gCBF_{ACZ}$ but 20 min after slow intravenous injection of 1 g of ACZ. Heart rate and arterial pressure were measured at the time of the two injections of the tracer (basal and ACZ).

Basal and ACZ SPECT images were then converted to basal and ACZ quantitative CBF images using $gCBF_{Basal}$ and $gCBF_{ACZ}$, respectively, by application of Lassen's linearization algorithm (Lassen et al., 1988). For subsequent voxelwise statistical analysis, basal and ACZ quantitative CBF images were normalized to the Montreal Neurological Institute (MNI) space. The image normalization was performed by applying DARTEL parameters (based on a fast diffeomorphic algorithm) obtained from MRI preprocessing (see the next subsection). Normalized images were then smoothed using a 14 mm-kernel to optimize sensitivity (Van Laere et al., 2002).

2.3. Volumetric MRI

Volumetric high-resolution MRI was also performed to characterize the MCI group regarding regional brain atrophy. Regional atrophy, particularly hippocampal, is a biomarker of neuronal injury of MCI due to AD (Albert et al., 2011; Sánchez-Catasús et al., 2017). Volumetric MRI also had two other functions: to correct for PVE in CBF SPECT images and to estimate spatial transformations that were used to normalize images to MNI space, as described above.

MRI acquisition was performed using a 1.5 Tesla Symphony scanner (Siemens, Erlangen, Germany). The acquisition protocol for volumetric MRI is described in details in our previous study (Melie-García et al.,

2013). The preprocessing steps were as follows: images were segmented into GM and WM; imported into the DARTEL toolbox and normalized to MNI space to generate warped and smoothed (12 mm-kernel) Jacobian modulated GM and WM images. GM/WM modulated images represent GM/WM volume images (GMV/WMV images). Global tissue volumes were estimated in the native space using the Voxel-Based Morphometry toolbox (VBM8: http://dbm.neuro.uni-jena.de/vbm8/).

For every subject, neurological/psychiatric/neuropsychological examinations, as well as SPECT and MRI, were carried out within a maximum interval of one month.

2.4. Construction of the CBF correlation (CBF_{corr}) network

For each group of subjects (MCI and control) in each condition (baseline and ACZ challenge), a CBF_{corr} network was constructed as a CBF correlation matrix (Melie-García et al., 2013). In short, 90 ROIs were defined using the AAL atlas (Tzourio-Mazoyer et al., 2002) and Pearson's correlation coefficients were calculated (across subjects) between all possible pairs of ROIs. Hence, the interregional correlation matrix (90 × 90 ROIs) was obtained gathering together all correlation coefficients. Self-correlations were excluded, implying a diagonal of zeros in the symmetric matrix. Prior to the correlation analysis, a linear regression was performed at every ROI to remove the effects of age, gender, age–gender interaction, and global CBF values. For computing the CBF correlation matrix, the correlation was carried out between the residuals of this regression instead of the raw regional CBF values. Fig. 1 shows CBF correlation matrices for each group in each condition.

For within-conditions and within-groups network metrics comparisons (see Sub-section 2.6.2), we obtained 1000 bootstrap samples (with replacement) of each CBF correlation matrix. Paired bootstrap samples were used for baseline and the ACZ challenge in each group.

2.5. Network metrics

In the following, we define *SA* (the mean strength of association) (Bullmore and Bassett, 2011) and *C* (the clustering coefficient) (Watts and Strogatz, 1998) to study ACZ-induced changes in the CBF correlation networks.

The *SA* for a particular brain region or node *i*, SA_{nodal} (*i*), is defined as the mean of the absolute value of Pearson's correlation coefficients ($Corr_{ij}$) of node *i* with the rest *N*-1 nodes in the network. Formally, SA_{nodal} (*i*) is calculated as:

$$SA_{nodal}(i) = \frac{1}{N-1} \sum_{\substack{j=1 \\ j \neq i}}^{N} |Corr_{ij}|$$

where *N* is the number of nodes (ROIs).

In simple terms, SA_{nodal} measures the correlation's mean (covariation's mean) of a node with the rest of the network. *SA* is also defined at the network level (SA_{global}) as the average of SA_{nodal}:

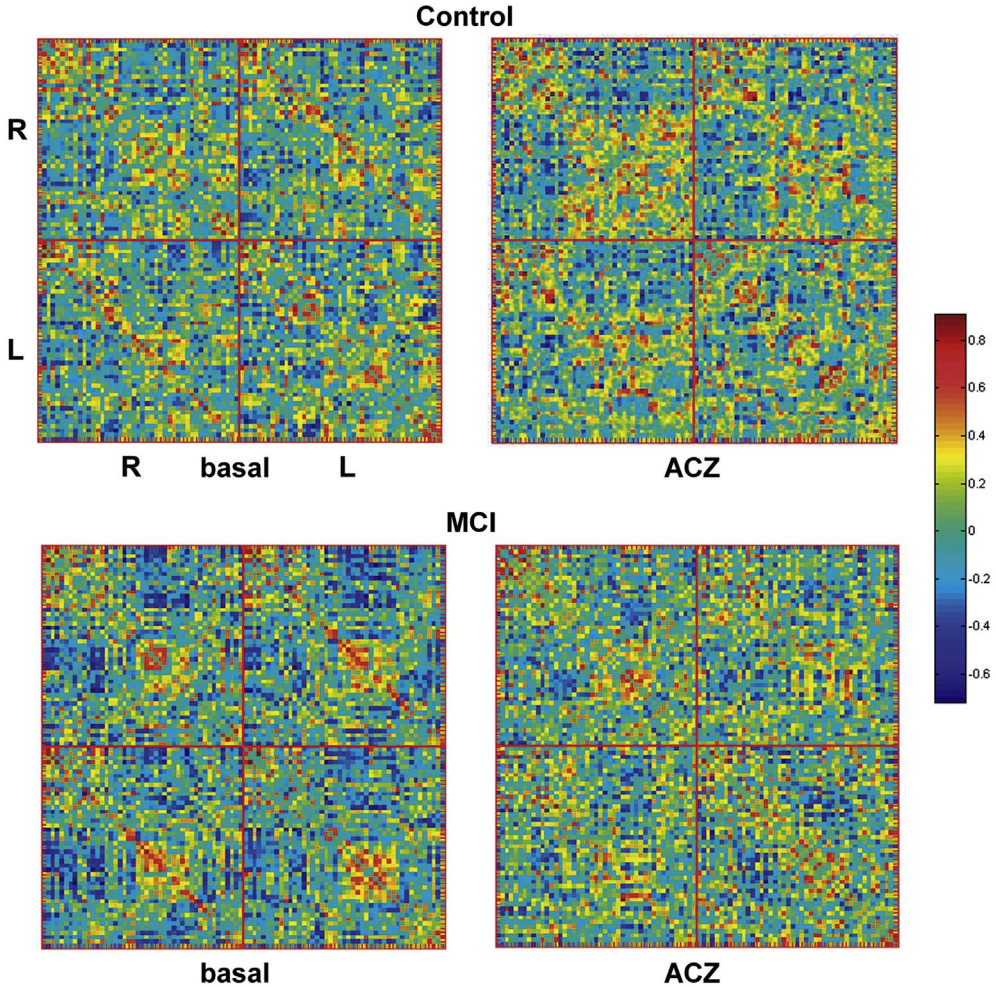

Fig. 1. CBF correlation matrices (CBF correlation networks) constructed using CBF SPECT data at basal and under the acetazolamide (ACZ) challenge for MCI and cognitively normal controls. The color bar indicates the value of the correlation coefficient coming from the CBF co-variations among 90 anatomical brain regions (AAL atlas). For the sake of clarity brain regions of the right (R) and left (L) hemispheres were separated.

$$SA_{global} = \frac{1}{N} \sum_{i=1}^{N} SA_{nodal}(i)$$

On the other hand, C is a measure of the tendency to cluster nodes into strictly connected neighborhoods (a measure of network segregation; i.e. local connectivity). Nodes are considered neighbors when a connection between them exists, which is not limited to a physical neighborhood concept. C_{nodal} (i), for a binary and undirected graph G, is the number of existing connections between the neighbors of node i divided by all neighbor's possible connections. Formally, C_{nodal} (i) is calculated as:

$$C_{nodal}(i) = \frac{1}{N} \sum_{i \in G} \frac{2t_i}{k_i (k_i - 1)}$$

where t_i is the number of triangles around node i (see below); and k_i is the degree of node i (number of links connected to node i); (for $k_i < 2$, C_{nodal} $(i) = 0$).

$$t_i = \frac{1}{2} \sum_{j,h \in G} a_{ij} a_{ih} a_{jh}$$

where a_{ij} is the connection status between i and j: $a_{ij} = 1$ when link (i, j) exists (when i and j are neighbors); $a_{ij} = 0$ otherwise ($a_{ii} = 0$ for all i).

In simple terms, C_{nodal} measures how well neighbors of a node are connected. C is also defined at the network level (C_{global}) as the average of C_{nodal}:

$$C_{global} = \frac{1}{N} \sum_{i=1}^{N} C_{nodal}(i)$$

For each CBF correlation matrix, SA_{nodal} and SA_{global} were calculated over the bootstrap samples. Since we used C defined for a binary (undirected) graph, C_{nodal} and C_{global} were calculated over bootstrap samples of thresholded binary adjacency matrices. Rather than restricting the analysis to a binary graph obtained by applying a single threshold value, C_{nodal} and C_{global} were calculated over a range of thresholds or 'sparsity degree' values. A sparsity degree of 0.9 means that 90% of the correlation matrix is discarded; consequently, only the highest 10% of the values is taken into account. Sparsity degrees ranging from 0.5 to 0.9 (in steps of 0.02) were used, yielding a set of 21 values. This procedure normalizes the networks to have the same number of nodes and edges, enabling the examination of C_{nodal} and C_{global}. The range of sparsity degree was chosen to allow for these network properties to be estimated and the number of spurious edges in each network minimized as indicated in previous studies (Achard and Bullmore, 2007; He et al., 2007; Sanabria-Diaz et al., 2013).

Before calculating C_{nodal} (as described above), the largest connected component (see Achard et al., 2006) of all bootstrap samples of CBF correlation matrices was computed. The minimum sparsity degree for the largest connected component (equal to the number of AAL nodes) was used as the upper limit of the sparsity degree range. This step guarantees that all C_{nodal} values come from fully connected CBF_{corr} networks. Then, the C_{nodal} mean curve (across the range of sparsity degree) was assessed over the bootstrap samples for every node and used as the C_{nodal} descriptor.

On the other hand, the descriptor used for C_{global} was the area under the curve (AUC) extracted from thresholding across the range of sparsity degree over bootstrap samples for each group and condition. Since the topology of the C_{global} curve is monotonic with the sparsity degree, the AUC is a suitable descriptor for characterizing its global performance. This descriptor was also adopted in previous studies (Sanabria-Diaz et al., 2013; Wu et al., 2012; He et al., 2009b).

Construction of CBF_{corr} networks and computation of network metrics was performed using the MorphoConnect toolbox (Melie-García et al., 2010) and subroutines of the Brain Connectivity toolbox (https://sites.google.com/site/bctnet/).

2.6. Statistical analysis

2.6.1. Changes in standard metrics

The data at the voxel level was analyzed by a 2 (group: Control and MCI) × 2 (condition: basal and ACZ) full factorial design as implemented in the SPM8 toolbox. Age and gender were modeled as nuisance covariates. The global effect was also controlled using proportional scaling.

We examined simple main effects of condition (positive and negative) in each group by t-contrasts for dependent samples; and simple main effects of group (positive and negative) in each condition by t-contrasts for independent samples. We also studied the interaction of group and condition (positive and negative).

A similar treatment (2 × 2 design) was also performed for global CBF values, controlling for age and gender.

As a supplementary morphometric analysis, differences at the voxel level between groups for GMV and WMV images were tested to evaluate regional brain atrophy in the MCI group. Comparisons were performed using the Student t-tests for independent samples through the SPM8 toolbox. The GMV and WMV images were masked using an absolute threshold of 0.25 to avoid as much as possible contamination by misclassified voxels. Age, gender, and total intracranial volume were controlled.

In all SPM analyses, the statistical threshold of $p = 0.01$ (peak level) was used. The extent threshold used was determined by the cluster of voxels significant at $p = 0.05$ (cluster level), corrected for multiple comparisons (family-wise error method - FWE) and after correction of non-isotropic smoothness. Anatomical regions were determined by comparing voxel and cluster location with the AAL atlas (Tzourio-Mazoyer et al., 2002). The most significant voxels were reported in MNI coordinates.

2.6.2. Changes in network metrics

Similar to the standard analysis, C and SA (global and nodal) were analyzed by a 2 × 2 design. To examine simple main effects of the condition in each group for each network metric (or simple main effects of the group in each condition), we computed the difference between the two conditions (or between the two groups) for the corresponding bootstrap samples. Then, we constructed the bootstrap distribution of the difference and computed the 95% BC (bias-corrected) bootstrap confidence interval (CI). A significant difference between conditions (or between groups) was considered when the CI did not contain the zero. For C_{nodal} and SA_{nodal}, we also corrected for multiple comparisons by Bonferroni adjustment.

Likewise, we studied the interaction of group and condition (global and nodal) by comparing simple main effects of condition between groups following the same procedure as described in the previous paragraph. For instance, the differences between conditions in control and MCI groups were subtracted and the 95% BC bootstrap CI was calculated for the subtraction. As before, if CI did not contain the zero, the interaction effect was considered statistically significant. Due to the exploratory nature of this study, we also examined the interaction for uncorrected values at the nodal level.

The network statistical analyses were performed using the MorphoConnect toolbox (Melie-García et al., 2010), while global CBF data was analyzed using STATISTICA software (Stat Soft, Inc., version 8.0). The significance level was set at $p < 0.05$.

3. Results

The administration of ACZ was well tolerated in all individuals. There were no significant differences between conditions (basal vs. ACZ) in both groups in heart rate (Control: 68.2 ± 9.9 vs. 67.2 ± 9.4 bpm, respectively, $p = 0.6$, paired t-test; MCI: 70.4 ± 9.4 vs. 67.4 ± 7.1 bpm, respectively, $p = 0.09$) and mean arterial pressure (Control: 106.9 ± 10.8 vs. 106.5 ± 9.9 mm Hg,

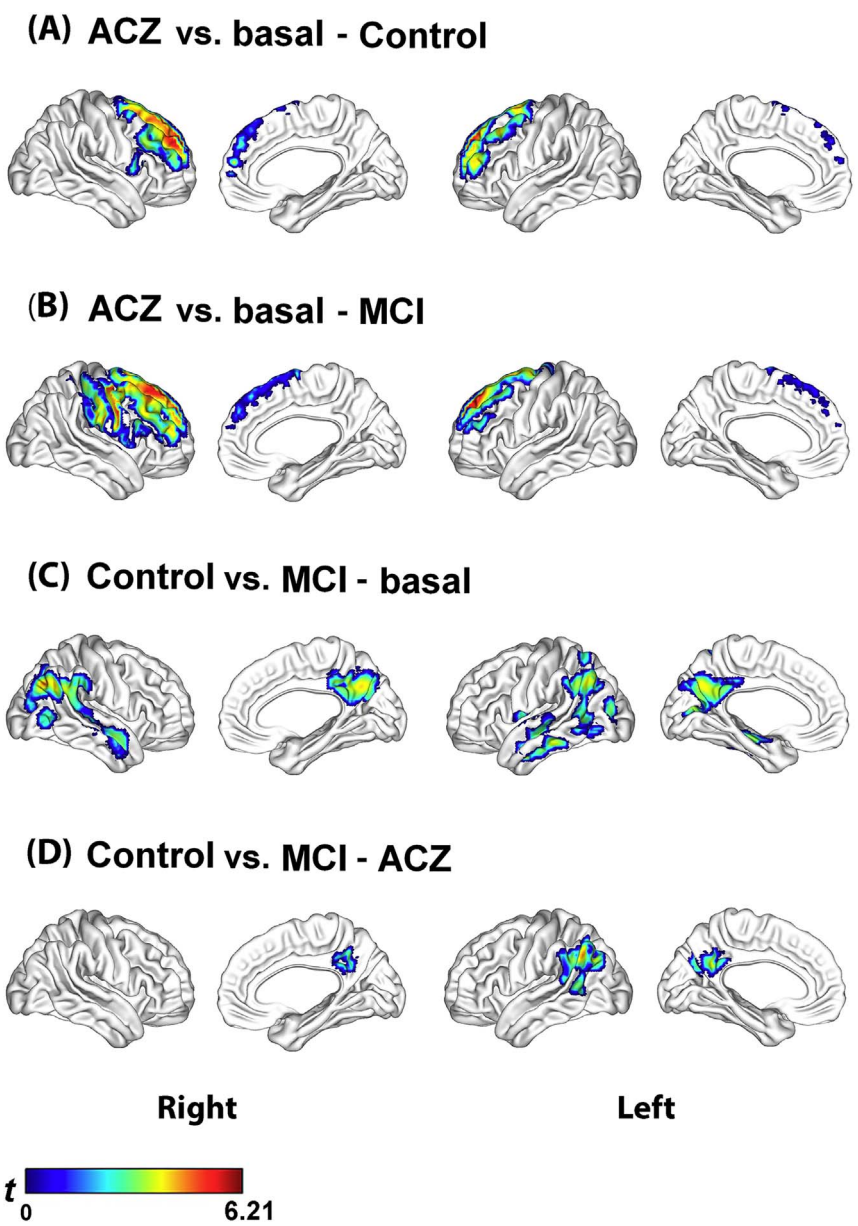

Fig. 2. CBF changes at the voxel level analyzed by a 2 (group: Control and MCI) × 2 (condition: basal and ACZ) full factorial design using statistical parametric mapping (SPM). Figures A and B show that the control and MCI groups had a similar regional pattern of CBF increase in frontal lobe bilaterally. Figures C and D show that the regional differences between groups were relatively similar in the two conditions, although less extensive in the ACZ condition. No interaction of the group by the condition was found.
SPM t-maps are visualized onto the cortical surfaces using the BrainNet Viewer package (http://www.nitrc.org/projects/bnv).

respectively, p = 0.8; MCI: 102. 8 ± 10.9 vs. 105.9 ± 10.8 mm Hg, respectively, p = 0.1).

3.1. Changes in standard metrics

At the global level, there was a significant increase in $gCBF_{ACZ}$ as compared with $gCBF_{Basal}$ in both groups (Control: 42.0 ± 5.5 vs. 54.9 ± 6.3 mL/min/100 g; $p < 10^{-6}$; MCI: 38.9 ± 6.7 vs. 51.1 ± 7.3 mL/min/100 g; $p < 10^{-6}$) (Supplementary Fig. S1). The percent of the increase in the control group (+ 31.4 ± 9.2) was comparable to that found in the MCI group (+ 32.7 ± 12.9). There were no significant differences between groups in the basal (p = 0.21) and ACZ conditions (p = 0.07). No significant interaction of group and condition was found (p = 0.75).

At the voxel level, the analysis of differences between condition within-group showed a similar pattern in the control and MCI groups. Both groups showed significant regional CBF increases mainly in frontal regions bilaterally, after removal of the effect of global CBF increase due to ACZ (Fig. 2.A and B, Supplementary Table S2). In the control group, the voxel with the lowest p-value was found in the right superior frontal gyrus (medial part) (MNI: x, y, z = 15, 56, 31; $P_{FWE} = 10^{-3}$, T = 6.21). In the MCI group, the right superior frontal gyrus (dorsolateral part) was the voxel with the lowest p-value (MNI: x, y, z = 15, 35, 55; $P_{FWE} = 10^{-3}$, T = 6.18). Neither group showed a significant regional decrease.

On the other hand, the group difference within-condition showed a regional CBF decrease in the MCI group as compared to the control group in the basal condition, mostly in temporoparietal regions bilaterally (Fig. 2.C, Supplementary Table S3). In the right angular gyrus was the voxel with the lowest p-value (MNI: x, y, z = 45, −70, 34; $P_{FWE} = 0.05$, T = 4.52). At the ACZ condition, the results were relatively similar to those observed in basal condition, although less extensive and the right temporoparietal region showed no difference as compared to the control group (Fig. 2.D, Supplementary Table S3). In

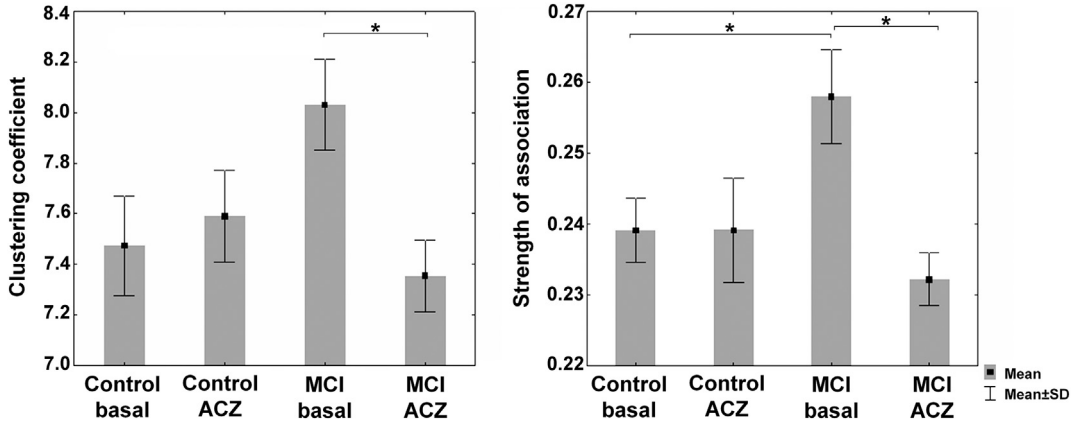

Fig. 3. Global clustering coefficient ($C_{globlal}$) and mean strength of association (SA_{global}) in the control and MCI groups in the two condition: basal and under the ACZ challenge. The data were generated by bootstrapping the CBF correlation matrices (1000 samples per group and condition). Comparisons were performed by estimating 95% bootstrap confident intervals (see main text for details). *Significant effect.

the left angular gyrus was the voxel with the lowest p-value (MNI: x, y, z = − 45, 61, 37; P_{FWE} = 0.004, T = 5.17). In the basal and ACZ conditions in the MCI group, as compared to the control group, also no significant regional CBF increases were found. No significant interaction of group and condition were observed neither positive nor negative.

3.2. Changes in network metrics

At the global level, the control group showed no significant changes of C_{global} and SA_{global} (no changes of CBF co-variation) in response to the ACZ challenge. In contrast to the control, the MCI group showed a decrease in $C_{globlal}$ and SA_{global} (Fig. 3 and Table 2; see also Supplementary Fig. S2).

Moreover, SA_{global} was higher in the MCI group as compared to the control in the basal condition (Fig. 3 and Table 2). Although not significant, a similar difference for $C_{globlal}$ in the MCI group was found (Fig. 3 and Supplementary Fig. S2). At the ACZ condition, no significant differences were observed for C_{global} and SA_{global} between the MCI and control groups (Fig. 3 and Table 2; see also Supplementary Fig. S2). However, unlike the standard analysis, we found a significant crossover interaction effect of group and condition for SA_{global} (Table 2). Thus, compared to the control group, the MCI group showed a specific decrease in SA_{global} induced by the ACZ challenge. For C_{global}, a similar interaction was observed although did not reach significance (Supplementary Fig. S2).

At the nodal level, the control group showed no significant change in C_{nodal} in response to ACZ after multiple comparisons correction (4.A and 4.B); while SA_{nodal} showed an increase in the right inferior temporal gyrus (Fig. 4.C) and decreases in the frontal superior and middle temporal pole on the left side (Fig. 4.D). In contrast to the control, the MCI group showed decreases in C_{nodal} in the hippocampus and the fusiform gyrus on the right side and in the dorsal medial prefrontal cortex on the left side (Fig. 4.E and F). In this group, SA_{nodal} increased in the postcentral gyrus (Fig. 4.G) and decreased in the superior frontal, middle frontal, lingual and fusiform gyri on the right side, and in the left middle occipital gyrus (Fig. 4.H).

On the other hand, the group difference within-conditions showed that in the MCI group, in the basal condition, C_{nodal} was increased in the inferior parietal lobe bilaterally and in lingual and fusiform gyri on the right side (Fig. 5.A and B); whereas SA_{nodal} was increased in the lingual gyrus bilaterally and in the right inferior temporal and left middle occipital gyri (Fig. 5.C and D). At the ACZ condition, both groups showed no significant changes in both C_{nodal} and SA_{nodal} (Fig. 5.E–H).

However, similar to global network metrics, there was a significant crossover interaction effect of group and condition for both C_{nodal} and SA_{nodal} (Fig. 6). Compared to the control group, the MCI group showed a specific decrease in C_{nodal} induced by the ACZ in the lingual, fusiform and superior temporal gyri on the right side after multiple comparisons correction (Fig. 6.A); and a specific decrease in SA_{nodal} in the middle frontal region and in the lingual, fusiform and inferior temporal gyri on the right side and in the left thalamus (Fig. 6.C).

When the interaction effects described above were examined less conservatively (uncorrected statistic), we found that the MCI group showed a specific decrease in C_{nodal} mainly in regions comprising the inferior parietal lobe and medial prefrontal cortex bilaterally, the parahippocampal gyrus and the lateral temporal cortex on the right side (Fig. 6.E and F). Both thalamus also showed a decrease in C_{nodal}. Moreover, a specific increase in C_{nodal} was found mainly in frontal and occipital regions on the right side, and in the anterior and posterior cingulate on the left side. Likewise, SA_{nodal} showed concurrent changes in C_{nodal} (increase or decrease) in several regions as shown in the Fig. 6.E–H. An opposite change in C_{nodal} and SA_{nodal} was also observed in the right middle frontal region (Fig. 6.E and G).

Table 2
Simple main effects and interactions of group and condition at the global level.

Effect	Mean (95% CI) - C_{global}	Mean (95% CI) - SA_{global}
ACZ vs. basal (Control)	0.12 (− 0.90 – + 0.63)	0.00004 (− 0.02 – + 0.009)
ACZ vs. basal (MCI)	− 0.68 (− 1.44 – − 0.97)[a]	− 0.026 (− 0.04 – − 0.01)[a]
Control vs. MCI (basal)	− 0.56 (− 1.28 – + 0.16)	− 0.019 (− 0.03 – − 0.003)[a]
Control vs. MCI (ACZ)	0.24 (− 0.61 – + 0.84)	0.007 (− 0.02 – + 0.02)
Interaction	0.79 (− 0.14 – + 1.75)	0.03 (+ 0.0006 – + 0.04)[a]

ACZ, acetazolamide; CI, confident interval.
[a] Significant effect.

3.3. Supplementary morphometric analysis

Regional GMV was decreased significantly in the lateral and medial temporal regions (including hippocampi) in the MCI group compared with the control group (Supplementary Fig. S3 and Supplementary Table S4). In contrast to GMV, no significant differences were observed between groups in WMV.

4. Discussion

This study investigated ACZ-induced changes in the topology of the CBF_{corr} networks in normal cognition and MCI subjects. We found that normal cognition and MCI show different patterns of *C* and *SA* changes,

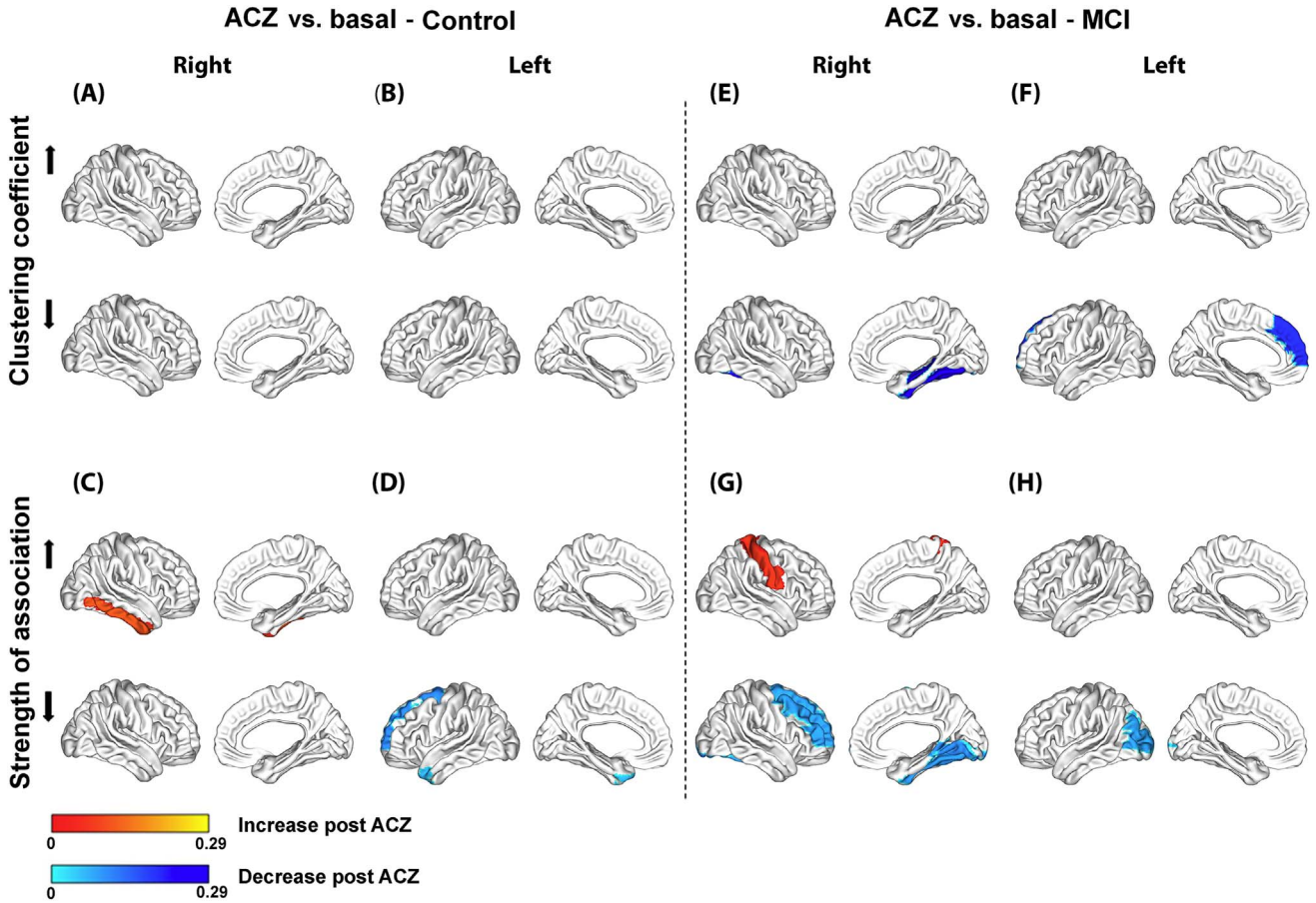

Fig. 4. Significant differences between condition within-group at the nodal level for the clustering coefficient (C_{nodal}) and mean strength of association (SA_{nodal}) in the control (A–D) and MCI groups (E–H).
Regional changes are mapped onto the cortical surfaces using the BrainNet Viewer package (http://www.nitrc.org/projects/bnv).

while the standard approach did not detect substantial differences. Thus, our findings support the concept that multivariate measures (i.e. co-variations) combined with a graph theoretical approach are more sensitive to identify complex pathological processes, as has found in other brain diseases (Bassett et al., 2012; He et al., 2009b). Univariate measures derived from the standard approach could be insufficient for capturing subtle (early) abnormal changes.

4.1. CBF imaging under the ACZ challenge

The global CBF increase in both groups verifies the reliability of the methodology used for CBF imaging under the ACZ challenge. The percent of the increase in the two groups was comparable to previous studies in healthy subjects using a similar methodology (Boles Ponto et al., 2004, for a review).

An interesting observation is the highest regional CBF increase in response to ACZ in frontal cortices in both groups (Fig. 2.A and B). As far as we know, this has not been previously reported. The highest frontal CBF is possibly caused by greater oxygen metabolism in these regions before ACZ administration. This explanation is substantiated by the fact that the neuronal activity is high in frontal regions during the resting state (Ingvar, 1979) and there is a direct relationship between the CBF response to the ACZ and pre-existing oxygen metabolic activity (Yamauchi et al., 2002).

Moreover, the basal temporoparietal CBF reduction observed in the MCI group as compared to the control group (Fig. 2.C) is the typical AD-like hypoperfusion pattern previously described (Herholz et al., 2002). The group difference in the ACZ condition was also relatively similar to those observed in the basal condition. Thus, the basal regional CBF reduction in the MCI group was not misery perfusion since microvessels responded to the ACZ. The basal hypoperfusion is likely mainly related to a reduced level of regional metabolic activity (Herholz et al., 2002).

4.2. Patterns of ACZ-induced changes in CBF correlation networks

The control (cognitively normal) group network showed only a little or almost no topological changes in response to the ACZ challenge (Figs. 3 and 4.A–D). That is, the control group network seems to have the capability to adapt to the challenge. Possibly, this reflects the process to maintain the brain microenvironment homeostasis (Iadecola, 2004), vital for brain function, in response to the vascular challenge induced by the ACZ (Vagal et al., 2009). In contrast, the MCI group network showed a decrease in C and SA, especially at the global level (Fig. 3), suggesting that the above process is possibly altered to some extent in the MCI stage not detected by the standard analysis. On the other hand, although speculative, the SA_{global} increase in the MCI group network in the basal condition might represent an adaptive mechanism in response to the effects of the pathological process.

Perhaps, the most revealing finding is the crossover interaction effect between group and condition, in particular, when analyzed in a less conservative way (Fig. 6.E–H). For example, the patterns of C_{nodal} and SA_{nodal} decreases (mainly C_{nodal}, the bottom of Fig. 6.E and F) partially correspond with the regional CBF reduction in the MCI group in the basal condition (Fig. 2.C). The overlap increases if the atrophy found in the MCI group is included (Supplementary Fig. S3), which suggests that these functional and structural abnormalities could be related to the ACZ-induced changes observed in the MCI group network since they are both biomarkers of neuronal injury of MCI due to AD

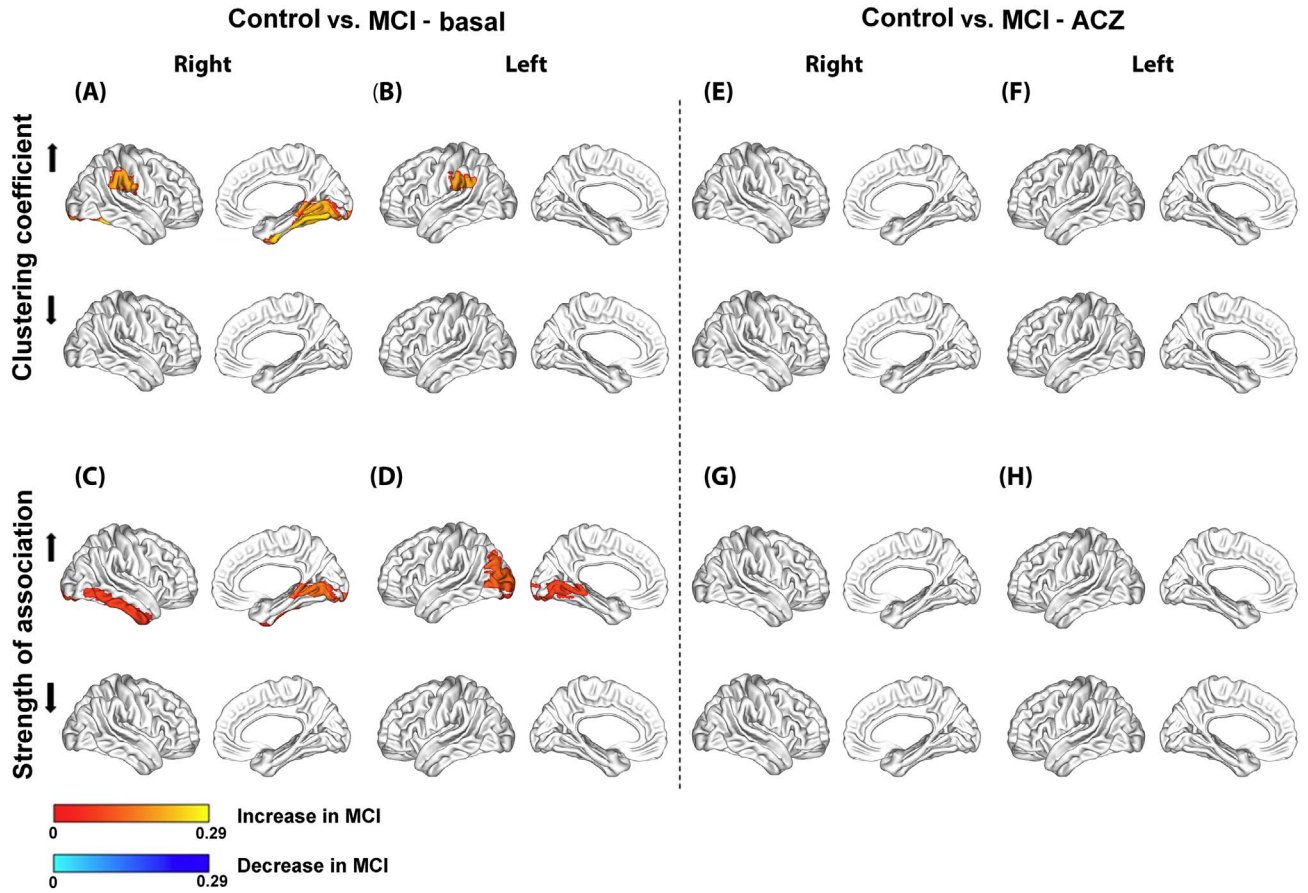

Fig. 5. Significant differences between group within-condition at the nodal level for the clustering coefficient (C_{nodal}) and mean strength of association (SA_{nodal}) in the basal (A–D) and ACZ conditions (E–H).
Regional changes are mapped onto the cortical surfaces using the BrainNet Viewer package (http://www.nitrc.org/projects/bnv).

(Sánchez-Catasús et al., 2017, for a review).

Interestingly, the patterns of C_{nodal} decrease (the bottom of Fig. 6.E and F) also overlap to a certain extent with the default mode network (DMN), which is very active in the resting state (Hafkemeijer et al., 2012, for a review). Thus, it is plausible that these patterns could be related to altered changes in the topology of the DMN's vascular component, considering that the CBF_{corr} network was studied in two resting states: pre-ACZ and under the effect of the ACZ. It is known that DMN also overlaps the brain network underlying the episodic memory (Rugg and Vilberg, 2013) that is specifically affected in MCI due to AD (Albert et al., 2011).

Furthermore, the DMN regions are also targets of the AD process (Ingelsson et al., 2004; Villain et al., 2012), which may disrupt CBF co-variation in response to the vasodilatory challenge. The available evidence suggests that various pathological mechanisms of AD may contribute to alterations of CVR as a result of damage to the cerebrovascular system (Glodzik et al., 2013, for a review). Nevertheless, such mechanisms could have less expression in the MCI stage, especially in patients with a low vascular load. Consequently, subtle CVR alterations would be difficult to detect by the standard approach, in agreement with previous studies with negative findings (Shim et al., 2015; Fromm et al., 2013; Anzola et al., 2011).

Moreover, the C_{nodal} increase in the MCI group network in the basal condition (the top of Fig. 5.A and B) also showed a partial correspondence with the C_{nodal} decrease induced by the ACZ (the bottom of Fig. 6.E and F). This overlap implies that in these regions C_{nodal} is changing from a high basal to a low ACZ value, thus being the regions with the greatest negative changes. Notably, these regions include the inferior parietal lobe bilaterally which also overlap with the regional CBF reduction in the MCI group in the basal condition (Fig. 3.C).

Of interest is also the opposite change of C_{nodal} (increase) and SA_{nodal} (decrease) in the right middle frontal region (the top of the Fig. 6.E and the bottom of the Fig. 6.G, respectively), which partially corresponds with the regional CBF increase in the MCI group (Fig. 2.B).

As a final point, let us consider some issues regarding our study population of MCI patients. The criteria for patient selection and the episodic memory reduction in the MCI group (Supplementary Table S1) indicate that our patients presented amnestic MCI. Furthermore, hippocampal atrophy in the MCI group (Supplementary Fig. S3 and Supplementary Table S4) suggests that most of our patients could evolve to AD dementia, with an intermediate level of certainty according to the latest diagnostic criteria for MCI due to AD (Albert et al., 2011). Still, we cannot exclude the possibility that some of our MCI patients evolve to another type of degenerative dementia as MCI is a complex heterogeneous condition.

4.3. Study limitations

First, some results at the nodal level and their interpretations should be taken with caution since they are based on an uncorrected statistic. Yet, these findings are meaningful given the partial correspondence found with the other results in this study using a corrected statistic. In order to increase the effect size at the nodal level, it may be necessary to increase the number of subjects and/or to use a more potent vasodilator stimulus in future studies. Second, our results are only valid at the group level. However, the present study is a necessary first step for a further study based on individual level. A recent study demonstrated that it is possible to estimate the individual contribution of a single subject to group-based correlation networks and to examine its association with clinical data (Saggar et al., 2015). A third limitation

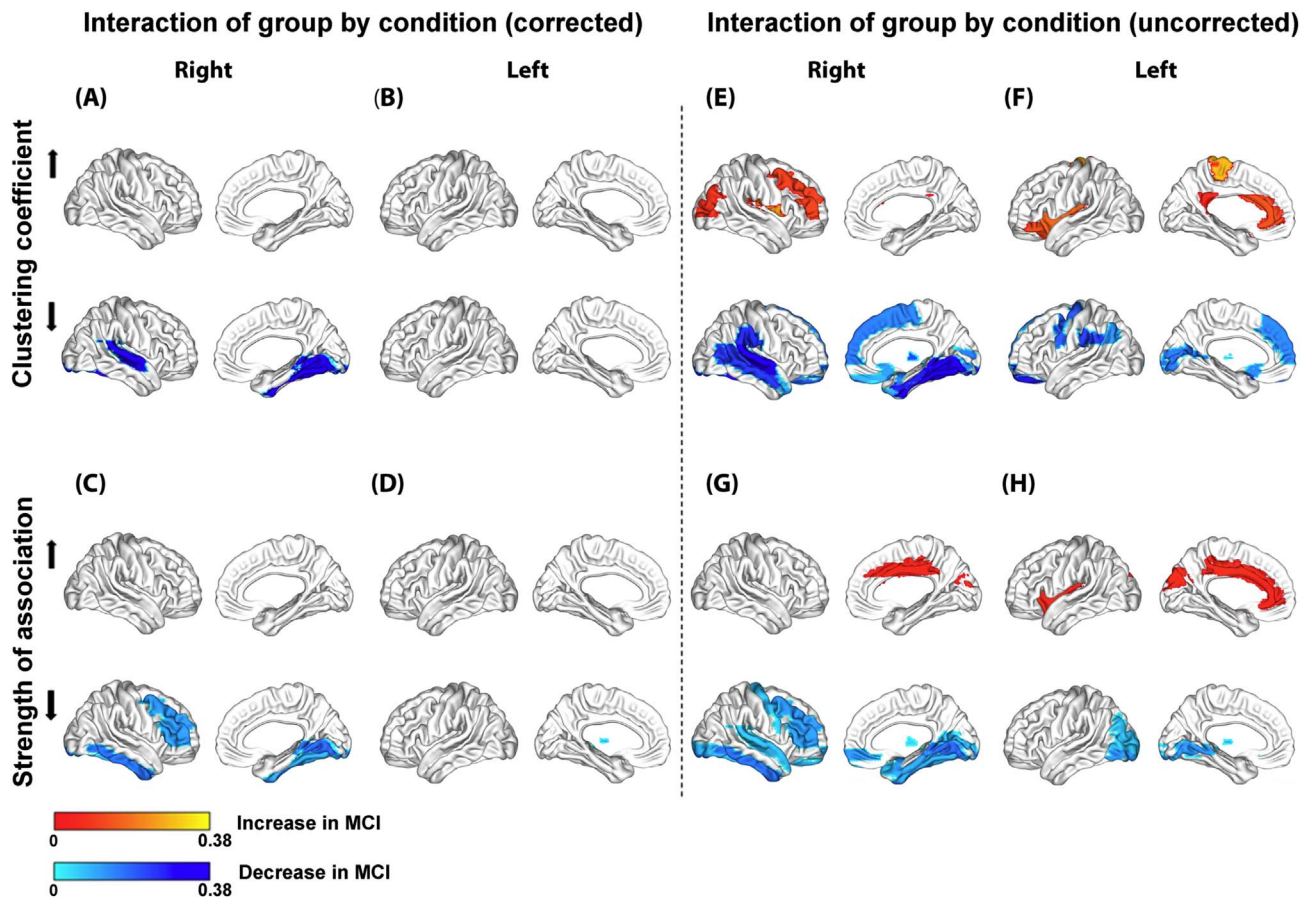

Fig. 6. Significant crossover interaction effects of group and condition at the nodal level for the clustering coefficient (C_{nodal}) and mean strength of association (SA_{nodal}) with Bonferroni correction (A–D) and without correction (E–H).
Regional changes are mapped onto the cortical surfaces using the BrainNet Viewer package (http://www.nitrc.org/projects/bnv).

is that this is a cross-sectional study, whereas longitudinal studies are needed to clarify the temporal evolution of the CBF_{corr} network along the continuum from normal aging to AD dementia. Four, graph theoretical analysis of the CBF_{corr} network has limitations that were discussed in our previous article (e.g. the use of Pearson's correlation instead of partial correlation; choice of parcellation scheme; possible variability of results with different sample sizes) (Melie-García et al., 2013). In addition, a recent study showed that the inclusion of global CBF as a confounding variable introduces artificial negative correlations in networks using resting state fMRI data (Carbonell et al., 2014), which might also be present in correlation networks using CBF SPECT. Nevertheless, all of these limitations are attenuated to some extent by studying the CBF_{corr} network in two different conditions, i.e. by analyzing the vasodilatory effect of ACZ after subtracting the effect of baseline. The vasodilatory effect of ACZ could be considered comparatively greater than the effects of the above methodological shortcomings.

4.4. Conclusions

This study suggests that graph theoretical analysis of ACZ-induced changes in the topology of the CBF_{corr} networks can detect subtle network-related CVR alterations in MCI not reflected by the standard approach. These alterations involve brain regions directly related to cognitive dysfunction in MCI. Our results also warrant further research on the individual level to develop a 'network'-based CVR biomarker of MCI due to AD.

Acknowledgements

The authors thank the collaboration of Drs. Yasser Iturria-Medina, Luis Juárez Orozco, Yurelis Ginarte and Fransje Reesink for their invaluable helps. The authors also thank the support of the Center for Neurological Restoration (CIREN), Havana, Cuba, and Department of Nuclear Medicine and Molecular Imaging, University Medical Center Groningen, the Netherlands.

Appendix A. Supplementary data

Supplementary data to this article can be found online at http://dx.doi.org/10.1016/j.nicl.2017.04.019.

References

Achard, S., Bullmore, E., 2007. Efficiency and cost of economical brain functional networks. PLoS Comput. Biol. 3 (2), e17.
Achard, S., Salvador, R., Whitcher, B., Suckling, J., Bullmore, E., 2006. A resilient, low frequency, small-world human brain functional network with highly connected association cortical hubs. J. Neurosci. 26 (1), 63–72.
Albert, M.S., DeKosky, S.T., Dickson, D., Dubois, B., Feldman, H.H., Fox, N.C., Gamst, A., Holtzman, D.M., Jagust, W.J., Petersen, R.C., Snyder, P.J., Carrillo, M.C., Thies, B., Phelps, C.H., 2011. The diagnosis of mild cognitive impairment due to Alzheimer's disease: recommendations from the National Institute on Aging-Alzheimer's Association workgroups on diagnostic guidelines for Alzheimer's disease. Alzheimers Dement. 7 (3), 270–279.
Alexander-Bloch, A., Giedd, J.N., Bullmore, E., 2013. Imaging structural co-variance between human brain regions. Nat. Rev. Neurosci. 14 (5), 322–336.
Anzola, G.P., Galluzzi, S., Mazzucco, S., Frisoni, G.B., 2011. Autonomic dysfunction in mild cognitive impairment: a transcranial Doppler study. Acta Neurol. Scand. 124 (6), 403–409.
Bassett, D.S., Nelson, B.G., Mueller, B.A., Camchong, J., Lim, K.O., 2012. Altered resting state complexity in schizophrenia. NeuroImage 59 (3), 2196–2207.

Boles Ponto, L.L., Schultz, S.K., Watkins, G.L., Hichwa, R.D., 2004. Technical issues in the determination of cerebrovascular reserve in elderly subjects using 15O-water PET imaging. NeuroImage 21 (1), 201–210.
Bullmore, E.T., Bassett, D.S., 2011. Brain graphs: graphical models of the human brain connectome. Annu. Rev. Clin. Psychol. 7, 113–140.
Cantin, S., Villien, M., Moreaud, O., Tropres, I., Keignart, S., Chipon, E., Le Bas, J.F., Warnking, J., Krainik, A., 2011. Impaired cerebral vasoreactivity to CO_2 in Alzheimer's disease using BOLD fMRI. NeuroImage 58 (2), 579–587.
Carbonell, F., Bellec, P., Shmuel, A., 2014. Quantification of the impact of a confounding variable on functional connectivity confirms anti-correlated networks in the resting-state. NeuroImage 86, 343–353.
Fromm, A., Lundervold, A.J., Moen, G., Skulstad, S., Thomassen, L., 2013. A vascular approach to mild amnestic cognitive impairment: a pilot study. Acta Neurol. Scand. Suppl. 196, 73–76.
Glodzik, L., Rusinek, H., Brys, M., Tsui, W.H., Switalski, R., Mosconi, L., Mistur, R., Pirraglia, E., de Santi, S., Li, Y., Goldowsky, A., de Leon, M.J., 2011. Framingham cardiovascular risk profile correlates with impaired hippocampal and cortical vasoreactivity to hypercapnia. J. Cereb. Blood Flow Metab. 31 (2), 671–679.
Glodzik, L., Randall, C., Rusinek, H., deLeon, M.J., 2013. Cerebrovascular reactivity to carbon dioxide in Alzheimer's disease. J. Alzheimers Dis. 35 (3), 427–440.
Hafkemeijer, A., van der Grond, J., Rombouts, S.A., 2012. Imaging the default mode network in aging and dementia. Biochim. Biophys. Acta 1822 (3), 431–441.
Hamilton, M., 1960. A rating scale for depression. J. Neurol. Neurosurg. Psychiatry 23, 56–62.
He, Y., Chen, Z.J., Evans, A.C., 2007. Small-world anatomical networks in the human brain revealed by cortical thickness from MRI. Cereb. Cortex 17 (10), 2407–2419.
He, Y., Chen, Z., Gong, G., Evans, A., 2009a. Neuronal networks in Alzheimer's disease. Neuroscientist 15 (4), 333–550.
He, Y., Dagher, A., Chen, Z., Charil, A., Zijdenbos, A., Worsley, K., Evans, A., 2009b. Impaired small-world efficiency in structural cortical networks in multiple sclerosis associated with white matter lesion load. Brain 132 (Pt 12), 3366–3379.
Herholz, K., Schopphoff, H., Schmidt, M., Mielke, R., Eschner, W., Scheidhauer, K., et al., 2002. Direct comparison of spatially normalized PET and SPECT scans in Alzheimer's disease. J. Nucl. Med. 43, 21–26.
Iadecola, C., 2004. Neurovascular regulation in the normal brain and in Alzheimer's disease. Nat. Rev. Neurosci. 5 (5), 347–360.
Ingelsson, M., Fukumoto, H., Newell, K.L., Growdon, J.H., Hedley-Whyte, E.T., Frosch, M.P., Albert, M.S., Hyman, B.T., Irizarry, M.C., 2004. Early Abeta accumulation and progressive synaptic loss, gliosis, and tangle formation in AD brain. Neurology 62 (6), 925–931.
Ingvar, D.H., 1979. “Hyperfrontal” distribution of the cerebral grey matter flow in resting wakefulness; on the functional anatomy of the conscious state. Acta Neurol. Scand. 60 (1), 12–25.
Iturria-Medina, Y., Sotero, R.C., Canales-Rodríguez, E.J., Alemán-Gómez, Y., Melie-García, L., 2008. Studying the human brain anatomical network via diffusion-weighted MRI and Graph Theory. NeuroImage 40 (3), 1064–1076.
Lassen, N.A., Andersen, A.R., Friberg, L., Paulson, O.B., 1988. The retention of [99mTc]-d,l-HM-PAO in the human brain after intracarotid bolus injection: a kinetic analysis. J. Cereb. Blood Flow Metab. 8 (6), S13–S22.
Melie-García, L., Sanabria-Diaz, G., Iturria-Medina, Y., Alemán-Gómez, Y., 2010. MorphoConnect: toolbox for studying structural brain networks using morphometric descriptors. In: 16th Annual Meeting of the Organization for Human Brain Mapping, (Barcelona, Spain).
Melie-García, L., Sanabria-Diaz, G., Sánchez-Catasús, C., 2013. Studying the topological organization of the cerebral blood flow fluctuations in resting state. NeuroImage 64, 173–184.
Morris, J.C., 1993. The clinical dementia rating (CDR): current version and scoring rules. Neurology 43 (11), 2412–2414.
Pillai, J.J., Mikulis, D.J., 2015. Cerebrovascular reactivity mapping: an evolving standard for clinical functional imaging. AJNR Am. J. Neuroradiol. 36 (1), 7–13.
Richiardi, J., Monsch, A.U., Haas, T., Barkhof, F., Van de Ville, D., Radü, E.W., Kressig, R.W., Haller, S., 2014. Altered cerebrovascular reactivity velocity in mild cognitive impairment and Alzheimer's disease. Neurobiol. Aging 36 (1), 33–41.
Rugg, M.D., Vilberg, K.L., 2013. Brain networks underlying episodic memory retrieval. Curr. Opin. Neurobiol. 23 (2), 255–260.
Saggar, M., Hosseini, S.M., Bruno, J.L., Quintin, E.M., Raman, M.M., Kesler, S.R., Reiss, A.L., 2015. Estimating individual contribution from group-based structural correlation networks. NeuroImage 120, 274–284.
Sanabria-Diaz, G., Martinez-Montes, E., Melie-Garcia, L., 2013. Glucose metabolism during resting state reveals abnormal brain networks organization in the Alzheimer's disease and mild cognitive impairment. PLoS ONE 8 (7), e68860.
Sánchez-Catasús, C.A., Stormezand, G.N., van Laar, P.J., De Deyn, P.P., Sánchez, M.A., Dierckx, R.A., 2017. FDG-PET for prediction of AD dementia in mild cognitive impairment. A review of the state of the art with particular emphasis on the comparison with other neuroimaging modalities (MRI and perfusion SPECT). Curr. Alzheimer Res. 14, 127–142.
Shim, Y., Yoon, B., Shim, D.S., Kim, W., An, J.Y., Yang, D.W., 2015. Cognitive correlates of cerebral vasoreactivity on transcranial Doppler in older adults. J. Stroke Cerebrovasc. Dis. 24 (6), 1262–1269.
Takasawa, M., Murase, K., Oku, N., Yoshikawa, T., Osaki, Y., Imaizumi, M., Matsuzawa, H., Fujino, K., Hashikawa, K., Kitagawa, K., Hori, M., Matsumoto, M., 2002. Assessment of acetazolamide reactivity in cerebral blood flow using spectral analysis and technetium-99m hexamethylpropylene amine oxime. J. Cereb. Blood Flow Metab. 22 (8), 1004–1009.
Tijms, B.M., Wink, A.M., de Haan, W., van der Flier, W.M., Stam, C.J., Scheltens, P., Barkhof, F., 2013. Alzheimer's disease: connecting findings from graph theoretic studies of brain networks. Neuorobiol. Aging 34 (8), 2023–2036.
Tzourio-Mazoyer, N., Landeau, B., Papathanassiou, D., Crivello, F., Etard, O., Delcroix, N., Mazoyer, B., Joliot, M., 2002. Automated anatomical labeling of activations in SPM using a macroscopic anatomical parcellation of the MNI MRI single-subject brain. NeuroImage 15 (1), 273–289.
Vagal, A.S., Leach, J.L., Fernandez-Ulloa, M., Zuccarello, M., 2009. The acetazolamide challenge: techniques and applications in the evaluation of chronic cerebral ischemia. AJNR Am. J. Neuroradiol. 30 (5), 876–884.
Van Laere, K.J., Versijpt, J., Koole, M., Vandenberghe, S., Lahorte, P., Lemahieu, I., Dierckx, R.A., 2002. Experimental performance assessment of SPM for SPECT neuroactivation studies using a subresolution sandwich phantom design. NeuroImage 16 (1), 200–216.
Villain, N., Chételat, G., Grassiot, B., Bourgeat, P., Jones, G., Ellis, K.A., Ames, D., Martins, R.N., Eustache, F., Salvado, O., Masters, C.L., Rowe, C.C., Villemagne, V.L., AIBL Research Group, 2012. Regional dynamics of amyloid-β deposition in healthy elderly, mild cognitive impairment and Alzheimer's disease: a voxelwise PiB-PET longitudinal study. Brain 135 (Pt 7), 2126–2139.
Watts, D.J., Strogatz, S.H., 1998. Collective dynamics of ‘small-world’ networks. Nature 393, 440–442.
Wu, K., Taki, Y., Sato, K., Kinomura, S., Goto, R., Okada, K., Kawashima, R., He, Y., Evans, A.C., Fukuda, H., 2012. Age-related changes in topological organization of structural brain networks in healthy individuals. Hum. Brain Mapp. 33 (3), 552–568.
Yamauchi, H., Okazawa, H., Kishibe, Y., Sugimoto, K., Takahashi, M., 2002. Reduced blood flow response to acetazolamide reflects pre-existing vasodilation and decreased oxygen metabolism in major cerebral arterial occlusive disease. Eur. J. Nucl. Med. Mol. Imaging 29 (10), 1349–1356.
Zavoreo, I., Kes, V.B., Morovic, S., Seric, V., Demarin, V., 2010. Breath holding index in detection of early cognitive decline. J. Neurol. Sci. 299 (1–2), 116–119.

SUPPLEMENTARY MATERIAL

The Supplementary Material includes:

Assessment of cognitive function in MCI and control groups.

Supplementary Tables S1-S4.

Supplementary Figures S1-S3.

Assessment of cognitive function in MCI and controls groups

The cognitive function was assessed for each participant by a neuropsychological battery comprising mnemonic and nonmnemonic specific tests. Mnemonic tests included Rey Complex Figure test (delayed recall) for episodic memory assessment, logical memories A and B (immediate recall) and paired associate learning (easy and hard-word pairs, immediate recall) of the Wechsler memory scale (WMS). Nonmnemonic tests comprised the copy of the Rey Complex Figure test, attentive matrices [1], token test [2], verbal fluency [3], digit span of WMS (forward and backward items), and Trail Making A and B tests.

All mnemonic test scores, except easy-word pair learning, showed significant reduction in the MCI group as compared with control group (Supplementary Table I). In contrast, all nonmnemonic test scores showed no significant differences between groups.

Supplementary Table S1. Cognitive function in MCI and control groups

	MCI (N=26)	Control (N=26)	p value
Mnemonic Tests			
Rey complex fig. (delayed recall)	9.4 ± 4.8	18.1 ± 5.2	10^{-6}
Logical memory A	9.9 ± 3.5	11.7 ± 3	0.02
Logical memory B	8.4 ± 3.4	10.2 ± 3.1	0.04
Easy-word pair learning	8.1 ± 1.3	8.6± 0.7	0.06
Hard-word pair learning	3 ± 2.4	5.7 ± 2.5	1.7×10^{-5}
Nonmnemonic Tests			
Rey complex fig. (copy)	31 ± 5.5	32.7 ± 4.4	0.16
Attentive matrices	40.9 ± 10	44. 9 ± 9.7	0.07
Token test	32.5 ± 3.1	33.5 ± 2	0.07
Verbal fluency	9.1 ± 3.6	10 ± 2.9	0.18
Digit span (forward)	5.6 ± 1.2	5.9 ± 1	0.16
Digit span (backward)	4.5 ± 0.8	4.9 ± 0.9	0.07
Trail Making A	42.7 ± 7.6	39.4 ± 4.7	0.08
Trail Making B	117.1 ± 22.2	107.9 ± 14.5	0.08

Data shown as mean ± S.D. Differences between groups were tested using ANCOVA, modeling group as a categorical independent variable and controlling for age, gender and level of education. Bonferroni was used as a post-hoc test.

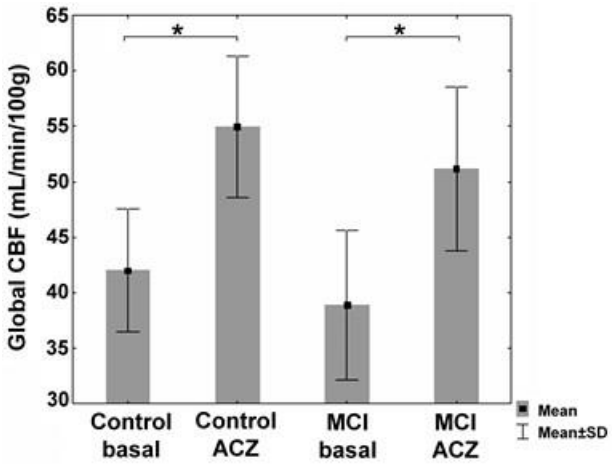

Supplementary Figure S1. Global CBF in the control and MCI groups in the two conditions: basal and under the acetazolamide (ACZ) challenge. Both groups responded similarly to the ACZ challenge by significantly increasing the CBF compared to the basal condition (*- $p < 10^{-6}$).

Supplementary Table S2. Brain regions with significant CBF increase due to ACZ challenge in MCI and control groups.

Group	p-value	Extent (voxels)	Brain regions
Control			
	0.002	1457	Right frontal lobe: precentral, superior (medial, dorsolateral and orbital), middle (including orbital) and inferior (opercular and triangular) gyri; rolandic operculum. Right postcentral and supplementary motor area.
	0.012	1028	Left frontal lobe: precentral, superior (medial and dorsolateral) and middle (including orbital) gyri. Left supplementary motor area
MCI			
	10^{-3}	2470	Right frontal lobe: precentral, superior (medial and dorsolateral), middle and inferior (triangular) gyri; and supplementary motor area. Right postcentral gyrus. Right insula.
	0.012	1027	Left frontal lobe: precentral, superior (medial and dorsolateral) and middle gyri; and supplementary motor area.

p-value corrected for multiple comparisons (FWE) at cluster level.

Supplementary Table S3. Brain regions with significant CBF decrease in the MCI group as compared to the control group at baseline and ACZ conditions.

Condition	p-value	Extent (voxels)	Brain regions
Basal			
	0.01	3435	Right temporoparietal cortices. Bilateral precuneus and posterior cingulate. Adjacent part of right occipital lobe and lateral temporal cortex.
	0.015	851	Left temporoparietal cortices. Adjacent parts of left occipital and temporal cortex. Left insula.
ACZ			
	0.013	1022	Bilateral precuneus and posterior cingulate. Left temporoparietal cortices.

p-value corrected for multiple comparisons (FWE) at cluster level.

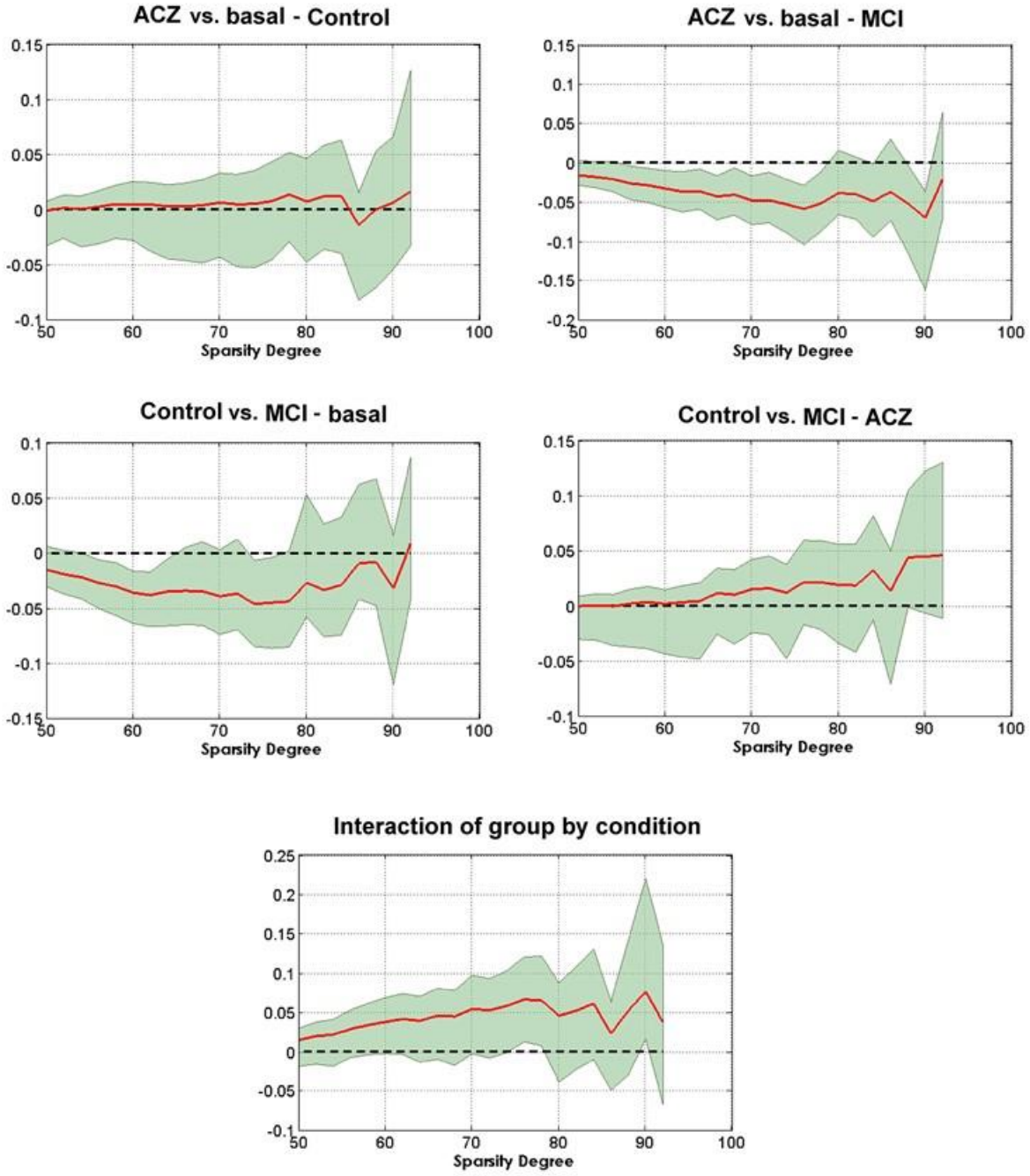

Supplementary Figure S2. Differences in the global clustering coefficient (C_{global}) across the range of sparsity degree. In red, the differences, the dashed line indicates the null hypothesis and the limits of the shaded area in green indicate the 95 percent BCa (bias-corrected) bootstrap confidence interval.

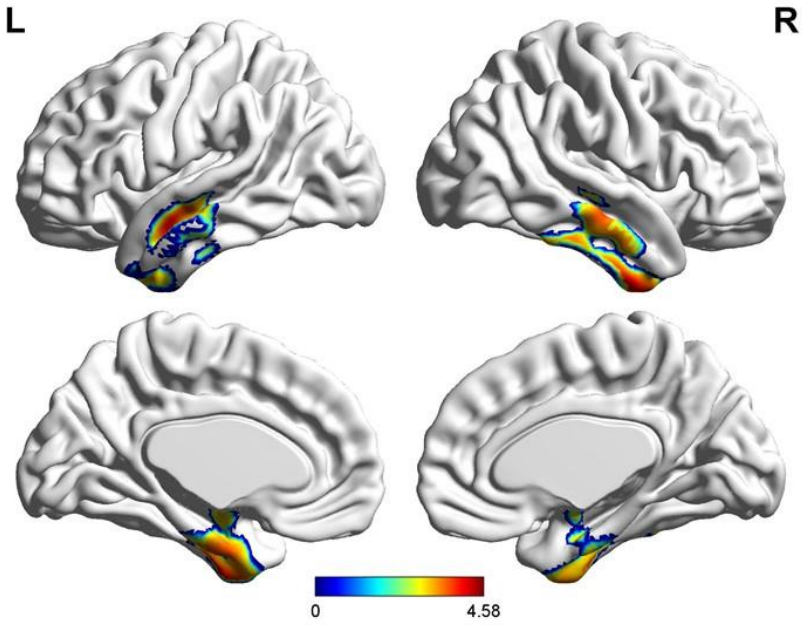

Supplementary Figure S3. Brain regions with a significant grey matter volume decrease in the MCI group as compared to the control group (see also Supplementary Table S4).

Supplementary Table S4. Brain regions with a significant gray matter volume decrease in the MCI group as compared to the control group.

p-value	Extent (voxels)	Brain regions
0.02	1265	Left medial temporal lobe (hippocampus, parahippocampal and amygdala).
0.04	1026	Left lateral temporal lobe (superior, middle and inferior gyri) and fusiform gyrus. Left temporal pole.
0.01	1659	Right medial temporal lobe (hippocampus, parahippocampal and amygdala). Right lateral temporal lobe (superior, middle and inferior gyri) and fusiform gyrus. Right temporal pole.

p-value corrected for multiple comparisons (FWE) at cluster level.

References

1. Spinnler H, Tognoni G (1987) Standardizzazione e taratura di test neuropsicologici. The Italian Journal of Neurological Sciences 8, suppl 6: pp. 1-20.
2. De Renzi E, Vignolo LA. The token test: A sensitive test to detect receptive disturbances in aphasics. Brain 1962; 85: 665-678.
3. Mondini S, Mapelli D, Vestri A. Esame neuropsicologico breve. Milan: Raffaello Cortina Editore; 2005.